Non-thermal atmospheric pressure plasma interacting with water for biological applications

Bo Liu

▶ To cite this version:

Thèse de doctorat

Non-thermal atmospheric pressure plasma interacting with water for biological applications

Thèse de doctorat de l'Université Paris-Saclay
Préparée à L'Ecole polytechnique

École doctorale n°564 – Physique en Ile de France (PIF)
Spécialité de doctorat : Physique

Thèse présentée et soutenue à Palaiseau, le 19 Septembre, par
M. Bo Liu

Composition du Jury:

Loic Rajjou	**Président**
Professeur des Universités, Université Paris-Saclay (INRA)	
Chedly Tizaoui	**Rapporteur**
Professeur, University of Swansea (College of Engineering)	
Ahmed Khacef	**Rapporteur**
Ingénieur de Recherche Université d'Orléans (CNRS, GREMI)	
Nofel Merbahi	**Examinateur**
Professeur des Universités, Université de Toulouse 3 (LAPLACE)	
Angelo Pierangelo	**Examinateur**
Ingénieur de Recherche, Ecole Polytechnique (LPICM)	
Françoise Corbineau	**Examinateur**
Professeur des Universités, Sorbonne Université (College of Engineering)	
Antoine Rousseau	**Directeurde thèse**
Directeur de Recherche au CNRS, Ecole polytechnique (Laboratoire LPP)	

Abstract

Non-Thermal-Plasmas (NTP) produced by electric discharges are weakly ionized gases, which keeps the gas temperature at near room temperature contrary to the electron temperature which can reach several electron-Volts. Applications of NTP to medicine and agriculture are new multidisciplinary research fields based on interactions of the Non-Thermal-Plasmas with living organisms. Electric field as well as Reactive Oxygen and Nitrogen Species produced by NTP may inactivate bacteria, stimulate skin regeneration (dermatology), tumor reduction (oncology) and seeds germination (agriculture). These new fields of research are based on the plasma-liquid chemistry. These new field of researches, based on the plasma-liquid chemistry are very promising and developing quickly. The objective of this work is based on both fundamental and applied researches in non-thermal atmospheric pressure plasma interacting with water for biological applications and aim at a better understanding of the physical and chemical processes of plasma-liquid interaction and of particularly the biological process of NTP treatments with seeds and *ex vivo* mice skin.

This manuscript is divided in five chapters: i) First a literature review is presented showing the state of the art of the plasma-liquid interaction, and the main advances of the application of NTP to seed germination and skin treatment; ii) Second, experimental set ups are described, in particular the manufacturing of plasma reactors using 3D printing; iii) then, the production of gaseous and aqueous reactive species formed by DBD plasmas was measured quantitatively and plasma-liquid interaction was analyzed; iv) Next, different varieties of seeds were selected to evaluate the effect of a DBD plasma treatment and the study of the mechanisms of NTP germination promotion was specifically investigated by treating mung bean seeds in different discharge conditions, in different mediums, in electric field alone and in different hydration levels of seeds; iv) Finally, Mueller parametric imaging (MPI) was applied to study the modification of *ex vivo* mice skin treated by a helium plasma jet.

Key words: Cold plasmas, plasma activated media, plasma medicine, plasma agriculture, plasma-liquid interaction, skin treatments, seeds treatment, Mueller polarimetric imaging.

Résumé

Les plasmas froids produits par les décharges électriques sont des gaz faiblement ionisés, ce qui maintient la température du gaz à une température proche de la température ambiante, contrairement à la température de l'électron qui peut atteindre plusieurs électron-volts. Les applications des plasmas froids en médecine et en agriculture sont des nouveaux domaines de recherche multidisciplinaires basés sur les interactions de ces plasmas avec des organismes vivants. Le champ électrique ainsi que les espèces réactives de l'oxygène et de l'azote peuvent inactiver les bactéries, stimuler la régénération de la peau (dermatologie), la réduction tumorale (oncologie) et la germination des graines (agriculture). Ce nouveau domaine de recherche, basé sur la chimie plasma-liquide, est très prometteur et se développe rapidement. L'objectif de ce travail est basé sur des recherches fondamentales et appliquées sur le plasma à pression atmosphérique non thermique en interaction avec l'eau pour des applications biologiques et vise à une meilleure compréhension des processus physiques et chimiques de l'interaction plasma-liquide et en particulier du processus biologique de traitements au plasma avec des graines et de la peau de souris ex vivo.

Ce manuscript est divisé en cinq chapitres: i) On présente tout d'abord une revue de la littérature présentant l'état de l'art concernant l'interaction plasma-liquide et les principales avancées en matière d'applications des plasmas froids à la germination des semences et traitement de la peau; ii) Deuxièmement, les dispositifs expérimentaux sont décrits, en particulier la fabrication de réacteurs à plasma utilisant l'impression 3D; iii) Ensuite, la production d'espèces réactives gazeuses et aqueuses formées par des plasmas de type DBD a été mesurée quantitativement et l'interaction plasma-liquide a été analysée; iv) Puis, plusieurs variétés de graines ont été sélectionnées pour évaluer l'effet un traitement par plasma DBD ; l'étude des mécanismes de promotion de la germination du plasma a été spécifiquement étudiée en traitant les graines de soja vert dans différentes conditions de décharge, dans différents milieux, avec un champ électrique seul et dans différentes conditions de cultures ou de niveau d'hydratation des graines; v) Enfin, l'imagerie paramétrique de Mueller (MPI) a été appliquée pour la modification de la peau de souris ex vivo traitées par un plasma à jet d'hélium.

Mots clés : Plasmas froids, milieu activé par plasma, médecine par plasma, agriculture par plasma, interaction plasma-liquide, traitements de la peau, traitement des semences, imagerie polarimétrique de Mueller

Acknowledgements

I would like to express my sincere appreciation to Antoine Rousseau, my supervisor, for providing me this opportunity and this PhD research subject to me, and also thanks for his continuous encourage and support during this three years' work. I am grateful to Antoine Rousseau for supporting me to participate in variety of international conference in other countries. These are extremely good opportunities knowing the latest cutting-edge research and communicating with the best researchers around the world. Thanks for him to provide me with sufficient experimental funding and equipment. Thanks for his patience for my poor knowledge about plasma and language in the beginning of my PhD. Finally, I sincerely thank him for treating me as a colleague and respecting my personal ideas and encouraging me to do what I want to do.

I would also like to express my appreciations to Dr Bruno Honnorat, my colleague, for giving me countless help in my first two years' work. I have to say that it is really difficult for someone who has only a background in chemistry and materials engineering but will do plasma research. Thank him for helping me to build up my plasma setup using 3D printer, to learn the diagnosis of plasma, to manipulate the plasma characterization equipment and to do the survival analysis, etc.

I thank my co-authors and my collaborator: Professor Loic Rajjou from L'Institut national de la recherche agronomique (INRA, JOUY-EN-JOSAS), for cooperation of seeds treatment with plasma and for the correction of my articles; Dr Angelo Pierangelo from Laboratoire de Physique des Interfaces et des Couches Minces (LPICM), for the cooperation of Mueller polarimetic imaging of mice skin and for the correction of my thesis.

I would like to thank another two valuable colleagues Constance Duchesne and Xianjie Wang. Thanks for their companionship during these three years. Thanks to Constance, an always energetic and optimistic girl, for the help in my work of skin treatment and the invitation to her hometown. I really enjoy the time staying near the sea and your father's delicious food. Thanks to Xianjie for the help on my work of plasma-liquid interaction. Thank you to be my neighbour for two years and offering

countless free dinner for me. I wish you both have a happy life every day.

I would like to thank my temporary colleagues Zixian Jia, Hang Yang, Chenyang Ding, Thierry Dufour, Nadira Frescaline, Jaime Arancibia and Sivachandiran Loganathan. Thanks for your help for my work.

I would like to also thank Cherifa Ighoud and Catherine Jegu, the Laboratory secretaries, for their help in purchasing experimental equipment and chemical medicine, booking tickets and paying for variety fees like conferences and summer school.

Thank my families and my friends in China to support and help me solving the loneliness and problems in life I have had in France alone.

Thanks to all other people who once helped me, if I forget to mention you here please don't mind.

Thanks for China Scholarship Council (CSC) to grant my three years PhD.

Lastly, I want to say working in LPP as PhD candidate and three years live in Paris would definitely be a preciously experience and memory in my life. I will treasure this experience and memory forever.

Thanks to all

Merci à tous

Bo

Contents

General introduction

Non-thermal plasmas (NTP) are weakly ionized gases having a gas temperature close to ambient temperature and an electron average energy of several electron-volts. NTP can be produced by electrical discharge in gases; they contain ions, electrons and neutral species. Electric field as well as Reactive Nitrogen and Oxygen Species (RNOS) produced by NTP can interact with living organisms. In the past few years, applications of NTP to biology such as agriculture and biomedicine have become stimulating multidisciplinary research fields. NTP treatments may stimulate seeds germination and plant growth (agriculture and agronomy); depending upon the dose, NTP can also induce cell destruction (necrosis) or cell programmed death (apoptosis) or, at the contrary, they can induce cell proliferation. However, due to the very high level of complexity, understanding is still poor concerning mechanisms involved in biological processes, in particular, the respective role of reactive species and electric field.

In the field of biological application of NTP to agriculture, NTP have been recently used to treat seeds with the aim of promoting seeds germination. Food crisis in terms of shortage and safety becomes a more and more important issue to face the population growth, reduced cultivated land, abused pesticide and deteriorated eco safety in the recent years. The most feasible and effective way is to improve the crop production in restrained cultivable land. Seeds are of critical importance for the production and security of food. The germination is the very complex physiological process through which a seedling grows from a seed. The quality of seeds germination is strongly related to the quality of seeds and the environmental stress. Seeds priming techniques aim at improving the seeds vigour and enhancing rapidity and uniformity of the germination. The potentialities of NTP as a new priming technology could be based on three key effects: first, the capacity of NTP to inactivate microorganisms; second, the ability to modify the seeds coat surface; third, the regulation of important metabolic activities of germination. Nevertheless, the complex underlying mechanisms of plasma-seeds interaction process still have not been fully described and understood. It is an important aspect of my thesis to

investigate which physical and chemical parameters produced by the NTP play a role on the germination of certain seeds.

A second aspect of my work is to investigate the biophysical and biochemical effects of NTP treatments on skin tissues. This preliminary study is related to NTP medicine and aims at exploring a fundamental aspect, which is the characterization of tissues after NTP treatment using a non-invasive spectroscopic diagnostic. Generally, for tumor reduction, relatively high doses (refer to the energy) of NTP are delivered which may damage tissues intentionally or not. On the other hand, the use of NTP for dermatology and cosmetology is increasing for healing skin wound, curing skin diseases, and caring skin health, etc… Here again, NTP, on one hand, can either inactivate bacteria or improve tissue repair, but on the other hand, can also be detrimental to the skin structure, depending the NTP treatment dose. The effect of NTP dose on dermatology can not only be indicated with cell activity, cell quantity and immunological activity, but also characterized with tissue structures. Collagen is a major component of the extracellular connective tissue matrix of the skin. The secretion and spatial structure of collagen can be affected by NTP. The structure of the skin is closely related to its physiological function. In general, the structures of pathological skin tissues are different to the healthy ones. Hence, the characterization of modification of microstructure of skin tissue treated by NTP can be valuable to indicate the effect of NTP treatment. An alteration of collagen spatial structure can cause the changes of the polarimetric properties of skin tissue.

In our work, Mueller polarimetric imaging (MPI) was used to characterize the skin tissue before and after NTP treatment. This could provide a useful characterization evaluating the performance of NTP treatment on dermatology, but very few related works have been done currently.

These new research fields are partially based on the plasma-liquid chemistry; they are very promising and develop quickly. The motivations of my PhD are based on both fundamental and applied researches in non-thermal atmospheric pressure plasma interacting with water for biology.

My three years of research at Laboratoire de Physique des Plasma (LPP), Ecole Polytechnique have been dedicated to: i) develop plasma reactors, ii) quantify the

reactive species produced by the NTP, iii) evaluate their potentialities for seed germination in collaboration with the L'Institut national de la recherche agronomique (INRA, JOUY-EN-JOSAS), iv) and explore the characterization of effect of NTP treatment on the modification of structure of mice skin using *ex vivo* Mueller polarimetric imaging in collaboration with Laboratoire de Physique des Interfaces et des Couches Minces (LPICM) at Ecole Polytechnique. My three years PhD is granted by the China Scholarship Council (CSC).

The thesis has been divided into six chapters.

Chapter 1 is the literature review. This chapter describes the topics of the present thesis, namely basic knowledge about NTP, plasma-liquid interaction process and biological applications of NTP. A special focus addresses the emerging field of applications of NTP for agronomy and dermatology, namely the stimulation of germination of seeds and skin treatments using a DBD plasma treatment and plasma jet treatment.

Chapter 2 is the description about the general experimental setups and principle of the related experimental measurement methods and techniques. It includes the design and fabrications of plasma sources, methods of quantitative and qualitative measurement of gaseous and aqueous species, protocols of seeds treatments and seeds germination, protocols of skin treatment with plasma jet and Mueller polarimetric imaging and description of principle of statistical analysis method used in the field of agronomy.

Chapter 3 investigates the physical and chemical process of plasma-liquid interaction using a single electrode plasma reactor in four different configurations. In this chapter, the plasma reactive species both in gaseous and liquid phase produced by the single electrode plasma setup are measured quantitatively. The discharge conditions of the touching bubble plasma using the single electrode plasma setup are optimized based on the production of aqueous species formed by the DBD plasma. The aqueous plasma reactive species produced by the 9-elelctrode plasma setup under the optimized discharge conditions are measured.

Chapter 4 is focused on the effects of DBD plasma treatment on a selection of eight types of seeds using the 9-electrode plasma setup. The selected seeds are Wheat,

General introduction

Mung Bean, Tomato, Radish, Mustard, Sticky Bean, Lettuce and Dianthus. The objective of this chapter is to select the type of seeds, which respond well to DBD plasma treatment.

Chapter 5 is a parametric study, varying the conditions of seed treatment in order to identify the key parameters. This study is made using an upscale 9 electrode reactor and the selected seeds are Mung Beans. The plasma treatments include seeds treatments with a DBD plasma in different discharge gases, different discharge times, different distances of seeds to water surface, different liquids and tap water in different pH values. Alternatively, electric field treatments will be compared to DBD plasma treatment.

Chapter 6 is an innovative study of the effect of plasma jet treatment on skin tissue using *ex vivo* Mueller polarimetric imaging. The skin samples are treated by a helium plasma jet in different doses by two different ways, that are plasma continuous treatment and plasma sequential treatment. The thermal treatments using an oven are used to heat mice skin with the aims of investigating the thermal effect of plasma jet on the modification of skin structure in the plasma jet treatments. The thermal treatment has been done in different temperature by two different ways, that are thermal continuous treatment and thermal sequential treatment.

Finally, the general conclusion of this study summarizes the main outcomes and points out the future perspective

Chapter 1: State of the art

This chapter describes the topics of the present thesis, namely basic knowledge about plasmas, plasma-liquid interaction process and biological applications of NTP. A special focus addresses the emerging field of applications of NTP for agronomy and dermatology, namely the stimulation of germination of seeds and skin treatments using a DBD plasma treatment and plasma jet treatment.

State of the art

1.1 General context of plasma

Plasmas are ionized and electrically neutral matter [1-3]. As the distinct fourth state of matter, plasmas are estimated to constitute more than 99% of the visible universe and its components mainly include free electrons and charged ions. In 1879, the famous British physicist and chemist William Crookes discovered the plasma. In 1928, American chemist and physicist Irving Langmuir and Tonks introduced the term plasma for the first time to describe the special form of matter in an energized gas tube. Plasma is obtained after ionization of the gas molecular structure by injecting energy such as heat or electromagnetic field. Plasmas contain electrons, ions, neutral atoms, and free radicals, and its total charge is zero.

1.1.1 Plasma classification

According to its thermodynamic equilibrium state, plasma can be divided into high temperature plasma (HTP), thermal plasma (TP), local thermal plasma (LTP) and non-thermal plasma (NTP). The average energies of neutral and/or charged particles in plasma and their relevant translational, rotational or vibrational degrees of freedom can be used to measure the temperature of plasma including ions, electrons and gas [3]. Temperature of electrons is equal to the temperature of the heavy particles in HTP. Gas temperature (T_g) in HTP can be as high as 10^9 K. This is typically the temperature of solar plasma or magnetic confinement fusion. Temperature of electrons, ions and gas in TP is same or nearly equal, but the temperature is lower than HTP, which is about 10^4 K. LTP is also known as "thermal plasma", but it does not reach a comprehensive thermodynamic equilibrium. Only local region between electrons and ions reach thermal equilibrium and the T_g is in the range of 10^3 K to 10^4 K. Plasmas driven by an Arc or radio frequency discharge are LTP. Non-thermal plasma is a state where gases are weakly ionized and the ionization degree of NTP is less than 0.01%. Ions, electrons and neutral species coexist in NTP, but electron temperature (T_e, 10^4-10^5 K) is significantly higher than that of heavy particles (ions and neutrals). Since ionization degree of NTP is low, the gas temperature of NTP is merely in room temperature ($T_g < 10^3$ K). Discharge of plasma can be in low pressure or at an atmospheric pressure.

1.1.2 Non-thermal plasmas (NTP)

NTP are produced by localized electric field-excited discharges and are generally considered to be partial discharges. It includes dielectric-barrier discharges (DBD), corona discharges (CD), constricted glows (CG), electron avalanches (EA), local Townsend discharges (localized Townsend discharges, LTD). The average energy of electrons in NTP is much higher than the energy of charged heavy particles, neutral molecules, and molecular fragments (free radicals, and atoms). Atmospheric pressure NTP are rich in chemical reactive species and have low gas temperature, which make them widely used in multiple fields. The DBD plasma and plasma jet are the ones which are mostly studied and selected for applications of NTP.

A DBD discharge is composed of a large number of filament-shaped breakdown channels (micro-discharges), and the plasma parameters of the micro-discharge channels can be controlled to change, so that the DBD technology can be optimized in various applications. The plasma jet that is mostly selected for biological applications can be a DBD discharge whereby the NTP is extended beyond the plasma generation zone into the vicinity of treated targets by propagating in the capillary channel flown by a noble gas; the length of a plasma jet can reach the level of meters.

DBD discharge often develops with Streamer breakdown mechanism in a non-uniform field at non-thermal. The streamer discharge has the properties of 1-10 ns of growth duration, ca. 0.5 µm mean free path, ca. 50 µm of ionization length, 100-200 µm of NTP radius, 100-1000 A.cm^{-2} of current density, 10^{14}-10^{15} cm^{-3} of electron density and 1-10 eV of mean electrons energy. When the breakdown field strength is reached, the DBD discharge produces the NTP. When the electrons are attached to other particles and participate in the recombination process to reduce the NTP conductivity, the NTP are also extinguished. When the electric field strength is slightly lower than the breakdown field strength, the microdischarge is interrupted. The electric field drop is caused by the charge build up at the filamentous NTP location. Filamentous microdischarges are weakly ionized NTP channels. The charge transferred generally increases with the discharge spacing and the dielectric constant of the dielectric and has no direct connection with the gas pressure. Regardless of the frequency and voltage characteristics of the open circuit, the micro-

discharge properties are independent of the external drive circuit and are related to gas properties and geometry of the electrodes. This latest statement may fail for nanosecond or sub nanosecond voltage rise time, where the applied electric field may reach values higher than the breakdown voltage.

Under atmospheric pressure condition, the excited state species produced in the NTP region undergo a rapid (0.1-100 µs range) de-excitation and recombination process leading to less reactive radicals which can diffuse outside the NTP region. The DBD device can be designed in a variety of styles like flat, cylindrical, single layer media, dual layer media, media locations that can be either floating or attached to the electrodes. The electrode spacing (including the medium) is from a few millimeters to few centimeters.

1.2 Applications of non-thermal plasmas

Until now, NTP have been widely applied in many fields including material science [4-6], space science and astronomy [7, 8], electronics science [9], chemistry and chemical engineer [3] and environment science [10-23]. More recently, the NTP have been found to have extremely high biological activity, especially in treating the organic living tissues in the fields of oncology [24-28], dermatology [29], stomatology [30, 31] and agronomy [32-38]. This work mainly focuses on the applications of NTP in environment field and in biological fields as they are related to the work of our group and our main topics of this thesis which are seeds treatments and skin treatments, which will be introduced in the following sections.

1.2.1 Applications of non-thermal plasmas in environmental fields

As a simple and environmentally friendly new technology, NTP have been successfully applied to solve the increasingly prominent environmental pollution problems, including volatile organic compounds (VOCs) degradation [12-14, 39-41], waste water purification [15-19, 42, 43] and toxic gases elimination [20-23]. The NTP applied in solving environmental pollution can be produced by a gliding arc

discharge [44-47], a corona discharge and a DBD discharge [47-49]. When reacting with NTP, these contaminant molecules are both collided by reactive particles (e.g. high-energy electrons) and oxidized by strong oxidative chemical species (e.g. Hydroxyl radicals and ozone etc).

Tizaoui et al. has conducted extensive researches in purifying waste water based on the oxidation by ozone formed by a gas discharge [42, 43, 50-52]. Khacef et al. has studied a series of works to remove the pollutants from the diesel exhaust with the NTP treatments [40, 53-56]. In our group, Barakat et al. decomposed VOCs through the oxidation by ozone produced by a DBD discharge [49, 57]; Jia [58] et al. found the oxidation of toluene can be intensified by combining the DBD plasma treatment with a catalyst in the plasma-catalysis configuration; Wang [48] et al. further to study the decomposition of ozone adsorbed on the surface of the Gobi dust.

1.2.2 Applications of non-thermal plasmas in biological fields

In the past few decades, applications of NTP to biology like agriculture and biomedicine are new multidisciplinary research fields based on interactions of the electric discharges (NTP) with living organisms. Electric field as well as Reactive Nitrogen and Oxygen Species (RNOS) produced by NTP have been found to have significant biological activity. In the field of agriculture, NTP have been used to promote seeds germination [59], to strength seeds tolerance of drought stress [60], to decontaminate infected seeds and plants [61], to stimulate plant growth [62], to improve yields [36], to package food [63] and to sterilize fruits and meats [64] etc. In addition, numerous researches of NTP in the field of biomedicine have been carried out [25-28, 65-78]. It is found that NTP can be a therapy of tumor, can inactivate bacteria, can stimulate cell or tissue regeneration, can coagulate blood, can modify skin and can cure chronic wound or other pathological organisms, etc. These new field of researches are very promising and developing quickly.

1.2.2.1 Applications of NTP in agriculture

Seeds treatment with NTP is one of the main applications of NTP in agriculture

and is one of the topics of the present work which will be introduced in detail in the following section. Food treatment with NTP is another important application in this field and will be introduced here.

NTP food treatment aims to be an innovative food preservation technology. The purpose of food preservation is to store food in its original fresh and nutritious state for a long time. To do so, food should be sterilized and kept in a condition that could avoid the contamination from bacteria and microorganisms and could inhibit visual deterioration like rancidity, dehydration and enzymatic browning reaction [79]. The conventional techniques preserving food are curing, cooling, freezing, pickling, canning, jellying, jugging, burial, fermentation, pasteurization, artificial food additives, modified atmosphere, high-pressure food preservation and bio-preservation etc [38-42]. Although these methods could make food kept in an edible level, the nutrition, texture and even safety of the food are destroyed partially or completely[79]. Packaging food in specific gas mixture at an atmospheric pressure is one of the most usual ways for fresh conservation. Gas mixtures with less oxygen or more CO_2 can significantly inhibit the action of bacteria, fungi and even viruses. Even though, the package food still faces problems that cell metabolism of food itself cannot be retarded, which causes food flavor reduction and natural deterioration. Cooling down the food conservation temperature can slow down the metabolism rate of food and microorganisms but is detrimental for food texture. High temperature disinfection can protect food from infection of bacteria but seriously reduce the nutrition of food. Pasteurization is a way to disinfect food at relative low temperature but only guarantees an inefficient sterilization.

NTP have exhibited its unique advantage in food conservation and food function modification. It can give a rapid food sterilization with little detrimental effect on food nutrition and flavors [38, 80-84]. This sterilization effect of NTP is associated to the strong oxidative ability of reactive chemical species produced by NTP, like radicals, ozone, and hydrogen peroxide. These species can either oxidize the cell membrane or damage the DND molecule of cell nucleus. Plasma reactive species can also indirectly induce the formation of intracellular radicals, which are more detrimental to microorganisms. Table 1.1 lists part of the works about the microbial inactivation effect of non-thermal plasma on foods.

Table 1. 1 Microbial inactivation by non-thermal atmospheric plasma

Microorganism	Substrate	Plasma source	Treatment time/min	Log reduction	Reference
S.enteritidis	Egg	DBD	90	4-5	[85]
S. aureus	Strawberry	Plasma activated water	-	2-4	[86]
E. coli	Lettuce	DBD	10	0.4-0.8	[87]
Yeast	Fruits	DBD	5	3	[88]
E. coli	Apple juice	DBD	0.4	5	[89]
E. coli	Fruits	Jet	0.4	3	[90]

The oxidative species of NTP not only have a broad and rapid bactericidal effect, but also possess a biological function; for example, NTP could improve the activities of endogenous enzymes. During a long storage, foods, especially fruits and vegetables, appear damaged because of the enzymatic browning [63]. If the activity of such kind of enzyme decreases, food then can be kept in a fresher state for a long time. In the recent work, researchers find the enzymatic activity of trypsin [91], polyphenol oxidase [92] and peroxidase [92] are inhibited when the corresponding foods are treated by NTP. The enzymes related to the NTP food preservation are increasingly becoming an effective technique which could not only preserve the food quality like color, texture and nutrient but also the safety, e.g. decontamination, microorganism inhibition and residual pesticide degradation etc.

1.2.2.2 Applications of NTP in biomedicine

1) Stomatology

NTP were first applied in dentistry for surface modification of dental implants. The modified surface shows an improved osseointegration, adhesive qualities and polymerization [67]. Applications of NTP in dentistry are further involving in microbicidal activities [31], endodontic treatment [93], periodontal regeneration [30] and tooth bleaching [94] etc. It is said that there are over 700 species of microbial coexist in human mouth and existing in a biofilm form [67]. Periodontal disease and caries that are the most common diseases are mainly caused by the bacteria living in our mouths. Since parasitic bacteria on dental tissues was found to be able to be sterilized effectively with NTP treatment, NTP have been paid more and more attention in stomatology. Until now, researchers have demonstrated that NTP have a significant biofilm removal effect like *bacillus cereus, escherichia coli,*

porphyromonas gingivalis, streptococcus mutans, enterococcus faecalis and geobacillus stearothermophilus etc [95-97]. Lu et al. found that the plasma reactive species, especially the reactive oxygen species can penetrate a 25.5 micrometers thickness of biofilm layer and kill the *E. faecalis* [98]. Miletic et al. applied NTP to treat human periodontal ligament mesenchymal stem cells and found cells migration and proliferation were inhibited but osteogenic differentiation is promoted [99].

2) Oncology

NTP have been used to treat various tumors. Currently, remarkable anticancer ability of NTP have been confirmed by dozens of *in vivo* and *ex vivo* experiments with various cancer cells including liver cancer cells, lung cancer cells, glioma cells, skin cancer, cervical cancer cells, bone cancer, myeloma cells, melanoma cells, central nervous [26, 27, 69, 73, 75, 100, 101]. Non-thermal plasma is a rich mixture and multiple ingredients of NTP have been proved to have anticancer effect. Reactive RNOS produced by NTP could induce apoptotic response of tumor cells, promote immune response of cell, stimulate angiogenesis and inactivate bacteria etc. In our group, Dr Bruno Honnorat [101] found that the hyperthermia effect produced by NTP could play an important role in anticancer. Although the specific mechanism behind the antitumor effect of NTP still remains unclear, numerous researches have proved that this physical technique could be a revolutionary tumor therapeutic method.

3) Dermatology

The skin tissue treatment with NTP is one of the most important applications of NTP in dermatology. It includes the therapies of hand and foot lice, herpes simplex, depigmentation scars [25, 102, 103], and particularly the wounded skin [104, 105]. NTP can also be used in skin care like facial skin reshaping, wrinkle removal and aged skin regeneration [106, 107]. In this section the application of NTP in healing wounded skin will be mainly discussed. The influence of NTP on the structure change of skin tissue will be introduced in the following section.

Wound healing starts from coagulation, then is followed by the process of vasoconstriction, inflammatory reaction, angiogenesis, fibroblast cells hyperplasia, and then is finished with dermal reconstruction [29]. NTP have been applied to treat

skin wound, especially for chronic wounds. Chronic, also called non-healing wounds, are the wound, which is hard to be repaired because of persistence of bacteria and biofilm formation. 20% to 50% of the chronic wound is infected with *Staphylococcus,* the most common detrimental bacteria hindering wound healing. All the wounds like diabetic foot ulcers, acne and cancerous ulcers may be chronic wound. The aim of conventional effective therapy is to remove necrotic tissue and inactivate the parasitic bacteria with antibacteria drugs. The use of NTP to treat chronic wounds is mainly based on its significant advantages in sterilization. In recent studies, the therapeutic effects of non-thermal plasma in the field of dermatology have been gradually attributed to not only the chemical activity, but also the physiological activity in the process of chronic wound healing [105, 108-110]. Researchers show that low dose of NTP treatment can induce the release of fibroblast growth factor-2 (FGF-2) [110]. It is an important signal for the growth factor of vascular endothelial and can induce the proliferation, migration and formation of endothelial cells [109]. NTP treatment has also been proved to improve the angiogenesis [104, 108]. Zhong et al. found that NTP produced by a DBD Air discharge can both induce HaCaT cells death and regulate the release of several cytokines [103].

In our group, Constance Duchesne and Nadira Frescaline applied a plasma jet to promote cutaneous healing and prevents infection in an in vivo model of third-degree burn wounds infected with S. aureus [104, 105]. She explored the effect of NTP on cellular viability, proliferation and migration of human origin cells including fibroblasts, keratinocytes, endothelial cells and monocytes in vitro, and on extracellular matrix formation and angiogenesis. She also investigated the effect of NTP on the in vivo model of third degree burn wound grafted with allogeneic skin. The major finding of her work was that NTP treatment can enhance burn wound healing and graft integration in a mouse burn wound model. The main results are that: i) NTP treatment have dose-dependent effects; ii) NTP are able to trigger key event for wound healing on a cellular level, including enhances fibroblasts and keratinocytes (KC) migration *in vitro*, upregulates collagen expression in primary fibroblasts, enhances cellular migration and extracellular matrix formation; iii) NTP enhance angiogenesis by increasing the eNOS signaling activation and upregulating pro-angiogenenic growth factors secretion of NTP-treated endothelial cells and iv) NTP significantly decrease bacteria (*S. aureus*) burden of graft and increases wound healing rate and graft integration.

1.3 Non-thermal plasma-liquid interaction

As have been discussed in the previous section, NTP have a great potential in applications in temperature-sensitive biological fields and these biological effects of NTP are strongly related the plasma reactive species. Note that, most of these biological targets are often covered by a layer of either physiological liquid or water. This liquid layer significantly affects the composition of plasma reactive species because of the plasma-liquid chemical process. This makes the studies of the plasma-liquid chemistry based on the biological applications of NTP very promising and developed quickly.

The plasma-liquid interaction is a complex physicochemical process. It involves diffusion and chemical reactions in the liquid and gas phase and at the gas-liquid interface, energy transfer etc. The main feature of this interaction is the formation of various aqueous chemical species including both long-lived and short-lived reactive nitrogen and oxygen species (RNOS). Numerous studies have shown that it is mainly those aqueous RNOS formed through the plasma-liquid interaction process that dominate the biological function of NTP on regulating those living organisms [75, 111, 112]. It is necessary to investigate this plasma-liquid interaction process in terms of diagnosing the properties of NTP in discharge with liquid, quantifying the amount of aqueous and gaseous RNOS and understanding the formation mechanism of RNOS. This will be helpful in improving the effect of NTP on biological applications. In this section, the properties of discharge with liquid in different configurations and part of the chemical reactions in this plasma-liquid interaction process will be briefly introduced.

1.3.1 Properties of discharge with liquids

Depending on the location of the NTP versus the liquid, discharges in liquids can be classified into three categories: i) direct gaseous phase discharge outside the aqueous phase, ii) multiphase discharge, iii) direct aqueous phase discharge.

1.3.1.1 Discharge above water surface

Discharges in gases and touching the water surface is the most used configuration for biomedical application. It could be DBD or plasma jet. In DBD discharges, the high voltage electrode could either be a nude metal or dielectric coated metal, and is usually fixed to the upper position of water. The region where NTP are produced changes with the position of ground electrode (Figure 1. 1).
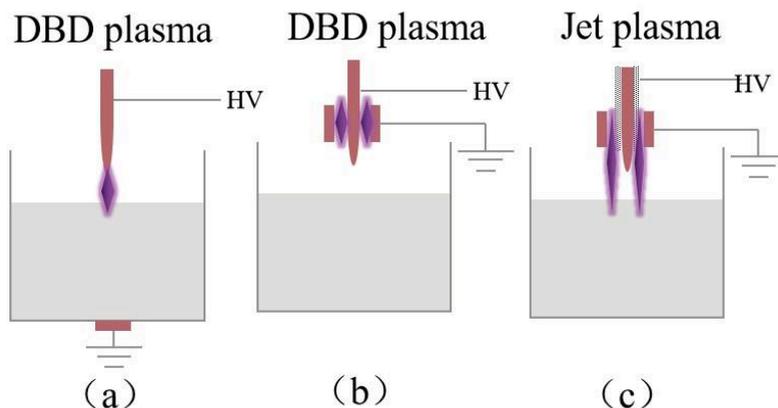
Figure 1. 1 Types of direct gaseous phase discharge outside the aqueous phase. (a) is a DBD plasma touching the water surface, (b) is a DBD plasma non-touching the water surface and (c) is a plasma jet touching water surface, the high voltage electrode is coated with dielectric. The figures are reproduced from [113]

In configuration a, the NTP are produced in the space between high voltage electrode and the water surface, and touches the water surface. On the other hand, in configuration b, the NTP are generated at some distance from the water surface and does not touch it. Only the long-lived reactive species produced by NTP can touch the water. The NTP produced in configuration c is called plasma jet. In this configuration, the high voltage electrode is often coated with a dielectric layer and the NTP can touch the water surface. Plasma jets is mostly selected for organic tissue treatments since the length of NTP formed with inert gas discharge is adjustable. It makes it possible to treat a target conveniently and safely far from the plasma source.

The NTP produced in these three configurations have a gas temperature close to room temperature, which are around 300-350K. The densities of the chemical

reactive species produced by such NTP are high, for instance concentrations of hydroxyl radical and oxygen atom, the very important biochemically active particles, are around $10^{19}m^{-3}$-$10^{21}m^{-3}$. Low gas temperature and ionization degree, and rich chemical reactive species, make NTP possible to be applied in biomedical applications.

1.3.1.2 Multiphase discharge
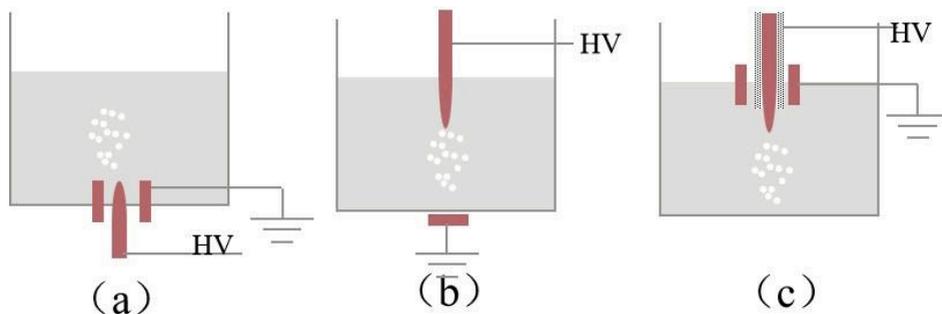
Figure 1. 2 Types of multiphase discharge. (a) is a discharge bubbling from bottom, (b) is a discharge bubbling form tap and (c) is a discharge bubbling from top but with the high electrode coated with a dielectric layer. The figures are reproduced from[113].

In order to increase the aqueous reactions of plasma reactive species with liquid and to promote the mass transfer from gaseous phase to liquid phase, multiphase discharge can be chosen. It mainly happens in bubbles or foams, or the NTP are ignited in gaseous phase but mixed with water droplets. Figure 1. 2 lists the part of common configurations of NTP sources selected for multiphase discharge. Configuration of discharge with bubbles is the usual selected one. For discharge in bubbles, a surface streamer is more inclined to be formed and propagates along the interface of gas-liquid [114]. In such streamers, temperature of electrons reaches 8-10 eV and density of electrons can be up to 10^{22} m^{-3} [115], which means liquid-gas interface is the place where NTP and large proportion of reactive species generate. Mass and thermal transfer is strengthened since most of the particles are produced close to the discharge surface.

1.3.1.3 Direct aqueous discharge

Direct discharge in water is a process in which the NTP are generated directly

inside the bulk water. In this configuration, high voltage electrode is usually immersed into water. The electrode can either be a bare metal or dielectric coated metal in a shape of plate, needle or dendritic. Discharges inside water need a much higher electric fields than discharges in gases, because of the collisions of electrons with surrounding dense water molecules. Formation and propagation of filamentary streamer inside water needs ca.1 MV/cm of electric field intensity [116]. The main properties of direct aqueous discharges are: NTP generation time is around 1-10 μs; the density of electrons is very high, which ranges from $10^{24}/m^3$ to $10^{26}/m^3$; gas temperature is more than 10 times higher than that in a DBD discharge, which is around 1000-7000 K; electron temperature is close to the one in local thermodynamic equilibrium (LTE); ionization degree of such discharge can be even up to 1; discharge current is in the amplitude of ampere and large amount of reactive species are formed [117-120].
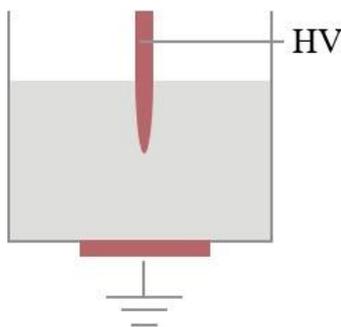
Figure 1. 3 Types of direct aqueous discharge without flow. The figures are reproduced from [113].

1.3.2 Chemical reactions in plasma-liquid interaction

Various aqueous RNOS are produced through the process of plasma-liquid interaction. Part of the aqueous RNOS like hydrogen peroxide (H_2O_2), nitrate (NO_3^-), nitric oxide (NO) and hydroxyl radical (OH radical) play crucial biological roles in the current NTP applications. The chemical reactions in this process are extremely complex. Lietz et al. simulated 1680 gaseous phase reactions and 448 liquid phase reactions, and a total of ca. 79 gaseous species and 83 aqueous species in the plasma-

liquid interaction with a GlobalKin model [121]. In this section, the transport process of RNOS produced by NTP from gaseous phase to liquid phase, and the main chemical reactions in aqueous phase will be discussed.

1.3.2.1 Transport process of RNOS from gas to liquid phase

The transport of matter is mainly due to molecular diffusion and convection. As shown in Figure 1. 4, this process includes three steps: i) the species is transferred from the gas phase to the interface of gas-liquid; ii) dissolution of the species to the interface; iii) mass transfer in the aqueous phase (the solute is transferred from the interface to the aqueous phase).
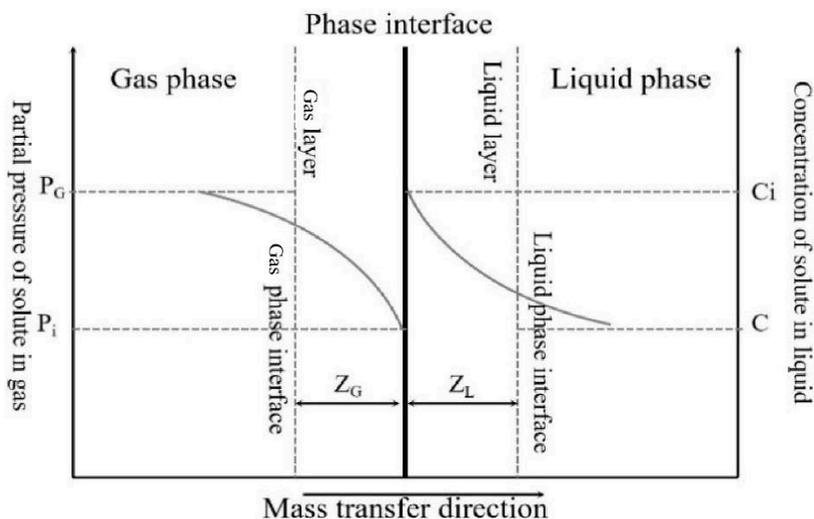
Figure 1. 4 Schematic diagram of two-phase mass transfer process. The figures are reproduced from[122].

The diffusion of NTP produced species in gaseous and interface phase follows the Fick's first law:

$$J = -D\frac{d\varphi}{dz} \qquad (1.1)$$

Where J is the diffusion flux, D is the diffusion coefficient, φ is the concentration and z is the diffusion position.

In the case of two-molecules diffusion, the rate of transfer of component A due to molecular diffusion and bulk flow can be calculated from the material balance and Fick's law. Molecular A diffusion rate equation N_A is:

$$N_A = J_A + (N_A + N_B)\frac{c_A}{c_M} \tag{1.2}$$

Where J_A is the diffusion flux of A, N_B is the diffusion rate of B, c_A is the concentration of A and c_M is the concentration of bulk flow.

Diffusion of NTP produced reactive species is equivalent to molecular diffusion model, since each concentration of them in liquid is negligible to water. In this case, Molecular A diffusion rate can be calculated by the equation:

$$N_A = \frac{D}{RTz}(P_{A1} - P_{A2}) \tag{1.3}$$

Where D is the gas diffusion coefficient, P_{A1} and P_{A2} are the partial pressure of A in different diffusion position, z is the diffusion distance, T_z is the diffusion temperature and R is the ideal gas constant. The diffusion coefficient of species is an important parameter in calculating diffusion distance of any species, e.g. electrolyte ions and molecules and nonelectrolyte molecules. In the case when the solute and solvent molecular radius ratio is greater than 5, diffusion coefficient can be roughly calculated by the equation of Stokes-Einstein:

$$D_{AB} = \frac{KT}{6\pi\mu_B r_A} \tag{1.4}$$

Where μ_B is the dynamic viscosity of fluid of solvent B and r_A is the radius of solute A.

The diffusion coefficient is a transfer property of a substance whose value is affected by temperature, pressure and mixture content. It is usually measured experimentally. Theoretically derived diffusion coefficient calculation formula can be sometimes huge different to the value measured by experiment. Generally, diffusion coefficient of gas species in gaseous phase is within the range of 10^{-6} -10^{-5} m^2/s; diffusion coefficient of electrolyte or non-electrolyte in aqueous phase is within the range of 10^{-10} -10^{-9} m^2/s. Diffusion coefficient of species in interface phase can be equivalent to gaseous phase since it is supposed that there is no resistance of mass

transfer both in liquid layer and gas layer.

NTP produced short-lived reactive species, like OH radical and NO radical, have been proved to play an important role in NTP biological application. Lifetimes of these species range from nanosecond up to micro seconds. In biological application, since the NTP treated target is often covered by a liquid layer in a thickness of micrometers to millimeters, it is necessary to clarify the diffusion distance of species with lifetime maximum to microsecond in bulk liquid phase. Rumbach et al. measured the diffusion distance of solvated OH radicals and electrons at a plasma-liquid interface and found that the distance limitation is typically in a range of 1-100 nanometers [123]. Landsay et al. claimed that aqueous OH radical and peroxynitrite (HONOO) can diffuse to a distance of 50 μm at interface phase [124]. This is the value without considering the convection.

1.3.2.2 Formation pathway of biochemical important aqueous species

1) Aqueous hydroxyl radical (OH radical)

OH radical is a highly reactive species with a 2.73 V of oxidation potential. Source of OH_{aq} radical ("aq" represents aqueous) can be either the aqueous reactions or solvation of OH_g ("g" represents gaseous) radical. Part of the aqueous reactions of OH_{aq} formations are listed in Figure 1. 5.

In this figure, OH_{aq} could be produced through the reaction of O_{aq} and HO_{2aq}, reaction of O_{aq} and H_{aq} and dissociation of water by electrons, UV, and metastable or excited state particles [125-128]. Luo et al. found the original sources of OH_{aq} mainly comes from water dissociated by electrons at high water concentration [126]. In the discharge of humid gas, it is found that density of OH_{aq} increases with the increasing of density of O_{aq} and HO_{2aq}, but the contribution of dissociation of water and combination of H_{aq} atom and O_{aq} are still the main source of OH_{aq} formation[126]. OH radical can also be directly formed by UV photolysis of water [125]. Excited nitrogen reactive species can form OH_{aq} by dissociating water molecules but in a very small proportion, according to the NIST chemical kinetics database. OH_{aq} has a short lifetime (from hundred nanoseconds to few microseconds) and can rapidly react with other species like H_{aq}, OH_{aq} and most of the organic

molecules, and can also be dissociated by electrons. Pathways of OH consumption are even more complicated in discharges of high energy density due to the complexity of water dissociation and fast aqueous reactions.
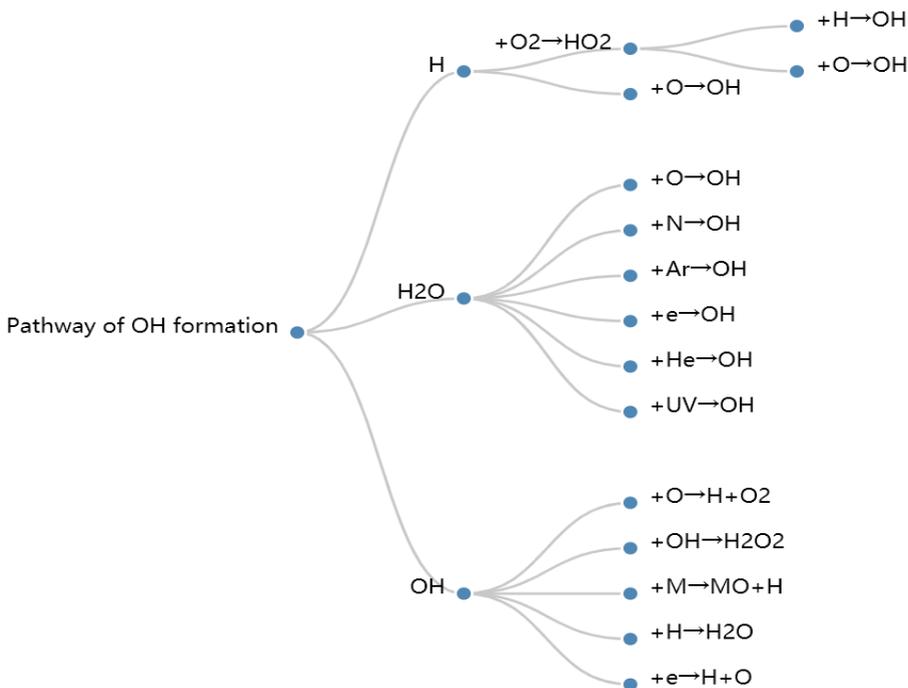
Figure 1. 5 Pathways of aqueous OH formation in discharge with water. All the species in the figure are in aqueous state. The reactive species, like O, N and other particles, could be in the forms of ions and atoms.

2) Hydrogen peroxide (H_2O_2)

H_2O_2 is an important biological reactive molecule involved in seeds dormancy breakdown, bacteria inactivation and cell oxidation stress. Chemically, H_2O_2 is a reactive oxygen non-planar species with a 1.8 V of oxidation potential. H_2O_2 exists in liquid phase with a 150.2 °C boiling point and -0.43 °C freezing point. In discharge with water, the pathways of H_2O_{2aq} formation mainly include solvation of H_2O_{2g} and various aqueous reactions [127-134], e.g. $OH_{aq}+OH_{aq}\rightarrow H_2O_{2aq}$, $HO_{2aq}+HO_{2aq}\rightarrow H_2O_{2aq}+O_2$. H_2O_{2aq} can be consumed in several ways, for example $H_2O_{2aq}+NO_2^-\rightarrow OONO^-+H_2O$. Aqueous H_2O_2 can either be formed in gaseous phase, or directly produced in the plasma-liquid interface or in liquid phase.

Takeuchi et al. studied the generation of H_2O_{2aq} and found that the production rate of H_2O_{2aq} significantly decreases when water electrode changes from cathode to anode [131]. They proposed that H_2O_{2aq} is mainly produced in gaseous phase then diffuse into bulk water. This is consistent with the work of Hefny et al. [130]. Gorbanev et al. also proved that all the detected H_2O_{2aq} are produced in gaseous phase using the methods of spin-trapping, hydrogen and oxygen isotopic labelling and electron paramagnetic resonance spectroscopy [127].

Chen et al. specially designed a helium DC discharge setup to compare the concentration of H_2O_{2aq} produced by i) dissolving gaseous phase H_2O_{2g}, or by ii) electrolyzing water or by iii) recombining OH_{aq} radicals, respectively [129]. It is found that recombination of OH_{aq} radicals is the dominating pathway of H_2O_{2aq} formation and this process mainly takes place in the water surface layer. This conclusion is similarly proved by He et al. who suggested that the H_2O_{2aq} is mainly formed through the recombination of OH_{aq} radical in plasma-water surface and water photolysis of ultraviolet and dissolution of H_2O_{2g} give no contribution to the formation of H_2O_{2aq} [135].

H_2O_{2aq} can also be produced directly inside the bulk water, but there is not a study indicating that the direct production of H_2O_{2aq} inside bulk liquid is the main source of H_2O_{2aq}.

3) Aqueous reactive nitrogen species

Aqueous reactive nitrogen species with a long lifetime are stable aqueous chemical ions and some of them are signaling molecules in biological physiological activities. For instance, NO_2^- is beneficial to trigger germination of seeds by participating in the regulation of seeds dormancy related endogenous hormone [136]. The existence form of aqueous reactive nitrogen species like $O=NOO^-$, O_2NOO^-, NO_2^- and HNO_3^-, are strongly related to the pH of liquid. In a liquid with pH larger than 6.8, these chemical species stay stable and in a state of ions. While, when pH is below 6.8, $O=NOO^-$ will be decomposed into OH_{aq} and NO_{2aq} radicals; when pH is lower than 5.9, O_2NOO^- decayed back to HO_{2aq} and O_{2aq}^- radicals; NO_2^- will mostly be transformed into NO_3^- by the reaction with H_2O_{2aq} when pH of liquid is below 3.5; when liquid is even more acidic (lower than 3.5), the reactive nitrogen species will mainly exist in the form of various radicals and nitric acid (HNO_{3aq}). In discharge

with water, reactive nitrogen species can be produced in gaseous phase, interface of gas-liquid phase and aqueous phase [119, 121, 137-140]. The aqueous reactive nitrogen species can be formed either through the aqueous reactions or from solvation of gaseous species. It is said that aqueous reactions of reactive nitrogen species formation involve 448 liquid chemical reactions [121]. Part of the related aqueous reactions are listed in Figure 1. 6.
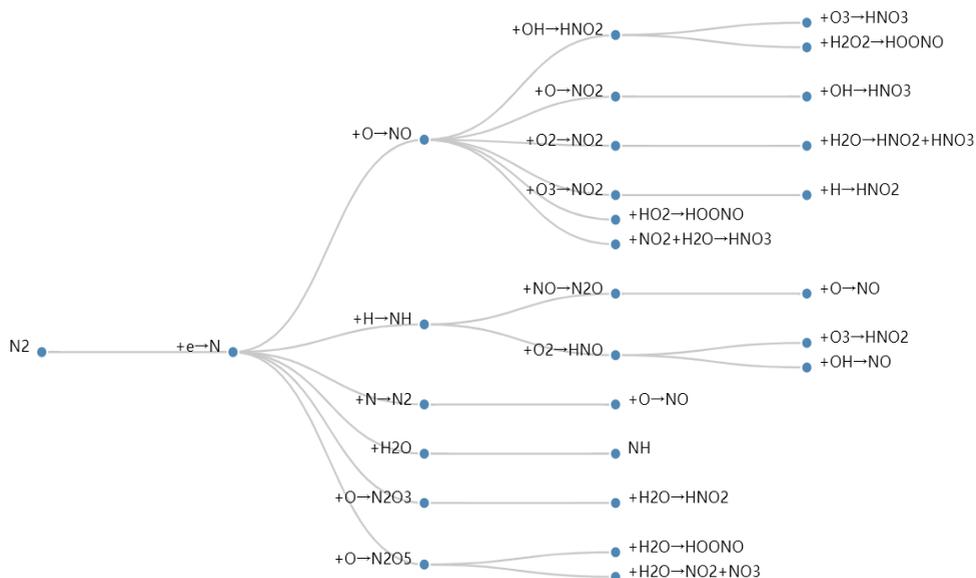
Figure 1. 6 Pathways of aqueous reactive nitrogen species formation in discharge with water. All the species in this figure are in aqueous state. The reactive species, like O, N and other particles, could be in the forms of ions and atoms.

1.4 Introduction of seed treatment with non-thermal plasmas

Food crisis in terms of shortage and safety becomes a more and more important issue to face the population growth, reduced cultivated land, abused pesticide and deteriorated eco safety in the recent years [80, 82, 84, 141]. A sustainable agriculture should answer to the food demand of the society in the present without compromising the ability of future generations to meet their own needs [142]. For this aim, the food production has undergone regulations in many areas in terms of

sustainability. It includes restricting chemical fertilizers, replacing pesticides, protecting existed arable land and improving cultivate techniques etc [84]. However, the most feasible and effective way to achieve sustainable agriculture in an economically viable way is to improve the crop production in restrained cultivable land. Seeds naturally become the most critical point, since they are of paramount importance to agriculture, conservation of plant genetic diversity and feed/food security.

Seeds germination is the most important physiological process by which a plant grows from a seed. Generally, a faster seed germination guarantee a better yield [143, 144]. Germination potential refers to the percentage of germinated seeds to the total number of seeds in the first 1/3 of the period of germination. Germination potential represents the capacity of seeds to germinate rapidly and uniformly and emerge seedlings in a wide range of adverse conditions [145, 146]. It is directly related to the plant growth, adaptation to stress and yield of crops in a large extent, and is a major trait for agriculture defined as seed vigour [147-149]. Seed vigour is the sum of seed germination and emergence rate, seedling growth potential, plant stress resistance and production potential, and is an important indicator of seed quality. Numerous works therefore have been done in improving seeds vigour, among which seed pre-sowing, also called seeds priming, has been regarded as a feasible, low risk and well-established technology [150-154]. Seed priming could lead seeds to germinate more quickly and efficiently. Currently, seeds priming has become an indispensable procedure in agriculture. More recently, NTP have shown potentialities to an innovative pre-sowing seed priming technique. The purpose of the NTP in seeds treatment is to increase the seeds germination percentage, to shorten the germination time and eventually to improve the food production. In this section, the traditional seeds priming technologies will be first discussed and the literature review about the effect of NTP on seeds germination will then be introduced in detail.

1.4.1 Traditional seed priming techniques

Traditional priming techniques include osmopriming, halopriming, hydropriming, matric priming, thermopriming, chemopriming, biopriming and physical priming like UV, ultrasound, ionizing radiation and radioisotopes etc. Next,

we will introduce the main traditional priming technologies and how priming technique works in seeds germination promotion.

1.4.1.1 Effect of priming techniques on seeds water-up in pre-germination

Seed germination is triggered by the absorption of water by the quiescent and non-dormant seeds, altogether with physiological and biochemical activities [145, 146] and terminates with the elongation of the embryonic axis and seedling growth [148, 155]. The germination related metabolism activities include reactivation of metabolism, resumption of cellular respiration, DNA and protein repair, translation and/or degradation of stored mRNAs and protein turnover [148, 149]. Priming techniques induce the trigger of specific metabolic activities of seed in advance when seeds start to absorb water [156]. Hydropriming is a process where seeds are soaked in water under optimal temperature conditions with or without aeration. One of the difficulty of this technique is to well control the water up-take to achieve uniform germination of seeds [157]. Osmopriming is a way to immerse seeds to osmotic solutions (mainly Polyethylene Glyco) at low water potential for a controlled seed water uptake [158]. Osmopriming performs a better germination promotion than hydropriming alone, but it is at a high cost and requires polluting chemicals. Water potential of the osmotic agent is a crucial parameter in osmopriming. Compared to PEG, effectiveness of less expensive alternatives like inorganic salts (e.g. NaCl, $NaNO_3$, $MnSO_4$ and KNO_3) [159], organic molecules (e.g. glycerol and $Na(C_2H_5-COO)$) [159] and even solid matrix reagents (coal, sawdust, vermiculite, calcined, kaolin, charcoal and commercial substrates such as AgroLig) [160] have been investigated. The results show that they either are less effective or can lead to an excessive hydration, which is detrimental to seeds germination. Increasing seeds hydration could also be achieved through physical techniques. In a recent work, Alberto [161] et al. claimed that the ultrasound treatment can reduce ~25% of the hydration process time of mung bean seeds and accelerate germination.

1.4.1.2 Effect of priming techniques on seeds cellular metabolisms

Germination is a very complex physiological activity, which is strongly related to endogenous seed dormancy, environmental stress and aging-related damage

during seed conservation, etc [149, 162-164]. The aim of seed dormancy is to prevent the germination of the seeds particularly when ecological conditions are unsuitable for germination [165]. Dormancy and germination are partially and mainly controlled by a dynamic balance between two antagonistic phytohormones: abscisic acid (ABA) and gibberellins (GAs) [165]. Mutants with defects in ABA and GA biosynthesis or signaling have supported direct evidence for the involvement of ABA in the acquisition and maintenance of dormancy and for GA in enhancing cell elongation leading to germination. These phytohormones act as secondary messengers in metabolism activities involved in the lessening of the dormancy and the occurrence of the germination [162, 166-168]. Biopriming is the typical priming technique performed by adding secondary metabolites, such as salicylic acid (SA), ABA or GA, in affecting seeds cellular metabolisms. Apart from biological hormones, chemical reagents can also be the signaling molecules or affect other cellular metabolism activities like enzyme performance or cellular respiration. Numerous evidences have proved that Reactive Nitrogen Species like NO and Reactive Oxygen Species like H_2O_2 are essential regulators in mediating or cooperating with the central role of classical phytohormones [136, 169-171]. Chemopriming is another commonly used technique by seed industry to increase/decrease germination rate in a relative efficient and controlled way. Currently, most of the conventional chemical or biological agents are still either too expensive or harmful to the environment and human health. Beneficial effects of UV radiation priming which has been applied as one of the physical priming techniques have been verified. Kacharava et al. exposed two varieties of kidney bean (*Phaseolus vulgaris var. oratus and var. ellipticus*), cabbage (*Brassica oleracea var. capitata and var. capitatarubra*) and beet (*Beta vulgaris, var. saccharifera and var. rubra*) seeds to UV radiation (intensities ranging from 460 to 760 mW/cm^2) and found that ABA, tocopherol and different pigments of seeds were changed [172].

1.4.1.3 Effect of priming techniques on seeds disinfection

The persistent yield reduction and safety issues in the agriculture and food sectors are mostly caused by micro-organisms such as fungal. Hence, decontamination priming technology is beneficial to improve the physicochemical and physiological properties of seeds for a food production in high quality and yield [84]. Common priming way to remove disease-causing fungi, bacteria and pests is

to adopt highly efficient pesticides, e.g. conventional disinfectants (sodium hypochlorite (NaClO) and hydrochloric acid (HCl)) [173], or fungicide-based Thiram [174]. Although chemopriming prevents seeds from damage of microorganisms, simultaneously improved the drug resistance of microorganisms. Non-chemical priming techniques like biological and physical ways also have been investigated. Beneficial microbes inoculation to seeds is proposed as a promising biopriming, which is applied to avoid of the risk of inhibitors or natural antagonistic microbes [152]. Ozone treatments can kill most of bacteria living on seeds without any environmental detrimental production. Reports about magnetic field, UV light or heavy ions radiation treatments on seeds show antibacteria property, but a slightly higher dose can change the positive effect of these priming techniques into negative or even destructive effect.

In summary, traditional priming techniques work in seeds germination promotion by either increasing seeds water uptake (e.g. Hydropriming and Osmopriming), or disinfecting seeds (e.g. chemopriming and biopriming) or regulating seeds metabolic activities (e.g. biopriming), etc. However, the conventional priming technologies still face series problems in terms of cost, efficiency and environmental protection, etc. It is found that NTP can integrate most of the advantages of the traditional priming technologies in germination promotion [175-177].

1.4.2 Seeds treatment with non-thermal plasmas

The application of plasma technology in agriculture originates from aerospace experiments. Space environment has features that are not available on Earth, such as ultra-vacuum, microgravity, high-energy particles, cosmic high-energy rays and magnetic fields. In the 1960s, former Soviet Union was the first country to carry out research on space mutation breeding. So far, United States, Europe, Russia, Japan, Canada and China etc have conducted space breeding experiments on dozens of crop varieties. Air-dried seeds were first used as research objects to study the effects of space environment on plant growth and development. For instance, in 1984, the Space Shuttle Challenger placed an additional portion of seeds in the board for an exposure of plasma and cosmic radiation in space for years. Upon the return of space

to earth for planting, an faster germination rate of these space-exposed seeds was successfully conducted thanks to the strong vitality and stress resistance in space [178]. Based on their early successful space experiments, the former Soviet Union started to simulate space environment by developing a high-voltage arc plasma reactor combined with an alternating electromagnetic field for seeds treatments in a microgravity condition during the free-falling movement [158]. Seeds were located inside the plasma space where a large amount of short ultraviolet light, charged particles, ozone and electromagnetic field and obtained a higher germination percentage and yield [158]. Since then, in the late of 1990s, numerous researchers from all over the world followed with this ground breaking work both in academic and engineer field till now.

As stated before, non-thermal plasma is a multi-component system containing charged particles (electrons, negative and positive ions), excited species, e.g. atoms and molecules (O_3 and H_2O_2), radicals ($^{\cdot}OH$ and $O_2^{\cdot-}$), electric field and UV photons. Some of the ingredients of NTP have been proved having the ability to regulate seeds hydration behavior and cellular metabolisms, and to disinfect microorganism, etc [175, 177, 179-182]. In the last twenty years, a large amount of NTP seeds treatments has shown competitive advantages of NTP on enhancing seeds germination potential, seedling resistances and yield in a low cost, rapid, simplicity, environmentally friendly way. Based on the configurations of gas discharge, seeds treatments are mainly divided into two models, which are NTP dry treatment and NTP wet treatment. NTP dry treatment is treating dry seeds directly during the discharge. The NTP wet treatment is to treat seeds in water or wet seeds directly during the discharge, which is called direct NTP wet treatment, or to treated seeds only the plasma activated water, which is called indirect plasma wet treatment. Following is the introduction of seeds treatment both with NTP dry and wet treatments.

1.4.3 NTP dry seed treatments

1.4.3.1 Plasma sources

NTP used to treat seeds vary with the plasma source, the working gas, the discharge pressure etc… The frequency of the input voltage can range from low

frequency 50-60 Hz to radio frequency and can work in AC or in pulsed mode. Discharge gas can be Air, Ar, O_2 and N_2 or a gas mixture. The selected NTP for seeds treatment can be formed in low pressure and atmospheric pressure. Geometries of plasma reactor are closely related to the efficiency of seeds treatment. Geometries of plasma reactor generally are designed to produce NTP with a large surface. The size of the NTP depends on the quantity of the seeds to be treated. Electrodes can be a plate-plate structure or a multiple needle in parallel structure.

1) Plate-plate electrode
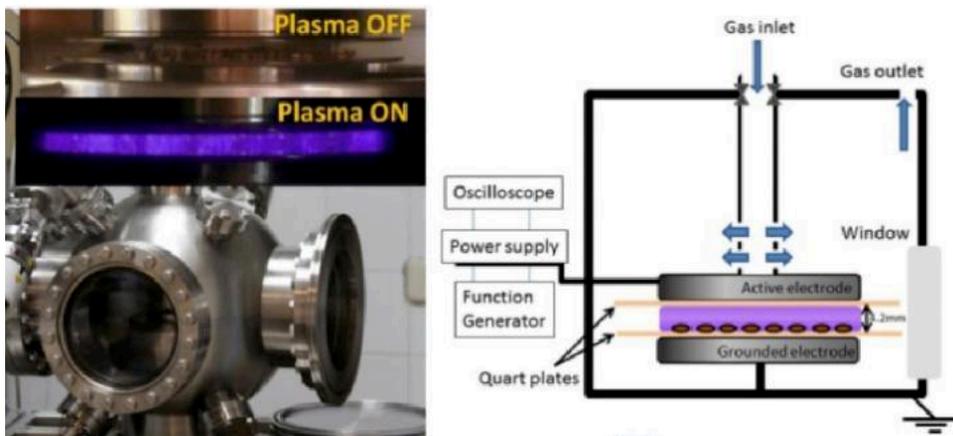
Figure 1. 7 DBD plasma reactor setups and electrical and operational schemes. Diameter of metal electrodes are 8 cm, dielectric disc one is 10 cm. Frequency and the voltage amplitude of the input signal are maintained constant at 1 kHz and 8.2 kV, respectively. Under these conditions the current is around 7 mA and consumed power is in the order of 6.4 W [182].

Discharge conditions of plasma reactor with plane electrodes usually select inner gas and low pressure. For discharge at an atmospheric pressure, the space between two planar electrodes is usually small and the formed NTP can be transformed into a hot arc plasma easily. Coating a dielectric on the plate electrode is a way to avoid this transform. However, sustaining a stable and uniform NTP is a challenge. Figure 1. 7 shows one of the plasma reactors with plate-plate electrode for seeds treatment. In the work of Gómez-Ramírez et al., Quinoa seeds are treated by an Air DBD plasma at a pressure of 500 mbar [182]. In this plasma reactor, two parallel-plate circular metal are used as electrodes and the gap electrodes is 4.2 mm. Continuous

NTP will be produced in the space of two electrodes where seeds will be placed. Mildaziene et al. used a 5.4 MHz RF plasma reactor which has a similar planar geometry and performs in Air at a pressure of 1.68 mbar to keep the NTP temperature low. The power density of this RF plasma is ca. 0.68 W/cm^2 [181].

2) Multiple needle array discharge structure

In order to keep the temperature of the plasma produced by a reactor with a plate-plate structure low, a low working pressure or a small gap between two plate electrodes are often selected. This make the structure of plasma reactor complicate and restrict the amount of plasma treated seeds (Treatment capability of NTP). Replacing the powered plate electrode with parallel array needle electrode can greatly reduce the engineer difficulty of setup and can easily produce the NTP with large discharge surface. plasma setup geometry in multiple needles structure is flexible. Treatment capability is dependent to the number of needle electrode. In the current related works, parallel array multi-needle electrode structure is most developed and applied for seeds treatments.
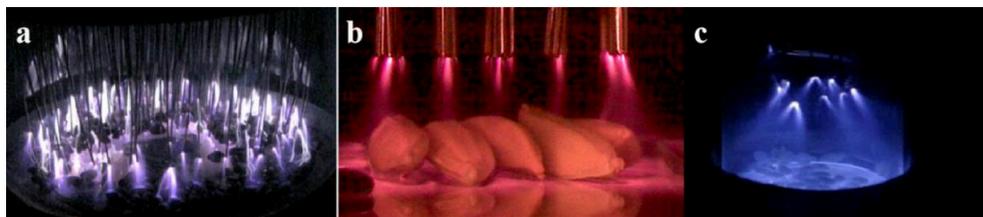
Figure 1. 8 Photos of various plasma source. a is a DBD discharge working in atmospheric pressure. The chamber is a 5 L borosilicate glass cylinder. 100 needle electrodes are installed inside and connected to an AC power supply. 1 kHz sine wave with high voltage of 38 kVpp for Air discharge and 11 kVpp for argon. NTP treatment time ranges from 30 s to 5 min under 100 sccm of gas flow rate. The gap between the needle tips and chamber bottom is around 13 mm [175]. b is an atmospheric hybrid corona discharge plasma (HCP). Conditions: DC High voltage was ∼ 14 kVpp, frequency is ∼700 Hz). HCP was obtained in atmospheric-Air ambient conditions. The measured power of operation was ∼4.8 W with a gap distance of ∼7 mm (An array of the tips was designed with 10×10 twin-tip electrodes covering an area of ∼4 cm^2) [177]. c is cotton seeds treatment under a DBD discharge [183]. The discharge voltage applies 32 kV at 1KHz [183].

Figure 1. 8 shows some photos of plasma reactor in parallel array multi-needle electrode structure. Gerard et al. investigated the effect of a DBD plasma on alleviating dormancy of cotton seeds by a home-made NTP array reactor under

atmospheric pressure (Figure 1. 8a) [175]. This reactor can treat approximately 350 cotton seeds per time. Figure 1. 8b is a plasma setup with a similar configuration to the plasma setup shown in Figure 1. 8a. It works in an open environment and cold NTP is generated by the ionization of ambient Air. With this plasma setup, Khamsen et al. enhanced the surface wettability of rice (*Oryza sativa L.*) seeds [177] and sunflower seeds [177, 180], and improved the final germination percentage. Plasma reactors with similar structure to the one shown in Figure 1. 8c has applied to treat other type of seeds. Saberi et al. treated wheat seeds (*Triticum aestivum L.*) by a radiofrequency (RF) plasma reactor operated with Air at 13.56 MHz [184]; Zhou et al. treated tomato seeds by DBD plasma at an atmospheric pressure (4.7-6.8 kV and 8-30 kHz) [185]; Dobrin et al. treated wheat seeds with a DBD discharge at an atmospheric pressure (15 kV, 50 Hz, 2.4 W) [186].

1.4.3.2 Effects of NTP treatments on seeds germination

Positive effect of NTP on seeds germination can be roughly attributed to the reasons summarized below:

1) Disinfection effect of NTP

Microorganism contamination of seeds is a key point, which determines the germination quality. NTP can inactivate pathogenic fungi and other microorganisms living on seeds coat, which keeps seeds safe and healthy [177, 187-189]. For instance, treating the soybean seeds infected with *Diaporthe/Phomopsis* by a DBD plasma significantly decrease the infection of soybean seeds [189]. How NTP inactivates bacteria?

i) Chemical sterilization of NTP

NO$_2$ produced by Air discharges is a well-known and broad range sterilant. It has been widely applied in disinfection of common bacteria, viruses, and spores. Even at a small concentration, NO$_2$ can degrade DNA in the spore core through nitration of the phosphate backbone [190]. Reactive oxygen species produced by NTP, e.g. H$_2$O$_2$ (E=1.776 vs SHE), singlet O (E=1.88 vs SHE), O$_3$ (E=2.076 vs SHE), OH radical (E=2.8 vs SHE) and various excited species, are

also known for inactivate microorganism because of their strong oxidative ability. Among them, H_2O_2 has been well widely used in medical sterilization, which enables to destroy 35%- 90% of pathogens in a short cycle time.

ii) Physical sterilization of NTP

The strong electromagnetic field produced by discharge can break cellular membrane, destroy internal molecular structures and cause cell dying by changing the electrostatic polarization of the microorganism [191]. UV light has the ability inhibiting bacteria replication by breaking organic biological macromolecular chain. Heat produced by the NTP could also inactivate microorganism by pyrolyzing DNA or RNA.

2) Seeds surface modification

Germination starts from water uptake. Thus, the capability of water absorption strongly affects the germination of seeds. Generally, increasing the seeds hydration is beneficial to break seeds dormancy and trigger biological metabolisms in advance. As mentioned before, the hydration promotion of seeds can be achieved via various priming techniques. The effects of NTP treatment on promoting water uptake largely depend on the modified coat surface of treated seeds. Seed coat is composed by a layer of polymer fibers, which may be etched or oxidized by reactive particles formed by NTP. So, how NTP treatments modify the surface of seeds coat and what is the relation between the modified surface and germination?

i) Seeds coat physical modification

The initial seed coat is usually smooth and often covered with a wax layer. Coat of seeds treated by NTP would become rough. It is the result of destruction of coated wax layer or even cellulose. The roughness of the seed coat is closely related to its water absorption capacity. Contact angle of seeds coat is an index of quantitative characterization of the wettability. The smaller the contact angle, the easier the water is to cover the surface of the seed coat (the better the wettability of seed coat). Khamsen et al. measured the contact angle of rice seeds treated by NTPand found the treated rice seeds coat shows an unobservable contact angle ($\sim 0°$), as shown in Figure 1. 9 [177]. It indicates that NTP treatments change the seeds coat from a hydrophobic interface (non-treated) to

a super-hydrophilic interface (treated-Air/Ar). The duration of water-uptake of seeds treated by NTP decrease to ∼1 min from initially ∼30 min and the accelerated seeds hydration promote the germination of rice seeds. Similar results have been found in seeds of *Mimosa caesalpiniafolia benth* [192], *Erythrina velutina [33]*, *oilseed rape [60]*, soybean (*Glycine max L. Merr cv. Zhongdou 40*) [193], wheat [194] and mung bean [195]. Researchers attribute the seed coat physical modification to the etching effect of those NTP reactive particles, e.g. electrons, atoms and radicals. Khamsen et al. considered ROS, mainly OH and O radicals, are the key particles that are responsible to the rice coat hydrophilic modification [177]. Pawlat et al. claimed reactive species e.g. NO_2, NO and O_3, produced by an Air NTP at an atmospheric pressure can sharpen the pattern structure of the upper epidermal layer of Thuringian Mallow (*Lavatera thuringiaca L.*) seed coat [196]. Dubinov et al. found that the UV light generated by NTP cause cracks on seeds coat and proposed it is the modified seeds coat that increases the germination rate of Altaic flax seeds (*Linum altaicum)* [197].

Figure 1. 9 Photos of contact angle of rice seeds[177]

ii) Chemical modification of seeds coat

Seeds coat modification can be a chemical process [34]. ROS generated by NTP, especially OH radicals, can decompose the organic polymer molecules of seeds coat through an oxidation process. The chemical composition and even chemical structure of the organic molecules of seeds coat then will be modified by the NTP treatment. Gómez et al. investigated chemical composition changes of the surface of Quinoa seed coat treated by a DBD and a RF plasma using X-ray photoemission spectroscopy (XPS) [182]. They found that the oxygen content of the outer parts of the treated dry quinoa seed was 2~3 times higher than non-treated seeds and the O is existed in the form of C-OH functional

groups which is a hydrophilic group. This makes the hydrophilic property of treated surface increased. Wang et al. observed the similar result by measuring infrared absorption of the surface of cotton seeds treated by NTP using FITR [198].

3) Metabolism activities regulation

NTP interaction with germination is a complex process, which not only involves physical and chemical modification of seeds, but also physiological activity regulation. Researchers have found that the NTP can significantly influence seeds cellular metabolisms [199-202].

i) Direct effect of NTP treatment on seeds cellular metabolism regulation

Direct effect of NTP on metabolisms is the effect directly provoked by NTP component like RNOS, UV light or electric field etc.

NTP can directly affect germination by generating to an oxidative stress. ROS deposited on the seeds surface or penetrating inside the seeds can directly induce an oxidation of seeds cell membrane lipid [189], and modify the normal redox state of seeds cells causing an oxidization stress [60, 162, 166, 167, 176, 200-203]. Although ROS, especially radicals, may cause damages to seeds cell, e.g. triggering a lipid peroxidation chain reaction or damaging migration of cell, etc. they also facilitate germination [204, 205]. Oxidative stress of ROS to seeds cell can induce the formation of intracellular superoxide radical, which stimulates cells to activate superoxide radical deuterase to scavenge the extra radicals. Normal cells also have another scavenge system to protect them avoid the damage from radicals. It is the seed storage proteins (SSPs). Researchers have proved SSPs can be largely oxidized by ROS produced by NTP [206, 207]. The abundant amount of SSPs makes it acting as an efficient ROS scavenger before transforming the radicals into other safe molecular by intracellular antioxidase of seeds cell. However, the oxidation of SSPs on the other hand promotes structural denaturation and proteolysis of proteins, which facilitates germination [206, 207].

Electromagnetic field formed by NTP can directly affect water structure of seeds cell [208-211]. Isobe et al. claimed that the water structure of morning

glory seed cell was greatly affected by a treatment of DC electric field (500 kV/m) based on the observation of relaxation time of water measured by H-NMR [212]. Zhao et al. suggested that electrostatic field priming can instantly increase onion (Allium cepa) seeds vigour and then accelerate germination, though the effects are short-lived [209]. Leong et al. reported that the treatment of pulsed electric field (PEF) (0.5–2 kV/cm) changed the levels of bioactive compounds and antioxidant enzyme activities in the shoots of wheatgrass seeds (*Triticum aestivum L.*) [211].

ii) Indirect effect of NTP on seeds cellular metabolism regulation

NTP can indirectly affect seeds dormancy by regulating cell endogenous hormones. Seeds dormancy blocks germination metabolisms, which is regulated by the phytohormones of abscisic acid (ABA), gibberellins (GA) and ethylene as described before. The endogenous phytohormone of the seed can be synthesized by selectively oxidizing the protein and mRNA or interacting with NO. Researchers have demonstrated that ROS can affect the synthesis of phytohormone [165, 169, 213]. ROS are capable of interacting with nucleic acids, proteins, DNA, and lipids since they can easily diffuse and penetrate into intracellular through membranes [165, 169]. The suitable interaction of ROS with proteins or lipids can release an oxidative signaling which could breaks seed dormancy and promotes seeds vigour [213].

NTP can improve the drought resistance of seeds indirectly by strengthening enzymes performance and increasing cell membranes permeability. Under a drought stress, the drought resistance of dry rape seed has been improved by a RF plasma treatment [60]. Researchers found that NTP treatment improves the antioxidant enzymes activities, e.g. superoxidase (SOD), peroxidase (POD) and catalase (CAT), and reduce the lipid peroxidation. Similar studies have been carried out by other researchers. Ling et al. claimed that RF plasma raised superoxide dismutase (SOD) concentration and catalase activities of oilseed rape seed [60]. Piza et al. suggested that NTP showed a significant decrease of lipid peroxidation of infected soybean seeds [189].

NTP can indirectly stimulate germination by inducing genetic variations. Zhang et al. reported that the germination and sprout growth of soybean seed are

promoted by an argon NTP and it is attributed to the enhancement of adenosine triphosphate (ATP) concentrations [176]. Authors found that the expression of alpha genes of ATP synthase subunit is affected by NTP treatment. ATP a1, ATP a2, ATP b1, ATP b2, ATP b3, target of rapamycin (TOR), growth-regulating factor (GRF) 1-6 are up-regulated and ATP MI25 mRNA expression is down-regulated [176].

1.4.4 NTP wet seed treatments

Although energy of NTP can accelerate the seeds germination either through strengthening the performance of metabolism activities or modifying the morphology of seeds coat in micro-nanoscale, direct NTP dry treatments may easily damage seeds under a higher NTP treatment dose. Ji [199] et al claimed that germination of *Coriandum sativum* seeds was strongly influenced by the transferred energy from NTP to seeds. This positive effect is proportionally enhanced with the increasing of transferred energy dose, till to the threshold energy over 0.65 J/seed. In direct NTP dry treatment, the density of reactive species interacting with seeds coat surface may be is high generating damages from excessive reactive species. Excessive reactive species can rapidly damage the cellular tissue, protein and even DNA of seeds cells and even lead to the death of the whole seeds by cleaving molecular bonds directly. Optimizing the dose of NTP treatment energy by adjusting discharge conditions like input voltage and treatment time is necessary. However, treating seeds in water by NTP can largely avoid seed damage caused by excessive treatments. Since the water layer covering seeds acts as a medium that blocks excessive reactive species depositing on seeds coat and transfers NTP energy to seeds uniformly. Besides, the plasma-water interaction produce large amount of aqueous chemical species, which have been proved to have a significant positive influence on seeds germination promotion [62, 214, 215]. Hence, NTP wet treatment, based on the plasma-liquid chemistry is very promising and develops quickly. NTP wet treatment aims at treating seeds in water or wet seeds directly during the discharge, which is called direct NTP wet treatment, or to treated seeds only the plasma activated water, which is called indirect plasma wet treatment.

1.4.4.1 NTP sources used in NTP wet treatments

A large variety of reactors used for seeds wet treatment have published so far. In many cases their structure is similar with the ones used in plasma-liquid interaction, including discharge in the gas phase above water surface [62, 214, 215], discharge in vertical water filming [35], discharge in bubbles [195], discharge in liquid sprays and discharge in foams [36].
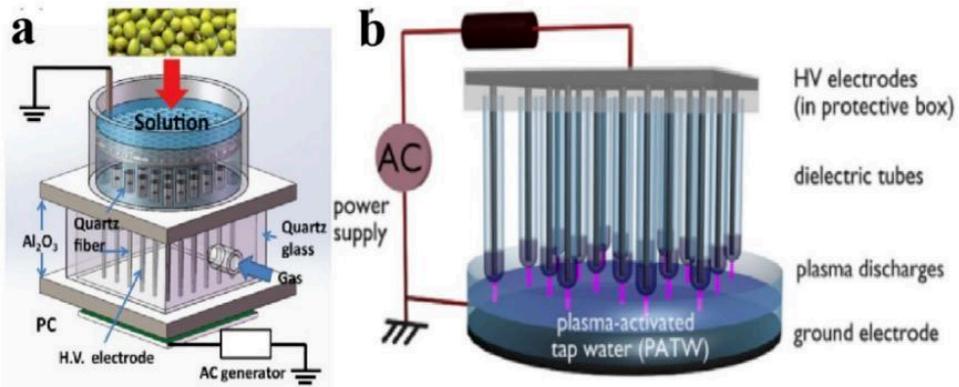
Figure 1. 10 The schematic diagram of the direct wet treatment on mung bean seeds using a microplasma arrays plasma source (a) and the activation of tap water using a multi-neddle electrode plasma source (b). Conditions: Sub figure a composes 36 microplasma jet units, feeding gases are He, N_2, artificial Air ('Air'), and O_2, flow rate is 2.0 standard liter per minute (SLM). Input voltage is bipolar AC with the peak voltage (VP) of 4.5 kV at an AC frequency of 9.0 kHz. The discharge power is 25 W. 100 uniform mung bean seeds are overspread on a filter screen which is placed 1 cm above the microplasma jet units. Treatment time is 10 min [195]. Sub figure b is composed with a matrix of 4*4 metal rods that are embedded in dielectric tubes and fixed with 4 mm distance to water surface. Output voltage is 12 kV_{AC} at 500 Hz, volume of tap water is 50 mL [62].

plasma reactor shown in Figure 1. 10a is a direct NTP wet treatment. Aqueous plasma reactive species generated by discharge in bubbles diffuse to the filter screen where seeds are overspread. In such configuration, all seeds are not only well contacted with aqueous plasma reactive species, but protected by water layer from the damages of high energy particles like electrons, radicals. Plasma reactor shown in Figure 1. 10b can produce the NTP touching the water surface and activating water. This plasma activated water, rich in various reactive species, is then used to water the seeds.

1.4.4.2 Mechanisms of NTP treatment on wet seeds

Plasma-liquid interaction can convert a fraction of the NTP energy into aqueous RNOS. It is often considered that NTP wet treatment is mostly an interaction process of aqueous chemical reactive species and seeds. Mechanisms of NTP wet treatment could be summarized as:

1) Disinfection effect of NTP

Aqueous reactive species include both long-lived species and short-lived species. Researches show that the plasma activated water has a bactericidal effect [35, 37, 82, 216, 217].

i) Long-lived RNOS

Long-lived reactive species are mainly the chemical stable substances like H_2O_2, NO_2^-, $ONOO^-$, NO_3^- and O_3, etc. Aqueous reactive nitrogen species, e.g. NO_2^-, $ONOO^-$ and NO_3^-, can acidify the NTP treated water. The acidified water has been proved to kill bacteria [35, 37, 82]. For instance, in the work of Oehmigen et al., bacteria of *Escherichia coli* and S*taphylococcus aureus* (10^6-10^8 cfu/mL) are completely inactivated by a DBD plasma, which is attributed to the acidification effect of NTP treated water [37]. Aqueous reactive oxygen species, e.g. H_2O_2 and O_3, are also proved have strong sterilization effect because of the oxidizing ability [35, 82, 195, 217].

ii) Short-lived RNOS

Short-lived reactive species, especially OH radical, have been widely proven to have a disinfecting effect. The bacteria inactivation effect of aqueous short-lived species largely depends on the density of species diffused to the seeds. As described in section 1.2, in the discharge where NTP is produced above water surface and touching the water surface, short-lived reactive species are mostly produced in gas phase and/or gas-liquid interface layer. Source of aqueous short-lived reactive species is the solvation of gaseous species and/or aqueous reactions like dissociation of water. Although a theoretical diffusion length of aqueous short-lived species in bulk water is only in the range of hundred nanometers to few micrometers, this diffusion can be significantly changed by the motion of fluid when there is a gas flow during discharge. Penetration

distance of the aqueous short-lived species can be up to several millimeters or even more. Hence, aqueous short-lived species can potentially have the disinfection effect.

2) Seeds surface modification

Unlike NTP dry treatment, the density of energetic particles like electrons or ions the surface of seeds coat in NTP wet treatment is negligible. However, it was reported that seeds coat is slightly modified [195]. Zhou et al. found that hydrophilicity of mung bean *(Vigna radiata L)* treated by an Air bubbles DBD microplasma (9kHz) is enhanced, which is attributed to the modification of seeds coat by aqueous ROS [195].

3) Metabolisms regulation of NTP

Similar to what has been reported in the case of dry treatment, long-lived and short-lived aqueous RNOS produced by NTP have been proved to play an important role in affecting metabolism activities of germination in the case of wet treatment [168, 170, 171, 218-220]. RNOS can break seed dormancy and regulate other metabolism activities by affecting endogenous hormones [168, 171, 219, 220]. Seeds can absorb RNS to produce NO through enzymatic conversion of nitrate reductase in seed cells. NO is an essential and important regulator in various physiological activities of germination. For instance, NO can break seeds dormancy by regulating the release of ABA, ethylene and GA [170, 218]. ROS can also break seed dormancy by affecting the performance of NADPH oxidase [221, 222]. H_2O_2 is another important secondary messenger of metabolism activity and it could interact with NO to regulate the endogenous phytohormones synthesis. Exogenously supplied H_2O_2 could regulate physiological activities. Puač et al. reported that the presence of H_2O_2 in the NTP treated water could activate the catalase (CAT) genes to synthesize enzyme, which leads to enhancement of germination of *paulownia tomentosa* seeds [223].

1.4.5 Summary of seeds treatment with NTP

Seeds treatments with NTP can be mainly divided into NTP dry treatments and NTP wet treatments. Although numerous researches have proved that NTP being one

of the seeds priming technologies can significantly promoting seeds germination, clarifying the plasma-germination interaction process is still a challenge. Currently, researchers mainly attribute to the effect of NTP on seeds germination promotion to the modification of seeds coat surface, disinfection of seeds and regulation of the germination metabolic process, etc. The effect of NTP on germination stimulation is strongly related to the seed types, plasma reactive species, electromagnetic field, NTP sources and NTP treatment dose, etc. It is of great significance to find out the dominant plasma parameters in exploring the mechanisms of germination promotion with NTP.

1.5 Introduction of Mueller polarimetric imaging and its potential application in skin treatment with non-thermal plasmas

In the field of dermatology, NTP have been used to treat skin with the aims of healing skin wound, curing skin diseases and regenerating skin, etc. Generally, for tumor reduction, relatively high doses (the dose here can be plasma discharge power or plasmas treatment time) of NTP are delivered which may damage tissues intentionally or not. On the other hand, the use of NTP for dermatology and cosmetology is increasing for healing skin wound, curing skin diseases, and caring skin health, etc… Here again, NTP, on one hand, can either inactivate bacteria or improve tissue repair, but on the other hand, can also be detrimental to the skin structure, depending the NTP treatment dose. The effect of NTP dose on dermatology can not only be indicated with cell activity, cell quantity and immunological activity, but also characterized with tissue structures. The structure of the skin tissues can be affected by NTP treatments [25, 224-228]. Hence, the characterization of modification of microstructure of skin tissue treated by NTP treatment can be valuable to indicate the effect of NTP treatment. Mueller polarimetric imaging (MPI) is one of the optical polarimetric imaging technologies enabling the observation of the polarization characteristics of the biological tissues, which has been widely applied in surgery, diagnosis of pathological cancerous organ tissues and diagnosis of diseased skin [229-232]. In this section, the principle of MPI and the its potentiality in characterizing the structure of skin tissue modified with NTP treatment will be briefly introduced.

1.5.1 Mueller polarimetric imaging

MPI is a powerful technique enabling to detect the changes of optical properties of mediums by calculating mathematically the Mueller matrices of mediums. Depolarization (Δ), linear retardance (δ) and orientation of eigenvalue axis (α) are the most analyzed polarimetric parameters of the Mueller matrices of biological mediums.

1.5.1.1 Polarization

Polarization is an inherent property of light. Polarized light means that the direction of vibration of the light vector (the electric field of the light wave) and the direction of propagation of the light wave are perpendicular to each other. Generally, the interaction of light and mediums can change the polarization state of light mainly through the independent process of scattering, birefringence and dichroic absorption. When polarized light scatters and propagates in mediums, photons that undergo little or no scattering retain their original polarization characteristics, while those that are scattered multiple times lose their polarization characteristics and become disordered. Polarization imaging preserves the signals from the subsurface scattering of mediums and the few scattered photons, while removes signals from multiple scattered photons deep in the tissue, thereby increases the contrast of tissue superficial imaging.

The Stokes vector is one of the methods to characterize the polarization state. It can be used to describe a fully polarized light, a partially polarized light and a completely unpolarized light. As shown in Equation 1.5, Stokes vector includes four measurable light intensities. I represents the total intensity of the light wave. Q represents the light intensity difference between the linear polarization component of the light wave of X direction and Y direction. U is the light intensity difference between the linear polarization component of the light wave of 45^0 direction and -45^0 direction. V is the light intensity difference between the right-handed polarized light and the left-handed polarized light.

$$S = \begin{bmatrix} I \\ Q \\ U \\ V \end{bmatrix} = \begin{bmatrix} I_H + I_V \\ I_H - I_V \\ 2I_{45^0} - (I_H + I_V) \\ 2I_R - (I_H + I_V) \end{bmatrix} \qquad (1.5)$$

1.5.2 Interpretation of Mueller matrices

With the mathematical quantitative calculations, the effect of the medium on incident polarized light is usually equivalent to a linear "transformation" matrix, that is a Mueller matrix. The Mueller matrix is a matrix of four rows and four columns (Equation 1.6), which is suitable for the case where the Stokes parameter represents polarized light.

$$A = \begin{bmatrix} M_{11} & M_{12} & M_{21} & M_{14} \\ M_{21} & M_{22} & M_{23} & M_{24} \\ M_{31} & M_{32} & M_{33} & M_{34} \\ M_{41} & M_{42} & M_{43} & M_{44} \end{bmatrix} \qquad (1.6)$$

A Mueller matrix of the target can be applied to connect the Stokes vector of the incident light and reflected light (Equation 1.7). It is a transfer function of Stokes vectors and can characterize comprehensively the polarization properties of mediums interacting with light. The Mueller matrix expression of the mediums can be conveniently calculated by measuring the Stokes parameters of incident light and reflected light.

$$\begin{bmatrix} I' \\ Q' \\ U' \\ V' \end{bmatrix} = \begin{bmatrix} M_{11} & M_{12} & M_{21} & M_{14} \\ M_{21} & M_{22} & M_{23} & M_{24} \\ M_{31} & M_{32} & M_{33} & M_{34} \\ M_{41} & M_{42} & M_{43} & M_{44} \end{bmatrix} \begin{bmatrix} I \\ Q \\ U \\ V \end{bmatrix} \qquad (1.7)$$

1.5.3 Mueller matrix decomposition parameters

The Mueller matrix includes all the polarization information of the medium, but the 16 elements of the Mueller matrix have no clear physical meaning. The Mueller Matrix Polar Decomposition (MMPD) is method for analyzing the Mueller matrix of the medium. In this study, Lu-Chipman algorithm is applied for MMPD [233]. This method decomposes the Mueller matrix of mediums into the product form of

three basic matrices, that is $M = M_R \cdot M_\Delta \cdot M_D$. These three matrices are used to describe the influences of the medium on the polarization state of light. By mathematically calculating the Mueller matrix of the medium, we can get the polarization states of light like scattering depolarization, phase delay, linear phase delay and optical rotation, etc. The following is a brief introduction to the mathematical processing of MMPD.

Suppose M is the Mueller matrix of the medium. Firstly, normalizing each element of M with M11,

$$M = M_{11}\begin{bmatrix} 1 & M_{12} & M_{13} & M_{14} \\ M_{21} & M_{22} & M_{23} & M_{24} \\ M_{31} & M_{32} & M_{33} & M_{34} \\ M_{41} & M_{42} & M_{43} & M_{44} \end{bmatrix} = M_{11}\begin{bmatrix} 1 & \vec{D}^T \\ \vec{P} & m \end{bmatrix} \tag{1.8}$$

Secondly, representing the decomposed matrices by the metrices below

$$M_R = \begin{bmatrix} 1 & \vec{D}^T \\ \vec{0} & m_R \end{bmatrix}, \ M_\Delta = \begin{bmatrix} 1 & \vec{0}^T \\ \vec{P_\Delta} & m_\Delta \end{bmatrix}, \ M_D = \begin{bmatrix} 1 & \vec{0}^T \\ \vec{D} & m_D \end{bmatrix} \tag{1.9}$$

Thirdly, obtaining the M_D according to equation 1.4 and equation 1.5, which is shown below

$$\begin{cases} D = \sqrt{M_{12}^2 + M_{13}^2 + M_{14}^2} \quad (0 \leq D \leq 1) \\ \vec{D} = [M_{12} \quad M_{13} \quad M_{14}]^T \\ m_D = \vec{D}\vec{D}^T(1 - \sqrt{1 - D^2}) + I\sqrt{1 - D^2} \end{cases} \tag{1.10}$$

Since,

$$M_\Delta M_R = MM_D^{-1} = \begin{bmatrix} 1 & \vec{0}^T \\ \vec{0} & m_R \end{bmatrix}\begin{bmatrix} 1 & \vec{0}^T \\ \vec{P_\Delta} & m_\Delta \end{bmatrix} = \begin{bmatrix} 1 & \vec{0}^T \\ \vec{P_\Delta} & m_R m_\Delta \end{bmatrix} = \begin{bmatrix} 1 & \vec{0}^T \\ \vec{P_\Delta} & m' \end{bmatrix} \tag{1.11}$$

Then M_Δ is obtained, as shown below

$$\begin{cases} \vec{P_\Delta} = \frac{\vec{P} - m\vec{D}}{1 - D^2} \\ m_\Delta = \pm[m'(m')^T + (\sqrt{\lambda_1\lambda_2} + \sqrt{\lambda_2\lambda_3} + \sqrt{\lambda_3\lambda_1})I]^{-1} \times [(\sqrt{\lambda_1} + \sqrt{\lambda_2} + \sqrt{\lambda_3})m'(m')^T + \sqrt{\lambda_1\lambda_2\lambda_3}I] \end{cases} \tag{1.12}$$

Where $\lambda_1\lambda_2\lambda_3$ is the eigenvalue of the matrix $m'(m')^T$.

Lastly, M_R can be obtained through $m_R = m_\Delta^{-1}m'$. M_R can also be represented in the product of linear phase delay matrix and optical matrix, as shown below:

$$M_R = \begin{bmatrix} 1 & 0 & 0 & 0 \\ 0 & cos^2 2\theta + sin^2 2\theta cos\delta & sin2\theta cos2\theta(1-cos\delta) & -sin2\theta sin\delta \\ 0 & sin2\theta cos2\theta(1-cos\delta) & sin^2 2\theta + cos^2 2\theta cos\delta & cos2\theta sin\delta \\ 0 & sin2\theta sin\delta & -cos2\theta sin\delta & cos\delta \end{bmatrix} \times \begin{bmatrix} 1 & 0 & 0 & 0 \\ 0 & cos2\Psi & sin2\Psi & 0 \\ 0 & -sin2\Psi & cos2\Psi & 0 \\ 0 & 0 & 0 & 1 \end{bmatrix} \quad (1.13)$$

Where δ, θ, Ψ represent the magnitude of the linear phase delay, the eigenvalue axis direction and the optical rotation of the linear phase delay, respectively.

According to the phase delay matrix M_R, the total phase delay can be obtained, as shown below:

$$R = R_L + R_C = arccos[\frac{tr(M_R)}{2} - 1] \quad (1.14)$$

Where R_L is the linear retardance, R_C is the circular retardance and the $tr(M_R)$ is the trace of the retarder Mueller matrix M_R. Based on the published literature [232, 234, 235], researchers have found that structure of organism tissues often exhibit a very low R_C in backscattering configuration and it is mostly the R_L in such mediums. Hence, according Equation 1.14, the magnitude of linear phase delay R_L (also be represented by δ) can be obtained, as shown below:

$$R_L = \delta = arccos(\sqrt{(M_{R22} + M_{R33})^2 + (M_{R32} - M_{R23})^2} - 1) \quad (1.15)$$

Meanwhile, the direction of the eigenvalue axis θ (the orientation of one eigenaxis of the medium, also called "Azimuth" or "δ" in this study) is obtained, as shown below:

$$\theta = \frac{1}{2}arctan\left[\frac{M_{R24}}{M_{R43}}\right] \quad (1.16)$$

Besides, the depolarization capability parameter Δ is defined as:

$$\Delta = 1 - \frac{|tr(M_\Delta)-1|}{3} \quad (0 \le \Delta \le 1) \quad (1.17)$$

1.5.2 The relation between the Mueller polarimetric parameters and structure of biological tissues

The degree of polarization is usually defined as the ratio of the intensity of fully polarized light to the total light intensity in a light beam. It is generally believed that the change of the polarization state is caused by the birefringence effect and the optical rotation/dichroism of the scattering medium. For example, when polarized light passes through a birefringent crystal with a certain gradient phase difference, the beam will have an interference superposition, which can cause the depolarization effect. The scattering itself can also causes the change of corresponding polarization state, such as multiple scattering which is the dominate depolarization process in biological tissues [236]. The scattering depolarization is strongly related to the surface topography (e.g. roughness) of the medium, and can also be affected by organic structure of biological tissue. Arilfer et al. found that the degradation of fibrous collagen in stroma enables to decrease the light scattering [237]. Pierangelo et al. attributed the decrease of the depolarization of pathological uterine cervix tissue to the disordered organization of collagen by comparing the MPI of healthy and pathological tissues in backscattering configuration [238].

Birefringence, also called double refraction is a common intrinsic property for anisotropic mediums with a non-equivalent axis. A birefringent medium can refract a beam of polarized light into two orthogonal polarized rays travelling at different velocities and directions. Fast axis is the optical axis of medium where polarized beam components moves the fastest. The opposite is the slow axis. δ represents the linear phase delay of the slow axis direction light vector with respect to the fast axis. It is an integrated indicator characterizing the birefringent medium and sometimes used to calculate the normalized birefringence of the anisotropic medium by dividing the thickness of medium with the measured value of retardance. A well-ordered biological tissue generally has anisotropic characteristics. Anisotropic mediums exhibit a significant birefringence which is tightly related to the structure of mediums [232]. When the structure of a biological tissues become disordered, the birefringence of the tissues can be affected. Polarization state of light of medium like retardance and depolarization degree can be changed by the birefringence of mediums. In the measurement of backscattering MPI of pathological uterine cervix

tissue, Pierangelo et al. observed a decreased birefringence and a disappearance of the linear retardance, compared to the healthy tissue [238]. Other pathological tissues like squamous epithelium (EMS) [239], uterine cervix [232, 238] and human skin basal cell carcinoma (BCC) tissues [240] were all found to have a declined retardance, compared to the corresponding healthy ones.

Azimuth is the orientation of the eigenvalue axis, which is represented with α. Bancelin et al. observed a linear retardance of an uterine cervical tissue using MPI and assumed the azimuthal orientation of collagen fibers is in parallel with orientation of the slow axis [241]. In the work of Vizet et al. who measured a *in vivo* MPI of subepithelial connective tissue in a backscattering configuration observed a low retardance and an erratic orientations due to the less well-defined inner organization of tissue [232]. Hence, α is strongly related to anisotropy of medium, particularly to the organization of collagen fibers.

1.5.3 The relation between structure modification of skin and non-thermal plasma treatment

The cutaneous tissue is mainly made of three layers, as shown in Figure 1. 11. The outermost layer is the epidermis which is composed of stratum basal, spinosum, granulosum, lucidum and corneum. This layer mainly contains Keratinocytes and also some immune cells like Langerhans cells and T cells. Dermis is a layer beneath the epidermis and is separated by the basement membrane. It is mostly consisted of the fibroblasts and the extracellular matrix. Hypodermis is mainly composed of adipocytes.

Collagen is a major structural protein and the most plentiful protein in skin that makes up 78-80% of skin. It is mainly distributed in the extracellular space of various connective tissues of mammals. Type I that is one of the five most common collagen types takes over 90% of the whole collagen in human body. The structure of skin is strongly related to this structural protein. In dermatology, collagen has been widely used in skincare, wound healing, cosmetic surgery, grafts, construction of the artificial skin and tissue regeneration etc [25, 224-228]. Latest researches show that the collagen applied in the mentioned applications can be significantly influenced by

the treatment of NTP. NTP can not only promote the secretion of collagen in in vivo treatments of skin under a low treatment dose, but also modify or even damage the triple helical structure of collagen in ex vivo treatments of skin at a high treatment dose [75, 224, 228, 242-244].
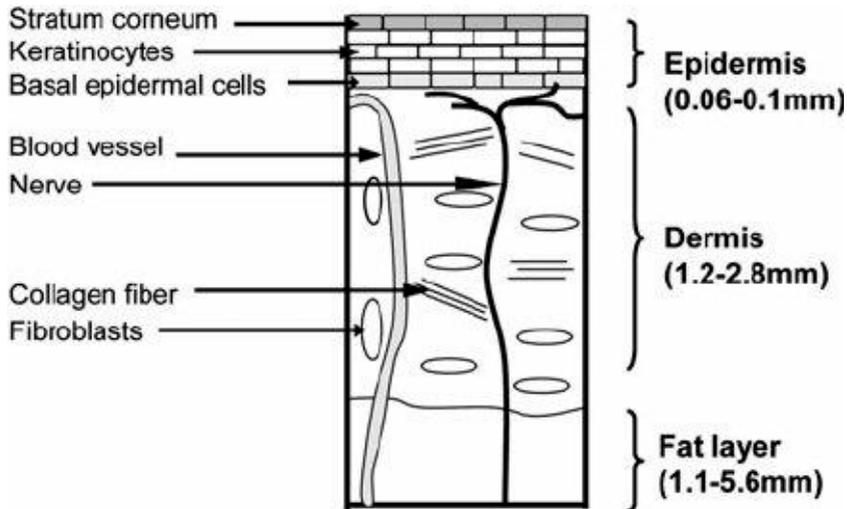
Figure 1. 11 Schematic representation of the skin structure [245]

The production of type I of collagen in wounded skin was found to be promoted by NTP, which accelerates the recovery of wound [105, 112]. Duchesne et al. related collagen secretion after NTP treatment in primary dermal fibroblasts to activation of SMAD and non SMAD TGF-β1 pathways [104, 105]. Besides, the physical and chemical structure of collagen was also sensitive to NTP treatment. In the work of Samouillan et al. who applied differential scanning calorimetry (DSC) to characterize the physical structure of collagen by evaluating the its thermal stability after NTP treatments, it was found that the physical structure of collagen is stabilized by NTP treatment [225]. Keyvani et al. observed the triple helical structure of dissolved collagen treated by NTP using the circular dichroism and found that a 270 second of NTP treatment can induce the full denaturation of collagen structure [246].

An alteration of spatial structure of collagen in skin can cause the changes of the structure of skin tissue. The polarization states of the light can be affected by the microstructure and optical properties of skin [247]. By characterizing the changes of polarimetric parameters state of skin treated with NTP treatment, we can detect and

even quantify the influence of NTP treatment on the structure modification of skin by characterizing the scattering property of light. For example, Δ can be used to evaluate the scattering properties of skin, δ enables to characterize the anisotropy of medium and α is a potential parameter indicating the orientation of the fibrous collagen. Normally, the skin tissue with a well-organized structure is a strong anisotropic medium, which has a strong polarimetric characteristic. The last chapter of this thesis will be dedicated to the influence *ex vivo* of a plasma jet to skin structure modification using Mueller Polarimetry diagnostics.

1.6 Summary and perspectives

NTP have been widely and successfully applied in the fields of material science, electronics science, chemistry and chemical engineer and environment science. Applications of NTP to biomedicine and agriculture are new multidisciplinary research fields based on interactions of the electric discharges (NTP) with living organisms. Electric field as well as Reactive Oxygen and Nitrogen Species (RNOS) produced by NTP may stimulate skin regeneration (dermatology), tumor reduction (oncology) and seeds germination (agriculture and agronomy). These new field of researches also make the plasma-liquid chemistry promising and develops quickly since aqueous RNOS formed by the reaction of NTP with the water covered on the surface of these living organisms have been proved playing a key role in these biological applications. DBD or plasma jet discharges are most types of NTP used in the literatures for such applications. Based on the literature review discussed in this chapter, the works related to plasma-liquid interaction, NTP seeds germination stimulation and NTP skin treatment can be summarized into:

1) For plasma-liquid interaction:
    i) The NTP can be formed in gaseous phase above the water surface, or in gas bubbles inside liquid or directly inside liquid phase; the configuration above water and in bubbles show high production of reactive species in liquids.
    ii) Aqueous reactive species can either mainly formed in liquid phase/liquid layer or mostly formed through the solvation of gaseous species produced in gaseous phase, depending on discharge conditions;

      iii) Short-lived gaseous species with a lifetime ranging from hundred nanoseconds to few microseconds can penetrate up to liquid phase to a depth of few micrometers.

2) For NTP germination stimulation:
   i) NTP can positively promote germination of seeds;
   ii) NTP promotes seeds water uptake by improving seed coat hydrophilicity;
   iii) NTP sterilize seeds chemically and physically;
   iv) NTP regulate seeds cellular physiological activities including enzyme performance, endogenous hormone secretion, drought resistance and genetic variations, etc.

3) For NTP skin treatment:
   i) NTP have been applied in skin care, aged skin regeneration, grafts, dermatological diseases and wound healing, etc;
   ii) NTP have an effective role of sterilization and blood coagulation;
   iii) NTP stimulate cell collagen regeneration and modify its structure of triple helical structure;
   iv) NTP regulate cells cellular viability, cell proliferation, cell migration, growth factors secretion and angiogenic, etc.

The aim of the present thesis is mainly to study the plasma-liquid interaction, to investigate the mechanisms of DBD plasma treatment on seeds germination promotion and to preliminarily explore the structure modification of *ex vivo* skin tissue caused by plasma jet treatment using Mueller polarimetric imaging. The main objectives of this thesis are:

1) to measure qualitatively the amount of plasma reactive species produced by the single electrode DBD plasma reactor and 9-electrode DBD plasma reactor under different discharge conditions;

2) to study the formation pathways of aqueous long-lived plasma reactive species produced by the single DBD plasma reactor;

3) to investigate the potential mechanisms about how the 9-electrode DBD plasma wet treatments stimulate germination of mung bean seeds by treating seeds in different discharge conditions, in different mediums, in electric field alone and in different hydration levels of seeds;

4) to preliminary explore the potentiality of Mueller polarimetric imaging in characterizing the structure modification of mice skin caused by a helium plasma jet.

Chapter 2: Experimental materials and methods

This chapter is composed by four parts: the plasma-liquid interaction, the seeds treatments, the skin treatments and the statistical method for data analysis. In the first part, the NTP source setup, the configurations of discharge, the diagnosis methods of NTP physical properties and plasma reactive species are introduced. In the second part, the plasma setup used for seeds treatment, the protocols of seeds treatment with NTP, electric field and chemical solutions, the optimization of seeds germination and the protocol of seeds water uptake measurement are described. In the third part, the plasma setup for skin treatment, the setup of Mueller polarimetric imaging (MPI) and protocols of skin treatment with NTP, oven and MPI are introduced. In the last part, the statistical analysis (survival test) of the seeds, necessary to obtain the significant difference between the control group and treated group, is introduced.

Experimental materials and methods

2.1 Plasma-liquid interaction

This section will introduce the single electrode plasma source setup, configurations of gas discharge and methods for measurements of plasma reactive species in the gas phase and liquid phase using chemical and physical techniques.

2.1.1 Plasma source setup
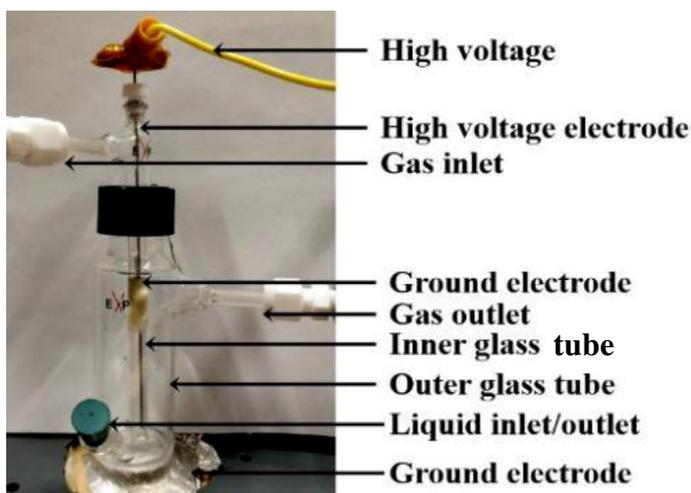
Figure 2. 1 Photo of single electrode DBD plasma setup

The single electrode DBD plasma source is built in order to study the plasma-liquid interaction by examining the plasma reactive species simultaneously formed in the gas and liquid phase. Controlled NTP can be produced for different discharge conditions. The single electrode DBD setup is shown in Figure 2. 1. The two cylinders constitute the body of the main part of the setup. Three nozzles are attached to the large cylinder, the one at the top and the one in the middle serve as gas outlets, the one at the bottom is used for liquid in- and outlet. A gas flow is guided through the small cylinder, at the top of this small inner glass tube, the high voltage electrode is mounted. The diameter of the inner tube is 3 mm and the diameter of the HV electrode is 1.2 mm. The position of ground electrode can be either on the out surface of the inner tube or under the bottom of the big cylinder, depending on the

configurations of discharges. A power supply delivering bipolar square waveforms with an amplitude in the range 0-18 kV at a frequency of 500 Hz is selected to produce the NTP using this setup.

2.1.2 Configurations of gas discharge

In order to study the chemical reactions between the plasma phase and the liquid phase using the closed single electrode plasma reactor (Figure 2. 1), two kinds of non-thermal plasma are designed, a touching plasma where the NTP touch the water and a non-touching plasma where the NTP do not touch the water.
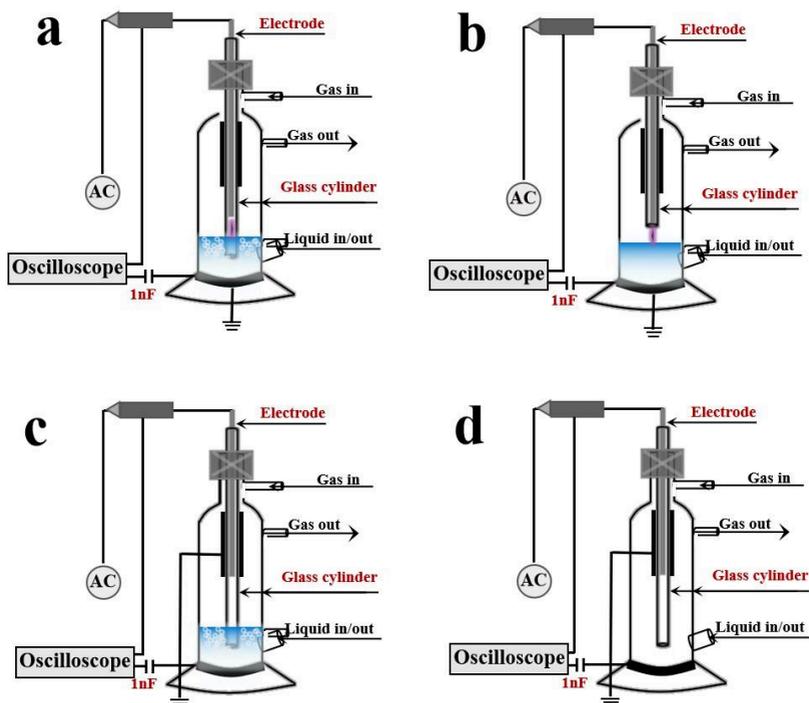
Figure 2. 2 Schematic of single electrode DBD plasma setup in different configurations. a is touching bubble plasma (TBP), b is touching non-bubble plasma (TNP), c is non-touching bubble plasma (NBP) and d is non-touching non-bubble plasma (NNP). The device is made of glass tubes. Liquid is placed on the bottom of the bigger diameter glass cylinder for NTP treatments. The diameter of the inner tube is 3 mm and the diameter of the HV electrode is 1.2 mm.

The kind of NTP is chosen by changing the position of the grounded electrode. When the grounded electrode is located at the bottom of the reactor, NTP will be generated in the gap between the tip of the high voltage electrode and the water surface. This is called a touching plasma (Figure 2. 2 a&b). If the inner tube is immersed inside the liquid for 1 mm, the configuration is called a touching bubble plasma (TBP, see Figure 2. 2a). If the inner tube is not immersed in the water, the configuration is called a touching non-bubble plasma (TNP, Figure 2. 2b). When the ground is located at the outer surface of the discharge the NTP will be produced in the space between the high voltage electrode and the glass tube. The configuration is then a standard cylindrical DBD. In this case the NTP is not in direct contact with the water, this is called a non-touching plasma (Figure 2. 2 c&d). Again, two configurations exist, when the capillary is immersed in the water for 1 mm, the configuration is called a non-touching bubble plasma (NBP, Figure 2. 2c). If the inner glass tube is not immersed into the water or when there is no water present in the setup, the configuration is called a non-touching non-bubble plasma (NNP, Figure 2. 2d). NTP physical and chemical diagnostics both in gas phase and liquid phase will be further implemented for each of these four plasma configurations.

2.1.3 Diagnosis of plasma electrical property

2.1.3.1 The waveform of the power supply

Passive probes PP08 (10 times attenuation) and PPE20kV (1000 times attenuation) are used to measure the input and measured voltages, the signal is displayed on the Lecroy Wave Runner 6 Zi oscilloscope (band-pass=2.5GHz). The typical waveforms of the power supply with a 500 Hz is shown in Figure 2. 3: the voltage increases from -1.5 kV to +10 kV in approximately 100 μs, and after some oscillations stabilizes at +2.5 kV. The peak to peak discharge voltage is 20 kV. The waveform signal is obtained via a series capacitor (100 nF), shown in Figure 2. 10. The positive cycle is succeeded by a similar negative cycle.
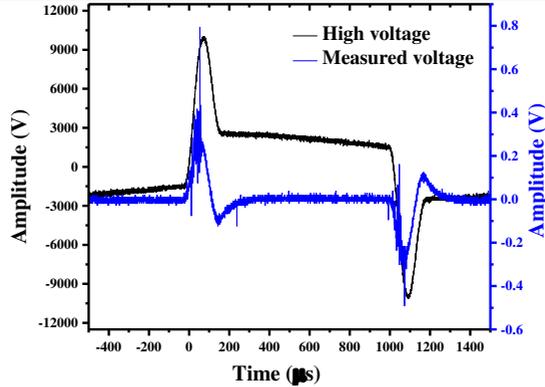
Figure 2. 3 Waveform of the voltage delivered by the 500 Hz power supply with 9-electrode plasma reactor. The black curve is the waveform of input voltage and the blue curve is the waveform is the measured voltage of the series capacitor (100 nF).

2.1.3.2 Protocol of current measurement
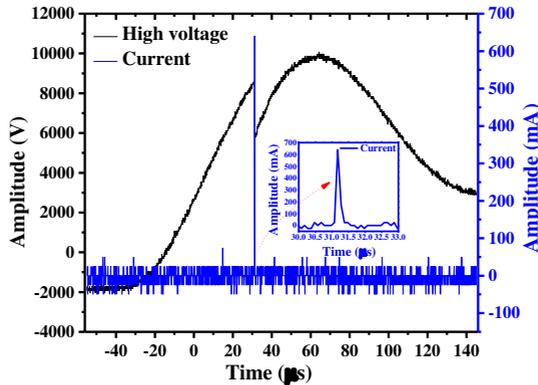
Figure 2. 4 Waveform of the current delivered by the 500 Hz power supply with the single electrode plasma reactor

In order to measure the discharge current, a 50 Ω resistor is series connected after the ground electrode of plasma setup. The current is calculated by

$$I = \frac{U_g}{R} \tag{2.1}$$

In this equation U_g is the voltage applied over the resistor and R is the resistance. The waveform of the voltage is monitored on the oscilloscope. The peak to peak input voltage is 20 kV. The typical waveform of the measured current over the series

resistor during the positive period is shown in Figure 2. 4.

2.1.3.3 Protocol of discharge power measurement

The average discharge power is measured by connecting a capacitor in series after the ground electrode of plasma setup.

Since:

$$I = \frac{dQ}{dt} = C \frac{dU_g}{dt} \tag{2.2}$$

With U_g the voltage over the capacitor and C the capacitance, the power can be calculated by

$$P = UI = CU \frac{dU_g}{dt} \tag{2.3}$$

In which U is the voltage of the high voltage electrode.

The average discharge power $\bar{P}$ can be obtained by integrating the power over one period:

$$\bar{P} = \frac{1}{T} \int_0^T CU \frac{dU_g}{dt} dt \tag{2.4}$$

U and U_g are monitored on the oscilloscope. A visual basic script (VBS) function is written in order to calculate the average power and display the calculated average power on the oscilloscope. Details of the VBS code for real time power calculations are shown in appendix B.

2.1.3.4 iCCD imaging of the discharge

The physical properties of the single electrode DBD plasma can be studied by analyzing the discharge patterns in the images recorded by the Andor Istar iCCD camera with Edmund Optics 50 mm FL (1:2.8) high resolution lens. Images of plasma propagation (camera gate 0.5-1 µs) are acquired and analyzed. In order to synchronize with the discharge initiation, the camera is externally triggered by the oscilloscope. The TGP110 10MHz signal generator is used to increase the output

signal from the oscilloscope to a 5 V square pulse signal that can trigger the iCCD camera. It has to be noted that the camera has an internal, nonregulated delay of approximately 200 ns.

2.1.3.5 Optical emission spectroscopy (OES)

OES is a widely used contactless plasma diagnostic technology for the qualitative and quantitative measurement of characteristics of various electron excited species within the plasma, including vibrational and rotational temperature, density and concentration etc. A monochromator, Shamrock 303i, Andor Technology, is connected to an optical fiber Ocean optics QP450-2-XSR 455 µm, which collect the light emitted by the plasma. After dispersion by the monochromator, spectra are acquired by Andor Istar iCCD mounted on the spectrometer. The monochromator entrance slit is connected to an optical fiber to collect the plasma emitted light. The entrance slit is 60 μm and the optical fiber is fixed at a 2 cm from the plasma. Emission spectra are recorded on iCCD Camera mounted on the spectrometer after dispersion by a 600 l/mm diffraction grating. The camera is triggered externally via the oscilloscope and the signal generator to synchronize with the discharge initiation with an adjustable delay. In order to capture the emission light of the whole positive or negative discharge process, camera gate is fixed at 50 μs to capture all the light.

2.1.4 Measurements of plasma gaseous species

A Fourier Transform Infrared (FTIR) ozone analyzer and NOx analyzer are used to analyze the plasma generated gaseous species generated by the single electrode DBD plasma reactor.

2.1.4.1 Fourier transform infrared spectroscopy (FTIR)

FTIR spectroscopy is used to obtain infrared absorption spectra and emission spectra of solids, liquids or gases. In this work, a FTIR spectrometer (high-resolution Nicolet 6700 from Thermo Fisher Scientific) is equipped with a 10 m optical-path

gas cell and a mercury cadmium telluride (MCT) detector. The MCT is cooled to 77 K by liquid nitrogen. The gas cell is maintained at 50 ˚C in order to prevent the adsorption of water and other gas species on the mirrors inside the gas cell. The software used for the acquirement of the spectrum is OMNIC. For each spectrum, 16 scans are needed. It takes 32 seconds to make these 16 scans and a resolution of 0.5 cm^{-1} can be reached.

2.1.4.2 Ozone analyzer

A commercial ozone analyzer (Environment S.A. O342e) is connected to the outlet of the single electrode plasma reactor. UV absorption of ozone is used to determine the concentration of ozone. The device is characterized by an accuracy of 0.1 ppm and a detection limit of 0.2 ppm. A pump is integrated in the ozone analyzer in order to collect gas, the optimal working flow is 1000 sccm. To reach the optimal working conditions, extra N_2 is added to the incoming gas, the N_2 acts as a supporting gas.

2.1.4.3 NO analyzer

A commercial NO_x analyzer (Ecotech, Serinus 40) is used to measure the concentration of nitric oxide (NO). The principle of this analyzer for NO measurement is to detect the intensity of the chemiluminescence intensity of activated NO_2* formed by the reaction of NO and ozone. The detection limitation of this analyzer is 0.4 ppb.

2.1.4 Measurements of plasma aqueous species

The concentrations of the three major aqueous long-lived species and one aqueous short-lived species, that are H_2O_{2aq}, NO_2^-, NO_3^- and OH_{aq} radical, are measured by spectrophotometric methods. The disposable PMMA cuvettes (10 mm of optical path) are used to measure the amount of long-lived species with a visible light spectrophotometer, and to measure the OH_{aq} radical with a fluorescence spectrophotometry.

2.1.4.1 Protocol of nitrite measurement

Numerous methods can be chosen for the quantitative detection of NO_2^- in water, reaction with Griess reagent is one of the most sensitive and accurate methods. In acidic medium, NO_2^- reacts with the Griess' Reagent (Sigma Aldrich-035553) and forms a pink colored azo-compound with a 1/1 stoichiometry. 900 µL of diluted (dilution factor between 2 and 9) samples are mixed with 100 µL of the commercial solutions of Griess' reagent. After 20 min of incubation: the absorbance of the solution is measured at 522 nm with a 10 mm cuvette. Chemical reaction in nitrite and Griess reagents is shown below:

(2. 5)
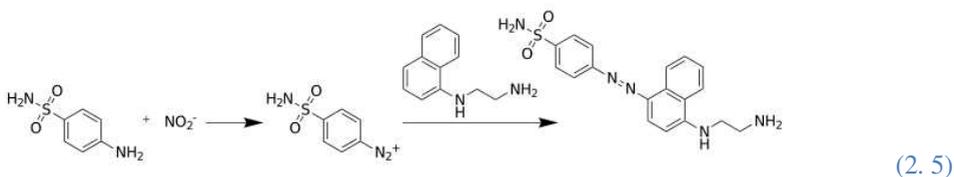
It is worth noting that there is a slight inference from H_2O_{2aq} with nitrite forming $ONOO^-$ in acidic conditions. An elimination of H_2O_{2aq} before NO_2^- measurement should be considered. This can be done by adding Catalase enzyme in the plasma treated liquid.
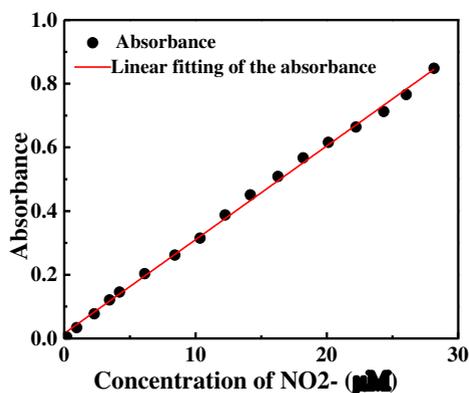
Figure 2. 5 Calibration curves of measurement of sodium nitrite solution with Griess reagents in different concentration ranges. Concentrations of nitrate ranges from 0.2 µM to 28 µM. Absorbance at λ= 522 nm as a function of concentration with absorbance (1-cm cells). The total volume of liquid is 1000 µL sample. 900 µL of samples were mixed with 100 µL of the commercial solutions of Griess reagents

As shown in Figure 2. 5, the calibration curves of NO_2^- solution are plotted with the concentration ranging from 0.2 μM to 28 μM. Higher concentration will be diluted with blank liquid. Fitting degree of this method is 0.99 and regression fitting equation is:

$$Y=0.02946X+0.01563 \tag{2.6}$$

Where Y is absorbance and X is concentration of nitrite solution.

2.1.4.2 Protocol of nitrate measurements

Nitrate quantitative measurements are generally done with Griess reagents. Before measuring, NO_3^- have to be selectively reduced to nitrite with reductants like vanadium (III) [248, 249], iron (II)/iron (III) [250] and enzyme [251]. Here a nitrate reductase is used to reduce it to nitrite. NO_3^- is measured with Nitrite/Nitrate Assay kit (Sigma-Aldrich 23479). The kit is used in accordance with manual instructions with the exception of one point: Deionized water is added to bring the total volume into 1 mL after incubation and before the measurement of the absorbance at 540 nm. Concentration of nitrate is obtained by subtracting the concentration of existed nitrite with the total concentration of the nitrite.

2.1.4.3 Protocol of hydrogen peroxide measurements

In the experiment with multi-electrode and single electrode plasma reactor, two independent methods measuring concentration of H_2O_{2aq} are chosen, based on the sensitivity of each methods and the concentration of H_2O_{2aq} in the plasma activated liquid.

Conversion of Titanium (IV) Oxysulfate ($TiOSO_4$) with H_2O_{2aq} to a compound having a very high absorbance is used for higher concentration experiments [252, 253]. The reaction equation is below:

$$Ti(OH)_3HSO_{4(aq)}+H_2O_{2(aq)}=Ti(O_2)OH^+_{(aq)}+HSO_4^-_{(aq)}+2H_2O \tag{2.7}$$
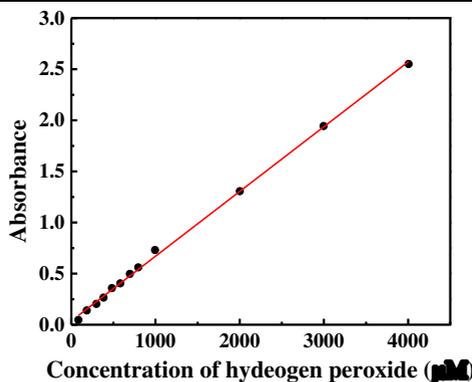
Figure 2. 6 Calibration curve of hydrogen peroxide concentration measurement with TiOSO$_4$. Absorbance at $\lambda = 408$ nm as a function of concentration with absorbance (1-cm cells). The total volume of liquid is 1000 μL sample. 900 μL of samples were mixed with 100 μL of the commercial solutions of TiOSO$_4$

In this method, there are no inferences from other species in the co-solvent plasma treated liquid and it has a wide measuring range. The total volume of liquid is 1000 µL sample. 900 µL of samples are mixed with 100 µL of the commercial solutions of TiOSO$_4$. Record the absorbance with 1-cm cells after a 10 min reaction time at 408 nm. In the Figure 2. 6, a linear increase still is shown when concentration reach up to a 4 mM. However, this reaction had a low sensitivity that the measuring concentration limitation is more than 29 µM. Fitting degree of this method is 0.99 and regression fitting equation is:

$$Y=0.000634X+0.003686 \qquad (2.\ 8$$

Where Y is absorbance and X is concentration of H$_2$O$_2$ solution.

Discharge with the 9-electrode plasma reactor can produce a large amount of the aqueous species, the minimum concentration of H$_2$O$_{2aq}$ has exceeded the detection limitation of the method with TiOSO$_4$ (29 µM). However, this method is not suitable for the measurement of H$_2$O$_{2aq}$ in the case of discharge with single electrode plasma reactor. The production of H$_2$O$_{2aq}$ is greatly decreased due to the low discharge power of single electrode plasma reactor. Another method with a higher detection limitation is selected for the measurement of H$_2$O$_{2aq}$ in a lower concentration.

Figure 2. 7 Calibration curve of hydrogen peroxide concentration measurement with Cu ions. Absorbance at λ= 453 nm as a function of concentration with absorbance (1-cm cells). The total volume of liquid is 800 µL sample. 800 µL of samples were mixed with 50 µL of the commercial solutions of the two reactants respectively

Spectrophotometric method using Copper (II) ion and 2,9-dimethyl-1,10-phenanthroline (DMP) is the alternative method measuring concentration of H_2O_2. Cu(II)-DMP can be reduced by hH_2O_{2aq} to form the $Cu(DMP)_2^+$ with a 1-1 stoichiometry [254, 255]. 800 µL of samples are mixed with 50 µL of the commercial solutions of the two reactants respectively. Record the absorbance of this solution after 10 min reaction time with 1-cm cell at 453 nm. This method exhibits a more sensitive detection limitation than titanium oxalate colorimetric method. It can measure a concentration as low as 5 µM. Species like nitrate, nitrite and radicals have no inference to the reduction reaction of Cu(II)-DMP. The fitting degree is 0.999. Regression fitting equation is:

$$Y=0.0115X-0.07577 \tag{2. 9}$$

Where Y is absorbance and X is concentration of hydrogen peroxide solution.

2.1.4.4 Protocol of hydroxyl radical measurement

Hydroxyl radical is measured by the method of fluorescence spectrophotometry. Hydroxyl radical can react with terephthalic acid (TPA, from sigma Aldrich, Ref 752525) to mainly form 2-hydroxyterephtalic acid (TPA-OH) that has a strong fluorescent signal with an excitation wavelength of 317 nm and an emission wavelength at 433nm. The reaction is below:

(2. 10)
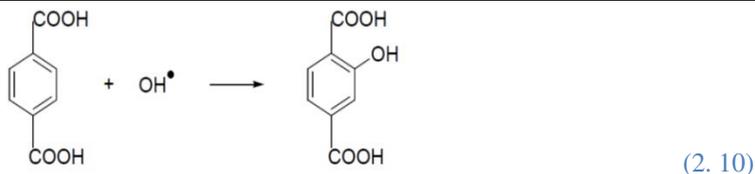
In this work, TPA solution with a concentration of 67 mM being hydroxyl capture agent is treated by NTP. Since the short-life and high chemical activity, only part of those NTP produced hydroxyl radical can react with TPA to form the fluorescent compound. After NTP treatment, the treated water is then transformed to the measurement of fluorescent intensity. Calibration curve is measured with pure TPA-OH (from sigma Aldrich, Ref 185361). The fitting degree is 0.998. Regression fitting equation is:

$$Y=299687X-44269 \tag{2. 11}$$

Where Y is intensity and X is concentration of hydroxyl radical. To be noted that here the concentration of hydroxyl radical only is only those that are captured by TPA.
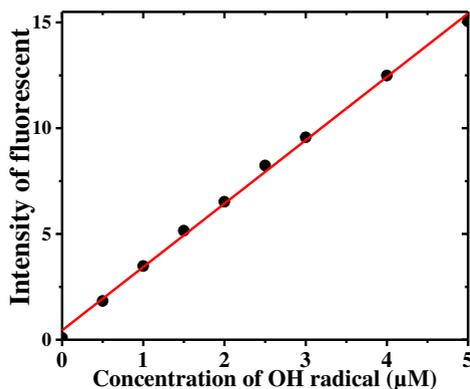
Figure 2. 8 Calibration curve of hydroxyl radical with the method of fluorescence spectrophotometry. Excitation wavelength is 317nm and an emission wavelength is 433nm.

2.2 Seeds treatments

This section will introduce the 9-electrode plasma setup used for seeds

treatments, the measurements of aqueous plasma reactive species formed with DBD plasma, protocols of seeds treatments including DBD plasma treatments, electric field treatments and chemical solutions treatments, and the optimization of seeds germination protocol.

2.2.1 Plasma source setup

In order to treat a large amount of seeds per time, it is necessary to build a device that can treat batches of at least 20 mL of water. Since the capacity of the single electrode plasma reactor is only 5 mL, this reactor setup is no longer sufficient. In order to increase the capacity of the reactor, a larger treatment surface is needed. Therefore a 9-electrode DBD plasma reactor is designed and selected for seeds treatments.

3D printing is used to develop the 9-electrode DBD plasma reactor, it allows the fabrication of more complex structures than the ones produced by conventional fabrication methods. 3D printing enables effective design and optimization in terms of geometry. The used printer material is polymer plastic, this is in general a good insulator and provides a strong plasticity. The printing parameters have to be optimized in order to prevent gas leakage and instabilities in the electric field. Among the alternations of printing parameters are the reduction of the z-layer thickness, the increase in density of the printed model and the selection of a suitable printing temperature, but also the suspension of precautions while printing. The whole setup is separated in two parts, the 3D printed plastic body and the gas channel where the NTP are generated which is made of glass. The capillary in which the NTP are generated is made out of glass to prevent etching, oxidization, deformation and melting. The maximum deformation temperature of polymer plastics is beneath 250 °C, and if the temperature gets higher by-products will be produced by etching and oxidizing and leakages will be caused by melting of the plastic. Since glass has a much higher deformation temperature, these problems play no part when a glass capillary is used.

2.2.1.1 Modeling of 9-electrode plasma setup

A model of the 3DS printed 9-electrode plasma setup is shown in Figure 2. 9. It is designed in an open-source software called Open SCAD. The device consists of three parts: a horizontally placed cuboid which is the main gas inlet, 9 integrated double-pass cones which are the gas outlets and a hollow cube which connects the cuboid and the cones. The gas enters the device through the cuboid channel and will pass through the hollow cube where it is equally divided over the 9 cylinders which are placed in the center of each cone. A stainless-steel electrode is fixed in the center of each cylinder. The detailed parameter is attached in Appendix A.
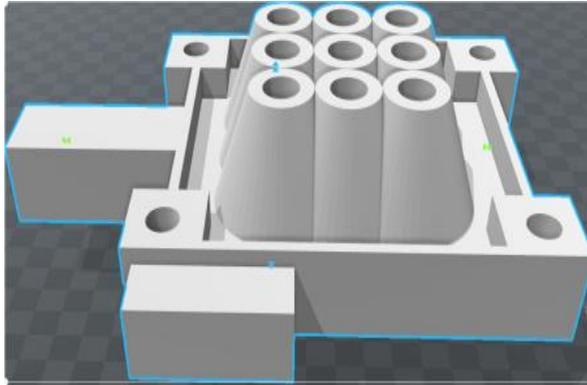
Figure 2. 9 3D model of 9-electrode DBD plasma setup

2.2.1.2 Setting of 3D-printer

The 3D printer used to print the setup is a Create-HS which is purchased from Leapfrog3D. A spool with plastic filament is placed in the machine and the plastic filament is motorial feed into the extrusion nozzle. The extruder heats the filament to printing temperature (about 220 °C for PLA or PETG). Important control parameters in the printing process are the printing speed, the temperature of the extruder, the size of the plastic layers and the cooling kinetics. The distance between the print head and the print surface is critical for printing quality, it depends on the height of the layers and is usually around 100 μm.

Experimental materials and methods

2.2.1.3 Assembling the 9-electrode plasma setup for seeds treatments

As mentioned, glass tubes will be used as the gas channel to form NTP. They are fixed in each central of the plastic cones, as shown in Figure 2. 10. The multi-electrode plasma setup is made of 3x3 glass dielectric tubes set in an array; glass tube inner diameter and outer diameters are 4 mm and 7 mm respectively. All the glass inner tubes are immersed into water for 1 mm to avoid the ambient Air diffusing into discharge zones. High voltage electrodes are made of stainless-steel wires (1.2 mm diameter and 100 mm length). The distance of all the HV electrodes to water surface is 7 mm. An annular aluminum connected to the bottom of the beaker being ground electrode and a series 100 nF capacitor is fixed after the ground electrode of plasma setup. The power supply used in seeds treatment is the same one used in plasma-liquid interaction, which has been discussed in section 2.1.3.1. The average discharge power is obtained by calculating the current through a series capacitor (100 nF), which has been shown in 2.1.3.3. In this setup configuration, NTP will be generated in the space between HV electrode tip and liquid surface.
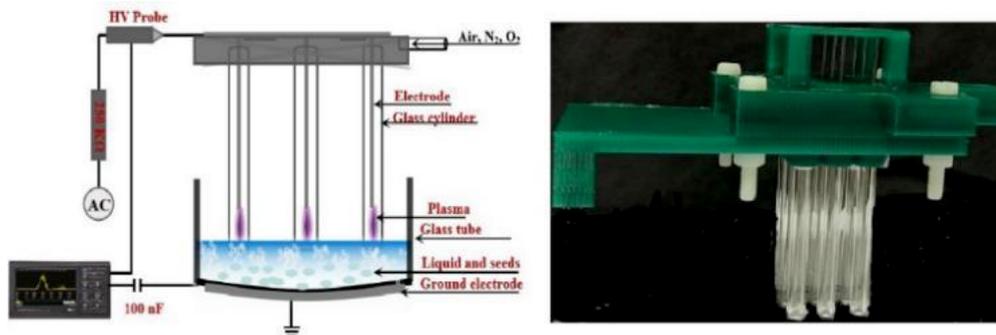
Figure 2. 10 Schematic diagram (left) and Photo (right) of the 3×3 array of glass tubes in side view of the plasma setup. The device is made of 3×3 glass tubes set in an array and fabricated by 3D printer. The gap between electrode and water surface is 7 mm.

2.2.2 Measurements of plasma aqueous species

The protocols of aqueous plasma reactive species refer to the methods discussed in section 2.1.4.

2.2.3 Protocols of seeds treatments with the DBD plasma reactor

2.2.3.1 Protocol of multiple seeds treatments

The seeds are treated with the DBD plasma reactor in two different ways. They can be treated in water directly during the discharge, which is called direct plasma wet treatment, or be treated only with the plasma activated water, which is called indirect plasma wet treatment. The schematic of NTP wet treatment is shown in Figure 2. 11. In this work, seeds of Tomato, Lettuce, Mung Bean, Sticky Bean, Radish, Dianthus, Mustard and Wheat are treated by indirect plasma treatments, and seeds of mung bean, wheat and mustard are also treated by direct plasma wet treatments.
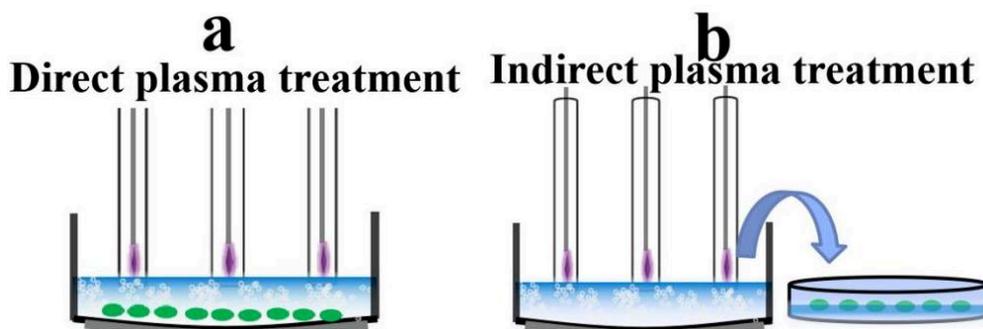
Figure 2. 11 Schematic of (a) direct plasma treatment with seeds and (b) indirect plasma treatment with seeds using the 9-electrode DBD plasma setup. The discharge conditions for all plasma treatments are same. The input voltage is 20kV peak to peak (Vpp=20kV) and the gas flow rate is 1.5 standard liters per minute (SLM). The power consumption measured for plasma treatment is ca. 3W. The discharge gas can be Air, N_2 or O_2. The plasma treatment time ranges from 1 min to 20 min. The inner glass tube is 1 mm immersed the liquid surface and the distance of HV electrode to water surface is 8 mm. The distance of seeds top surface to water surface is 5 mm.

For direct plasma wet treatment, seeds are placed at the bottom of a glass beaker which also contains the liquid that will be subject to plasma treatment (20 mL), when the NTP are turned on. After the direct plasma wet treatment, the seeds are soaked in the plasma treated liquid for several hours in order to stimulate further germination. The seeds are directly soaked in the plasma treated liquid for further germination is the indirect plasma wet treatment. The liquid used to be treated by NTP can be the

tap water, or the acidified tap water or the sodium nitrate solutions.

2.2.3.2 Protocol of direct plasma wet treatments with mung bean seeds in different distances to water surface

First, placing a 3D printed porous discs (PLA) at the bottom of the beaker. Second, putting the mung bean seeds on the surface of this PLA discs and watering 20 mL tap water into the beaker. Next, treating seeds with the DBD plasma for different times. Last, soaking the plasma treated seeds with the plasma treated liquid for further germination. The distance of seeds top surface to water surface can be 1 mm, or 3 mm or 5 mm by increasing the thickness of PLA discs, as shown in Figure 2. 12.
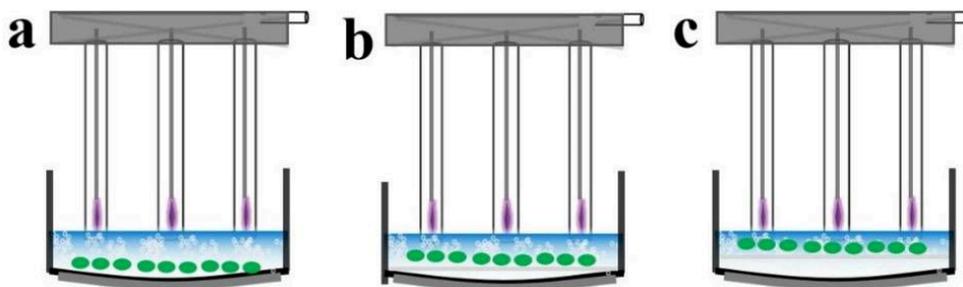
Figure 2. 12 Schematic of direct plasma wet treatment with seeds in different positions using the 9-electrode DBD plasma setup. The distance of top surface of seeds to water surface is 5 mm in Figure 2. 12 a, is 3 mm in Figure 2. 12 b and is 1 mm in Figure 2. 12 c. The seeds tough the inner glass tubes in Figure 2. 12 c. The input voltage is 20kV peak to peak (Vpp=20kV) and the gas flow rate is 1.5 standard liters per minute (SLM). The power consumption measured for NTP treatment is ca. 3W. The discharge gas can be Air, N_2 or O_2. The NTP treatment time ranges from 1 min to 20 min. The inner glass tube is 1 mm immersed the liquid surface and the distance of HV electrode to water surface is 8 mm. The distance of seeds top surface to water surface can be 1 mm, or 3 mm or 5 mm by placing a 3D printed porous discs at the bottom of the beaker.

2.2.3.2 Protocols of mung bean seeds treatments with the DBD plasma in different conditions

In the following plasma treatments, mung bean seed is selected to investigate the mechanisms of NTP affecting the process of seed germination. It is treated not only by plasma treatments but by electric field alone and chemical solutions.

The NTP treatments with mung bean seeds are listed below.

i) Direct plasma wet treatments with immersed seeds: First, immersing 60 dry seeds to the beaker containing 20 mL liquid. Second, treating seeds with NTP for different times. Last, soaking the plasma treated seeds with the plasma treated liquid for further germination;

ii) Direct plasma wet treatments with soaked seeds: First, soaking the seeds in two different ways. Immersing all the seeds (the total number of seeds ranges from 120 to 240) fully in a beaker containing 100 mL tap water for different times, or semi-immersing every 15 seeds in one Petri dish (diameter = 55 mm, height = 10 mm) with 2 paper layers and 5 mL tap water for different times. Then, treating the soaked seeds with NTP according to i);

iii) Indirect plasma wet treatment with dry seeds: First, treating the 20 mL liquid with NTP without any seeds immersed in the liquid. Then, soaking the dry seeds with plasma treated liquid for further germination.

2.2.4 Protocols of electric field treatments
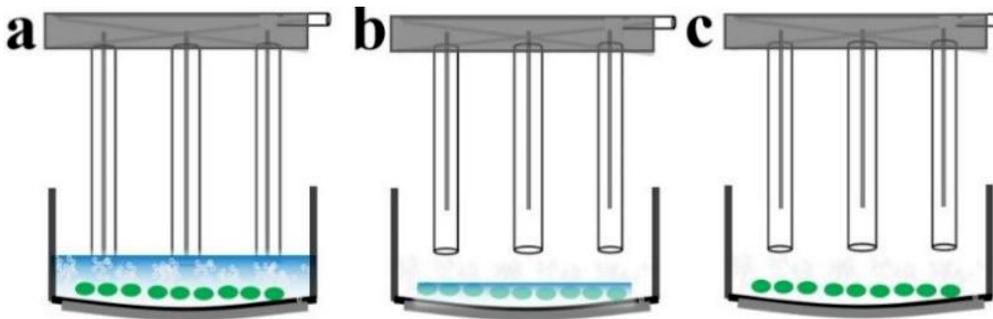
Figure 2. 13 Schematic of electric field treatment with seeds using the 9-electrode in different conditions. The seeds in configuration a can be immersed seeds or soaked seeds, in configuration b is wet seeds and in configuration c is dry seeds

The configuration described in this section is used to study the effect of the electric field on the germination of mung bean seed. The contribution of the electric field to the germination process is investigated under different treatment conditions,

as shown in Figure 2. 13. The treatment time in all experiments is 4 minutes. There is not a gas in all the electric field treatments. The power consumption for electric field treatment is less than 10 mW for all E-field treatments.

The electric treatments with mung bean seeds are listed below.

iv) E-field treatment with immersed seeds (Figure 2. 13a): First, immersing 60 dry seeds in a beaker with 30mL tap water. Second, adjusting the position of high voltage electrodes to make all of these electrodes touching the water surface. Then, treating seeds with electric field. Last, soaking the electric field treated seeds with tap water for further germination. In this configuration, the seeds are located 12 mm beneath the tips of the high voltage electrodes, and the amplitude of the peak to peak voltage Vpp is in the range between 1 and 20kV. It is checked that no detectable RNOS are formed in the liquid. The measured H_2O_2, and NO_2^- concentrations are below the detection limits (typically 5 µM for H_2O_2 and 1 µM for NO_2^-) of the methods described in previous works [9];

v) E-field treatment with soaked seeds (Figure 2. 13a): First, semi-immersing every 15 seeds in one Petri dish (diameter = 55 mm, height = 10 mm) with 2 paper layers and 5 mL tap water for different times. Then, treating the seeds with electric field according to iv);

vi) E-field treatment with wet seeds (Figure 2. 13b): First, immersing all the seeds (the total number of seeds ranges from 120 to 240) fully in tap water for several seconds. Second, treating 60 soaked seeds with electric field without tap water. Last, soaking the electric field treated seeds with tap water for further germination. In this configuration, the seeds are placed at the bottom of an empty beaker with a distance of 12 mm to tips of the high voltage electrodes. The amplitude of the voltage Vpp is ranging from 1 to 20kV. The absence of a discharge is checked by the measurement of the power consumption and measuring whether light emission is absent;

vii) E-field treatment with dry seeds (Figure 2. 13c): First, placing 60 dry seeds at the bottom of an empty beaker 16mm below the tips of the high voltage electrodes. Second, treating the seeds with electric field. Last, soaking the

electric field treated seeds with tap water for further germination. In this configuration, the amplitude of input voltage Vpp is 20kV. The absence of discharges is checked by measuring whether light emission and power consumption are absent.

2.2.5 Protocols of chemical treatments

The aim of seeds treatments with chemical solutions is to investigate the role of NTP reactive aqueous species on the germination promotion. In this study, the used chemical solutions include H_2O_2, sodium nitrite ($NaNO_2$) and sodium nitrate ($NaNO_3$). The concentration of H_2O_2 is 40 μM, the concentration of $NaNO_2$ is 110 μM and the concentrations of $NaNO_3$ have 230 μM, 500 μM, 1 mM, 5 mM and 7 mM. The procedures of seeds treatment with these chemical solutions are same to i) for direct plasma wet treatment and are same to iii) for indirect plasma wet treatment.

2.2.6 Optimization of germinating protocol

Investigating the biological effect of NTP on germination is one of the main purposes in this work. Optimization of the germination protocol is needed in order to select the best germination conditions and guarantee the reliability of the entire experiment. Seed germination is a complex process. The reproducibility of this process depends on the control of several important external environmental conditions, including temperature, water, oxygen level and exposure to light.

Water is required for germination. Mature seeds often contain a small amount of water molecules, which are chemically bonded into water clusters. Before cellular metabolism and growth of such dry seeds can resume, sufficient water content is needed to activate enzymes which could transform starch, proteins or oils into metabolically useful chemicals for providing of nourishment.

Oxygen is required for germination metabolism. In the dormant state, seeds require little oxygen quantities because the respiratory rate is weak. However, a gradually increasing demand of oxygen used in aerobic respiration is necessary

during the germination process. This is the main source of energy of metabolic activity before the formation of photosynthesis of leaves. Oxygen source can be either found in soil pore spaces or absorbed from atmospheric Air. If a seed is buried too deeply within the soil or the soil is waterlogged, the seed can be oxygen deprived.

Temperature impact germination metabolism and seedling growth rates. Any seeds often have their own proper germination temperature interval, and they will less germinate or even not germinate at all over or below the suitable temperature range. Even within this temperature range, the seed germination rate could be significantly affected by the ambient temperature. Germination rate of most seeds are sensitive to temperature that higher temperature fastens germinate rate or reduce germination in a converse temperature, generally.

Light or darkness have the ability to start the seed germination. Most of the common seeds are not sensitive to light or darkness during the whole germination process, but there are also some seeds whose germination can be affected by light. For instance, the species grown in forest settings will not germinate until an opening in the canopy allows sufficient light for growth of the seedling.

Here, experiments about germination in different conditions, including filter paper, temperature and light irradiation, are carried out to optimize the germination protocol. Wheat seed is selected to study the role of filter paper in germination since it is the first target chosen for the investigation of seed treatment with NTP in this work. Mung bean as the main target for the investigation of NTP biological effect is selected to study the effect of temperature and light irrigation on germination.

2.2.6.1 Filter paper

Seeds germination needs suitable amounts of water and oxygen at the same time. Filter paper as a porous material can be an ideal storage carrier supporting water and oxygen, and it has been applied for germination of many seeds [34, 176, 186, 198]. The filter paper exposes seed semi-immerse in water so that water and oxygen can be sustained simultaneously in the whole process of germination. To verify if filter paper can supply enough water and oxygen for germination, wheat seeds is selected to germinate with and without filter paper.
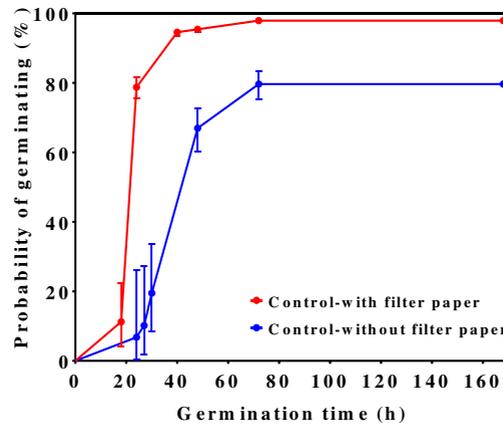
Figure 2. 14 Influence of filter paper on germination rate of wheat seeds. Germination with light irradiation at a temperature of ca. 22 °C and humidity of ca. 40 %. 15 seeds are soaked in each Petri dish with 5 mL tap water for germination. Petri dish is covered in the first two days. After that, the cover is removed and 3 mL water is supplied daily. The experiment is done with 240 seeds for control group without filter paper and 120 seeds for tested group with filter paper. All the curves represent the Kaplan-Meier estimator of the probability of germinating, error bars represent the 95 % confidence interval (Greenwood) and the P-value between each two groups is calculated based on Log-rank (Mantel-Cox) test.

Figure 2. 14 illustrates the comparison among probability of germinating curves of seed germination with and without filter paper. Germination rate of seeds with filter paper is much higher than that of germination without filter paper at each of the time points. P-value of these two curves is much smaller than 0.001. 95 % of the seed can be generated at germination time of 40 h when germinating with paper, while only 45% of seeds can be generated when germinating without filter paper. In this latter case, only 80 % of seeds are germinated even at the 160 h of germinating time. To be noted that, in the case of germinating without a filter paper, the non-germinated seeds in the terminated germination time point are censored data, which should be pointed out since they may have rotten and would never germinate. In summary, filter paper is the prerequisite material for germination.

2.2.6.2 Germinating light irradiation

Mung bean seeds are used to study the influence of light irradiation on germination. Since room temperature is 19 °C, temperature of experiment with seeds

germinating in darkness is equivalent to room temperature, however, because of light irradiation temperature of experiment with seeds germinating in light increase to ca. 21 °C. When exposed to light, seeds grow for a 16-hour photoperiod of artificial light (horticultural dimmable LED panel providing two wavelength peaks at 460 nm and 636 nm; 150~260 μmol.m^{-2}.s^{-1}). In order to keep the same temperature for these two experiments, a fan is used to cool down the higher temperature caused by light irradiation.
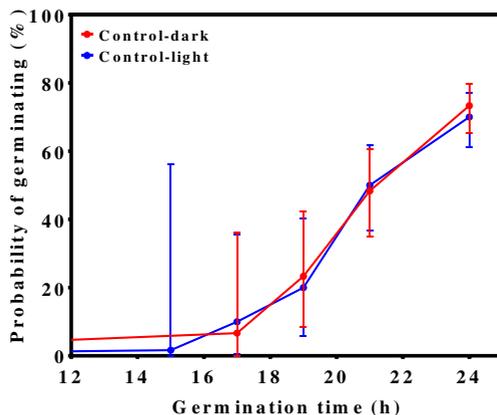
Figure 2. 15 Influence of light irradiation on germination rate of mung bean. Germination temperature is ca. 19 °C and humidity is ca. 40 %. 15 seeds are soaked in each Petri dish with 5 mL tap water for germination. The represented experiment is done with 120 seeds for each group. All the curves represent the Kaplan-Meier estimator of the probability of germinating, error bars represent the 95% confidence interval (Greenwood) and the P-value between each two groups is calculated based on Log-rank (Mantel-Cox) test.

In Figure 2. 15, the two curves show a same trend with a p-value of 0.807, indicating light irradiation is not a variable which is affecting the germination of a mung bean. Although, these two curves have several places where there is an interception, in Log-rank test, the assumption of proportional hazards here could still be valid when two curves are similar. Actually, light is generally a dispensable factor for common seed species during germination. In this work, experiments done in early time is irradiated with light but the rest are carried out in darkness during germination.

2.2.6.3 Germination temperature

Temperature is a sensitive variable affecting seeds germination. All the seeds tested in this work are bought from market for commercial use, which means those seeds are already in a state of maximum germination ability. In such cases, it is easy to influence the germination curve by changing the temperature, even in a small interval germination probably can significantly change. In this work, for each experiment the maximum temperature gradient is close to zero and less than 1 °C with and without light. Mung bean seeds is selected to germinate at 21 °C and 19 °C. In order to compare germination curves with seeds germinating in different temperatures, all the rest variables should be constant. Considering the fact that light irradiation has no influence on germination, 21 °C of germination temperature is achieved by light irradiation, while germinating in darkness is the way to keep germination temperature at 19 °C that is the room temperature.
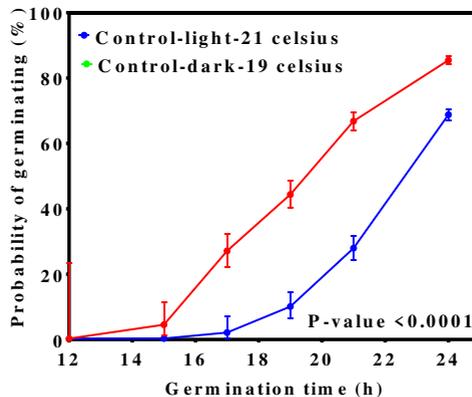
Figure 2. 16 Influence of temperature on germination rate of mung bean. 660 mung bean seeds are tested with germinating temperature at 21 °C and 1320 mung bean seeds are germinated at 19 °C. Germination humidity is ca. 40%. 15 seeds are soaked in each Petri dish with 5 mL tap water for germination. All the curves represent the Kaplan-Meier estimator of the probability of germinating, error bars represent the 95 % confidence interval (Greenwood) and the P-value between each two groups is calculated based on Log-rank (Mantel-Cox) test.

Apparently, Figure 2. 16 shows that the measured points of the germination curve with seeds germinating at 21 °C are almost three times higher than the seeds germinating at 19 °C in each germination time point. After germinating for 17 hours,

seeds under 19 °C start to germinate, while ca. 30% of seeds under 21 °C have already germinated. At 24 h, germination percentage of seeds under 21 °C is still 10% bigger than that of seeds under 19 °C. In summary, temperature is a variable which has a significant effect on germination. Therefore, in each independent experiment, experiment of control group is always carried out with corresponding treated group at the same time, and an appropriate statistical method is applied.

2.2.6.4 germination conditions

Based on the results of germination protocol optimization experiments, the germination conditions used in this study are: Seeds are placed in Petri dishes containing two layers of filter paper (WHA 1003055, Sigma Aldrich). Germination can either be processed with light or in darkness. When germination with light irradiation, seeds have grown under a 16-hour photoperiod of artificial light (horticultural dimmable LED panel providing two wavelength peaks at 460 nm and 636 nm; 150~260 µmol.m^{-2}.s^{-1}). Germination relative humidity range from 35 % to 45 %. Germination temperature is 19 °C if germinating in darkness and is 21 °C if germinating in light. A volume of 5 ml of liquid is added for soaking. The liquid is either tap water or NTP treated water. Each group (with 60~120 seeds) is repeated several times to assay the reproducibility of the experiments.

2.2.7 Protocol of water uptake of mung bean seeds

Seeds water adsorption is determined at room temperature (ca.18 °C) and relative humidity of ca 40 % using gravimetric method. Seeds that received different treatments are germinating in darkness. Before each weighting, water on the seeds surface coat is removed by absorbent paper. Water adsorption is the percentage of seeds weight increment of each time and is calculated with the formula below:

$$\text{Water adsorption increment} = \frac{W_{t_0} - W_t}{W_{t_0}} \qquad (2.12)$$

Where t_0 is the seeds initial weight and t is the weight after adsorption of each time point.

2.2.8 Morphological images of Mung bean seeds

Morphological images of mung bean seeds coat are characterized by Scanning electron microscopy (SEM, Hitachi S-4800, voltage is 1 kV). A ca. 7nm thickness of Au layer (30mA deposition current, Ar discharge and 40 s deposition time) is deposited onto the seeds coat surface to increase its conductivity by a sputter coater (EMTECH, K550X).

2.3 *Ex vivo* mice skin treatments

This section will introduce the NTP treatment setup, the Mueller polarimetric imaging setup, the protocols of skin treatment with a plasma jet and an oven, and the protocol of *ex vivo* Mueller polarimetric imaging with mice skin.

2.3.1 NTP source setup

The plasma jet is used to treat the mice skin. It is fabricated with the 3D printer and the detailed parameters of this setup has been described in the thesis of Dr Bruno Honnorat who used it to study the effect of this plasma jet on tumor therapy [101]. The brief structure parameters of this setup are described here and the photo of this setup is shown in Figure 2. 17. It is made of PLA. The helium gas is injected from top of the setup and passes through a vertical channel. The HV electrode is placed in a hole which is located at a distance of 60 mm to the gas outlet. A graphene is placed inside the hole to increase the conductivity of HV electrode. The HV electrode and the discharge gas is separated by a PLA layer with a diameter of 1 mm. The skin sample is grounded. NTP will be formed inside the gas channel and is blown out of the nozzle with a diameter of 2 mm and flows to the samples. Different distances of nuzzle to skin surface and input voltages are selected depending on the experiments. A power supply delivering sinusoidal waveforms with an amplitude in the range 0-7 kV at a frequency of 10 kHz is selected to produce the NTP using this setup.
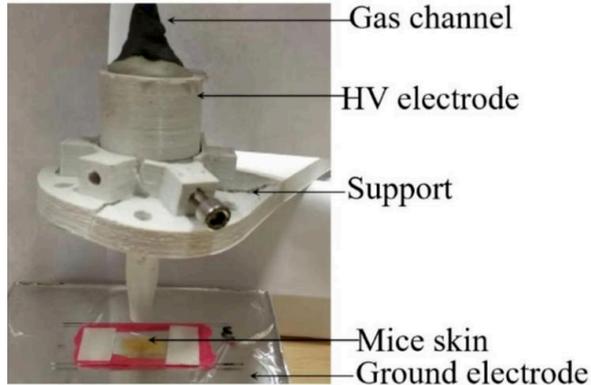
Figure 2. 17 The photo of NTP single jet

2.3.2 Mueller polarimetric imaging setup

The polarimetric setup used in this study is Mueller polarimetric imaging (MPI) operated in a backscattering configuration. Briefly, it is constituted by a LED lamp (Opto-Engineering LTPRW3W/W, 3 W power), a polarization state generator (PSG), a polarization state analyzer (PSA) and a Charge-Coupled Device (CCD) camera (Allied Vision Stingray F080B), as shown in Figure 2. 18. The LED lamp provides an incoherent white light which is used to illuminate the medium. PSG is aimed to modulate the incoming light into distinct specific polarization states and constructed by a linear polarizer and two tunable ferroelectric liquid crystal (LC) working as a quarter-wave plate with fixed retardation. PSA composes the same structure with PSG but in reverse order. Light goes through the PAG and interacts with medium, and the backscattered light from the medium is then collected and analyzed by PSA, and lastly measured by the intensity of the scattered light by the CCD with a resolution of 800×600 pixels. There is a filter wheel installed behind both the PSG and PSA, which is applied to hold the dichroic retarders and wavelength filters, respectively. Wavelengths of 550 nm and 650 nm, and a broad band optical filter (Thorlabs FB550-40, 40 nm FWHM) are selected in this study. 16 images corresponding to 4 different polarization states of incoming and outcoming light are collected to calculated the Mueller matrices of the medium at each wavelength
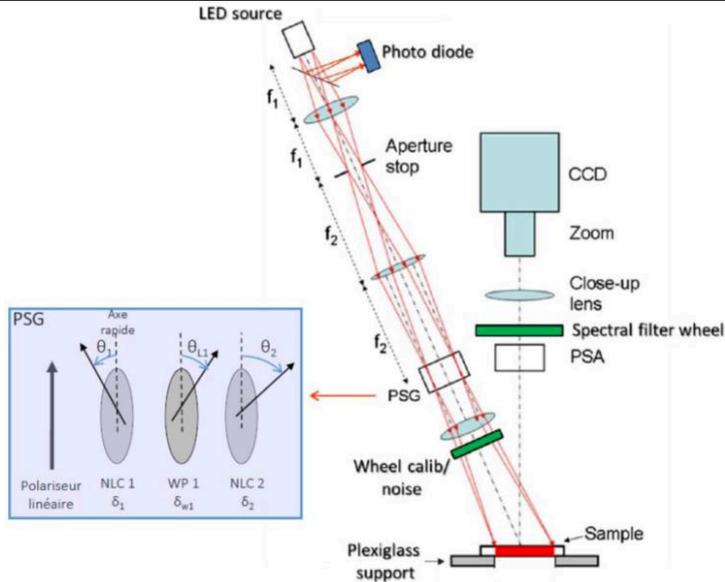
Figure 2. 18 Schematic of experimental setup for the backscattering Mueller matrix measurement *[239]*

2.3.3 Protocols of *ex vivo* mice skin treated by plasma jet treatments

There are two different ways to treat the mice skin with a plasma jet. The first way is called plasma continuous treatment in which the skin is treated by NTP continuously. The second way is called plasma sequential treatment. In this way, the skin is first treated by NTP for 1 min and then is measured with MPI. After the first measurement of MPI, the same skin is treated by NTP for another 1 min and then is measured with MPI for the second time. The same skin in the sequential treatment is treated by NTP for 9 times in total.

The procedures of plasma continuous treatments are:

1) Connecting the ground electrode on the surface of one side of a glass slide using an annular aluminum;

2) Putting the skin on the surface of other side of the glass slide;

3) Placing the sample under the nozzle of plasma jet, the distance of nozzle to skin surface is 10 mm;

4) Treating continuously different skins with the helium plasma jet for 0.5 min, 1 min, 2 min and 6 min, respectively;

5) Measuring the temperature of skin during the whole process of NTP treatment using the IR camera;

6) Placing the NTP treated skin on the surface of an ice before measuring with MPI.

The procedures of plasma sequential treatments are:

1) Treating the skin with NTP for 1 min based on the same procedures of plasma continuous treatments;

2) Placing the NTP treated skin on the surface of an ice before measuring with MPI;

3) Repeating the same procedures with the same skin for NTP treatment and MPI treatment in several times.

Discharge conditions for all NTP treatment are same. The helium flow rate is 1500 sccm, the distance of high electrode to skin surface is 10 mm and the input voltage is 15 kV peak to peak. The discharge power for all samples is around 2.8±0.3 W. Skin temperature is measured by an IR camera. The NTP treated skin is always stored on the surface of an ice before and after the measurement of MPI. We defined a term "SAP" to represent the zone of skin affected by the NTP treatment, and a term "SNAP" to represent the zone of skin non-affected by the NTP treatment. The untreated skin (without treated by NTP) is name with CTRL

2.3.4 Protocols of *ex vivo* mice skin treated by thermal treatments

There are two different ways to treat the mice skin with a heating. The first way is called thermal continuous treatment in which the skin is heated by an oven continuously. The second way is called thermal sequential treatment. In this way, the skin is first heated by an oven for 1 min and then is measured with MPI. After the measurement of MPI, the same skin is heated by oven for another 1 min and then is measured with MPI for the second time. The same skin in the thermal sequential

treatment is heated by oven for 6 times in total. The temperature of the oven selects 60 ℃ and 50 ℃. The thermally treated skin is always stored on the surface of an ice before and after the measurement of MPI.

The procedures of thermal continuous treatments are:

1) Putting the skin on the surface of a glass slide and keeping the initial temperature of skin is 20 ℃ (room temperature) before heating with the oven;

2) Heating continuously different skins in the oven for 1 min, 2 min and 6 min, respectively;

3) Measuring the temperature of skin right after the thermal treatment using the IR;

4) Placing the thermally treated skin on the surface of an ice before measuring with MPI.

The procedures of plasma sequential treatments are:

1) Putting the skin on the surface of a glass slide and keeping the initial temperature of skin is 20 ℃ (room temperature) before heating with the oven;

2) Heating the skin in the oven for 1 min;

3) Measuring the temperature of skin right after the thermal treatment using the IR;

4) Placing the thermally treated skin on the surface of an ice before measuring with MPI;

5) Repeating the same procedure with the same skin for thermal treatment and MPI treatment in several times.

2.3.5 Protocol of Mueller polarimetric imaging of mice skin measurement

The measurement method of MPI of medium can be generally divided into the following steps:

6) Calibrating MPI with a rough metallic plate based on the procedure of Eigenvalues Calibration Method (ECM) [256];

7) Importing the parameters of measurable wavelengths (550 nm) and image numbers of acquisition (16);

8) Selecting suitable exposure time based on different skin samples;

9) Measuring the Mueller matrices of skin samples;

10) Collecting the data from camera with LabVIEW;

Decomposing the Mueller matrices of skin samples based on the method of Lu and Chipman algorithm using MATLAB

2.4 Statistical method for data analysis

Statistical analysis is performed to find if the different treatments have a biological effect or not. The aim is to determine if the treated groups are significantly different from a control group, which is not treated. The null hypothesis H0 is the statement that there is no relationship between two measured phenomena. It is crucial to test H0, from the result of this test it can be concluded whether there are grounds to believe in a relation between the two phenomena. The p-value is used to quantify the statistical significance of a result under the assumption that H0 is true. A statistically significant result is an outcome that would be unlikely if the null hypothesis was verified. The p-value is the probability to obtain the actual observed results when H0 is true. If the p-value is less than the chosen significance level (α), the observed data is sufficiently inconsistent with H0 and H0 may be rejected. Here $\alpha = 0.05$ is chosen. In this work, the survival test is used for statistical analysis.

2.4.1 Principle of survival analysis

Survival analysis is a branch of statistics used to analyze the expected time duration for one or more events to happen. Survival analysis attempts to answer what the proportion of an event which will survive past a certain time duration is, and if

and to what extend a particular characteristic increases or decreases the probability of survival. In the case of survival, events can be a death in biological organisms, the failure in mechanical systems and even a changing of data. Traditionally only a single event occurs for each subject, after which it is dead, broken or occurred. The theory outlined below assumes well-defined events at specific times; other cases may be better treated by models which explicitly account for ambiguous events. The study of recurring events is relevant in system reliability, and many areas of social sciences and medical research. In this work, the time starts at the beginning of a germination observation to the end of this process. The subject, here is seed, the germination is treated as an event. The survival function is the probability that a subject is subject to an event during the observation time. If a subject does not encounter an event at the end of germination process, it is called as censored.

The survival function can in general be calculated by several methods:

1) To describe the survival times of members of a group
    i) Life tables
    ii) Kaplan-Meier curves
    iii) Survival function
    iv) Hazard function

2) To compare the survival times of two or more groups
    i) Log-rank test
3) To describe the effect of categorical or quantitative variables on survival
    i) Cox proportional hazards regression
    ii) Parametric survival models
    iii) Survival trees
    iv) Survival random forests

2.4.2 Methods used in this work

In this work, Kaplan-Meier model and Cox model were chosen for survival analysis.

Macro-commands programmed in VBA are used to format the data in Microsoft

Excel. The statistical analysis is performed in software environment R [188] and packages "survival" [257], "muhaz" [258] and "survminer" [259] are used. The graphs are drawn with GraphPad Prism version 6.01 for Windows, (GraphPad Software, La Jolla California USA, www.graphpad.com). Solid lines represent the Kaplan-Meier estimator; the error bars represent the 95% confidence interval computed according to Greenwood asymmetrical formula [260]. The Cox model of shared frailty is used to analyze series of data [261, 262].

2.4.2.1 Kaplan-Meier model

The Kaplan-Meier model or Kaplan-Meier survival estimator is a non-parametric statistic used to estimate the survival function from event data [263, 264]. It takes the censored data into account and requires few assumptions. During the experiments, the number of germinated seeds is observed as a function of time in discrete time points. The graph representing the Kaplan-Meier curve is an estimator of the probability of germinating of a group. The survival function $S(t)$ for this work is calculated with the formula below:

$$\hat{S}(t) = \prod_{0 \leq t \leq T}(1 - h_t) \tag{2. 13}$$

Where t is a time when at least one event occurs before the end of observation time T, h_t is ratio of the number of events (germinated seeds) and the subjects (seeds) known to germinate (have not yet had an event or been censored) at time t.

Although the Kaplan-Meier estimator is one of the most frequently used methods of survival analysis, its usability is limited for multi independent variables comparisons, continuous independent variables and survival adjusted by covariates. In this work, the objective is to quantify the differences between the multi treated groups and control groups, treated groups between each-over and to determine if plasma treatment modifies the instantaneous probability of germinating at any time. In addition, plasma is a complex multi parameters mixture, which means such survival curve is probably affected by more than one variable or even by covariables. It is therefore necessary to further investigate these systems with other more useful models. There are statistical methods to treat this kind of data and provide a p-value for comparing multi control and treated groups. For example, the Cox Model is a

method, which provides p-values and a quantification of the difference between two groups [261, 262]. In this work, the Cox model was chosen to compare difference among multi variables and to analyze how different they are.

2.4.2.2 Cox model

Cox regression is a model using parent-number analysis for exploring the relationship between the survival of an event and several explanatory variables. The purpose of the Cox statistical analysis is to seek which variable has the most important impact on the occurring of an event (here is germination). When discussing cox regression, there are two parts that need to be clarified first, namely the survival function and the hazard (or risk) function.

The survival function is the probability that a subject can survive after a time point that is expressed by *t*. The function can be estimated by the one below:

$$S(t) = P(T > t) = \int_t^\infty f(u)du \qquad (2.\,14)$$

where *S(0)* equal to 1 and *S(∞)* equal to 0.

The hazard function *h(t)* is the probability that an individual (here is seed) will experience an event (here is germination) within a time interval approaching zero, given that the individual has survived up (here is germinated seed) to the beginning of the interval. The hazard function is given by

$$h(t) = \frac{\frac{-d[S(t)]}{dt}}{S(t)} = \frac{f(t)}{S(t)} \qquad (2.\,15)$$

Where *t* is the time point. The hazard function *h(t)* is related to the lifetime, which represents the probability of event divided by the value of the survival function at a certain point in time. The longer the time (the larger *t*), the smaller the survival function *S(t)* (the survival function is the decrement function). When it is assumed that the probability density *f(t)* is the same for any point in time, increasement in the risk function value *h(t)* implies shortening of the expected survival time.

Experimental materials and methods

The instantaneous hazard rate is the limit of the number of events per unit time divided by the number at risk within a time interval approaching zero [265]. Here the instantaneous risk of germination is the limit of the number of germinated seeds per unit time divided by the number of non-germinated seeds, as the time interval trend towards 0. The formula is given below.

$$h(t) = \lim_{\Delta t \to 0} \frac{P(\leq T < t + \Delta t / T \geq t)}{\Delta t} = \frac{-\partial S(t)/\partial t}{S(t)} \tag{2.16}$$

where T is the time variable and t is the time point.

Combine equation 1.1 and 2.1,

$$S(t) = exp(-\int_0^t h(u)du) \tag{2.17}$$

$$h(t) = \lambda \tag{2.18}$$

$$S(t) = exp\left(-\int_0^t h(u)du\right) = exp(-\lambda t) = e^{-\lambda t} \tag{2.19}$$

$$f(t) = h(t) * S(t) = \lambda e^{-\lambda t} \tag{2.20}$$

When studying hazards time zero covariates (initial factors), it is assumed that these factors have a consistent proportion of hazards' effects and risk ratio for a certain risk factor cannot be changed over time. This is a very important hypothesis, that is called the Proportional Hazard hypothesis (PH hypothesis), it has to be verified first. Under such a PH hypothesis of the classic Cox regression, the ratio of the instantaneous risk of germination of treated groups and control group is deemed as constant. Because the λ is a constant, the Cox regression can be therefore induced with the formula below:

$$log(HR(X)) = log\left(\frac{h\left(\frac{t}{x}\right)}{h_0(t)}\right) = \beta_1 x_1 + \beta_2 x_2 + \cdots + \beta_k x_k + \varepsilon \tag{2.21}$$

Where β is the regression coefficient for all of the predictors (or independent variables) x.

Hazard ratio *(HR(X))* in Cox model is a specific value of the predicted hazard for two risk rates which correspond to the conditions described by two levels of

covariable *X*. It is interpreted as the survival chance. The ratio of the hazard functions is given by regression coefficient β which is the estimator of treatment effect. A positive regression coefficient for an explanatory variable, in this work, means that the hazard for seed germination having a high positive value on that particular variable is high. Conversely, a negative regression coefficient implies a better prognosis for germination with higher values of that variable.

To be noticed, the Cox model in this work takes frailty and crossing of survival curves into account.

The frailty is a model which provides an evaluation for random factor effect from associated but unobserved heterogeneity. This unobserved random factor could modify multiplicatively the hazard function of one or multiple subjects. We consider that control and treated groups share the same frailty. However, the data which used to build survival curves are usually done in different days, especially for repetitive tests. It will less reasonable to attribute the so called "overnight" independent tests share a same frailty without any verified. Such question is addressed by the so-called "time-to-event analysis", which are also used for survival analysis in medicine. Cox proportional hazard modelling is one of the models analyzing time-to event. Such analysis enables to take into account and quantify the effect of frailty, which is not the case with a stratified analysis along the day of the experiment or, much worse, data pooling without precaution.

In the absence of a clear violation of the hypothesis of Proportional Hazard (PH) required by Cox model, the first step of the analysis is to test if the frailty term must be taken into account or not. If the frailty term is associated with a p-value < 0.05, the term is kept in further analysis, else the data corresponding to the different days of the experiment are pooled [261]. The validity of PH hypothesis was systematically analyzed with the Schoenfeld Residuals Test (SRT). PH hypothesis is not rejected when the p-value of the SRT is ≥ 0.05. In this case, Cox model is valid and the p-value (with or without frailty term) between treated and control group will be computed. Ratio of the risk of germination of treated group vs. control group then will be obtained. The increase in the probability of germinating of treated group vs. control group was reported in the form of. For instance, a ratio of 1.6 will be reported as an increase of the instantaneous risk of germination of +60% of treated group

compared to its corresponding control group. However, if PH hypothesis was rejected, the building of two Cox models then was tried for a partition in two time-subsets defined by t $<$ ti and t $\geq$ ti, in which *t* is the germination time and *ti* is the subset germination time. If PH hypothesis was verified separately in the two subsets, the result will be calculated and reported in the tables 1-2. Otherwise, the increase in the instantaneous probability of germinating due to NTP treatment will not be defined and only the p-value given by the Mantel-Haenszel test stratified along the days of the experiments will be reported. In another case, if there is a crossing among the probability of germination curves, which also implies a violation of PH hypothesis, the building of two Cox models is tried for the two time-subsets preceding and following the crossing. If PH assumption is rejected and no crossing of survival and hazard function is observed, the use of Cox model is rejected. The p-value enabling the comparison of germination curve is then calculated with the Mantel-Haenszel test stratified along the days of the experiments. However, in these two situations, Mantel-Haenszel tests lose power: it means that the probability of rejecting the null hypothesis when the alternative hypothesis is true is lower than in the case where PH hypothesis is true. Nevertheless, the test can still be used [260]. If p<0.05 we consider that there is a significant difference between treated and control seeds. If p>0.05 the consideration regarding the power of the test does not allow to conclude and it would be necessary to develop more complex model; for example time-dependent Cox model [260]. This last case was not encountered since all the violation of PH-assumption were overcome either by the building of Cox models in two time-subsets (if PH hypothesis is verified separately in these two subsets) or the observation that the Mantel-Haenszel test rejects the null hypothesis. When PH assumption is verified, the increased risk of germination of treated group compared to control group was obtained.

2.4.2.3 Log-rank test

The log-rank test that is equivalent to the Mantel Haenszel method is a hypothesis test to compare the hazard functions of two survival distributions at each observed time if the assumption of PH is true. If the calculated P-value is lower than 0.05, the two groups of survival curve have a statistically significant difference, otherwise, they are possessing a same distribution. If there is a crossing between two

survival curves, then one group has a higher risk at early time points and the other group has a higher risk at late time points. This could just be a coincidence of random sampling, and the assumption of proportional hazards could still be valid. But if the sample size is large, the log-rank can only be helpful with two independent analysis in each separate part when the survival curves cross near the middle of the time course.

Experimental materials and methods

Chapter 3: Non-thermal Plasma-liquid Interaction

This chapter aims to investigate the physical and chemical processes of plasma-liquid interaction using cylindrical Dielectric Barrier Discharges. We want to characterize and quantify the reactive species produced in gas and liquid phase. Two types of reactors, described in detail in Chapter 2 are used in the present chapter. First, a single electrode plasma setup used for the study of plasma-liquid process is designed into 4 different configurations. As described in chapter 2, this reactor is a closed reactor where the gas composition and the presence of water can be controlled independently using inlets and outlets. Second, a 9-electrode DBD plasma setups is characterized in order to be used in Chapter 4 and 5 for seeds germination. This reactor may be flown by various gases but is open Air contrary to the single electrode reactor described before. The NTP are produced in different gases, which are Air, N_2 or O_2. The produced NTP either touch the water surface and are called a touching plasma, or they do not touch the water surface and are called a non-touching plasma as described in Chapter 2 (Figure 2. 2). For the sake of clarity, a similar figure showing the different configurations is shown in Figure 3. 1.

The main difference between "touching" and "not-touching" configurations is that in the non-touching case, the ground is located outside the DBD tube in a cylindrical geometry. Only the flowing post-discharge is in contact with the water. On the other hand, in the touching case, the NTP are ignited between the tip of the electrode and the surface of the water, and is in direct contact with the water.

The gas flowing though the DBD tube(s) may also bubble inside the water. The non-touching plasma are divided into non-touching non-bubble plasma (NNP) and the non-touching bubble plasma (NBP) depending if there is water on the bottom of plasma reactor or not (Figure 3. 1). In this chapter, the NNP is used to diagnose the reactive gaseous species whereas the NBP are applied to detect the reactive species formed in the treated liquids. The touching plasma can also be divided into touching

non-bubble plasma (TNP) and touching bubble plasma (TBP), depending if the gas channel is immersed in the water or not (Figure 3. 1). In this chapter, the TNP is mainly used to determine the physical properties of touching plasma whereas the TBP is used to study the effect of the plasma parameters on the production of long-lived species in liquid. TBP is also used to determine the best conditions for seeds treatment.

After a somehow detailed characterization of the single DBD discharge tube in the four operating conditions listed above (touching vs non-touching, bubbling vs non-bubbling), the 9-electrode plasma reactor using for seeds treatments is characterized in order to quantify reactive species produced in water.
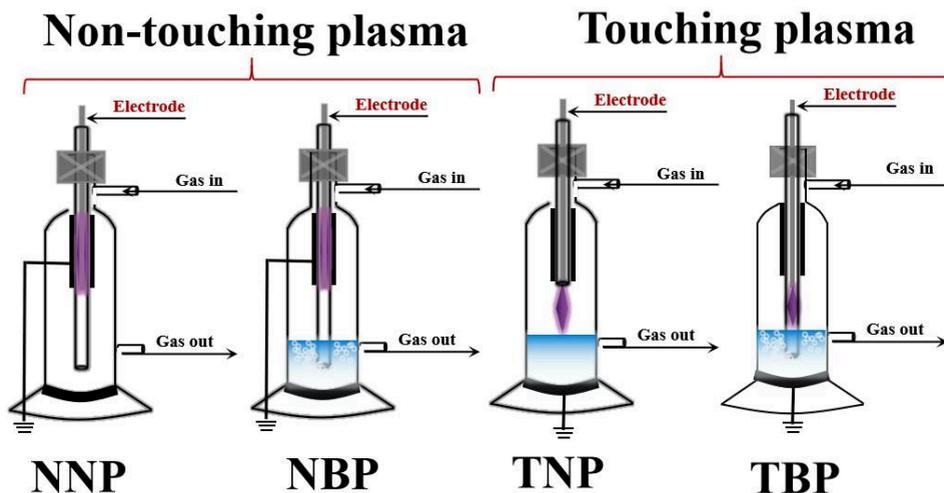
Figure 3. 1 Schematic of single electrode DBD plasma setup in different configurations. NNP is non-touching non-bubble plasma, NBP is non-touching bubble plasma, TNP is touching non-bubble plasma and TBP is touching bubble plasma. The device is made of glass tubes and the diameter of the inner glass tube is 3 mm. High voltage electrodes are stainless-steel and an annular aluminum is used as ground electrode and series connected with a 1 nF capacitor for the power calculation. The high voltage power supply delivers bipolar square waveform with amplitude in the range 0-18 kV at a frequency of 500 Hz. Liquid is placed on the bottom of the bigger diameter glass cylinder for NTP treatments.

This chapter is organized in 3 different parts. The first section is to diagnose the plasma reactive species formed by the single electrode plasma setup and to analyze the potential formation pathways of the selected aqueous species. The second section

is to investigate the physical property of touching plasma and the effect of discharge parameters on the production of aqueous reactive species using the single electrode plasma setup. The last section is to quantify the amount of aqueous species produced by the 9-electrode plasma setup.

The discharge parameters can be optimized by choosing the best discharge conditions, in order to do so the concentration of NO_2^-, NO_3^- and H_2O_{2aq} in the NTP treated water have to be evaluated. By choosing proper discharge conditions, the performance in producing the chemical compounds can be optimized. The adjustable parameters are the discharge voltage, the gas flow rate, the discharge time and the electrode height. A single electrode plasma reactor will be used to optimize the parameters in the touching bubble plasma configuration. The discharge gas consists of O_2, N_2, Air and Ar. The conditions of each parameter that are tested are:

1) Discharge voltage selects 15 kV, 17.5 kV, 20 kV, 22.5 kV and 25 kV;

2) Gas flow rate includes 50 sccm, 100 sccm, 200 sccm, 300 sccm and 600 sccm;

3) Discharge time chooses 0.5 min, 1 min, 2 min, 4 min and 6 min;

4) Electrode height contains 3 mm, 5 mm, 7 mm, 10 mm and 14 mm.

3.1 Diagnosis of plasma reactive species in gaseous and aqueous phases

We use multiple characterization methods to identify and/or quantify the plasma reactive species produced by NTP in the gaseous and the aqueous phases (Chapter 2). FTIR enables to measure simultaneously different species in the gas phase. Using ozone analyzer, we can rapidly obtain the concentration of gaseous ozone (O_{3g}) for concentration above 0.1 ppm. Using NOx analyzer, we synchronously measured the concentration of gaseous nitric oxide (NO_g) and gaseous nitrogen dioxide (NO_{2g}) (measurable limitation of 0.4 ppb). In order to measure NO_2^-, NO_3^- and H_2O_{2aq} in the liquid phase we used spectrophotometry methods.

3.1.1 Measurement of the reactive species produced by NTP in the gaseous phases

3.1.1.1 Measurement of gaseous species produced by non-touching plasma

1) Concentration of O_{3g}

Let us now check the Non-Touching plasmas condition, when the NTP are ignited inside the DBD tube; The conditions may be dry or humid (without liquid water), or with liquid water at the bottom of the reactor. In this latter case, the flowing post-discharge is in contact with the water in bubbling or non-bubbling mode. The concentrations of O_{3g} produced both in dry (the solid lines) and humid gas (the dash lines) are quantitatively measured by an O_{3g} analyzer. We studied the effect of the gas flow rate but also of the nature of the used gas on the O_{3g} production (Figure 3. 2).

No O_{3g} is detected in N_2 discharges. O_{3g} productions of Air discharges (Figure 3. 2a) and O_2 discharges (Figure 3. 2b) are significantly affected by the flow rate. Between 150 and 250 sccm, O_{3g} concentration increases with the flow rate for all discharges. However, O_{3g} concentration gradually decreases when the flow rate is above 250 sccm. No difference can be seen between Air-NBP and Air-NNP in terms of O_{3g} concentration. Regarding gas humidity, we can also observe that dry O_2-NNP gives a similar O_{3g} production as dry O_2-NBP. However, less O_{3g} is produced by

humid O_2-NBP compared to dry O_2-NBP, especially at low flow rate. Both dry Air and O_2 discharge produce more O_{3g} than humid gas discharge at the same flow rate. The amount of O_{3g} produced by both dry and humid O_2 NTP is higher than Air discharge at the same flow rate. The maximum O_{3g} concentration is about 392 ppm for dry Air NTP, 157 ppm for humid Air NTP, 657 ppm for humid O_2 NTP and over 900 ppm for dry O_2-NNP and O_2-NBP. Note that there is a strong error bar in the curves of dry O_2 NTP when flow rate below 250 sccm. This error bar induces a significant difference in the concentration of O_3 between dry O_2-NNP and O_2-NBP. This is mainly due to the fact that the discharge of dry O_2 is not stable at the low flow rate.
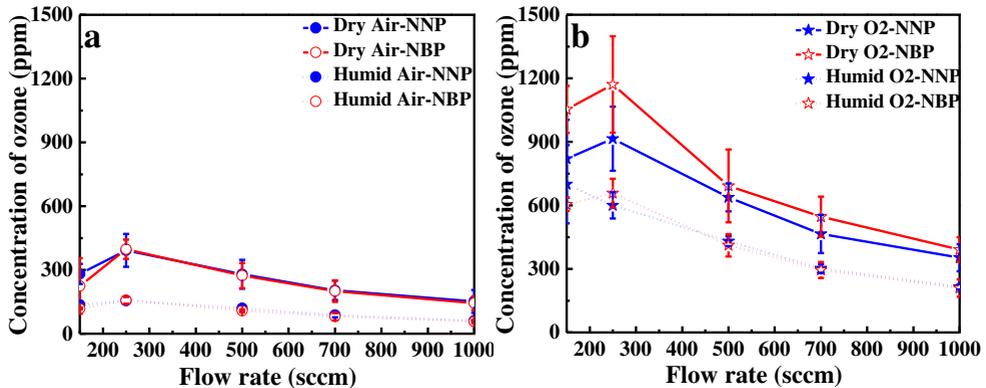
Figure 3. 2: Concentrations of O_{3g} measured by ozone analyzer. a is the Air discharge and b is the O_2 discharge. All concentrations of ozone are recorded when the production of ozone becomes steady. Discharge conditions: 20 kV of input voltage, 1000 sccm of gas flow rate (N_2 is used as a balance gas and used to make the whole flow rate reach 1000 sccm), treatment time = 4 min. Discharge power of gases are 312±49 mW for dry Air, 322±37 mW for humid Air; 293±43 mW for dry O_2, 321±35 mW for humid O_2 and 271±4 mW for dry N_2. Humid gases are saturated gases at 20 °C. For bubble NTP, the volume of water is 5 mL and the 1mm of the inner tube is immersed in water. Results are represented as mean ± standard deviation.

Non-bubble plasmas and the one of bubble plasma lead to very similar production of ozone in the gas phase. Besides, water vapor decreases the production of O_{3g} formed by Air and O_2 discharge. This is because ozone is mostly formed by the recombination of O_g atoms and O_{2g} molecules [266], but the existence of H from the dissociation of water vapor can consume the O_g radicals forming OH_g radical [121].

2) Measurement of reactive species in gas phase using infrared spectroscopy

The results are shown in Figure 3. 3. The infrared spectrum of dry Air-NNP shows the peaks of O_{3g} at 1050 cm^{-1} and 2100 cm^{-1}, the peak of HNO_{3g} at 1310 cm^{-1} and the peak of N_2O_g at 2200 cm^{-1}. Infrared spectrum of dry O_2-NNP only shows the peaks of O_{3g} at about 1050 nm and 2100 cm^{-1}. No peak is observed iwo daon the spectrum of dry N_2-NNP, which was expected. In the discharge in dry Air, the infrared peak of NO_g (1858 to1902 cm^{-1}) is not observed.
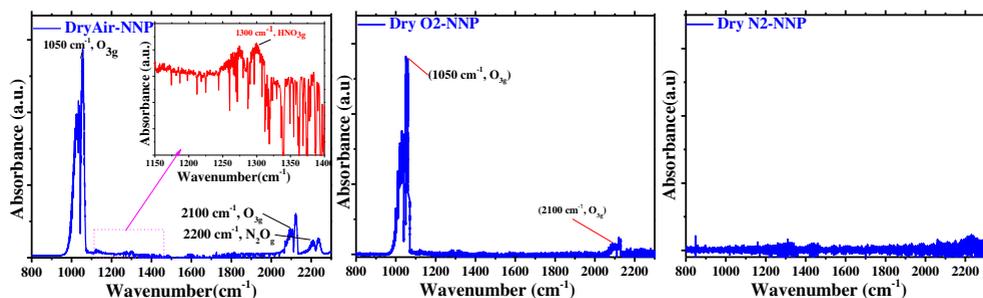
Figure 3. 3 Infrared spectra of feed gases of dry Air, O_2 and N_2. Discharge conditions for all discharges: 20 kV of input voltage, 1000 sccm of gas flow rate (300 sccm of discharge gas and 700 sccm of N_2). Discharge power of gases are 312±49 mW for Air; 293±43 mW for O_2 and 271±4 mW for N_2. The peaks of 1050 cm^{-1} and 2100 cm^{-1} are O_{3g}, the peak of 1310 cm^{-1} is HNO_{3g} and the peak of 2200 cm^{-1} is N_2O_g.

NO analyzer (detection limit equals to 0.4 ppb) can measure an even lower concentration of NO_g than the current FTIR, but does not detect any NO_g. These results indicate that the NO_g may be rapidly oxidized into other reactive nitrogen species. This has been recently reported by Sivachandiran et al. that the concentration of NO_g and NO_{2g} produced in a DBD plasma decreases with increasing concentration of O_{3g}. Authors showed that all NO_g and NO_{2g} are converted into N_2O_5 and/or HNO_{3g} when amount of O_{3g} exceeds the amount of NO_g [267]. In our study, the transit time between the reactor and the detection is ca. 1.4 seconds in the case of the NO_x detector and more than 2 min in the case of FTIR (the volume of the gas cell is 2 L). Then, all the NO_g and NO_{2g} are oxidized into dinitrogen pentoxide (N_2O_5) and/or HNO_{3g} by the large amount of O_{3g} (more than 300 ppm, *cf.* Figure 3. 2) produced by Air discharges. N_2O_5 is an unstable oxidizer and is existed in a solid state under room temperature, which is not shown in the infrared spectra. HNO_{3g} peaks is visible in the infrared spectra. NO_{2g} can react with water vapor to form

HNO$_{3g}$ and the water vapor comes from Air bottle.

3.1.1.2 Measurement of gaseous species produced by touching plasma

1) Concentration of O$_{3g}$
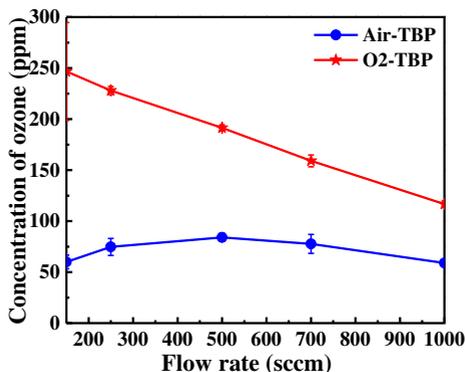
Figure 3. 4 Concentrations of O$_{3g}$ measured by ozone analyzer. All concentrations of ozone are recorded when the production of ozone becomes steady. Discharge condition are similar for all NTP: 20 kV of input voltage, 1000 sccm of gas flow rate (N$_2$ is the balance gas and used to make the whole flow rate reach 1000 sccm), 7 mm of height of HV electrode to water surface and 4 min of treatment time. Discharge power of gases are 533±14 mW for Air, 564±18 mW for O$_2$ and 510±15 mW for N$_2$. For bubble NTP, the volume of water is 5 mL and the inner tube is immersed in water for 1 mm. Results are represented as mean ± standard deviation.

Let us now check the touching plasmas condition, when the NTP are ignited between the high voltage electrode and the surface of the water in bubbling or non-bubbling mode. The concentrations of O$_{3g}$ produced by Air-TBP, N$_2$-TBP and O$_2$-TBP are shown in Figure 3. 4. O$_{3g}$ concentrations of O$_2$-TBP continuously decrease as the gas flow rate increases. No O$_{3g}$ can be detected in N$_2$-TBP, meaning that despite the presence of water vapor, ozone is not produced in our conditions with a nitrogen NTP. The effect of the gas flow rate on the production of O$_{3g}$ is less important than in Air-TBP. Compared with non-touching plasmas (Figure 3. 2), the amount of O$_{3g}$ produced by touching plasmas are significantly lower. The maximum of O$_{3g}$ concentration is 246 ppm for O$_2$-TBP and 84 ppm for Air-TBP.

2) Measurement of reactive species using infrared spectroscopy

The infrared spectra of gaseous species of touching bubble plasmas are shown in Figure 3. 5. Infrared spectrum of Air-TBP is similar to the one of Air-NNP, which shows the peaks of O_{3g} at 1050 cm^{-1} and 2100 cm^{-1}, the peak of HNO_{3g} at 1310 cm^{-1} and the peak of gaseous N_2O at 2200 cm^{-1}. Infrared spectra of O_2-TBP only shows the peaks of O_{3g} at about 1050 nm and 2100 cm^{-1}. No infrared peak is observed in the spectra of N_2-TBP.
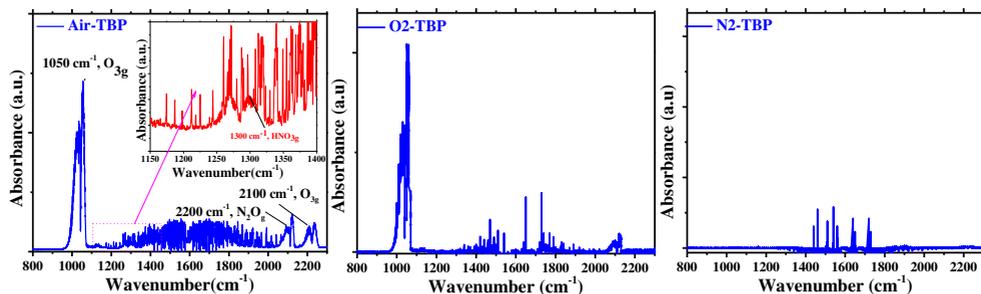
Figure 3. 5 Infrared spectra of feed gases of discharges of dry Air, O_2 and N_2. Discharge condition for all touching bubble plasmas is the same, it is 20 kV of input voltage, 7 mm of height of HV electrode to water surface, 1000 sccm of flow rate (300 sccm of discharge gas and 700 sccm of N_2) and 8 min of treatment time. Discharge power are 633±14 mW for Air, 664±18 mW for O_2 and 610±15 mW for N_2. For bubble NTP, the volume of water is 5 mL and the inner tube is immersed in water for 1 mm. The peaks of 1050 cm^{-1} and 2100 cm^{-1} are O_{3g}, the peak of 1310 cm^{-1} is HNO_{3g} and the peak of 2200 cm^{-1} is N_2O_g.

3.1.2 Measurement of plasma reactive species in the liquid phase

In this section we quantified the concentrations of NO_2^- and H_2O_{2aq} produced by touching plasmas in the liquid phase using spectrophotometric methods. NO_2^- is detected using Griess reagent and H_2O_{2aq} is measured using Copper (II) ion and 2,9-dimethyl-1,10-phenanthroline (DMP) (see section 2.2.3). The detection limits of these two methods are 1 µM and 5 µM, respectively.

3.1.2.1 Diagnostics of aqueous species produced by Non-touching Bubbling Plasmas

Concentrations of NO_2^-, NO_3^- and H_2O_{2aq} produced by NBPs for different gas flow rates are shown in Figure 3. 6. The blue color represents the H_2O_{2aq}, the red color represents the NO_3^- and the pink color represent NO_2^-. The solid lines represent

the concentration curves of the species produced by the dry gases discharges and the dash lines represent the concentration curves of the species produced by the discharges of humid gases.
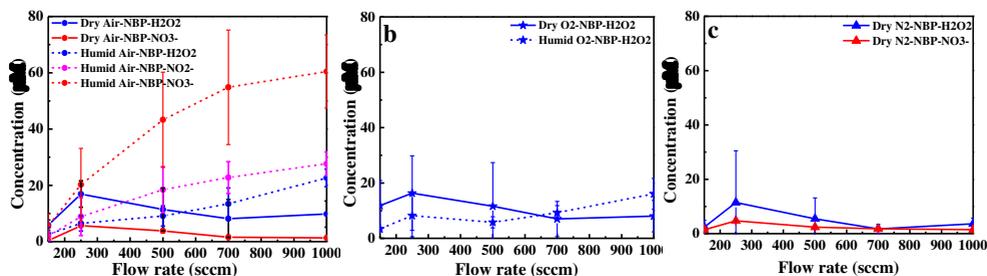
Figure 3. 6: Concentrations of NO_2^-, NO_3^- and H_2O_{2aq} produced by NBPs at different flow rates. Discharge condition for all NTP: 20 kV of input voltage and 4 min of treatment time. Discharge power of gases are 312±49 mW for dry Air, 322±37 mW for humid Air; 293±43 mW for dry O_2, 321±35 mW for humid O_2 and 271±4 mW for dry N_2. Volume of water is 5 mL and the inner tube is immersed inside water for 1 mm. Results are represented as mean ± standard deviation.

In the case of dry gases discharge, H_2O_{2aq} and a small amount of NO_3^- are detectable in the water treated by Air-NBP and N_2-NBP. However, NO_2^- could not be measured (below 1 μM). Only H_2O_{2aq} is detected in the water treated by O_2-NBP (figure 3.5b). Production of NO_2^-, NO_3^- and aqueous H_2O_2 is affected by flow rate. Aqueous H_2O_2 concentration produced by dry Air-NBP is similar to the one produced by dry N_2-NBP and O_2-NBP. In both cases, the concentration increases when the gas flow rate increases from 150 sccm to 250 sccm, but then decreases when flow rate is greater than 250 sccm. These results are also true for NO_3^-. Maximum concentration of NO_3^- and H_2O_{2aq} is 5.6 μM and 17 μM respectively. NO_2^-, NO_3^- and H_2O_2 are detected in the water treated by humid Air-NBP. Only H_2O_{2aq} is detected in the water treated by humid O_2-NBP. Unlike NBPs of dry gases, the production of all aqueous species in humid gases NBPs are increased rather than reduced when flow rate exceeds 250 sccm. Production of H_2O_{2aq} of humid Air-NBP is slightly higher than humid O_2-NBP at the same flow rate. Maximum concentration of H_2O_{2aq} for humid Air-NBP and humid O_2-NBP is about 23 μM and 18 μM. Amounts of NO_2^- in discharges of dry Air-NBP are too low to be detected, but in Air-NBP NO_2^- concentration significantly increased to peak at 28 μM. The amount of NO_3^- is about 2-3 times higher than the amount of NO_2^-. NO_3^- concentration peak

is at 60uM at a 1000 sccm.

3.1.2.2 Measurement of aqueous species produced by Touching Bubbling Plasmas
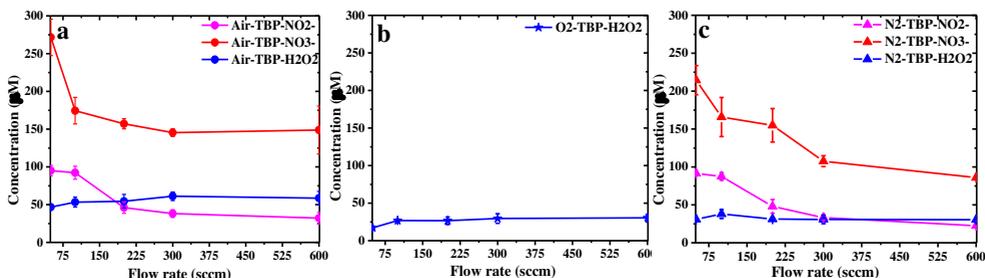
Figure 3. 7 Concentrations of NO_2^-, NO_3^- and H_2O_{2aq} produced by Air touching bubble plasma (a), O_2 touching bubble plasma (b) and N_2 touching bubble plasma (c) at different flow rates. All concentrations of aqueous species are the total production of 2 min of NTP. Discharge condition for all NTP is similar for all the devices: 20 kV of input voltage, 7 mm of height of HV electrode to water surface and 2 min of treatment time. Average discharge power of Air, N_2 and O_2 discharge is respectively about 634 mW, 627 mW and 691 mW. The volume of water is 3 mL and the inner tube is immersed in water for 1 mm. Results are represented as mean ± standard deviation.

Concentrations of NO_2^-, NO_3^- and H_2O_{2aq} produced by TBPs at different gas flow rates are shown in Figure 3. 7. The blue color represents the H_2O_{2aq}, the red color represents the NO_3^- and the pink color represent NO_2^-. In the case of TBPs, NO_2^-, NO_3^- and H_2O_{2aq} can be detected in the water treated by both Air-TBP and N_2-TBP. However, only H_2O_{2aq} is detected in the water treated by O_2-NBP. Production of NO_2^- and NO_3^- of Air-TBP and N_2-TBP strongly depend of the flow rate. Indeed, their concentrations strongly decrease with the flow rate. However, the production of H_2O_{2aq} does not depend of the flow rate for all the TBP. Air-TBP produce a similar amount of NO_2^- than N_2-TBP, but produce more NO_3^- than N_2-TBP. The amount of NO_3^- produced by both Air-TBP and N_2-TBP is higher than the amount of NO_2^- produced by the two devices. The amount of aqueous H_2O_2aq produced by N_2-TBP is similar to the one produced by O_2-TBP but is lower than the one produced by Air-TBP. At a flow rate of 50 sccm, the water treated by N_2-TBP contains about 100 μM of NO_2^- and 225 μM of NO_3^-. The water treated by Air-TBP contains about 100 μM of NO_2^- and 275 of μM NO_3^-. When flow rate is increased to 600 sccm, the concentration of NO_2^- in the water treated by Air-TBP and N_2-TBP is reduced to

about respectively 40 μM and 35 μM, whereas the concentration of NO_3^- is decreased to 100 μM in the water treated by N_2-TBP and to 175 μM in the water treated by Air-TBP. Average concentrations of H_2O_{2aq} in the water treated by Air-TBP, N_2-TBP and O_2-TBP are 50 μM, 42 μM and 38 μM, respectively.

3.1.3 Analysis of the formation of NO_2^-, NO_3^- and H_2O_{2aq} produced by Non-Touching Bubbling Plasmas and Touching Bubbling Plasmas

In this section, the potential pathways of aqueous NO_2^-, NO_3^- and H_2O_{2aq} formation are analyzed. As discussed in section 1.2.2.2 (Chapter 1), the formation pathways of H_2O_{2g} can be due to the combination of radical of OH_g (Equation 3.1) and HO_{2g} (Equation 3.2) and the formation pathways of H_2O_{2aq} can be due either to the following reaction in liquid (Equation 3.3 and Equation 3.4) or to the solvation of gaseous H_2O_{2g} (Equation 3.5). As shown below:

$$OH_g + OH_g \rightarrow H_2O_{2g} \tag{3.1}$$

$$HO_{2g} + HO_{2g} \rightarrow O_{2g} + H_2O_{2g} \tag{3.2}$$

$$OH_{aq} + OH_{aq} \rightarrow H_2O_{2aq} \tag{3.3}$$

$$HO_{2aq} + HO_{2aq} \rightarrow O_2 + H_2O_{2aq} \tag{3.4}$$

$$H_2O_{2g} + H_2O \rightarrow H_2O + H_2O_{2aq} \tag{3.5}$$

NO_2^- and NO_3^- can be formed via aqueous reactions (Equation 3.6, Equation 3.7 and Equation 3.8) or through the solvation of gaseous species (Equation 3.9 and Equation 3.10). As shown below:

$$NO_{aq} + OH_{aq} + H_2O_{aq} \rightarrow H^+ + NO_2^- \tag{3.6}$$

$$N_2O_{3aq} + H_2O_{aq} \rightarrow H^+ + NO_2^- \tag{3.7}$$

$$NO_{2aq} + H_2O_{aq} \rightarrow 2H^+ + NO_3^- + NO_2^- \tag{3.8}$$

$$HNO_{2g} + H_2O_{aq} \rightarrow H_2O_{aq} + NO_2^- + H^+ \tag{3.9}$$

$$HNO_{3g}+H_2O_{aq}\rightarrow H_2O_{aq}+NO_3^-+H^+ \qquad (3.\ 10)$$

During plasma-liquid interaction, a previous publication emphasized that the formation pathway of aqueous reactive species involves 448 liquid chemical reactions [121].

3.1.3.1 Pathways of H_2O_{2aq} formation

<u>Summary of the results for the different discharges</u>

Our different results show that in the case of Non-touching Bubbling Plasmas and Touching Bubbling Plasmas, H_2O_{2aq} is detectable in the water treated by discharges of Air, N_2 and O_2. The amount of H_2O_{2aq} produced by the dry Air-NBP is similar to dry O_2-NBP, but humid Air-NBP produce more H_2O_{2aq} than humid O_2-NBP (Figure 3. 6). Air-TBP is equivalent to humid gas discharge, which similarly produce more H_2O_{2aq} than the one produced by an O_2-TBP (Figure 3. 7). The effect of gas flow rate on the production of H_2O_{2aq} shows an opposite effect between dry gas NBPs and wet gas NBPs. Indeed, a higher flow rate decreases the amount of H_2O_{2aq} in the case of dry gas NBPs whereas it increases the amount of H_2O_{2aq} in the case of humid gas NBPs. Production of H_2O_{2aq} for all TBPs is less influenced by the gas flow rate.

<u>Formation pathway of H_2O_{2aq} for Non-touching Bubbling Plasmas</u>

H_2O_{2aq} in NBPs-treated water are most probably formed through the solvation of H_2O_{2g} since most of the radicals formed in the discharge zone cannot reach water surface. H_2O_{2g} is formed by the combination of radicals of OH_g (Equation 2.22) or HO_{2g} (Equation 2.23) and these gaseous radicals mainly come from the dissociation of water vapor by electrons or excited species [121]. Production of H_2O_{2g} is then positively correlated with the density of water vapor in the discharge region.

In dry gas NBPs, the water vapor in the discharge zone is strongly affected by the gas flow. Indeed, the bigger the flow rate, the fewer water vapor in the discharge zones. This is the reason why increasing the flow rate (greater than 250 sccm) can restrict the production of H_2O_{2aq}. Increasing the flow rate on the other hand transfers more H_2O_{2g} to dissolve in water via bubbles, which induces more H_2O_{2aq}. This is

only true when the flow rate is small, (below 250 sccm). In humid gas NBPs, the density of water vapor does not depend of the flow rate. Increasing the flow rate promotes the dissolution of H_2O_{2g} and increase H_2O_{2aq} concentration.

Formation pathway of H_2O_{2aq} for Touching Bubbling Plasmas

H_2O_{2aq} in TBPs can be formed either through the solvation of H_2O_{2g} or through aqueous reactions, since the NTP touch the water surface. The production of aqueous H_2O_2 is little influenced by the gas flow rate, which indicates that H_2O_{2aq} is mostly formed in water layer or bulk water through one or more aqueous reactions (e.g. Equation 3.3 and Equation 3.4). Note that the amount of H_2O_{2aq} produced by TBPs is about twice as much as NBPs at the same flow rate. It means that aqueous reactions contribute more than the solvation of H_2O_{2g} for the formation of H_2O_{2aq} by TBPs. Based on the literatures[129, 135, 137, 138, 268], the aqueous reactions for the formation of H_2O_{2aq} are mainly due to the combination of radical of OH_{aq} (Equation 3.3) and HO_{2aq} (Equation 3.4). The formation of HO_{2aq} radical involves O_2 ($H+O_2\rightarrow HO_2$). Although there is no O_{2g} in N_2 discharge, H_2O_{2aq} is still detected in both N_2-TBP and N_2-NBP, indicating that the formation of H_2O_{2aq} through the combination of HO_{2aq} is probably negligible in this case. On the other hand, the presence of OH_{aq} radicals is detected in the water treated by the 9-electrode plasma reactor using fluorescence spectrophotometry (Figure 3. 24). This result implies that the combination of OH_{aq} radical is the main source of H_2O_{2aq} in TBPs.

3.1.3.2 Pathways of NO_2^- and NO_3^- formation

Summary of the results for the different discharges

In the case of NBPs, NO_3^- is detected in the water treated by all feed gas discharges. NO_2^- is detected in the water treated by humid gas discharge, but its concentration is negligible in dry gas discharges (below 1 μM, Figure 3. 6). In the case of TBPs, both NO_3^- and NO_2^- are detected in the water treated by Air-TBP and N_2-TBP (Figure 3. 7). The effect of the gas flow rate on the production of NO_3^- and NO_2^- shows an opposite effect in TNPs and NBPs of humid gas. A high flow rate decreases the amount of NO_3^- and NO_2^- in TBPs contrary to the NBPs of humid gas,

which produce more NO_3^- and NO_2^- for high flow rate. Production of NO_3^- in NBPs of dry gas increases with low flow rate, but decreases when gas flow rate over 250 sccm.

Formation pathway of NO_3^- and NO_2^- for Non-touching Bubbling plasmas

NO_3^- and NO_2^- in the NBP configuration can only be formed through the solvation of gaseous species for the same reason than H_2O_{2aq}. NO is the initiating species for the formation of RNOS [137-140, 217, 269]. It can be rapidly oxidized into other gaseous species such as N_2O_{3g}, NO_{2g}, HNO_{2g}, HNO_{3g} and NO_{3g} in gas phase[267].

$$NO_g + O_g \rightarrow NO_{2g} \qquad (3.\ 11)$$

$$NO_g + O_{3g} \rightarrow NO_{2g} + O_{2g} \qquad (3.\ 12)$$

$$NO_g + OH_g \rightarrow HNO_{2g} \qquad (3.\ 13)$$

$$NO_{2g} + H_g \rightarrow HNO_{2g} \qquad (3.\ 14)$$

$$HNO_{2g} + O_{3g} \rightarrow HNO_{3g} + O_{2g} \qquad (3.\ 15)$$

$$NO_{2g} + OH_g \rightarrow HNO_{3g} \qquad (3.\ 16)$$
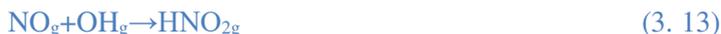
In NBPs of dry Air and N_2, both NO_g and NO_{2g} are probably secondly oxidized into HNO_{2g}, HNO_{3g} or NO_{3g} …, based on the infrared spectra of gaseous species (Figure 3. 3). The solvation of these gaseous species is probably the main source of NO_2^- and NO_3^-. Amounts of NO_3^- and NO_2^- in NBP of humid Air and N_2 are increased, compared to the NBP of dry gases. NO_g can react with OH_g radical coming from water dissociation to form HNO_{2g} (Equation 3.13). The solvation of HNO_{2g} is then one of the sources of NO_2^-. HNO_{2g} can be further oxidized into HNO_{3g} (e.g. Equation 3.15). That is why the amount of NO_3^- can be greater than the one of NO_2^-. Since the solvation of gaseous species is the main source of NO_3^- and NO_2^- in NBPs, the dissolution of gaseous species will be strengthened when the flow rate increase as shown in Figure 3. 6.

Formation pathway of NO_3^- and NO_2^- for TBP

NO_3^- and NO_2^- in TBPs can either be formed through aqueous reactions or the

solvation of gaseous species. Productions of aqueous NO_2^- decrease when the flow rate increases (Figure 3. 7a). As discussed before, the production of OH_g radical decreases when the flow rate increase since the humidity of the gas in the discharge area is reduced. Then the concentration of the HNO_{2g} produced decreases at a higher flow rate. This is considered to be one of the reasons why NO_2^- is decreased at a higher flow rate and this result indicates that the solvation of RNOS contribute to the formation of NO_2^-. Note that the concentration of NO_2^- shows a sharp decrease when flow rate increase to 300 sccm and become nearly stable at a higher flow rate (Figure 3. 7). Besides, TBPs produce more NO_2^- than NBPs. It means that NO_2^- can also be directly formed in water layer or even bulk water through the aqueous reactions, e.g. solvation of N_2O_3 (Equation 3.7) or the reaction of NO_{aq} with OH_{aq} radical (Equation 3.6). This is also true for NO_3^- that it can be formed both in gas phase and liquid phase, e.g. Equation 3.8 and Equation 3.10, etc. Besides, NO_2^- and HNO_{2g} can be further oxidized into NO_3^- and HNO_{3aq}, which cause the production of NO_3^- is higher than NO_2^-.

3.2 Investigations of touching plasmas

As discussed before, touching plasmas produce more aqueous reactive species than non-touching plasmas. The aqueous reactive species produced by the reaction of NTP with water are key factors in NTP biological applications. In this section, we focus on touching plasmas to treat tap water. The single electrode plasma reactor is used to produce both a Touching Bubbling Plasmas and Touching Non-bubbling Plasmas. Air-TNP is used to observe the physical properties of NTP interacting with water, including discharge power, plasma propagation and plasma excited species. The TBPs are used to study the effect of the discharge parameters on the production of NO_2^-, NO_3^- and H_2O_{2aq}. The adjustable parameters include the input voltage, the plasma treatment time, the gas flow rate and the height of HV electrode to the water surface. For seeds treatments using the 9-electrode plasma reactor, a TBP configuration will be selected. We choose this configuration to avoid the diffusion of ambient Air into the plasma discharge region since this reactor works in open Air conditions. The discharge conditions of 9-electrode plasma setup are selected based

on the optimal conditions of the TBPs of the single electrode plasma reactor.

3.2.1 Diagnostics of physical properties of Air Touching Plasmas

Discharge current and images of propagations of the plasma are investigated in this subsection.

3.2.1.1 Discharge current

The discharge current waveform is obtained by connecting a resistor of one-ohm in series between the plasma and the ground. In the process of Air discharge, there is only one current peak in the discharge process of both positive and negative plasma. The discharge currents are shown in Figure 3. 8. Intensity of the discharge current of positive polarity is about 600 mA. The current takes about 10 ns to reach the maximum intensity and then exhibits a sharp decrease in about 80 ns and then lasts for about 1.5 μs. The intensity of the discharge current of negative polarity is about 800 mA. The current takes about 15 ns to reach the maximum intensity and exhibits a sharp decrease in about 100 ns and then lasts for more than 1 μs.
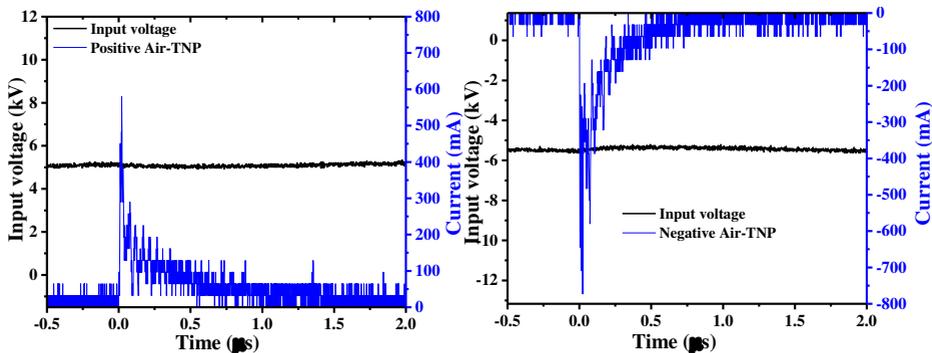
Figure 3. 8 Current of the Air-TNP for discharges of positive polarity and negative polarity. The height from the HV electrode to the water surface is 3 mm, the NTP are contacting with tap water surface, Air flow rate is 300 sccm and the input voltage is 20 kV$_{P-P}$.

3.2.1.2 iCCD images of Air-TNP

The images of the NTP are taken by an Andor Istar iCCD camera using Edmund

Optics 50 mm FL (1:2.8) high resolution lens. The camera gate is 50 ns and is triggered externally via the oscilloscope and the signal generator in order to be synchronized with the discharge initiation. The delay of the iCCD camera is varied in order to follow the dynamic of the discharge. However, Due to the slow rise time of the high voltage power supply (typically 100 μs), a large jitter exists between the discharge voltage and current and no accumulation is possible. Hence, each photo is taken in a single shot. The current is monitored with the oscilloscope to determine the beginning of the discharge. 0 ns correspond to the time when the current rise up. The iCCD images of Air discharge of positive polarity are shown in Figure 3. 9 and negative polarity are shown in Figure 3. 10.
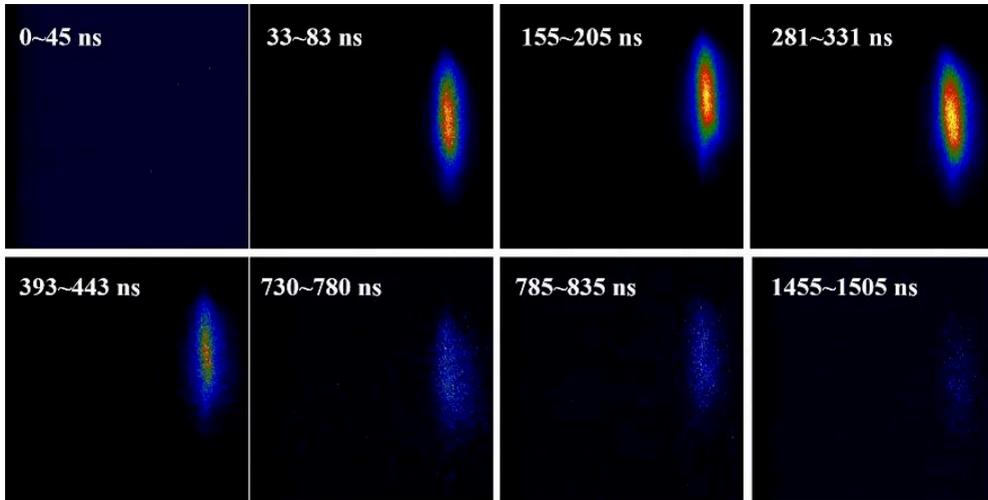
Figure 3. 9 iCCD images of plasma driven by an Air-TNP of positive polarity at an atmospheric pressure. Camera gate is 50 ns. HV electrode is fixed 3 mm above the tap water surface and discharge voltage on HV electrode is 20 kV$_{p-p}$, Air flow rate is 300 sccm and the plume is contacting with tap water surface. 0ns is the start of rise up time of current.

In the propagation of positive plasma, no light emission is observed during the first 50 ns after the breakdown. The light emission detected by camera begins within a time interval of 50 to 80 ns and reaches the maximum intensity in about 300 ns. A rapid drop occurs when the light intensity of positive plasma reaches the maximum. Then, the rate of decline slowly slows down and light emission can last for 1500 nanoseconds.
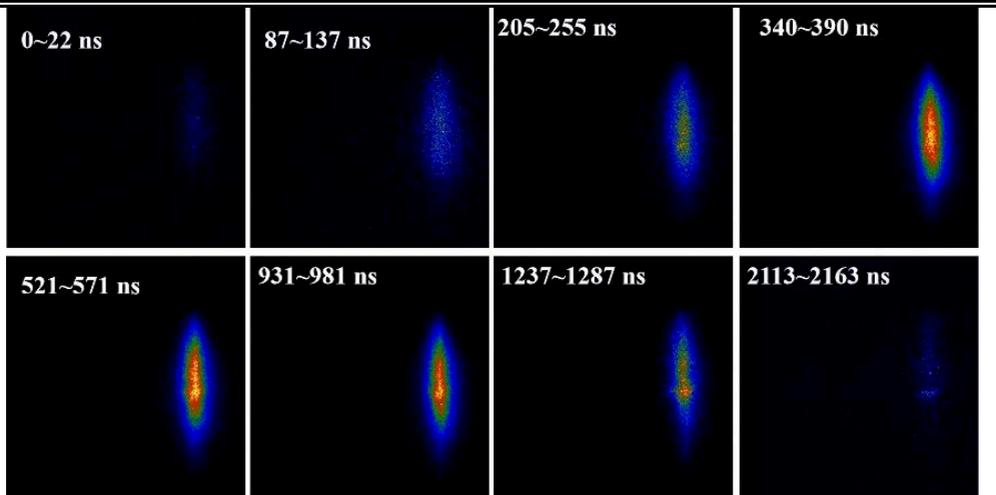
Figure 3. 10 iCCD images of plasma driven by an Air-TNP of negative polarity at an atmospheric pressure. Camera gate is 50 ns. HV electrode is fixed 3 mm above the tap water surface and discharge voltage on HV electrode is 20 kV$_{p-p}$, Air flow rate is 300 sccm and the plume is contacting with tap water surface. 0 ns is the start of rise up time of current.

In the propagation of negative plasma, light emission is detected during the first 20 ns after the breakdown but light intensity is very weak. The intensity of the light emission of the negative plasma shows a slow increase process, which reaches a maximum intensity in 400 ns. Intensity of the light does not exhibit a rapid decrease after reaching the peak and maintains nearly 1000 ns at the state of the maximum light intensity. The light emission of negative plasma has a longer time than the light of positive plasma since it sustains more than 2000 ns.

3.2.1.3 Optical emission spectra of Air-Touching Non-Bubble Plasmas

The monochromator entrance slit is connected to an optical fiber to collect the plasma emitted light. The entrance slit is 60 μm and the optical fiber is fixed at a 2 cm from the plasma. Emission spectra are recorded on iCCD Camera mounted on the spectrometer after dispersion by a 600 l/mm diffraction grating. The camera is triggered externally via the oscilloscope and the signal generator to synchronize with the discharge initiation with an adjustable delay. In order to capture the emission light of the whole positive or negative discharge process, camera gate is fixed at 50 μs to capture all the light. The spectra of Air positive and negative plasmas are shown in Figure 3. 11.
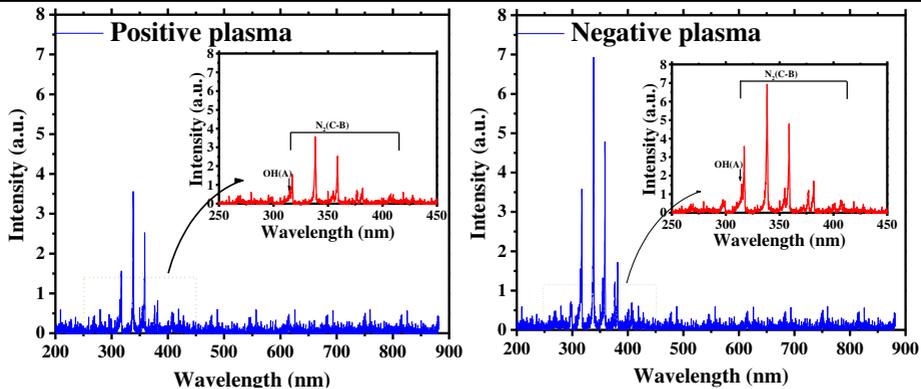
Figure 3. 11 Emission spectra of the Air positive and negative plasmas. HV electrode is fixed 3 mm above the tap water surface and discharge voltage on HV electrode is 20 kV$_{p-p}$, Air flow rate is 300 sccm and the plume is contacting with tap water surface. Emission is accumulated along entire discharges volume.

It is observed that the emission spectrum lines of the negative plasma are same with the positive NTP except for the intensity that negative plasma is about twice as big as that of the positive plasma. Spectrum lines of positive and negative plasma are mainly concentrated in the range of 290-450 nm, which correspond to the second positive bands of nitrogen ($N_2(C^3\Pi_u \rightarrow B^3\Pi_g)$) and OH ($A^2\sum^+$, v'=0$\rightarrow X^2\Pi$, v''=0) and have a maximum lifetime of microsecond. The emission spectrum lines of the transition include OH (A-X, 308), N_2 (1-0, 316 nm), N_2 (0-0, 337 nm), N_2 (0-1, 358 nm), N_2 (1-3, 375 nm), N_2 (0-2, 380 nm), N_2 (1-4, 400 nm), N_2 (0-3, 406 nm), etc. The emission bands of the active oxygen atom are not observed. The measurement of OH spectrum band is due to the water. The emission lines of the NO_y system (NO(A-X)) between 200-300 nm, second emission order of N_2 (B-C) between 600-800 nm and the active oxygen atom of 777 nm and 845 nm were not detected.

3.2.2 Optimization of working conditions for the single electrode DBD in the Touching Bubble Plasmas configuration

The production of gaseous and aqueous reactive species by a Touching Bubble Plasmas for different gases and flow rates has already been compared in section 3.1.2.2. The objective of the present section is to investigate the effect of adjustable discharge parameters of TBPs such as the NTP treatment time, the gas flow rate, the

input voltage and the height from the electrode to the water surface treatment time, height and voltage, on the production of aqueous reactive species (Table 3.1). The reactor is the single electrode discharge and the NTP gas can be Air, O_2 or N_2. Quantitative analysis of concentrations and yields of aqueous species of NO_2^-, NO_3^- and H_2O_{2aq} are also presented. Yield of species (nmol/J) is the ratio of species amount (nmol) and consumed energy (J).

$$Yield=CV/Pt$$

Where C is the concentration of solution, V is the volume of the plasma treated water, P is the discharge power and t is the plasma treatment time.

Table 3. 1 Adjustable parameters of the discharges of Air, O_2 and N_2 in the configuration of touching bubble plasmas using the single electrode plasma reactor.

	Treatment time min	Flow rate sccm	Input voltage kV	HV electrode height mm
Air discharge O_2 discharge N_2 discharge	0.5, 1, 2, 4, 6	50, 100, 200, 300, 600	15, 17.5, 20, 22.5, 25	3, 5, 7, 10, 14

3.2.2.1 Effect of NTP treatment time on the production of aqueous species
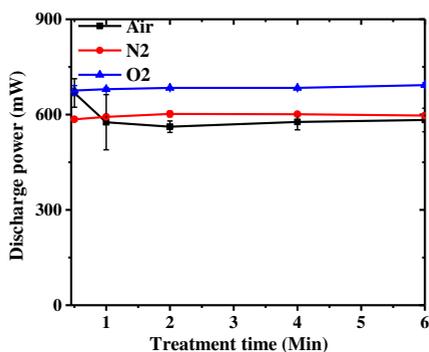
Figure 3. 12 Discharge power of Air, N_2 and O_2 at different treatment times. Discharge conditions: flow rate is 300 sccm, height of electrode to water surface is 7 mm, input voltage is 20 kV and volume of tap water is 3 mL.

The power of the gas discharge in function of the NTP treatment times is shown in Figure 3. 12. Gases discharge power are not influenced by the treatment time, which means that the discharges of all gases are stable. The average power of the Air

discharge is about 585 mW, N_2 discharge is about 596 mW and O_2 discharge is about 683 mW.
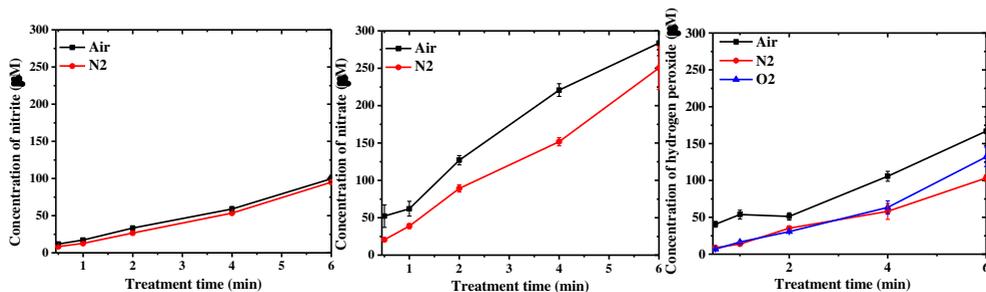
Figure 3. 13 Concentration of NO_2^-, NO_3^- and H_2O_{2aq} at different treatment times. Discharge conditions: Flow rate is 300 sccm, height of electrode to water surface is 7 mm, input voltage is 20 kV and volume of tap water is 3 mL.

The concentrations of NO_2^-, NO_3^- and H_2O_{2aq} in NTP treated water at different treatment times are shown in Figure 3. 13. The production of all the species increases linearly with the NTP treatment time. The amount of NO_2^- produced by the Air-TBP is the same than the one produced by the N_2-TBP. However, Air-TBP produces more NO_3^- than N_2-TBP. Both Air-TBP and N_2-TBP produce more NO_3^- than NO_2^-. For instance, concentration of NO_3^- and NO_2^- produced in Air-TBP treated water for 4 min is 225 μM and 57 μM, respectively. Concentration of NO_3^- and NO_2^- produced in N_2-TBP treated water for 4 min is 153 μM and 53 μM, respectively. Concentration of NO_3^- and NO_2^- formed by O_2-TBP is below the detection limit (1 μM). The amount of H_2O_{2aq} produced by N_2 is similar to the one of the O_2 discharge, but is lower than the one of Air discharge.

Yields of NO_2^-, NO_3^- and H_2O_{2aq} at different treatment times are shown in Figure 3. 14. The yield of the three species is constant over the considered treatment times and does not depends much on the discharge gases. NO_2^- produced by Air-TBP shows a similar yield with N_2-TBP, which is stable at 1.5 ± 0.25 nmol/J. Air-TBP shows a higher yield of NO_3^- than N_2-TBP. The yield of NO_3^- produced by Air-TBP is stable at 4 ± 0.25 nmol/J and the one of NO_3^- produced by N_2-TBP is stable at 1.5±0.25 nmol/J. The yield of NO_3^- is about 3 times higher than the one of NO_2^- in both Air-TBP and N_2-TBP. Discharge of all gases show a similar yield of H_2O_{2aq} that yield is stable at 1.6 nmol/J for Air-TBP, 1.5 nmol/J for N_2-TBP and 1.3 nmol/J for

O$_2$-TBP.
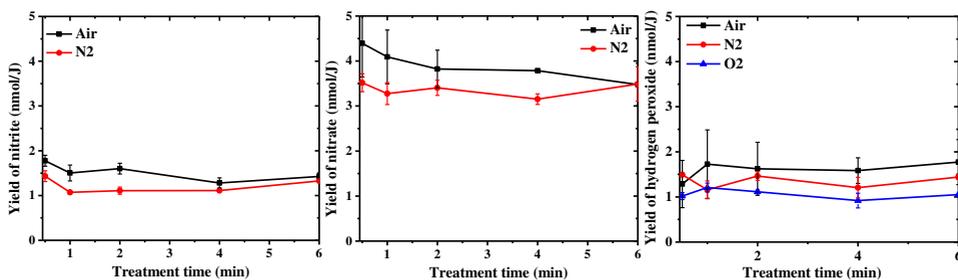
Figure 3. 14 Yield of NO$_2^-$, NO$_3^-$ and H$_2$O$_2$at different treatment times. Discharge conditions: Flow rate is 300 sccm, height of electrode to water surface is 7 mm, input voltage is 20 kV and volume of treated tap water is 3 mL.

3.2.2.2 Effect of the gases flow rate on the production of aqueous species

The discharge power at different gas flow rates is shown in Figure 3. 15. Sustaining the NTP generated by O$_2$-TBP requires more energy than Air-TBP and N$_2$-TBP. The power of Air-TBP is similar to N$_2$-TBP. Discharge power slightly decreases when the gas flow rate increases. At a flow rate of 50 sccm, the power of Air, N$_2$ and O$_2$ discharge is about 650±12 mW, 653±29 mW and 737±14 mW, respectively. When the flow rate increases from 50 sccm to 600 sccm, the power of Air, N$_2$ and O$_2$ discharge slightly decrease to about 617±11 mW, 600±23 mW and 645±9 mW respectively.
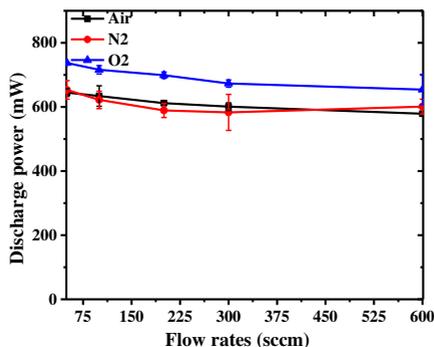
Figure 3. 15 Discharge power of Air, N$_2$ and O$_2$ at different gas flow rates. Discharge conditions: Treatment time is 2 min, height of electrode to water surface is 7 mm, input voltage is 20 kV and volume of tap water is 3 mL.

The concentrations of NO_2^-, NO_3^- and H_2O_{2aq} produced by Air, N_2 and O_2 discharge at different gas flow rates are shown in Figure 3. 7. The effect of the flow rate has already been discussed in section 3.1.2.2. The production of NO_2^- and NO_3^- are strongly affected by the flow rate, while the production of H_2O_{2aq} for all NTP is not influenced by the gas flow rate.
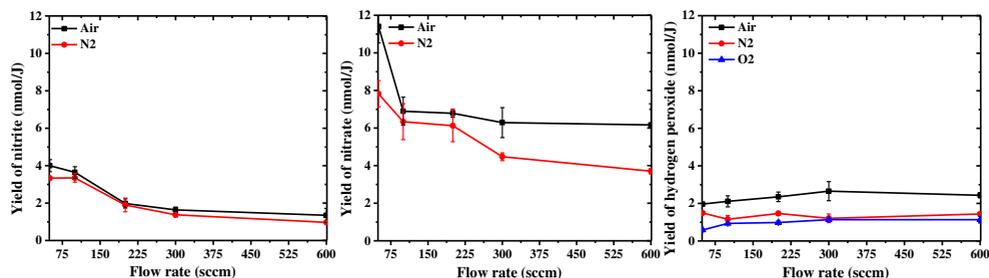
Figure 3. 16 Yield of NO_2^-, NO_3^- and H_2O_{2aq} at different flow rates. Discharge conditions: Treatment time is 2 min, height of electrode to water surface is 7 mm, input voltage is 20 kV and volume of tap water is 3 mL.

The yields of NO_2^-, NO_3^- and H_2O_{2aq} at different flow rates are shown in Figure 3. 16 for the different NTP. Increasing the gas flow rate decreases the yield of NO_3^- and NO_2^-. The yields of NO_2^- produced by Air-TBP and N_2-TBP reach about 3.5 nmol/J at a flow rate of 50 sccm. When flow rate increases to 600 sccm, the yield decreases to about 1.8 nmol/J. The yield of NO_3^- produced by Air-TBP is 11 nmol/J at a flow rate of 50 sccm and is about 7 nmol/J at a flow rate of 600 sccm. The yield of NO_3^- produced by N_2-TBP is 8 nmol/J at a flow rate of 50 sccm and is 4 nmol/J at a flow rate of 600 sccm. The yields of H_2O_2 produced by Air-TBP, N_2-TBP and O_2-TBP are not influenced by the flow rate. The average yields of H_2O_2 produced by Air-TBP, N_2-TBP and O_2-TBP are 2 nmol/J, 1.6 nmol/J and 1.5 nmol/J, respectively.

3.2.2.3 Effect of the distance from the high voltage electrode to the water surface on production of aqueous species

The power of gas discharge at different heights is shown in the Figure 3. 17. The result shows that the discharge power is significantly affected by the height of the HV electrode to water surface. The discharge power decreases when the height of the HV electrode is either too big (e.g. 14 mm) or too small (e.g. 3 mm). When the

height increases from 3 mm to 7 mm, the power of Air-TBP increases from 276 mW to 1029 mW, the power of N_2-TBP increases from 273 mW to 938 mW and the power of O_2-TBP increases from 197 mW to 1178 mW. However, when the height increases from 7 mm to 14 mm, the power of Air-TBP decreases to 175 mW, the power of N_2-TBP decreases to 290 mW and the power of O_2-TBP decreases to 31 mW. Electrical breakdown of the gas between the HV electrode and the water surface forms NTP touching the water surface. Increasing the height of the HV electrode to the water surface is equivalent to increase the capacitance of the discharge gas and the gas breakdown voltage. The discharge power increases with the height of the HV electrode. However, when the HV electrode is too high, the input voltage will not be sufficient to form a stable NTP. That is the reason why the consumed power rapidly decreases, especially when the height is over 10 mm.
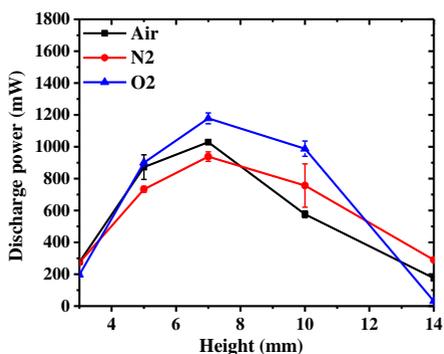
Figure 3. 17 Discharge power of discharge of Air, N_2 and O_2 at different heights. Discharge conditions: Flow rate is 300 sccm, treatment time is 2 min, input voltage is 20 kV and volume of tap water is 3 mL.

The concentrations of NO_2^-, NO_3^- and H_2O_2 produced by Air, N_2 and O_2 discharge for different heights are shown in Figure 3. 18. The amounts of reactive species are substantially positively related to the discharge power. The maximum amounts of species are produced when the electrode is fixed at the position of 7 mm. The Air-TBP produce a similar amount of NO_2^- to the N_2-TBP, but produce more NO_3^- than the N_2-TBP. When the height increases from 3 mm to 7 mm, the concentration of NO_2^- increases from 1 μM to 40 μM, the concentration of NO_3^- increases from 10 μM to 120 μM for Air-TBP and from 20 μM to 108 μM for N_2-TBP. But when the height increases from 7 mm to 14 mm, the concentration of NO_2^-

decreases from 120 μM to 20 μM, the concentration of NO_3^- decreases from 10 μM to 120 μM for Air-TBP and from 108 μM to 16 μM for N_2-TBP. The production of H_2O_{2aq} is strongly influenced by height but is less affected by discharge gas. The maximum concentrations of H_2O_2 formed by Air-TBP, N_2-TBP and O_2-TBP discharge are about 50 μM, 50 μM and 70 μM, respectively.
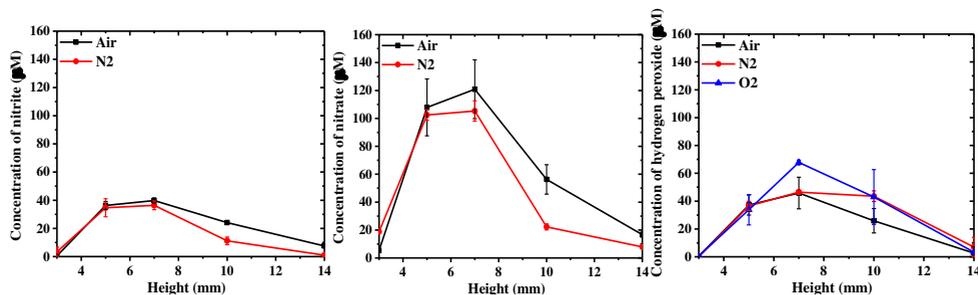
Figure 3. 18 Concentration of NO_2^-, NO_3^- and H_2O_{2aq} t different heights. Discharge conditions: Flow rate of all gases is 300 sccm, treatment time is 2 min, input voltage is 20 kV and volume of tap water is 3 mL.

Yields of NTP formed NO_2^-, NO_3^- and H_2O_{2aq} at different flow rates are shown in Figure 3. 19. Apparently, the height of HV electrode have a strong effect on the yields of reactive species. The maximum of yield of NO_3^- and NO_2^- are obtained when the electrode is fixed at the position of 5 mm. The maximum yield of NO_2^- produced by Air-TBP and N_2-TBP is same, which is about 1.2 nmol/J. The yields of NO_3^- produced by Air-TBP are higher than yield of NO_3^- produced by N_2-TBP. When the height increases from 3 mm to 7 mm, the yield of NO_3^- increases from 0.5 nmol/J to 3.7 nmol/J for Air-TBP and increases from 1.5 nmol/J to 3 nmol/J for N_2-TBP. When the height increases from 7 mm to 14 mm, the yield of NO_3^- decreases from 3.7 nmol/J to 1.5 nmol/J for Air-TBP and decreases from 3 nmol/J to 1.3 nmol/J for N_2-TBP. Yield of H_2O_{2aq} is not influenced by discharge gas when the discharge is stable. The maximum of yield of H_2O_{2aq} is about 1±0.2 nmol/J when the height of HV electrode is fixed at the position of 5 mm. Since the power of O_2 discharge rapidly decreases to 31 mW at a height of 14 mm because of the unstable discharge, the yield of H_2O_{2aq} directly increases to 2 nmol/J.
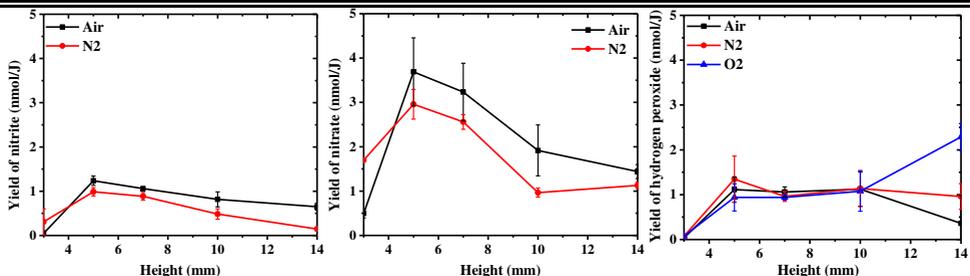
Figure 3. 19 Yields of NO_2^-, NO_3^- and H_2O_{2aq} at different heights. Discharge conditions: Flow rate is 300 sccm, treatment time is 2 min, input voltage is 20 kV and volume of tap water is 3 mL.

3.2.2.4 Effect of the input voltage on the production of aqueous species
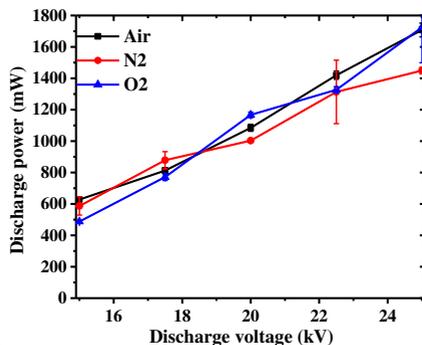
Figure 3. 20 Discharge power of discharge of Air, N_2 and O_2 at different input voltages. Discharge conditions: Flow rate is 300 sccm, height of electrode to water surface is 7 mm, treatment time is 2 min and volume of treated tap water is 3 mL.

The power of the gas discharge at different input voltages is shown in Figure 3. 20. The discharge power is linearly increasing with input voltage. There is not a significant difference among the power of different gases. O_2-TBP is unstable when the input voltage is lower than 20 kV and that is the reason why its power is even lower than Air-TBP and N_2-TBP at an input voltage of 15 kV and 17.5 kV. The maximum discharge power is 1708 mW for Air-TBP, 1449 mW for N_2-TBP and 1800 mW for O_2-TBP

The concentrations of NO_2^-, NO_3^- and H_2O_2 produced by Air, N_2 and O_2 discharge at different input voltages are shown in Figure 3. 21. Increasing the input voltage produces more reactive species. Air-TBP produces the same amount of NO_2^-

than N_2-TBP, but the NO_3^- produced by Air-TBP has higher amount than N_2-TBP. NTP exhibits better conversion of reactive species at higher input voltages. The amount of NO_3^- produced by Air-TBP increases by 537 % from 51 µM to 325 µM from 15 kV to 25 kV compared to 371 % from 50 µM to 240 µM for N_2-TBP. The amount of NO_2^- produced by Air-TBP increases by 421 % from 24 µM to 125 µM from 15 kV to 25 kV compared to 273 % from 26 µM to 97 µM for N_2-TBP. The amount of H_2O_{2aq} increases with the discharge voltage but are less affected by the type of gas. The maximum concentrations of H_2O_{2aq} in treated water is similar for Air-TBP, N_2-TBP and O_2-TBP and is about 100 µM. The amount of H_2O_{2aq} produced by TBPs increases by ca. 300 % from 25 µM to 100 µM from 15 kV to 25 kV.
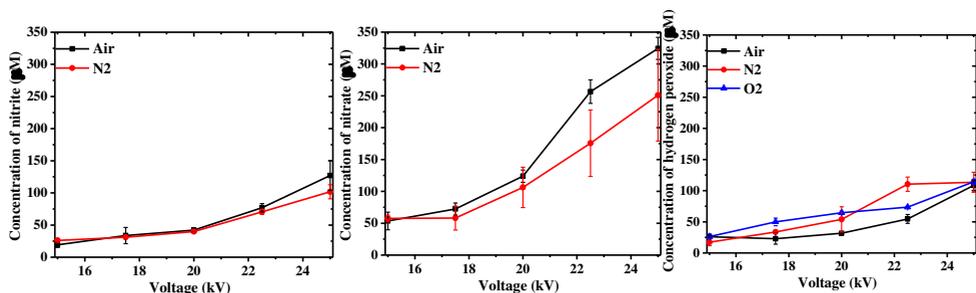
Figure 3. 21 Concentration of NO_2^-, NO_3^- and H_2O_{2aq} at different input voltages. Discharge conditions: Flow rate is 300 sccm, height of electrode to water surface is 7 mm, treatment time is 2 min and volume of tap water is 3 mL.

The yields of NO_2^-, NO_3^- and H_2O_{2aq} in different discharge are shown in Figure 3. 22. NO_2^- produced by Air-TBP leads to the same yield with N_2-TBP at different input voltages, but the NO_3^- produced by Air-TBP has higher yields than N_2-TBP. NTP exhibits better conversion of reactive species at higher input voltages. The yield of NO_3^- produced by Air-TBP increases by 140.34 % from 2.33 nmol/J to 5.6 nmol/J from 15 kV to 25 kV compared to 61.14 % from 2.29 nmol/J to 3.69 nmol/J for N_2-TBP. The yield of NO_2^- produced by Air-TBP increases by 170.37 % from 0.81 nmol/J to 2.19 nmol/J from 15 kV to 25 kV compared to 43.27 % from 1.04 nmol/J to 1.49 nmol/J for N_2-TBP. The yields of H_2O_{2aq} does not depend on the applied voltage. The maximum yield of H_2O_{2aq} produced by Air-TBP, N_2-TBP and O_2-TBP discharge is 1 nmol/J, 1.5 nmol/J and 1.4 nmol/J, respectively.
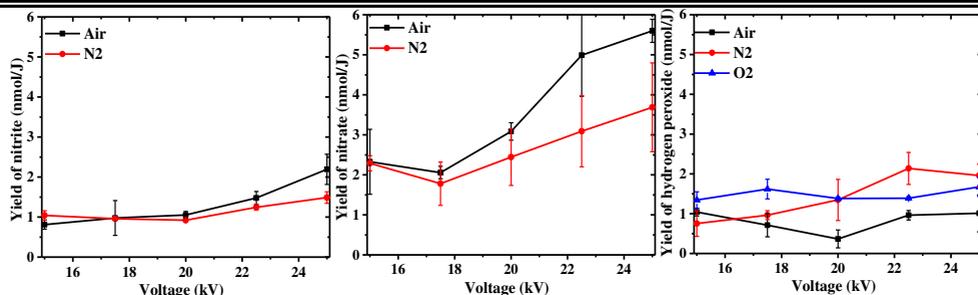
Figure 3. 22 Yield of NO_2^-, NO_3^- and H_2O_2 at different input voltages. Discharge conditions: Flow rate is 300 sccm, height of electrode to water surface is 7 mm, treatment time is 2 min and volume of tap water is 3 mL.

3.3 Selection of discharge conditions of 9-electrode plasma reactor

In the case of TBPs produced by the single electrode plasma setup, it is found that the production of aqueous species i) decreases with the gas flow rate, ii) increases with the input voltage and, iii) is maximized when the height of HV electrode to water surface is fixed at 7 mm. For the reason that the touching plasma produces the highest yield of aqueous plasma reactive species, a TBP configuration will be selected for the 9-electrode plasma reactor. The extremity of the glass tubes of 9-electrode NTP is immersed inside water for 1 mm in order to bubble the discharge gas in water. The optimization of the discharge conditions in term of NO_2^-, NO_3^- and H_2O_{2aq} concentration has been done for a single-electrode device and the optimization is used for the 9-electrode device. Hence, the discharge condition of 9-electrode plasma reactor is: 1500 sccm of total gas flow rate, about 7-8 mm of height and 20 kV_{p-p} of input voltage. The amount of NO_2^-, NO_3^-, H_2O_{2aq} and OH_{aq} radicals produced by the Air-TBP, N_2-TBP and O_2-TBP under the selected discharge conditions using the 9-electrode plasma reactor are determined in this section. The corresponding discharge power and yield of aqueous species are compared to the single electrode plasma reactor and the summary of the results is shown in Table 3. 2 and Table 3. 3Table 3. 3 for both devices.

3.3.1 Production of aqueous species in the water treated by 9-electrode plasma reactor

The potential of 9-electrode DBD plasma treatments to induce changes in the

concentration of long-lived RNOS in plasma-activated water are monitored as a function of the treatment time as a result of Air, O_2 and N_2 NTP treatment respectively. The amount of NO_2^-, NO_3^- and H_2O_{2aq} in NTP treated water are shown in Figure 3. 23. In the experimental conditions we selected, the concentrations of all species increase linearly with the NTP treatment time. N_2 and Air NTP lead to similar production of NO_2^-, NO_3^- and H_2O_{2aq}. pH is almost constant during NTP treatment (between 7.45 and 7.55).
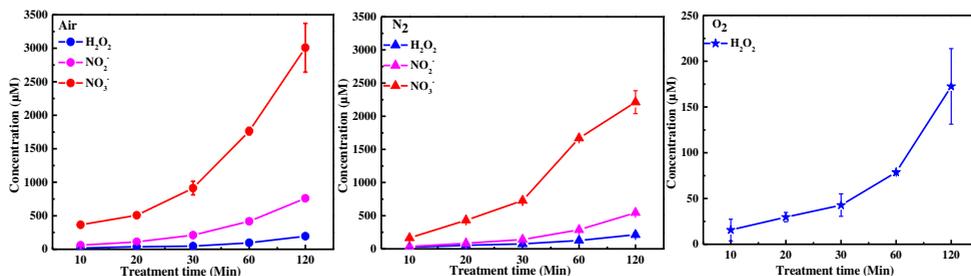
Figure 3. 23 Concentration (±standard deviation) of NO_2^-, NO_3^- and H_2O_{2aq} as a function of treatment time in plasma activated water for Air, N_2 and O_2 NTP (Vpp=20kV, Φ=1.5 SLM, Height of HV electrode to water surface ranges from 7 to 8 mm, tap water: V_L= 100 ml)

Similar to what was observed in the case of the single tube, only ROS are produced in O_2 discharge plasma activated water. O_2 NTP treatment produces no RNS due to the absence of nitrogen source. The production of H_2O_{2aq} does not depend upon the gas mixture, which is consistent to single electrode plasma reactor. RNS production in plasma-activated water is due to the dissolution of nitrogen oxides generated via the reactions between dissociated nitrogen species and oxygen-containing species as described earlier. The reason why Air NTP produces more RNS than N_2 is probably due to the O_2 contained in Air, which is an alternative source of ROS by O_2 ionizing. The formation of this excess of ROS, such as OH radical which reacts with nitrogen species to form more nitrate and nitrite, compared with N_2 discharge. The generated ROS can further be oxidized to form $NO_2^{\bullet}$ into $NO_3^{\bullet}$, which causes a higher concentration of NO_3^- than NO_2^- both in Air and N_2.

OH$_{aq}$ radical was measured by the method of fluorescence spectrophotometry. OH$_{aq}$ radical can react with terephthalic acid (TPA) to mainly form 2-hydroxyterephtalic acid (TPA-OH) that has a strong fluorescent signal with an

excitation wavelength of 317 nm and an emission wavelength at 433 nm.

The potential of 9-electrode plasma treatment to induce changes of the concentration of $^{\cdot}OH_{aq}$ radical in plasma-activated TPA solution are monitored as a function of the treatment time as a result of DBD discharge of Air, O_2 and N_2, respectively. As shown in Figure 3. 24, OH_{aq} is detected in the water treated by Air-TBP, N_2-TBP and O_2-TBP, and its concentration increases linearly with the treatment time. O_2-TBP trapped the bigger amount of OH_{aq} radical, followed by the Air-TBP and N_2-TBP. It should be note that the amount of trapped OH_{aq} radical is not the total production of OH_{aq} radical, only part of OH_{aq} radical can be trapped by TPA [270]. The maximum lifetime of OH radical is in microseconds and it can rapidly react with other species like NO_{aq}, NO_{2aq} and itself [133]. For instance,

$$OH_{aq}+OH_{aq}\rightarrow H_2O_{2aq} \text{ (Equation 3.1)}$$
$$OH_{aq}+NO_{aq}\rightarrow NO_2^-+H^+ \text{ (Equation 3.6)}$$
$$OH_{aq}+NO_{2aq}\rightarrow NO_3^-+H^+ \text{ (Equation 3.8)}$$
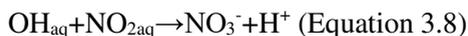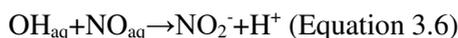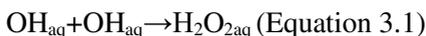
The rate constant of OH_{aq} radical with TPA is 4.4×10^9 $M^{-1}\cdot s^{-1}$ [270], and the reaction rate constant of OH_{aq} radical with OH_{aq} radical, NO_{aq} and NO_{2aq} is 5.5×10^9 $M^{-1}\cdot s^{-1}$, 2×10^{10} $M^{-1}\cdot s^{-1}$ and 3×10^{10} $M^{-1}\cdot s^{-1}$, respectively [271]. The OH_{aq} radicals produced by Air and N_2 NTP are mostly depleted by species like NO_{aq} and NO_{2aq}. Thus, TPA solution treated by Air-TBP and N_2-TBP capture significantly less OH_{aq} radicals than TPA solution treated by O_2 NTP
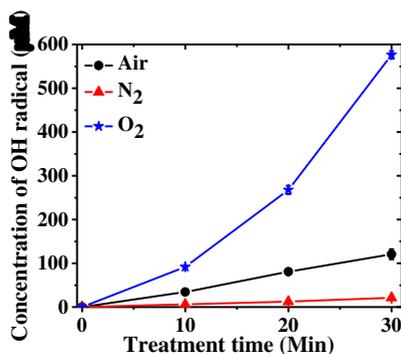
Figure 3. 24 Concentration (±standard deviation) of $^{\cdot}OH_{aq}$ radical as a function of treatment time in plasma activated water for Air, N_2 and O_2 NTP (Vpp=20kV, Φ=1.5 SLM, Height of HV electrode to water surface ranges from 7 to 8 mm, tap water: V_L= 100 ml)

3.3.2 Comparison of the yield of the aqueous species produced by the 9-electrode and the single electrode plasma reactor

The comparison of the discharge power of TBPs of Air, N_2 and O_2 between the single electrode and the 9-electrode plasma reactors is shown in Table 3. 2. The discharge power of the 9-electrode plasma reactor is about 3 W for the Air-TBP, 2.88 W for N_2-TBP and 3.68 W for O_2-TBP. Discharge power of 9-electrode plasma reactor is only about three times higher than the corresponding power of single electrode plasma reactor, which means it is not all electrodes can produce NTP simultaneously in one discharge cycle.

Table 3. 2 Comparison of power of touching bubble plasmas of different discharge gases between single electrode and 9-electrode plasma reactors (± standard deviation). Discharge conditions of single electrode plasma reactor: 300 sccm of flow rate, 7 mm of height of HV electrode, 20 kV of input voltage and 3 mL of tap water. Discharge conditions of 9-electtrode plasma reactor: 1500 sccm of total flow rate, 7-8 mm of height of HV electrode, 20 kV of input voltage and 20 mL of tap water.

Discharge gas / Setup	Discharge power/mW		
	Air	N_2	O_2
Single electrode reactor	634±32	622±27	716±13
9-electrode reactor	3015±91	2875±73	3675±203

Table 3. 3 Comparison of yield of aqueous species produced by touching bubble plasma in different discharge gases between single electrode and 9-electrode plasma reactors. The yield is defined as the ratio of the total amount of species in nmol divided by energy consumption in Joule (J). Discharge conditions of single electrode plasma reactor: 300 sccm of flow rate, 7 mm of height of HV electrode, 20 kV of input voltage and 3 mL of tap water. Discharge conditions of 9-electtrode plasma reactor: 1500 sccm of total flow rate, 7-8 mm of height of HV electrode, 20 kV of input voltage and 20 mL of tap water

Discharge gas / Setup	Yield (nmol/J)						
	Air discharge			N_2 discharge			O_2 discharge
	NO_2^-	NO_3^-	H_2O_2	NO_2^-	NO_3^-	H_2O_2	H_2O_2
Single electrode reactor	1.98	6.78	2.35	1.90	6.13	1.46	1.44
9-electrode reactor	3.7	18	1.5	3	14	1.5	1.04

In order to compare the efficiency of the energy transfer of these two types of

plasma reactor, the yield of NO_2^-, NO_3^- and H_2O_{2aq} produced by the two touching bubble plasmas are compared. The results are shown in Table 3. 3. The 9-electrode plasma reactor gives a higher yield of NO_3^- and NO_2^- than the single electrode plasma reactor. The yield of NO_3^- increases up to three times and the yield of NO_2^- increases by 1.50 times at most. The yield of H_2O_{2aq} is constant. 9-electrode plasma reactor shows a similar yield of H_2O_{2aq} to the single electrode plasma reactor in N_2-TBP, but shows an even lower yield of H_2O_{2aq} in Air-TBP and O_2-TBP.

3.4 Summary

In this chapter, we investigate the physical and chemical process of plasma-liquid interaction using a single electrode plasma reactor in a Dielectric Barrier Discharge configuration. To do so, the plasmas-formed reactive species both in gaseous and aqueous phase are firstly quantified. NTP produced by Air, N_2 and O_2 discharge either touch the water surface (which is called touching plasmas) or are generated at few centimeters away for the water surface and have no direct contact with it (which is called non-touching plasmas). In the first case, short-lived species such as ions, electronically excited species, O or OH radicals… interact with the water surface; on the other hand, in the non-touching case, only long-lived species such as O_3, NO, NO_2, HNO_3 … produced by the NTP may react with water. Such NTP are applied to study the reactive gaseous and aqueous reactive species, and to select the best discharge conditions, which produce the most aqueous reactive species for an upscaled plasma reactor containing 9 electrodes set in an array. Main conclusions are

1) Detection of plasma reactive species in gas phase
    i) The O_2 discharge produce more O_{3g} than Air discharge, no O_{3g} are formed in N_2 discharge;
    ii) Dry gas discharge produces more O_{3g} than humid gas discharge;
    iii) The O_{3aq} cannot be formed via the solvation of O_{3g};
    iv) NO_{2g} and NO_g are not detected in gas phase using FTIR;

2) Productions of NO_2^-, NO_3^- and H_2O_{2aq} in Non-Touching Bubble Plasmas configuration

    i) The productions of all species in dry Air-NBP, dry O_2-NBP and dry N_2-NBP are dependent to gas flow. Productions of species increase first and then decrease as the growing of flow rate;

    ii) The productions of all species in humid Air-NBP and humid O_2-NBP are dependent to gas flow. Productions of species increase continuously as growing of flow rate;

3) Productions of NO_2^-, NO_3^- and H_2O_{2aq} in Touching Bubble Plasmas configuration

    i) The productions of H_2O_{2aq} in Air-TBP, O_2-TBP and N_2-TBP are independent to gas flow and gas mixtures. Productions of H_2O_{2aq} is constant in different flow rates;

    ii) The productions of NO_2^- and NO_3^- in Air-TBP, O_2-TBP and N_2-TBP are dependent to gas flow. Productions of species decrease continuously as glowing of flow rate;

4) Potential pathways of NO_2^-, NO_3^- and H_2O_{2aq} formation

    i) NO_2^- and NO_3^- are mainly formed in water layer or aqueous phase through both the solvation of gaseous nitrogen species and aqueous reactions for touching plasma, and are mainly formed by the solvation of HNO_{2g} and HNO_{3g} for non-touching plasma;

    ii) H_2O_{2aq} is mainly formed in the upper water layer or aqueous phase through the combination of OH_{aq} radicals for touching plasma, and is mainly formed by solvation of H_2O_{2g} for non-touching plasmas;

5) Effect of adjustable parameters of touching plasma on productions of NO_2^-, NO_3^- and H_2O_{2aq}

    i) Species concentrations increase linearly with the NTP treatment time, meaning their yield is constant;

    ii) Concentrations and yields of NO_2^- and NO_3^- depends very much of the gas flow rate and distance because of hydrodynamic contrary to H_2O_{2aq}, which is not influenced by the flow rate;

    iii) Species concentrations and yields increase linearly with the input energy;

6) Productions of aqueous species using the 9-electrode plasma reactor in the touching bubble plasmas configuration

    i)   Discharge conditions select 1500 sccm of total flow rate, about 7-8 mm of height and 20 kV input voltage;

    ii)   The productions of NO_2^-, NO_3^-, H_2O_{2aq} and OH_{aq} radical increase linear with NTP treatment time;

    iii)   Air discharge produces more NO_2^- and NO_3^- than N_2 discharge;

    iv)   The productions of H_2O_{2aq} does not depend upon the gas mixture;

    v)   The productions of NO_3^- is about 3 times higher than NO_2^- in both Air discharge and N_2 discharge;

    vi) O_2 discharge produces the most OH_{aq} radical and followed by Air discharge and N_2 discharge.

Chapter 4: Non-thermal Plasma on Seeds Biological Effects

In the literature, numerous varieties of seeds have been treated by different types of NTP to increase seeds vigour or decrease the germination period. As reported in Chapter 1, the effect of NTP treatment on seed germination may be significantly affected by the NTP compositions and seed species. For instance, the germination percentage of both wheat seeds [194] and mung bean seeds [195] is positively enhanced by the treatment of dielectric barrier discharge Air plasma; the germination percentage of rice seeds (*Oryza sativa L.*) is increased after a treatment of microcorona discharge on a single dielectric barrier [177], while is not affected by atmospheric Air plasma jet treatment [272]. It is interesting to study how non-thermal atmospheric plasma affects seeds germination and to understand the links between the physical process of the NTP treatment and the observed biological effect on seed germination. The purpose of this chapter is i) to investigate if germination of seeds is selectively affected by a DBD plasma wet treatment, and ii) to select the seeds giving a positive germination response to NTP as the research target to study the biological effect of DBD plasma wet treatment.

Treating dry seeds by NTP directly is called plasma dry treatment. Another way, is plasma wet treatment, where immersed or wet seeds are directly treated by NTP or soaked with plasma activated water, as described in chapter 2.

For this purpose, eight different important crop seeds, including mung bean, radish, mustard, tomato, lettuce, dianthus, wheat and sticky bean, are selected to be treated by the multi-electrode plasma reactor. These seeds are shown in Figure 4. 1. In the present study, wet seeds are treated by NTP both in an indirect and direct way. Indirect plasma treatment is to treat/soak seeds with the plasma activated water and direct plasma treatment is to treat the seeds and water at the same time (immerse seeds inside water). The objective of direct plasma wet treatment is to check the seeds response to the combined effect of short-lived and long-lived reactive species

produced by NTP as well as the presence of UVs, charged particles and electric field. At the opposite, an indirect plasma wet treatment provides only "long" lived-species. "Long" meaning having a life-time of 1-2 min minimum which is the average time between the production of the plasma activated water and the watering of seeds.

Unlike plasma dry treatment, the reason why plasma wet treatment improves seed germination is attributed to the chemical and/or biological influences on germination process of aqueous chemical reactive species formed by NTP [35, 37, 82, 168, 171, 195, 217, 219, 220].

Figure 4. 1 Photographs of the seeds of this study in a plastic Petri-dish (diameter = 55 mm, height = 10 mm)

4.1 Effect of indirect plasma treatment on seeds germination

Radish, mung bean, wheat, tomato, lettuce, mustard, Dianthus and sticky bean have been selected to investigate the indirect plasma treatment effect on their germination (Figure 4. 2). Table 4.1 summarizes the total number of experimental seeds and the number of seeds germinating in one Petri dish.

Table 4. 1 Total number of tested seeds and the number of seeds in one Petri dish for germination. In this experiment, all seeds will be treated using an indirect NTP.

Name of seeds	Total number of seeds	Number of seeds in one Petri dish
Mung bean	135	15
Mustard	375	30
Radish	145	20
Tomato	135	20
Lettuce	105	30
Wheat	130	15
Dianthus	120	30
Sticky bean	125	5

The seeds are placed in Petri-dishes containing two layers of filter paper (Whatman 1003055, Sigma Aldrich). A volume of 5 ml of liquid is added for soaking. The liquid either can be non-treated tap water for the seeds in control group or NTP treated water for groups with the plasma treated seeds. Each experiment is repeated several times to ensure the reproducibility and to provide a good estimate of the statistical significance of the results. Germination is processed under a 16-hour photoperiod of artificial light (horticultural dimmable LED panel providing two wavelength peaks at 460 nm and 636 nm; 150~260 $\mu mol.m^{-2} \cdot s^{-1}$). Germination relative humidity ranges from 35 % to 45 %. The germination temperature is 21 °C, the interval of each temperature is below 2 °C. During the first 48h, Petri-dishes are covered with a lid to avoid the water evaporation. For seeds with a germination time over two days, 5 mL of tap water or NTP treated water will be added into each petri-dish per day to maintain a sufficient amount of water. Here mustard and mung bean seeds germinate within two days, while radish, wheat, lettuce, dianthus and sticky bean within five days. Tomato seeds are the slowest to germinate requiring 10 days. In the following, the germination time refers to the time when seeds are placed in

Petri-dishes for germination. All germination curves are shown in Figure 4. 2.
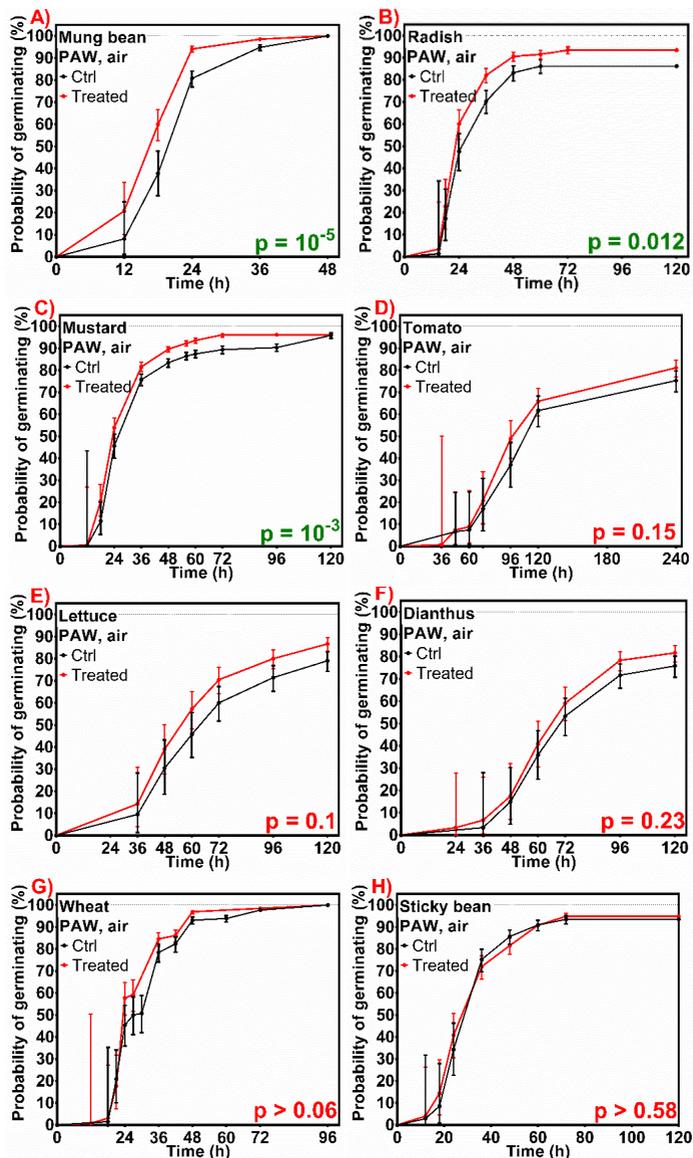
Figure 4. 2 Probability of germinating (%) for various seeds as a function of germination time (h). The seeds of treated group are exposed to the plasma activated water produced by Air NTP during 4 min (V_{pp}= 20 kV, Φ=1.5 SLM, tap water volume=100 mL). The control group uses tap water. All germination curves represent the Kaplan-Meier estimator of the probability of germinating, error bars represent the 95% confidence interval (Greenwood) and the P-value between each two groups is calculated based on Log-rank (Mantel-Cox) test described in Chapter 2 and is listed at the bottom right of the figures.

In Figure 4. 2, on can see that different types of seeds exhibit a broad diversity of responses to NTP treatment. The germination rate of NTP treated groups for mung beans, radish, and mustard seeds is significantly different from the control group. The corresponding statistical p-value are 10^{-5}, 10^{-3} and 0.012 for these three types of seeds respectively. Since Proportional Hard hypothesis, defined in Chapter 2, is verified for the three datasets, we can obtain the ratio of the instantaneous risk of germination in treated group vs. control group. It appears that the instantaneous risk of germination is increased by +73%, +38% and + 29% for mung bean, radish, and mustard seeds respectively. On the other hand, tomato, lettuce, dianthus, wheat and sticky bean, show no germination boost after an indirect treatment. At this stage, the conclusion is that different seeds selectively respond to the NTP generated long lifetime aqueous chemical species. As shown in chapter 3, Air NTP treatment produces a known amount of ROS and RNS. The concentration of Air NTP produced aqueous H_2O_2, NO_2^- and NO_3^- is ca. 40 µM, 102 µM and 220 µM, respectively. These chemical components could influence germination chemically and biologically, as described in chapter 1. Figure 4. 2 shows that our tested seeds react differently to plasma activated water. This diversity can be probably ascribed to their particular responses to the NTP formed ROS or RNS.

Mung bean and mustard are selected for the experiment with immersed seeds directly treated by NTP (direct plasma wet treatment) since they show a positive germination response to indirect plasma treatment. Although germination promotion of wheat is insignificant, it is also selected to be directly treated by NTP, because it was shown in the literature that such a treatment could accelerate the germination rate [36, 184, 194, 273].

4.2 Effect of direct plasma treatment on seeds germination

To investigate the germination response of seeds to both long-lived and short-lived chemical aqueous RNOS produced by NTP altogether with UV, radicals and electric field, mung bean, mustard and wheat are selected to be treated by direct plasma with the same plasma reactor.

Table 4. 2 lists each case the total number of seeds and the number of seeds in one Petri dish for germination. In this experiment, 240 seeds for mung bean, 240 seeds for mustard and 240 seeds for wheat.

The germination condition is identical to the conditions on indirect plasma treatment: in each Petri dish, there are 15 mung bean seeds, 15 wheat seeds and 30 mustard seeds are germinating. The seeds are placed in Petri-dishes containing two layers of filter paper (WHA 1003055, Sigma Aldrich). A volume of 5 ml of liquid is added for soaking. The liquid is either non-treated liquid by NTP for the control seeds or plasma treated liquid for the plasma treated seeds. Each group of samples (with 60~120 seeds) are repeated several times to assay the reproducibility of the experiments. Germination is processed under a 16-hour photoperiod of artificial light (horticultural dimmable LED panel providing two wavelength peaks at 460 nm and 636 nm; 150~260 $\mu mol.m^{-2}.s^{-1}$). Germination relative humidity range from 35% to 45%. Germination temperature is 21°C, interval of each temperature is below 2°C. During the first 48h, petri-dishes are covered to avoid the water evaporation. For seeds with a germination time over two days, 5 mL of tap water or NTP treated water are added into each petri-dish every day to maintain a sufficient amount of water. Here mustard and mung bean seeds germinate within two days, while wheat within five days. The initial germination time chosen is the beginning of seeds soaking time in Petri dishes. All germination curves are shown in Figure 4. 3 and all curves represent the Kaplan-Meier estimator of the probability of germinating, error bars represent the 95% confidence interval (Greenwood) and the P-value between each two groups is calculated based on Log-rank (Mantel-Cox) test and is listed at the bottom right of the figures. The comparison of treated and control groups shows a significant different if p-value < 0.05, Otherwise, the difference is not statistically significant. The p value is indicated on each figure.

Table 4. 2 Number of NTP directly treated seeds and the number of seeds in one Petri dish for germination

Name of seeds	Mung bean	Mustard	Wheat
Total number of seeds	240	240	240
Number of seeds in one Petri dish	15	30	15

Figure 4. 3a shows the influence of Air direct plasma treatment on mung bean seeds: the germination rate is significantly accelerated after NTP treatment. Proportional Hard hypothesis is verified in this case and the instantaneous risk of germination is increased by +161%. According to the comparison of germination instantaneous risk, this NTP positive effect on germination promoting of direct treatment is better than the indirect plasma treatment. It means other NTP parameters than long-lived chemicals species also participate in this NTP germination interaction.

In the case of wheat, as shown in Figure 4. 3b, no statistically significant effect of direct plasma treatment is measured, similarly to indirect plasma treatment. Germination rate curve of mustard (Figure 4. 3c) exhibits a statistically significant improved effect when only soaked with the NTP activated tap water, as shown in Figure 4. 2c. However, this positive effect is dramatically reversed when treated by NTP directly. The direct treatment slows down the germination rate instead. However, the germination percentage of the treated group at 35 h is same as the control group indicating mustard seeds can recover from this inhibition effect.
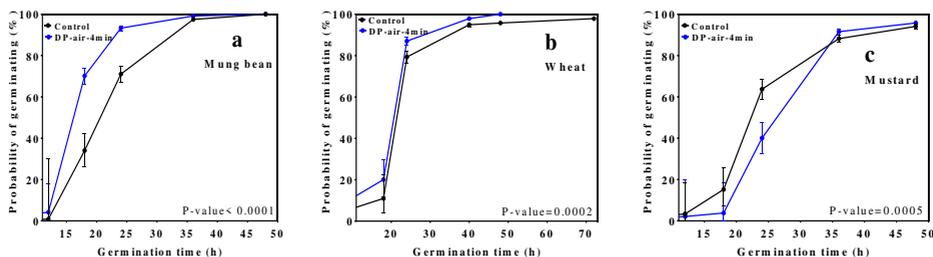
Figure 4. 3 Probability of germinating (%) for seeds as a function of germination time (h). The conditions are: 240 seeds for each group; Air discharge time is 4 min with 20 kV of Vpp, 1.5 SLM of flow rate and 20 mL of tap water in each treatment. Germination is processed in Petri dishes with light irradiation under a temperature of ca. 21 °C, humidity of ca. 40% condition and 5 mL liquid in each of them. 30 seeds are placed in one Petri dish for mustard and 15 seeds both for mung bean and wheat seeds. For seeds with a germination time over two days, 5 mL of blank liquid or plasma treated liquid are added into each petri-dish every day to maintain necessary germinating water. The initial germination time choose the beginning of seeds soaking time.

4.3 Summary

The purpose of this chapter is to verify the biological effects of non-thermal DBD plasma on the selected eight types of seeds and select the appropriate seeds being the target to explore how this NTP biological effect works, by using a multi-electrode plasma reactor. Eight different types of seeds, including wheat, mung bean, tomato, radish, mustard, sticky bean, lettuce and dianthus, are first indirectly treated by Air DBD plasma. Part of the seeds exhibit a positive germination response to NTP treatment are then selected to be treated using direct plasma treatment. Conclusions are:

1) Germination of seeds is differently affected by DBD plasma wet treatments depending upon the type of seed;

2) After an indirect plasma wet treatment, germination rate of mung beans, radish, and mustard is statistically increased, while there is no statistical effect on tomato, lettuce, dianthus, wheat and sticky bean;

3) After a direct plasma wet treatment, germination rate of mung bean is greatly increased whereas the germination of wheat, although statistically significant, show a small positive effect. The germination of mustard seeds is delayed by a direct plasma wet treatment. This last result is also interesting because mustard seed germination is favored by indirect plasma wet treatment.

4) Mung bean exhibits a positive germination response both to indirect plasma wet treatment and direct plasma wet treatment, it is selected as the main target used to fully explore how this NTP improving germination in the next step.

In summary, both plasma direct and indirect wet treatment are proved to be able to affect seeds germination selectively. The working factors could either be those long-lived chemical components produced by NTP, or others parameters like species in short lifetime, electric field and UV light etc. Since mung bean exhibits a positive germination response both to indirect plasma treatment and direct plasma treatment, it is selected as the main target used to fully explore how this NTP improving germination in the next step.

Chapter 5: Investigations of non-thermal plasmas positive stimulation mechanism on probability of mung bean seed germination

In the previous chapter, we have shown that mung bean seeds respond positively to both direct and indirect plasma wet treatments. Each NTP parameter may play an important role in stimulating the germination process. In our protocol described in Chapter 2 and 4, seeds are immersed inside water during the plasma direct wet treatment. It means that reactive species produced by the NTP react firstly with the liquid prior interacting with the surface of the seeds. Water layer around the seeds acts as a medium, which uniformly transfers NTP produced species to the seeds and forms an aqueous solution of dissolved RNOS. At the same time, this water layer may also be regarded as a buffer layer preventing the seeds from being excessively damaged by the short-lived particles (e.g. excessive oxidative). In this work, since seeds in most of the tests are covered by a thick water layer, highly reactive species (radicals and charged particles) with a short lifetime (from hundred nanoseconds to few microseconds) do not interact directly with the seeds. Some studies point out that the UV light produced by the NTP is also a variable which could affect seed germination. But when seeds are covered with a water layer, most of the energy of UV light is absorbed by the water, partly for water photolysis to generate aqueous RNOS. The effect of UV on germination may be linked to the interaction between aqueous chemical species and seeds. It is therefore reasonable to assume that aqueous RNOS are the main potential candidates responsible for the effect on the process of seed germination. Electric field is another key parameter, since electromagnetic field treatment is also novel and effective technology that has shown positive results in germination [210, 274-278]. According to the published literature, it is believed that NTP have the potential to either accelerate or inhibit germination by affecting the process of hydration and metabolism.

The objective of this chapter is to clarify the mechanisms and biological effects induced by NTP. In order to investigate the processes of NTP-germination interaction, the key working NTP parameters must firstly be identified, followed by the description of mechanisms which may potentially affects germination.

5.1 Quantification analysis of NTP produced aqueous species in tap water

NTP-produced aqueous RNOS have been associated with a positive shift in the germination process. Formation of RNOS such as HONOO could acidify NTP-treated liquid, which allows NTP to disinfect seeds directly. NTP-produced ROS like H_2O_{2aq} could indirectly affect germination by either participating in regulating dormancy as signaling molecule or causing oxidative stress that triggers cellular metabolisms. Highly reactive species, such as OH_{aq} radical, have been shown to have a positive effect on germination [177]. The concentration of some the species, such as NO_2^-, H_2O_{2aq}, OH radical and NO_3^- produced by NTP must be determined in order to identify the potential role of them on germination stimulation.
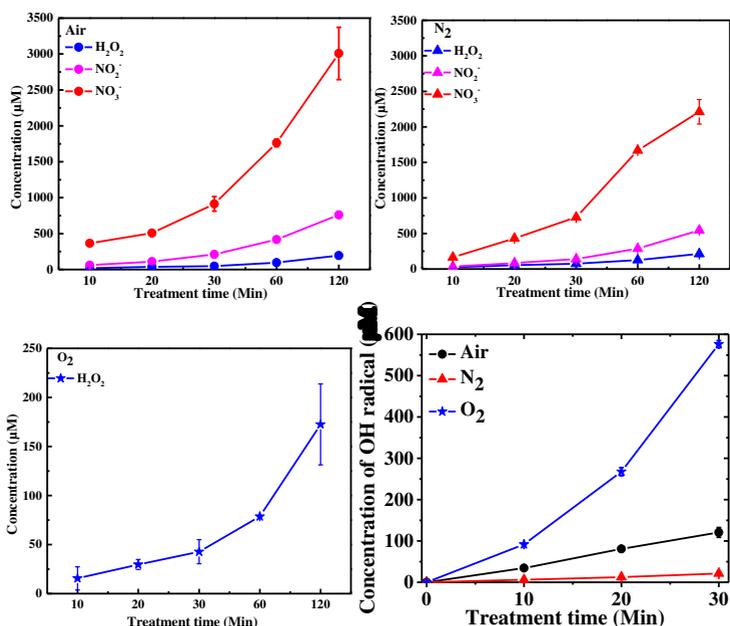
Figure 5. 1 Concentration (±standard deviation) of NO_2^-, NO_3^-, aqueous H_2O_2 and aqueous OH radical as a function of treatment time (min) in plasma treated liquid for Air, N_2 and O_2 NTP (Vpp=20kV, Φ=1.5 SLM, tap water: V_L= 100 ml and TPA-2Na solution: V_L= 100 ml)

The production of aqueous species has been described in Chapter 3 and we

briefly recall here the mains results. The potential of DBD plasma treatment to induce changes in the concentration of long-lived ROS/RNS in plasma activated water are monitored as a function of the treatment time; Three different gases are flown in the 9-electrode DBD plasma reactor presented in Chapter 3 as a result of Air, O_2 and N_2 NTP treatment, respectively. The formation of NO_2^-, NO_3^-, H_2O_{2aq} and OH_{aq} radical in NTP treated water are shown in Figure 5. 1.

In the considered experimental conditions, concentrations of NO_2^-, NO_3^- and H_2O_{2aq} increase linearly with the NTP treatment time. N_2 and Air NTP lead to similar production of NO_2^-, NO_3^- and H_2O_{2aq}. pH is almost constant during NTP treatment (between 7.45 and 7.55). Only ROS are produced in O_2 discharge plasma activated water. O_2 NTP treatment produces no RNS due to the absence of nitrogen source, but interestingly H_2O_2 concentration does not depend upon the operating gas. Aqueous OH radicals are detected in the TPA solutions treated by NTP of Air, N_2 and O_2, and the concentrations also linearly increase with treatment time. O_2 NTP produce the highest concentration OH_{aq} radical, followed by the Air and N_2 NTP

5.2 Roles of NTP activated aqueous RNOS in regulating germination

Germination of seeds starts with water adsorption and then follows with the triggering of seeds transition from the quiescent state of the dry seeds to the metabolic reactivation of germinating seeds [163, 279]. Oxidation processes by reactive species produced by the NTP could strengthen the ability of seeds to absorb water by increasing wettability of seeds coat. This has been proven by Zhou [195]et al. who used the following protocol: mung bean seeds are soaked in water and treated by a DBD plasma for 10 min (9kHz and 25W of discharge). Authors found that the morphology of mung beans seeds coat was modified by the Air NTP and the hydrophilicity of mung bean was significantly enhanced. The related surface modification was attributed to the surface oxidation caused by ROS.

Also, germination is the result of the endosperm cap weakening and the embryo elongation growth. It has been demonstrated that ROS are involved both in weakening mechanical force imposed by the endosperm and promoting embryo

growth potential [280]. Figure 5. 2 shows a simplified scheme of the germination process involving phytohormones. Reactive long-lived and short-lived species of oxygen and nitrogen (RNOS) are key molecules to activate and interact during the germination process. Seeds dormancy alleviation and induction of germination are regulated by the balance between various phytohormones, including abscisic acid (ABA), gibberellins (GA) and ethylene [162, 166, 167, 169]. Indeed, inhibition of germination by endogenous seed dormancy is related to low ROS and RNS levels. Promoting water adsorption triggers the intensification of biological metabolism inside seeds in term of various enzyme performances, ROS and RNS formation, mobilization of stored soluble protein and even endogenous phytohormones synthesis of seeds, which are beneficial to break dormancy and further to speed up germination. Reactive species produced by the NTP may also increase signaling molecules regulating endogenous hormones involved in the dormancy breaking. In brief, those aqueous RNOS produced by NTP on one hand promote seeds water uptake in early germination stage, on the other hand strengthen the performance of various cellular metabolism activities, especially when seeds are in a high-water content.
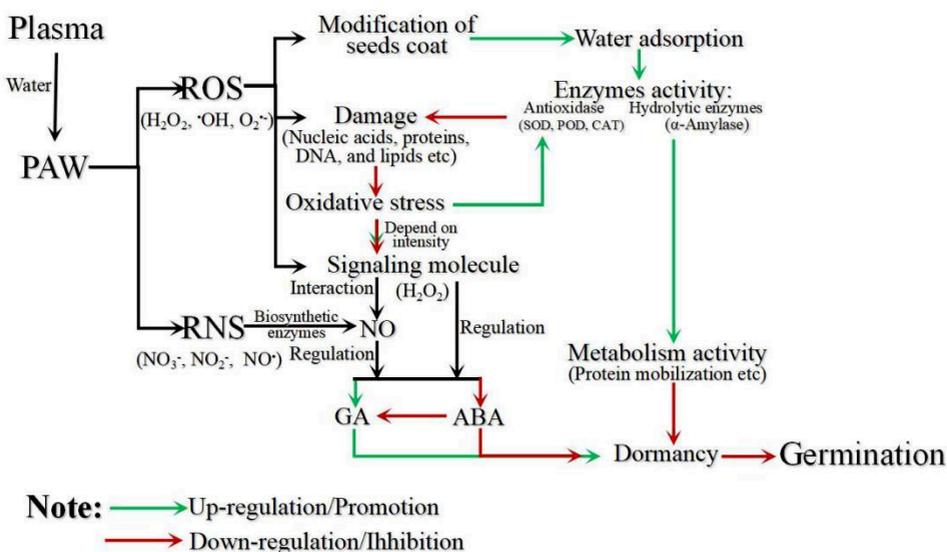
Figure 5. 2 Diagrammatic sketch of the mechanisms that could explain plasma effect on seed germination [214]

In this section, the influence of NTP produced aqueous RNOS on mung bean
seeds germination is investigated. The following parameters have been investigated
in order to understand the respective role of short-lived versus long-lived species and
ROS versus RNS:

1) The treatment time;

2) The gas composition;

3) Direct or indirect treatment, or treatment with chemicals such as NO_3^-, NO_2^- and H_2O_{2aq};

4) The role of pH;

5) The distance between the seeds and the water surface;

5.2.1 NTP discharge in tap water

The water used in this work is tap water. The ground electrode is fixed on the
out surface of the bottom of a glass beaker, which contains the water to be treated by
NTP. Pure O_2, N_2 or Air are the selected discharge gases treating mung bean directly
and indirectly. Figure 5. 3 shows that the effect on mung bean seeds germination
strongly depends on the treatment modalities. It appears that:

1) plasma direct wet treatment enhances significantly ($p < 0.05$) the
probability of germinating in treated group for all gas and treatment
times (sub-figure B, D and F);

2) only Air NTP shows a significant enhancement of the probability of
germinating for plasma indirect-treated groups (sub-figure C compared
to A and E);

3) treatment time has no effect in the range 2 min~6 min.
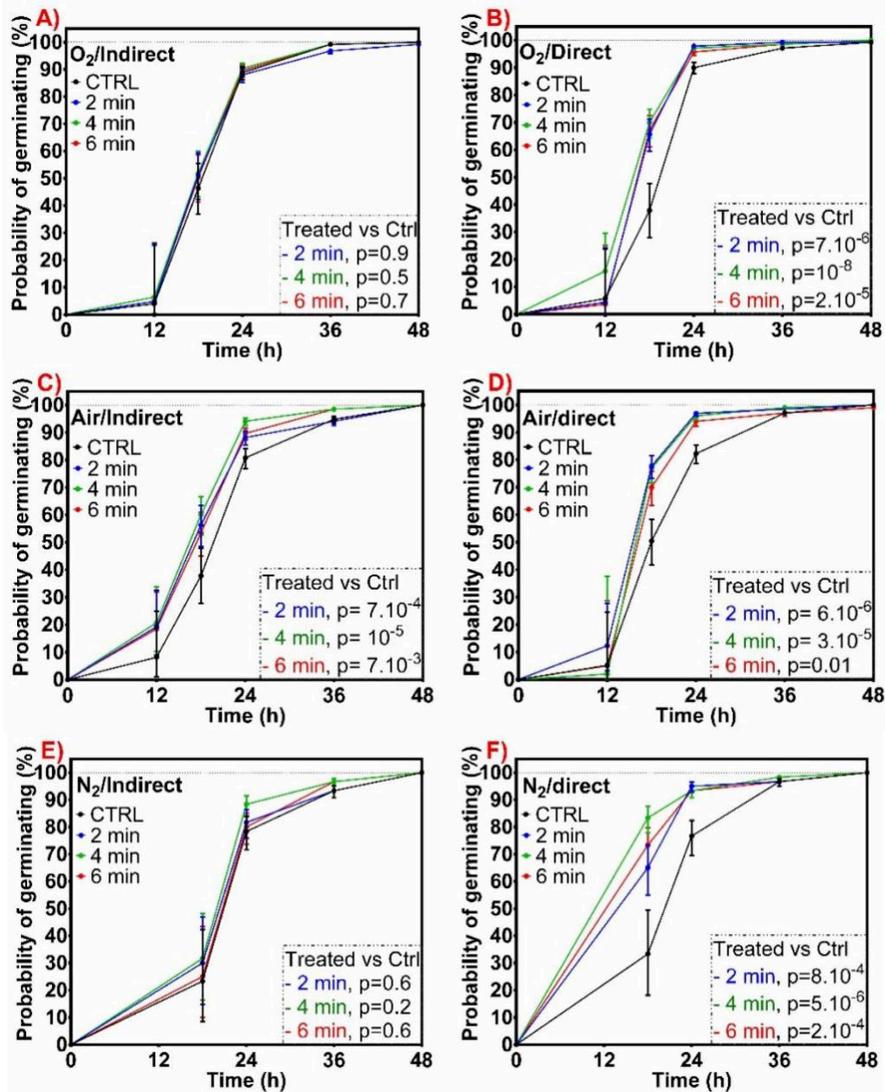
Figure 5. 3 Probability of germinating (%) as a function of time (h) of mung bean seeds. Discharge protocol for all experiments is same that discharge voltage is 20 kV of Vpp, gases flow rate is 1.5 SLM. Germination is processed in Petri dish with light irradiation under a temperature of ca. 21 °C, humidity of ca. 40% condition and 5 mL liquid in each of them. 15 seeds are germinated in one Petri dish with a cover. t=0 is the beginning of NTP treatment time. All germination curves represent the Kaplan-Meier estimator of the probability of germinating, error bars represent the 95% confidence interval (Greenwood) and the P-value between each two groups is calculated based on Log-rank (Mantel-Cox) test and is listed at the bottom right of the figures.

5.2.1.1 Effect of the NTP treatment time on germination
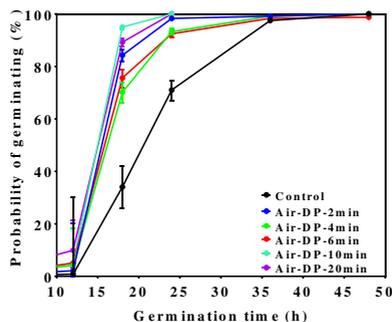
Figure 5. 4 Effect of Air direct plasma treatment time on germination of mung bean. Discharge protocol for all experiments is same that discharge voltage is 20 kV of Vpp, gases flow rate is 1.5 SLM. Germination is processed in Petri dish with light irradiation under a temperature of ca. 21 °C, humidity of ca. 40% condition and 5 mL liquid in each of them. 15 seeds are germinated in one Petri dish with a cover. The initial germination time choose the beginning of NTP treatment time. All germination curves represent the Kaplan-Meier estimator of the probability of germinating, error bars represent the 95% confidence interval (Greenwood) and the P-value between each two groups is calculated based on Log-rank (Mantel-Cox) test and is listed at the bottom right of the figures.

Figure 5. 3 shows that effects of treatment time ranging from 2 to 6 min are equivalent on germination. This is probably because the treatment time interval is too small to exhibit a difference, since concentrations of quantified long-lived aqueous species detected in water treated with NTP (6 min) are only 3 times higher than that of water treated with NTP for 2 min. To verify if NTP treatment time could affect germination, tests with a longer NTP treatment time were carried out for direct treatment in Air. Initial germination time is the beginning of NTP treatment time. Results are shown in Figure 5. 4. Germination rate of all plasma treated seeds are remarkably increased, but it is not the longer treatment time the faster germination rate. This confirms the germination of mung bean seeds is not sensitive to NTP treatment time in that time range and that even a short treatment time (2 min) produces a substantial enhancement of the germination rate at 20h.

5.2.1.2 Direct versus indirect treatment: an insight into the role of short-lived species

Indirect plasma wet treatment exposes seeds to long-lived reactive species

(H_2O_{2aq}, NO_2^-, and NO_3^- …). Based on the results shown in Figure 5. 3, the effect of plasma activated water is significantly lower than that of the direct plasma wet treatment. Note also, that the increment of liquid temperature is less than 3°C during 6 min of direct plasma wet treatment.
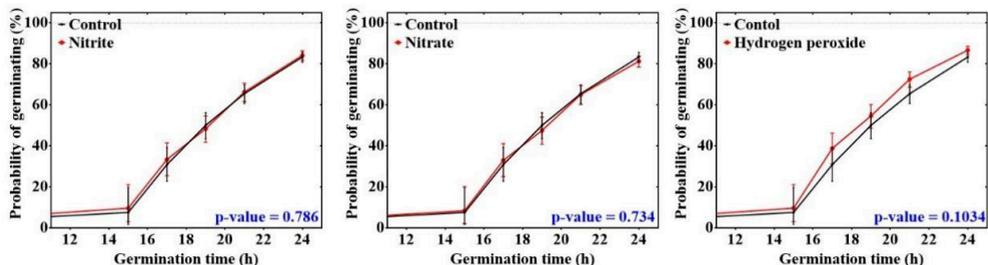
Figure 5. 5 Effect of chemical solutions on germination of mung bean. Concentration of H_2O_{2aq}, NO_2^-, and NO_3^- is 40 μM, 110 μM and 230 μM, respectively. Germination is processed in Petri dish with light irradiation under a temperature of ca. 21 °C, humidity of ca. 40% condition and 5 mL liquid in each of them. 15 seeds are germinated in one Petri dish with a cover. The initial germination time choose the beginning of NTP treatment time. All germination curves represent the Kaplan-Meier estimator of the probability of germinating, error bars represent the 95% confidence interval (Greenwood) and the P-value between each two groups is calculated based on Log-rank (Mantel-Cox) test and is listed at the bottom right of the figures.

Alternatively, chemical solutions with the concentrations equivalent to those produced by the NTP were added to the seeds. The concentration of each of these chemicals (H_2O_{2aq}, NO_2^-, and NO_3^- …) are equivalent to the concentrations produce by a 6 min NTP treatment (concentration of H_2O_2, NO_2^-, and NO_3^- is 40 μM, 102 μM and 220 μM, respectively). 240 seeds in each group are used being treated either by NO_2^-, NO_3^- or H_2O_{2aq} (Figure 5. 5). In addition, test with seeds germinated in nitrate solutions of various concentrations are also carried out (Figure 5. 6); 120 seeds for that of various concentrations of sodium nitrate ($NaNO_3$) solution test. Germination protocol is same as previous test.

As can be seen in Figure 5. 5, germination rates in all groups are not affected by any of these chemical components, although H_2O_{2aq} and NO_3^- have been widely proven to be important signaling molecules in regulating germination. In Figure 5. 6, seeds germinated in solutions with concentration over 1 mM show a lower

germination rate and germination percentage compared with seeds germinated in tap water (control group). This inhibition effect increases with a higher concentration, especially in $NaNO_3$ solution concentration of 5 mM and 7 mM. The effect of NTP-produced long-lived RNOS on germination strongly depend on the concentration. The effect is a negative effect and increases with the concentration of nitrate
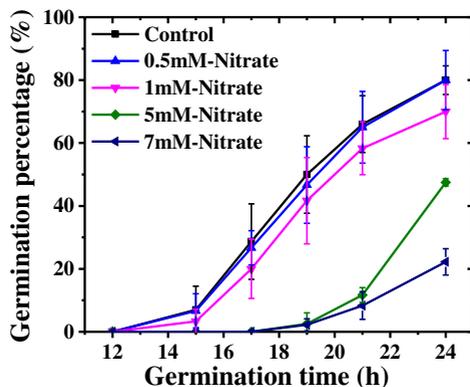
Figure 5. 6 Effect of concentration of sodium nitrate on germination of mung bean. Germination is processed in Petri dish with light irradiation under a temperature of ca. 21 °C, humidity of ca. 40% condition and 5 mL liquid in each of them. 15 seeds are germinated in one Petri dish with a cover. The initial germination time choose the beginning of NTP treatment time. All germination curves represent the Kaplan-Meier estimator of the probability of germinating, error bars represent the 95% confidence interval (Greenwood) and the P-value between each two groups is calculated based on Log-rank (Mantel-Cox) test and is listed at the bottom right of the figures.

On the other hand, as shown in Figure 5. 3, Air direct plasma wet treatment shows a statistically significant increase in the rate of germination. This is probably caused by some other short-lived reactive species, possibly in synergy with the electric field. For instance, it is likely that indirect treatment also exposes seeds to species whose lifetime ranges from few seconds to few minutes such as NO, O_3, peroxynitrites. Nevertheless, the effect of plasma activated water is much less than the one of direct plasma treatment.

5.2.1.3 Reactive Oxygen Species versus Reactive Nitrogen Species

O_2 NTP produces ROS only, whereas N_2 and Air NTP produce ROS and RNS

(Figure 5. 1). First, as shown in Figure 5. 3, N_2, O_2, and Air NTP lead to the similar germination enhancement for direct plasma wet treatment. Second, as seen before in Figure 5. 1, N_2, O_2 and Air NTP produce comparable H_2O_2 concentration. N_2 and Air NTP produce NO_2^-, NO_3^-, NO, $ONOO^-$ in addition, which are not present in the case of O_2 NTP. It is therefore tempting to conclude that ROS is/are the key species, which trigger mung bean germination in direct plasma wet treatment. For indirect plasma wet treatment, RNS could also be involved, as they are present in the case of indirect plasma wet treatment using Air a carrier gas (Figure 5. 3C); this is the only condition where indirect plasma wet treatments show a positive effect on mung beans germination. ROS are capable of interacting with most biomolecules, including nucleic acids, proteins, DNA, and lipids [165, 169]. They can easily diffuse and penetrate into intracellular through membranes to play a role in plant physiological activities such as an oxidative signaling and/or oxidative stress; the oxidative signaling leads to the breaking of seed dormancy and promotes germination vigor [213].

From previous experiments, it can be concluded that, in the case of direct plasma wet treatment, short-lived ROS play probably a key role in boosting germination since direct treatment gives a much better effect than indirect treatment. As mentioned before, the effect of ROS on seeds germination is achieved either through modification of seeds surface coat or by causing oxidation stress and acting as a signaling molecule. Short-lived ROS play a more significant effect on seeds germination because of their strong oxidizing capability: in one hand, it accelerates water adsorption by oxidizing seeds surface; or on the other hand, they may cause threaten like lipid oxidation or DNA damage, etc… However, it is not possible to exclude the role of short-lived RNS (NO and $ONOO^-$ etc.) since a small increase of the germination is observed in the case indirect Air treatment (Figure 5. 3B) but not in the case of indirect O_2 or N_2 treatment (Figure 5. 3A & E). NO and NO-donor molecules are expected to break the dormancy [164]. RNS are mainly adsorbed to produce NO. NO acting as an essential regulator in various processes of plant growth and development participates in seeds dormancy alleviation through regulating endogenous hormones like ABA catabolism and ethylene and or GA production [170, 218].

5.2.2 NTP discharge in acidic tap water

Numerous works consider the acidification of plasma treated liquid could be one of the major reasons which gives rise to the germination enhancement for the treated seeds, since it could promote seeds water uptake by softening and sterilizing coat surface [35, 37, 195]. In our case, the pH of tap water is about constant during the NTP treatment. However, to test if this acidification is a potential variable affecting germination of mung bean, sulfuric acid is added to tap water before the NTP treatment.

5.2.2.1 Germination in acidic tap water without NTP treatments

Tap water with four different pH values including 7.5 (pure tap water), 6, 4.5 and 3 are selected in this test. 120 seeds in each group are directly germinated in these solutions in Petri dish with light irradiation under a temperature of ca. 21 °C, humidity of ca. 40% condition. 5 mL liquid in each Petri dish with 15 seeds germinating. Initial germination time is the beginning of NTP treating time. Germination rate curves are shown in Figure 5. 7.
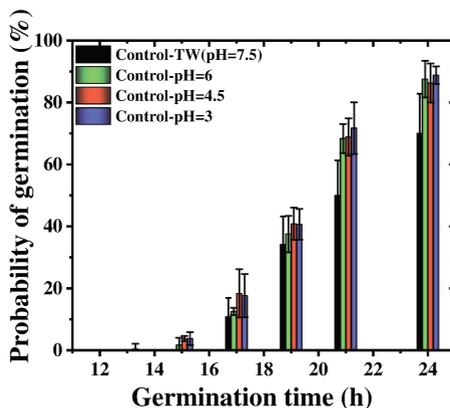
Figure 5. 7 Effect of pH value of tap water on germination of mung bean. Germination is processed in Petri dish with light irradiation under a temperature of ca. 21 °C, humidity of ca. 40% condition and 5 mL liquid in each of them. 15 seeds are germinated in one Petri dish with a cover. The initial germination time choose the beginning of NTP treatment time.

In Figure 5. 7, it can be seen that the germination percentage in all group is similar at a germination time before 20 h, but seeds soaked in acidified (pH lower than 7.5) show a higher germination rate than that of control (pH equal to 7.5) after this germination time. In summary, for pH lower than 6, the germination is faster than in tap water

5.2.2.2 Germination in acidic tap water with plasma direct wet treatment
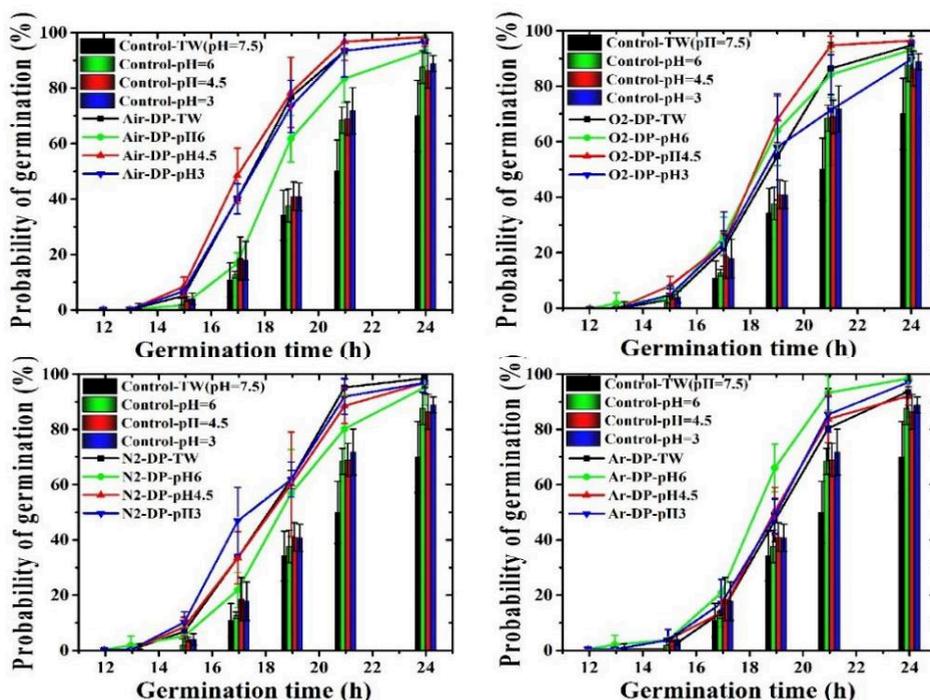
Figure 5. 8 Effect of Air direct plasma treatment on germination of mung bean seeds in tap water with different pH values under Air, O_2, N_2 and Ar discharge. 120 seeds in each group are treated in replicated tests. 20 mL relevant liquid with 60 seeds is treated for 4 min by NTP in each of discharge gas. Discharge protocol for all experiments is same that discharge voltage is 20 kV of Vpp, gases flow rate is 1.5 SLM. Germination is processed in Petri dish with light irradiation under a temperature of ca. 21 °C, humidity of ca. 40% condition and 5 mL liquid in each of them. 15 seeds are germinated in one Petri dish with a cover. The initial germination time choose the beginning of NTP treatment time. All germination curves represent the Kaplan-Meier estimator of the probability of germinating, error bars represent the 95% confidence interval (Greenwood) and the P-value between each two groups is calculated based on Log-rank (Mantel-Cox) test and is listed at the bottom right of the figures.

As shown before, a lower pH value benefits to the acceleration of mung bean germination; tests with mung bean seeds being treated by NTP directly in this acidified tap water are further carried out to see if this acidification effect enhances the influence of NTP treatment on germination boosting. The germination protocol is same as the previous test. The initial germination time is the beginning of the NTP treating time. Germination rate curves are shown in Figure 5. 8.

In this figure, germination curves of all plasma treated seeds present an accelerated germination rate, compared to NTP non-treated seeds, and independently of the pH value. It can therefore be assumed that the NTP biological effect in mung bean seeds germination does not relate to water acidification.

5.2.3 NTP discharge in tap water with seeds at different positions from the water surface

The direct treatment of seeds with NTP exposes them to long-lived, but also short-lived species, such as OH radical, O_2^- radical, singlet oxygen, depending upon the operating NTP gas. In this study, OH_{aq} radical has been confirmed to exist in the NTP treated water and been measured (see Figure 5. 1). Accordingly, we target NTP produced short-lived RNOS as key potential candidate in accelerating the germination of mung bean.

These short-lived RNOS are mostly produced near the water surface by reactions between water molecules and various high energy particles like electrons, ions, metastable and radicals etc. Passing through a millimeter thickness of water layer is inevitable before these short-lived particles reach seeds. However, diffusion distance of these reactive species is mostly in micro meters. For instance, OH_{aq} lifetime in water is 100 ns~2 ms, and its diffusion coefficient is 2.3×10^{-9} m^2/s. Hence a typical diffusion length is in the range of hundred nm to few µm, which is much smaller than the thickness of water above the seeds (5 mm). This should discard hydroxyl radicals as a potential ROS triggering mung bean seeds germination; however, it was recently claimed that OH_{aq} radical could be produced in the bulk of saline water exposed to an argon plasma jet via ultraviolet photolysis of H_2O and H_2O_{2aq} [125]. Besides, movement of NTP treated water caused by discharge gas flow could

facilitate these active components to diffuse to a deeper depth that touches seeds. Hence such particles have the possibility affecting germination and the most potential RNOS candidates that could boost mung bean seeds germination could be OH_{aq}, NO_{aq}, $ONOO^-$ or O_{3aq}, whose lifetime is in the range of nanoseconds to few seconds.

Since most of the reactive species are generated near the water surface, through which they probably diffuse and dissolve in water, it is reasonable to assume that the closer the NTP source is to the water surface the higher the concentration of these particles. Seeds are more likely to come in contact with the chemical particles if the distance of the seeds to the water surface is reduced. In this case, if it is the short-lived ROS that dominantly enhance germination, germination rate of mung bean seeds will definitely be influenced by strengthening the action of these energy particles on germination.

5.2.3.1 Air and N_2 discharge in tap water

Air and N_2 discharge are selected to treat mung bean seeds at different positions for the investigation of the role of short-lived particles. In this test, distance of seeds to water surface is decreased by immersing a cylindrical porous seed holder inside water. The height of these cylinders is 1mm, 3mm and 5mm respectively. Placing seeds on the top of the cylinder, the distance of the seeds to the water surface is then adjusted to 5 mm, 3 mm and 1 mm. In this test, since NTP treatment time ranging from 2 min to 6 min are selected to treat seeds. All seeds are germinated in same conditions as previous tests. Initial germination time is the beginning of NTP treating time.

The results are shown in Figure 5. 9. In this figure, all NTP treated germination curves exhibit an enhanced germination rate compared with control group. Germination curves of seeds with 2 min N_2 treatment in positions of 1 mm, 3 mm and 5 mm do not show statistically significant differences between each over (p-values between each group are over 0.05). When treated with N_2 NTP for 4 min and 6 min, germination curves of seeds located in 1 mm, 3 mm and 5 mm still behave in a similar behavior, indicating that the germination is not influenced by the distance

between the seeds and the NTP in the case of N_2 discharge. In Air NTP, curves are more scattered but still, with the error bars and no statistical significance. Hence, we conclude that no definite effect is observed when varying the distance between the seeds and the surface of the water during NTP treatment using N_2 or Air as a carrier gas.
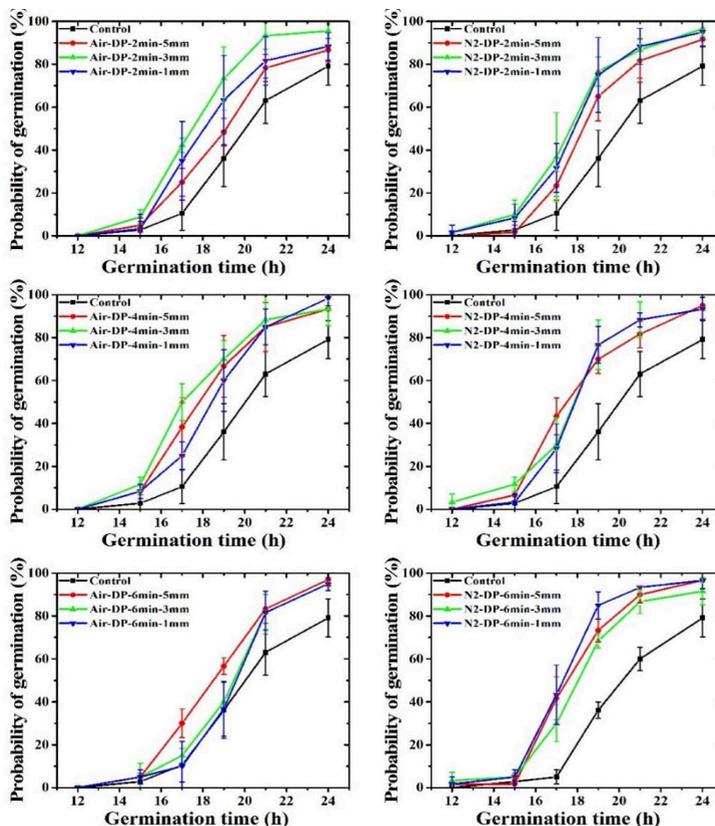
Figure 5. 9 Effect of Air and N_2 NTP treatment with seeds in different distances to water surface on germination of mung bean. 20 mL tap water with 60 seeds is treated for 4min by NTP per treatment. Replicated experiments use 360 seeds for control group and 60 seeds for each group of the rest plasma treated seeds. Discharge protocol for all experiments is same that discharge voltage is 20 kV of Vpp, gases flow rate is 1.5 SLM. Germination is processed in Petri dish with light irradiation under a temperature of ca. 21 °C, humidity of ca. 40% condition and 5 mL liquid in each of them. 15 seeds are germinated in one Petri dish with a cover. The initial germination time choose the beginning of NTP treatment time. All germination curves represent the Kaplan-Meier estimator of the probability of germinating, error bars represent the 95% confidence interval (Greenwood) and the P-value between each two groups is calculated based on Log-rank (Mantel-Cox) test and is listed at the bottom right of the figures.

5.2.3.2 Effect of short-lived aqueous species on germination

As mentioned before, despite the convection due to the treatment using bubbling NTP, the concentration of those short-lived aqueous species theoretically is assumed to have vertical gradient decreasing from the top to the bottom of the beaker. Highly reactive species such as aqueous OH react with few micrometers and may not reach the seeds. Less reactive species such as ozone and NO may diffuse in the bulk but we cannot draw definite conclusions from our experiments.

5.3 Role of the electric field in stimulating mung bean seed germination

In previous section, series of experiments have been done to investigate the role of NTP produced aqueous species, namely short-lived species. Results show that the apparent germination rate improvement cannot be directly connected to long or short-lived reactive species such as RNOS, as the distance between the seeds to the surface does not seem to play a role on the germination rate. In the following, we intend to check the influence of the electro-magnetic field produced by the NTP on the germination percentage.

Actually, it has been reported in the literature that magnetic field has already been applied to prime seeds. Sudsiri et al. increased germination percentage of Oil palm (*Elaeis guineensis*) seeds from 0% to 96 % after being exposed to magnetic DC fields with intensities of 2.5, 5.0, 7.0, 9.0 and 11.0 mT for 1, 2, 3, 4 and 5 h by the end of day-30 [210]. Moon et al. accelerated germination rate of tomato seeds by 1.1-2.8 times after a treatment of AC magnetic flux densities ranging from 3 to 1000 G [278].

On the other hand, AC and DC electric field is another physical seed priming technology which has been investigated with success. In the study done by Acosta-santoyo et al., germination percentage of ryegrass seeds was increased by 75% after an electrostatic field treatment [281]. This positive effect is also demonstrated in the work of Wang et al. with aged rice seeds [275]. Loss of viability or vigor in aged

seeds can cause a decrease of the germination percentage, which brings great economic losses every year. In their study, metabolism activities index of aged rice seeds including activity of SOD, POD and CAT and membrane lipid peroxidation were significantly increased by a high-voltage electrostatic field with the intensity ranging from 250 to 450 kV/m for more than 30 min treatment. For AC electric field, Dymek et al. showed that exposure of germinating barley seeds to a pulsed electric fields affects radicle emergence but influence seeds' gross metabolic activity less [282]. While in the test of wheatgrass (*Triticum aestivum* L.) seeds treated by pulsed electric field (PEF) (0.5-2 kV/cm), glutathione level and activities of SOD, CAT, glutathione reductase, glutathione peroxidase and ascorbate peroxidase in the resultant seedlings were increased with the PET treatment, done by Leong et al [211]. Furthermore, Galindo et al. found that PET with an intensity of up to 500 V/m can decrease the cell wall permeability of potato tissue in a fast way that within 30s after the PET treatment by observing a slower diffusion of the fluorescent dye FM1-43 through the cell wall [276].

Accordingly, the main objective of this section is to evaluate the role of the electric field on mung bean germination. This investigation is undertaken to determine if exposing mung bean seeds to an electric field would produce a change in the rate of germination of these seeds and if this change would be affected by the electric field intensity and type of the electric field used. For this purpose, a new protocol is operated: the high voltage electrodes touch the water to avoid the formation of a gas gap NTP.

5.3.1 Modeling of E-field exposure

To better understand the role of the electric field on germination influence, the distribution of electric field is first computed in the absence of NTP. The E-field is calculated by solving Poisson's equation when the potential of the electrodes is equal to 20 kVp-p. The simulations are performed for the experimental configurations with or without water. A three-dimensional full-size model of the experimental setup is built in the commercial software COMSOL-multiphysics, shown in Figure 5. 10.
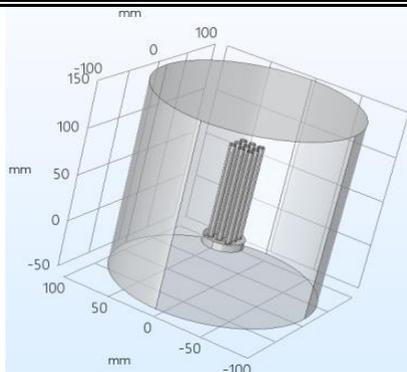
Figure 5. 10 Model of three-dimensional full-size of multi-electrode plasma reactor
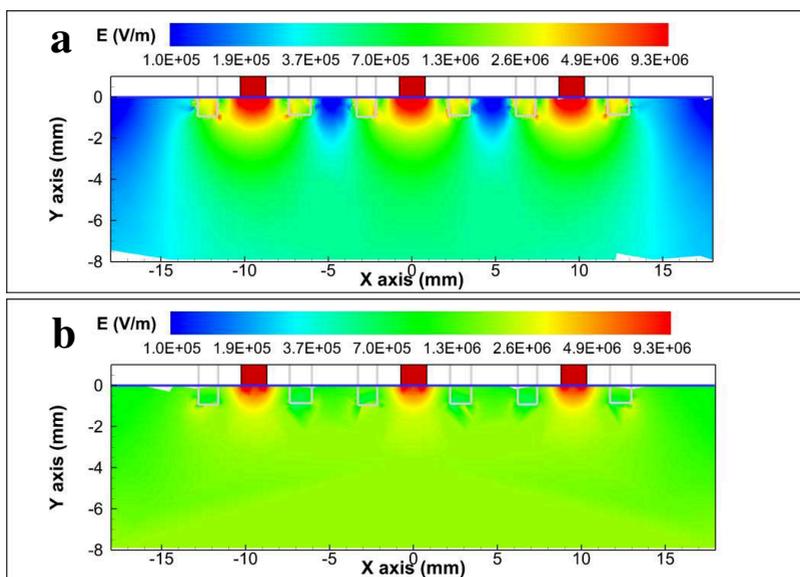
Figure 5. 11 Magnitude of the electric field in the vicinity of high voltage electrodes at potential V= 20 kV. (a) with water. (b) without water. Y axis is the height in beaker, 0-level is water surface. The white squares represent the section of the glass tubes. The red squares are the section of the cylindrical high voltage electrodes. The thickness of glass beaker is ca. 1mm. The ground is at the bottom of beaker (z=-9mm).

Figure 5. 11 shows the magnitude of the electric field in a vertical section of the beaker. In this model, water and glass-tubes are considered as a pure dielectric material with relative permittivity ε_r=80 and ε_r=6 respectively. The electrodes are perfectly conductive. Without water, the E-field is concentrated near the electrodes

and dielectric tube. At the vicinity of the seeds (their top is located 5 mm below the water surface in the standard protocol), the field amplitude is 10~30 kV/cm. The value of the electric field is lower in the presence of water. Indeed, at the seed position, the field is in the range 3~7 kV/cm. Note also that the values of electric field exposure are 20 times lower if the electrode are at potential V=1kV. Such voltage corresponds to the smaller condition of voltage tested E~0.15~0.35 kV/cm for immersed seeds.

5.3.2 Effect of electric field treatments on germination of mung bean
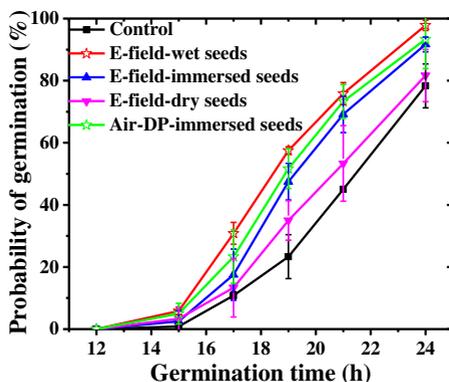
Figure 5. 12 Comparisons of mung bean seeds germination among electric field treatment for wet seeds, immersed seeds, dry seeds and NTP Air NTP direct treatment on immersed seeds. E-field test conditions: high voltage electrode happen to touch water surface, discharge voltage (Vpp) choose 20kV, treatment time choose 4min, pH is 7.5, volume of tap water is 30 mL and power is less than 10 mW. NTP test conditions: flowing gas is Air, discharge voltage (Vpp) choose 20kV, NTP treatment choose 4min, pH is 7.5, volume of tap water is 20 mL and power for NTP treatment is ca. 3W. Germinations are processed in Petri dish in darkness under a temperature of ca. 19 °C, humidity of ca. 40% condition and 5 mL liquid in each of them. 15 seeds are germinated in one Petri dish with a cover. The initial germination time choose the beginning of treatment time. All germination curves represent the Kaplan-Meier estimator of the probability of germinating, error bars represent the 95% confidence interval (Greenwood) and the P-value between each two groups is calculated based on Log-rank (Mantel-Cox) test.

Dry seeds (condition vii), wet seeds (condition vi) and immersed seeds (condition iv) are treated by electric field for 4 min, respectively. In this test, seeds treated by an Air NTP is used for a comparison with seeds treated by electric field.

All seeds are germinated in the same conditions as the previous experiments except that seeds are germinated in the dark. t=0 is the beginning of NTP or electric field treatment time. The results are shown in Figure 5. 12 plotting the time evolution of the seed germination percentage for the 4 different treatment conditions plus the control. Two main conclusions can be drawn: a) dry seeds electric field treatment (condition vii) does not seem to significantly improve seeds germination performance compared to the control (p value=0.43); b) wet seeds and immersed seeds electric field treatments (conditions vi and iv) give the same germination boost as direct plasma (DP) treatment (condition i), the p values between NTP treatment and electric field treatment of wet seeds is 0.24, which shows no statistical difference.

5.3.2.1 Comparison of the effect of electric field and plasma direct wet treatment on germination of mung bean

Based on Figure 5. 12, electric field alone promotes mung bean seeds germination as efficiently as direct plasma wet treatment, if seeds are placed inside water or covered with a thin layer of water during electric field exposure (the p value compared to the control group is 10^{-4}). It indicates that the electric field produced by gas discharge is likely to play the dominant role of NTP treatment on enhancing germination of mung bean seeds. The effect of electric field is not sensitive to NTP treatment time (see Figure 5. 3 and Figure 5. 4). This is consistent with the work of Yang [283] et al who reported that 5 to 40 min of electrostatic field (1-2.5 kV/cm) treatment time show a same effect on germination of *Sorbus pohuashanesis* seeds. Wheaton [208] et al. also found that the duration time of electric field treatments does not affect seeds germination by treating soybean and corn seeds with both AC and DC electric field (500-5000V/m).

5.3.2.2 Comparison of the effect of electric field treatment on germination of dry and non-dry seeds

As shown in Figure 5. 12, electric field strongly improves the germination rate of dry and non-dry mung bean seeds. Germination curve of dry seeds treated by electric field exhibits no significant effect on germination enhancement compared to

non-treated seeds. Apparently, electric field is able to boost the rate of germination provided that the seed are immersed in water or even covered by a water layer prior to electric field treatment. It means water is crucial in improving germination rate of mung bean seeds in electric field treatment. This has also been found in the work of other researchers. Zhao et al. claimed that the effect of electrostatic treatment (10 kV/cm) on acceleration of germination rate of Onion (*Allium cepa*) seeds is significantly strengthened when treating seeds immersed in water (in hydration process) [209]. Sudsiri et al. reported that the promoting effect of the electromagnetic DC field treatment on germination percentage of Oil palm (*Elaeis guineensis*) becomes more effective if the seeds absorbed water prior to electric treatment [210].

Table 5. 1 Statistical comparison of the instantaneous probability of germinating of mung bean seeds

Number of seeds	Subset compared	Significant difference? (p-value)	Increase of the instantaneous risk of germination
VS			
CTRL (n=540)	E-field-dry seeds (n=300)	NO (p=0.4)	—
CTRL (n=840)	Direct NTP (n=600)	YES (p<2e-16)	PHH false
CTRL (n=600)	E-field-immersed seeds (n=240)	YES (p<2e-16)	+ 66% /CTRL (for ti ≥21h)
CTRL (n=240)	E-field-wet seeds (n=240)	YES (p=3e-7)	+67 % /CTRL
E-field-immersed seeds (n=240)	Direct NTP (n=480)	YES (p=4e-3)	-22%/immersed seeds
E-field-wet seeds (n=240)	Direct NTP (n=120)	NO (p=0.6)	—

The statistical analysis of several experiments (started at different days) using electric field treatment with seeds in different state is summarized in Table 5. 1. The results confirmed by the calculations of p-value associated with several experiments is consistent with the main conclusion drawn from Figure 5. 12. Besides, the increase of the probability of germinating characterizes the importance of the observed effect on germination. It appears that the two treatments using only electric field with dry seeds and immersed seeds increase the instantaneous risk of germination by ~+66 %. Note also that NTP treatment is similar to electric field on seeds covered with water layer. Hence, electric field alone can promote mung bean seeds germination as

efficiently as direct plasma treatment, if seeds are placed inside water or slightly wet during electric field exposure.

5.3.3 Effect of the electric field amplitude on germination of mung bean
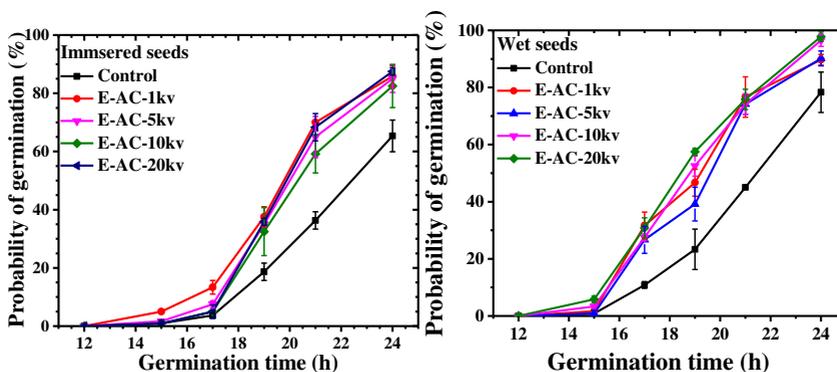
Figure 5. 13 Effect of the applied voltage amplitude (without NTP) on the probability of wet mung bean seeds germinating (left) and immersed mung bean seeds (right). Treatment time for all is 4min, volume of treated tap water is 30 mL and pH is 7.5. t_0 is the beginning of electric field treatment time. Represent experiments are done with 240 for control and 120, for all rest electric field treated groups. Germination is processed in Petri dishes in darkness under a temperature of ca. 19 °C, humidity of ca. 40 % condition and 5 mL liquid in each of them. 15 mung bean seeds are germinated in one Petri dish with 5 mL NTP treated water or tap water. All the curves represent the Kaplan-Meier estimator of the probability of germinating, error bars represent the 95 % confidence interval (Greenwood) and power consumptions measured were below 10mW (detection limit) for all treatment conditions.

By comparing the electrostatic electric field intensity at the position of seeds (about -5 mm in Y axis) with and without water, it is found that water decreases the electric field intensity from 10~30 kV/cm to 3~7 kV/cm, according to the simulation shown in Figure 5. 11. The strength of electric field at the position of seeds in electric field treatment with dry seeds is bigger than with immersed seeds. It is then probably the electric field intensity that strongly affect the germination promotion of mung bean seeds. Therefore, electric field with different amplitudes are applied to treat mung bean seeds. Wet seeds and immersed seeds are treated by electric fields produced by input voltage of 1 kV, 5 kV, 10 kV and 20 kV, respectively. The results are shown in Figure 5. 13.

In Figure 5. 13, germination rate of all electric field treated seeds is improved, but there is not a statistically significant difference among them, which indicates effect of electric field in the 1~20 kV of interval on germination promoting is equivalent. In the work of Morar et al. who carried out a test exposing bean seeds (*Phaseolus vulgare*) naturally infected with *Colletotrichum lindemuthianum* with a 50-Hz electric fields ranging from 2 to 16 kV/cm for up to 30 s, germination energy of infected bean seeds is distinctly improved with more than 99 % of the treated seeds germinated while only 30 % for control seeds, but this effect was independent of the field amplitude [284]. However, Moon et al. [278] found the germination rate of tomato seeds was accelerated by the treatment of AC electric field with an intensity of 4~12 kV/cm, but was inhibited when intensity of electric field is over 12 kV/cm. In the present work, according to Figure 5. 11, magnitude of the electric field in the vicinity of seeds in wet seeds treatments is about 10~30 kV/cm at potential V= 20 kV and about 0.5~1.5 kV/cm at potential V= 1 kV; in immersed seeds treatment is about 3~7 kV/cm at potential V= 20 kV and about 0.15~0.35 kV/cm at potential V= 1 kV. It means the effect of electric field treatment on germination promotion of mung bean seeds cannot be affected by magnitude of electric field ranging from 0.15~30 kV/cm.

Table 5. 2 Statistical comparison of the instantaneous probability of germinating: effect of the electric field on wet seeds and immersed seeds

Number of seeds	Subset compared		Significant difference?	Increase of the instantaneous risk of germination
	VS		(p-value)	
E-Field-immersed seeds	CTRL (n=600)	1 kV (n=240)	YES (p=4e-15)	PHH false
	CTRL (n=780)	10 kV (n=300)	YES (p<2e-16)	PHH false
	CTRL (n=600)	20 kV (n=240)	YES (p<2e-16)	+ 66% /CTRL (for ti ≥21h)
	1 kV (n=240)	20 kV (n=240)	NO (p=0.4)	—
E-Field-wet seeds	CTRL (n=240)	1 kV (n=120)	YES (p=3e-8)	PHH false
	CTRL (n=240)	10 kV (n=120)	YES (p=7e-11)	+115%/CTRL
	CTRL (n=240)	20 kV (n=120)	YES (p=3e-7)	+67%/CTRL
	1 kV (n=120)	20 kV (n=120)	NO (p=0.2)	—

Table 5. 2 summarizes the results of the statistical analysis when the results of experiments started at different days are combined. The level of statistical significance of the effect of electric field is very high ($p < 3e\text{-}7$) for all conditions and all voltage considered. Moreover, no significant statistical difference appears between the treatments performed with different peak to peak voltage. Indeed, the p-value between 1 kV and 20 kV treatments is 0.4 for immersed seeds and 0.2 for wet seeds. Such result is consistent with the assumption that the effect of electric field on germination is not sensitive to voltage above a certain threshold of voltage. Another kind of statistical test and experiments should be performed to investigate the statistical equivalence of the groups treated.

So far, the conclusions about the experiments performed on Mung Bean concerning germination are:

1) direct plasma wet treatment is more effective than indirect plasma wet treatment whatever the carrier gas is;

2) Electric field treatment leads to an effect comparable with the effect of direct plasma wet treatment;

3) Dry treatment using electric field does not increase the germination rate.

At this stage, it is interesting to discuss the possible mechanisms leading to the observed germination boosting effect, particular, the role of the water uptake in the germination process.

5.4 Mechanisms of the effect of NTP and electric field on germination of mung bean interaction

It is known that germination starts from water adsorption; the process of water uptake for seeds in germination is called germination hydration. Generally, this process can be divided into three main stages [161, 285]. For mung bean seeds, stage I (also called imbibition phase) is the seeds physical water uptake and is usually considered without -or with little- metabolism. This stage lasts for around 10 hours

depending on germination conditions such as temperature, humidity, seeds initial moisture etc. Stage II (also called activation phase) is a process where enzymatic transformation of meristematic cells and initiation of metabolic activities take place, and shows a limited water uptake; this stage is generally short for mung bean seeds (around 2 hours) [23]. Stage III (also called growth phase) starts with the beginning of visible germination (appearance of radicle elongation). In this section, the focus is put on how NTP and/or electric field affect hydration process of mung bean seeds in stage I. First, mung bean seeds with different initial moisture were prepared for NTP treatments, so that it could be determined if treatments exert some influence on seeds water uptake; second, experiments using NTP and/or electric field on germinated seeds but in different stage are carried out to observe if metabolisms are influenced. In addition, morphology of seeds surface and water adsorption isotherms of seeds are also investigated.

5.4.1 Morphological imaging of mung bean seeds coat surface

The surface morphological changes are identified using SEM imaging and shown in Figure 5. 14. The surface of a dry untreated seed (Figure 5. 14a) contains fragments with a characteristic size varying from nanometers to tens of micrometers. These irregularly shaped, randomly distributed fragments are probably outer cuticle wax composed of hydroxylated fatty acids [286]. This profile is typical of the cuticular waxes of many legume species [286, 287]. After 3h of germination, it can be seen in Figure 5. 14b that surface of untreated seeds coat shows less amounts of small size fragments but still has the larger one. This washing effect is remarkably strengthened in the seeds treated by NTP compared to the untreated ones; the treated seed surface becomes smother and only tiny fragments can be observed (Figure 5. 14d). However, no marks of being etched and signs of crack on treated seeds surface are noticed. After 20h of germination, porous and rough surfaces are formed, as can be clearly seen in image of untreated seeds (Figure 5. 14c) and image of plasma treated seeds (Figure 5. 14e). All these two seeds show a flat surface and no fragments.
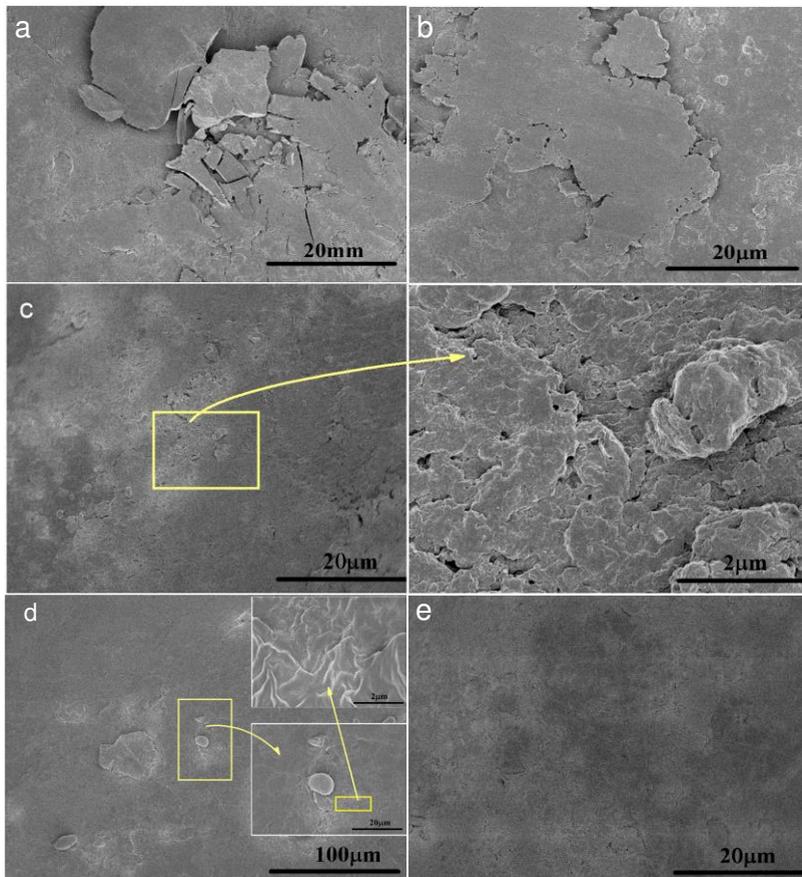
Figure 5. 14 Scanning electron micrographs of mung bean seed coats: Surface of untreated dry seed (a), surface of untreated seeds at 3h (b) and 20h (c) of germination time, surface of plasma treated seeds at 3h (d) and 20h (e) germination time

5.4.2 Water uptake of mung bean seeds during germination process

During the process of seeds germination, the sequence of germination stage is governed by seeds water uptake from external substrate. As shown in Figure 5. 15, the hydration curve of seeds can either have a downward concave shape (DCS), meaning that water uptake, fast at the beginning, decreases gradually with the increase of imbibition time, or show a sigmoidal behavior, which has a lag phase before the rapid water influx rate. Lag phase is an adaption period where seeds are

in a state of low rate of water uptake. The two forms of water uptake are differentiated by the mass transfer rate at the beginning of the process [288].
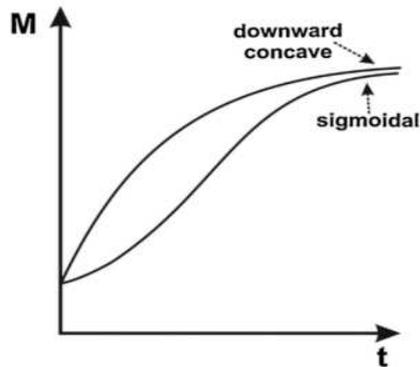
Figure 5. 15 General behavior of grains during hydration: downward concave (DCS) and sigmoidal shapes [288]

The driving force that enhances water absorption by the seeds is the low water potential of seeds. Water potential (Ψ) expressed as pressure units is a measure of the energy of the water in the seed. It drives water movement that flows water molecules from high potential to low potential. Pure water has the highest potential value, that is 0 MPa. Water potential of dry seeds usually range from -50 to -350 MPa. Therefore, during stage I Ψ inside the seed approaches equilibrium with external. In this stage, water penetrates or diffuses into seeds through different channels, which depend upon the particular seed constituents. For mung bean, Miano [161] et al. have shown that its coat is not or almost not porous when the moister level (water content) of the dry seed is below 15-20% d.b. In addition, it was recently shown that the hilum - also called eye, which is the mark left on a seed coat by the former attachment to the ovary wall, is porous and is probably the entrance gate for the primary water uptake. Hence, in the first phase of the hydration process, water principally comes through the hilum, then, a directional structure progressively guides water to the radicle, to the cotyledon and then to coat-cotyledon space. When Ψ inside and outside seeds reach the same value, stage II starts and follows with stage III.

200 seeds (~7 g) in each group are chosen for water uptake experiments. The

initial moisture content of mung bean seeds is 6.83 % d.b. Procedures of NTP and electric field treatments are same with previous tests. All groups are germinated in a big Petri dish with a filter paper. Results have been shown in Figure 5. 16.
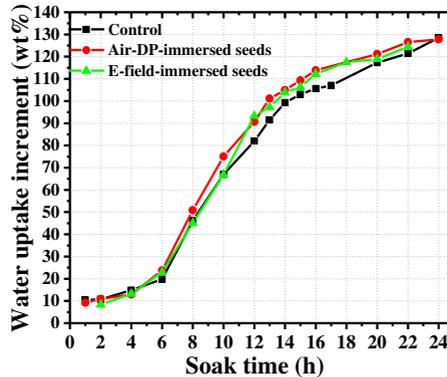
Figure 5. 16 Water uptake curves of mung bean seeds during germination process

The hydration process of mung bean seeds is known to have a sigmoidal form for low initial moister content and a DCS shape for initial moister level higher than 20 % [288]. In our case, the initial moister level is low and a sigmoidal shape is observed with or without treatment. As can be observed, germination time interval between 0 to 14 h is attributed to the imbibition phase (stage I). At the end of this stage, water uptake rate decreases sharply at germination time of 17 h. This is the beginning of the activation phase (stage II). After that, water uptake rate increases again in the (stage III).

Lag phase in imbibition stage exhibits a similar period for all groups and lasts 6 h. However, seeds treated by NTP and electric field display a slight faster water uptake rate in the rapid hydration process than that of untreated seeds. In this period, NTP and electric field treated seeds exhibit the same water uptake rate in the end of stage I. Time dividing line for activation phase in the curves of treated seeds is not clear. However, based on the hypothesis that all the tested seeds possess the same equilibrium moisture, the starting time of stage II for treated group is 13 h versus 14 h for untreated group; this indicates that the NTP or electric field has a little influence in triggering stage II. In the growth phase (stage III), the water uptake of treated

seeds gradually reaches the same value as untreated seeds.

In general, hydration process of mung bean seeds with 6.83 % d.b. of initial moisture behave in sigmoidal form. Hydration behavior of mung bean seeds can be changed by initial moisture of seeds. The higher initial moisture the faster water uptake rate[161].

5.4.3 Link between mung bean germination and treatments of NTP and electric field

One of the hypotheses we can make to explain effects of electric and NTP treatment is that the acceleration of germination of mung bean seeds by NTP or electric field can be attributed to the boost of hydration and/or germination related metabolic activities. In short, stage I is mostly a physical process of water uptake, and the metabolisms governing the initiation of seeds germination is unlikely to be triggered during this period due to the low water content of seeds; gradually, metabolism activities will be increased because of a higher hydration levels, at least for an activation of enzymes for radical scavenging [289]. When hydration level approaches the equilibrium, germination process enters stage II, where series of biochemical reactions will be prepared and activated. Since only a small amount of water will be further absorbed during this process, treatments by NTP or electric field should be related more to germination related metabolisms. Stage III is the growth phase in which a lot of vital physiological activities are processing. These activities include reserve mobilization, phytohormonal regulation, glyoxylate cycle and respiration process. The duration of stage III is important because germination is considered to be completed prior the embryo growth is initiated. In the present study, the germination is considered and validated when the length of sprout reaches half-length of mung bean seeds. During this period, water absorption of seeds is no longer mainly restricted by permeability of cell wall and membrane but also by cell osmotic potential. This is tightly related to cellular metabolic processes, which could also be influenced by the NTP or electric field treatments. In order to determine the influence of NTP or electric field treatments on germination hydration and metabolic process, tests with seeds in different initial moistures are carried out.

5.4.3.1 Does a full immersion of seeds in water before treatment accelerate germination?

Generally, the faster the uptake of water by the seeds, the higher the rate of seed germination [177, 193]. It was reported in the literature that the water uptake curve and water uptake rate increase with the initial seed moisture[161].

One hypothesis we could make is that NTP or electric field treatments improve germination by affecting hydration process to some extent. If the hypothesis that NTP treatment influences the seeds water uptake is true, effects of NTP on regulating seeds germination should be affected by changing the initial water content of seeds. To verify this hypothesis, mung beans seeds are fully immersed into water for a given time to increase their initial moisture before any NTP treatment. The influence of this immersion process on cellular metabolism activities of seeds is first investigated by immersing seeds before germination in Petri dishes for few hours. Mung bean seeds are totally sunk into water for 1h, 2h, 4h and 6h, respectively. All seeds germinate in Petri dishes after immersion. The percentages of germinated seeds are shown in Figure 5. 17 as a function of time.
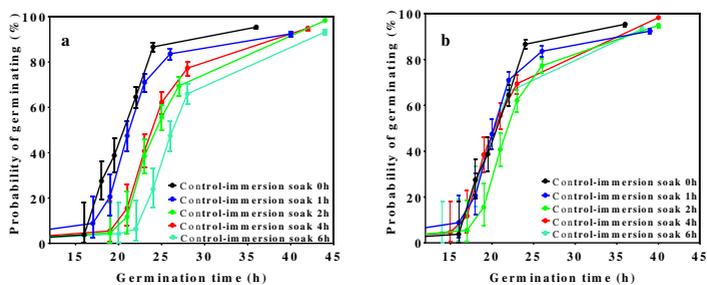
Figure 5. 17 Effect of full immersion time with tap water on germination rate of mung bean. The time reference in fig a) is the start of full immersion and the reference time in fig b) is the start in Petri dishes (after immersion time). 240 seeds are used for each group. Germination is processed in Petri dishes with light irradiation under a temperature of ca. 21 °C, humidity of ca. 40% condition and 5 mL tap water in each of them. All the curves represent the Kaplan-Meier estimator of the probability of germinating, error bars represent the 95% confidence interval (Greenwood) and the P-value between each two groups is calculated based on Log-rank (Mantel-Cox) test.

In Figure 5. 17a, the abscissa axis is the time since the seeds are immersed into

water. Germination rate of seeds soaked for 1 h is slower than seeds without an immersion, but significantly faster than seeds soaked for 2 h, 4 h and 6 h. It indicates the immersion process significantly delays germination of mung bean. Note that all seeds reach 100 % germination rate. According to Figure 5. 17a, it is concluded that full immersion process for few hours slows down germination rate without affecting the final germination percentage. In order to investigate if this immersion process causes influence on metabolism activities of seed cells, the beginning of germination time is shifted to the time when seeds are placed in Petri dishes (after full immersion), as shown in Figure 5. 17b. In this figure, all germination curves are superimposed, which means that the seeds do not germinate during full immersion although they absorb water, even for a 6h of immersion time. This is likely due to a lack of oxygen during immersion. Full immersion of seeds into water for hours increases the water content of seeds, but the water absorbed by seeds fail to accelerate germination rate. According to Figure 5. 17b, it seems that immersion process can increase the initial water content of seeds without affecting cellular metabolism activities. This is contradiction with result published by Miano [161] et al. who showed on mung bean seeds (*Vigna radiata*) that increasing the moister of seeds would speed up the germination process. The reason of this contradiction is an open question.
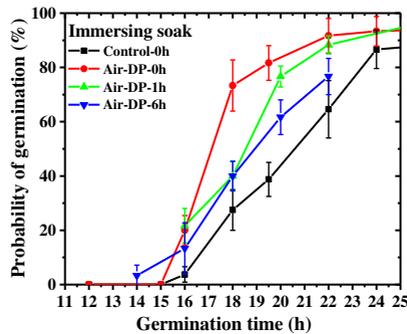
Figure 5. 18 Effect of NTP treatment on germination of pre-immersed mung bean seeds. The initial germination time choose the beginning of germination in Petri dishes. The conditions are: 240 seeds for each group; Air discharge time is 4 min with 20 kV of Vpp, 1.5 SLM of flow rate and 20 mL of tap water in each treatment. Germination is processed in Petri dishes with light irradiation under a temperature of ca. 21 °C, humidity of ca. 40% condition and 5 mL liquid in each of them. 15 mung bean seeds are germinated in one Petri dish with 5 mL NTP treated water or tap water. All the curves represent the Kaplan-Meier estimator of the probability of germinating, error bars represent the 95% confidence interval (Greenwood) and the P-value between each two groups is calculated based on Log-rank (Mantel-Cox) test.

The influence of NTP treatments on germination hydration process of seeds is then investigated by treating the immersed seeds before germination in Petri dishes. After the immersion process, soaked seeds and non-soaked dry seeds are treated by Air NTP for 4 min. After NTP treatment, all seeds germinate in Petri dish. The beginning of germination time for all seeds is the time when seeds germinate in Petri dish. Comparison of NTP effects on germination of seeds with different initial moisture is displayed in Figure 5. 18.

All plasma treated seeds conditions show an accelerated germination rate, compared to non-treated seeds. Among them, NTP exhibits the best performance when the full pre-immersion time is 0, with a germination rate 4 times higher than that of non-treated seeds at 18 h of germination time; the effect of NTP on germination promotion is weakened when seeds are immersed into water for a long time prior to NTP treatment. Seeds with shorter pre-immersion time have a faster germination rate than seeds with a longer pre-immersion time. Apparently, performances of NTP treatment on accelerating germination rate of mung bean seeds decrease when increasing seeds initial moisture. This shows that the NTP treatment, to be effective, should be applied prior water uptake by the seeds.

As shown before, it is likely that the first step of water uptake goes through the hilum leading to an increase of the membrane permeability. However, if the permeability is increased too quickly, a large leakage of electrolyte inside the seed will be produced and the seed will be damaged [290-292]. On the other hand, NTP treatment or only electric field treatment have also been reported to be able to decrease the permeability of seeds cell membrane when seeds are in hydration process [275, 293].

Note that 6 h of immersion cannot fully hydrate seeds as shown on Figure 5. 16. In Figure 5. 18, seeds immersed for 6 h prior NTP treatment still have a better germination potential than the control group. The effects of seeds hydration on germination widely vary with hydration time, positively or negatively and even death [294]. Mung bean germination is sensitive to oxygen and longtime immersion could cause seed rotting.

5.4.3.2 Effect of treatments of NTP and electric field on metabolic activity of germination

In order to compare the effect of NTP and electric field treatments on seeds in higher hydration levels and to explore the relations between treatments and metabolic activities of germination, seeds are treated at different stages of the germination process. 15 seeds per Petri dish is semi-immersed with 5 mL liquid in darkness. Contrary to the conditions of Figure 5. 17 and Figure 5. 18, seeds are not fully immersed and are not deprived of oxygen.

Based on the germination hydration curve shown in Figure 5. 16, five hydration (germination) times ranging from germination stage I to stage II are selected. The germination time include four points in imbibition phase (2 h, 4 h and 6 h in early hydration process and 11 h in rapid hydration process) and one point at 16h in activation phase. The germinated seeds are then treated by NTP or electric field. Responses of seeds at different hydration levels to the treatment of NTP and electric are shown in Figure 5. 19 as a function of the time since the seeds are soaked into water.
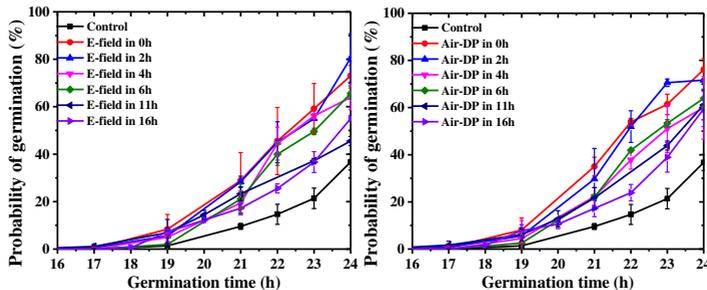
Figure 5. 19 Effect of NTP (right) and electric field (left) treatments on germination of mung bean seeds in different germinated stages. The initial germination time choose the beginning of seeds soaking time. The conditions are: 240 seeds for each group; Air NTP discharge time is 4 min with 20 kV of Vpp, 1.5 SLM of flow rate and 20 mL of tap water in each NTP treatment; Non-gas electrode treatment time is 4 min with 20 kV of Vpp and 30 mL of tap water in each electric field treatment. Germination is processed in Petri dishes in darkness under a temperature of ca. 19 °C, humidity of ca. 40% condition and 5 mL liquid in each of them. 15 mung bean seeds are germinated in one Petri dish with 5 mL NTP treated water or tap water. All the curves represent the Kaplan-Meier estimator of the probability of germinating, error bars represent the 95% confidence interval (Greenwood) and the P-value between each two groups is calculated based on Log-rank (Mantel-Cox) test.

Let us draw some remarks:

1) The germination of all treated group is accelerated compared with untreated seeds;

2) Similar to results obtained in the case of Figure 5. 18, for which seeds were fully immersed, the positive effect of both NTP and electric field on germination promotion gradually decreases with the treatment is applied later in the germination process. Then, it is concluded that the higher the degree of germination of seeds, the weaker the effect of NTP and electric field on promoting germination;

3) However, even if the positive effect of the NTP and electric field treatment decreases with higher hydration, this effect is still positive, even when the treatment happens 16h after the beginning of the germination process (stage II). Hence the germination improvement can be attributed to the influence of treatments on those germination related metabolic activities, since stage II is also a time when plenty of various metabolic activities start. This is consistent with the results from works of Wang [275] et al, Dymek [282] et al and Leong[211] et al etc;

4) It is remarkable that the decrease of the positive effect of the treatment with the delay time is much less in the case of a standard germination process (Figure 5. 17b), when the seeds are fully immersed (Figure 5. 17a).

In summary, treatments of NTP or electric field treatment improve germination of mung beans seeds mainly through the interaction with germination-related hydration and metabolic processes.

5.5 Summary

This chapter pointed investigated the respective role of NTP, chemicals, electric field treatment on mung bean seeds germination at different initial level. For this purpose, identification of key NTP parameter affecting germination is first

investigated. The investigated parameters include various NTP produced aqueous particles with both long lifetime and short lifetime, and electric field. Seeds with different initial moisture and germinated seeds are chosen to be treated by NTP or electric field to clarify how germination of seeds is improved.

1) Effect of NTP produced aqueous species on mung bean seeds germination

    i) Germination curves of seed directly treated with NTP show faster germination than that of indirect plasma treated seeds in all gases discharge; this argues in favor of the role of short-lived species produced in liquid phase by NTP;

    ii) Germination promoting effect of NTP treatment is not sensitive to the treatment time in the scanned range;

    iii) Acidification could increase germination rate for seeds without NTP direct treatments but could not further assist in strengthening NTP boosting effect;

    iv) There is no effect of the distance from the seeds to the water surface of their germination percentage, which indicates that very short-lived ROS, e.g. OH, are maybe not the main candidates to affect germination.

2) Effect of electric field on mung bean seeds germination

    i) Electric field intensity of 20 kV at the position of the seeds top surface is 10~30 kV/cm without water and 3~7 kV/cm at the same position with water;

    ii) Germination curves of seeds treated by electric field show same promoting effect with seeds treated by NTP;

    iii) Wet seeds and immersed seeds response to electric field in a similar way and both with a much better performance in germination promotion than that of dry seeds;

    iv) Intensity and treating time of electric field have very littles influence on germination;

v) Water is necessary in accelerating germination rate of mung bean of electric field.

3) The relation between germination of mung beans and treatment with NTP and electric field alone

i) No marks of being etched and signs of crack on seeds surface are noticed;

ii) Germination of seeds treated by NTP is similar to the seeds treated by electric field;

iii) Influence of NTP on germination relates to seeds hydration process that the higher the degree of hydration of seeds, the weaker the effect of NTP and electric field on promoting germination;

iv) Treatments of NTP or electric field treatment improve germination mainly through the interaction with germination related hydration and metabolic processes.

Chapter 6: Characterization of effect of helium plasma jet treatment on the modification of structure of mice skin using *ex vivo* Mueller polarimetric imaging

Collagen is a major component of the extracellular connective tissue matrix of the skin. Under low dose treatment, Non-Thermal Plasmas (NTP) may promote the secretion of collagen in *in vivo* treatments of skin and at the cell level in *in vitro* experiments [104]. At higher dose treatment, NTP may modify or even damage the triple helical structure of collagen in *ex vivo* treatments of skin [75, 224, 228, 242-244]. An alteration of its spatial structure can cause the changes of the structure of skin tissue. The modification of the microstructure of the skin tissue can further affect its optical properties and greatly change its polarimetric signature. Numerous publications have showed that polarimetric parameters of transmitted or reflected light can provide very useful information about the microstructure of biological tissues [229-232, 238-240, 247]. For example, depolarization (Δ) can be used to evaluate the scattering properties of medium [237], linear retardance (δ) enables to characterize the anisotropy of medium [238] and orientation of eigenvalue axis (also called Azimuth, labeled with α) is a potential parameter indicating the orientation of the fibrous collagen [241]. Mueller polarimetric imaging (MPI) is an optical imaging technique enabling the comprehensive characterization of polarimetric properties of different types of samples, such as biological tissues. It has been widely applied for improving detection and surgery of cancer for different types of biological tissues, such as cervix, colon and skin [229-232]. Therefore, the aim of this chapter is to detect and visualize the influence of a helium plasma jet treatment on the modification of the microstructure of *ex vivo* mice skin by characterizing its polarimetric properties in terms of Δ, δ and α. Based on the literature [295, 296], thermal effect of NTP treatment is an important factor modifying the structure of

collagen. Hence, the experiments with skin being heated with an oven aims to simulate this thermal effect on the modification of skin microstructures in a NTP treatment and have been specifically carried out. The Mueller matrices of skins tissues treated with plasma treatments or thermal treatments are measured by the MPI in a backscattering configuration.

Images named CTRL belong to the control group and correspond to polarimetric parameters characterizing untreated skin before NTP treatments or thermal treatments. We define a term "SAP" to represent the zone of skin affected by plasma and a term "SNAP" to represent the zone of skin non-affected by plasma. As shown in Figure 6. 1, in the skins treated with NTP, the peripheral skin adjacent to SAP can also be affected by plasma and the region inside SAP appears different zones with distinct δ. According to the δ of skin, we define Z1 is the region containing the entire SAP and the peripheral skin around SAP, which has a different retardance from SNAP; Z2 is the entire region of SAP; Z3 is the central part of SAP and this region has a different δ to the edge zone of SAP. CTRL that is the untreated skin has the same position and size with Z1.
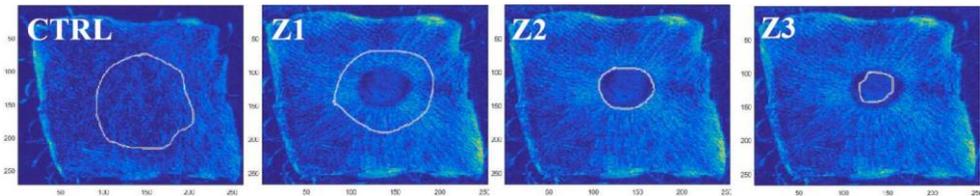
Figure 6. 1 Regions of the cycle selected zone in the image of δ of skin treated with NTP. Z3 is inside Z2 which is inside Z1.

In this chapter,

1) the skin is treated with a helium plasma jet either in a continuous treatment or a sequential treatment. The term of "P-Xmin-Z1" represents the Z1 zone of skin treated with NTP for a X min continuous treatment, the term of "P-Xmin-Z2" represents the Z2 zone of skin treated with NTP for a X min continuous treatment and the term of "P-Xmin-Z3" represents the Z3 zone of skin treated with NTP for a X min continuous treatment. The term of "P-1min*N-Z1" represents the Z1 zone of skin treated by a sequence of N times

1 min NTP treatment, The term of "P-1min*N-Z2" represents the Z2 zone of skin treated by a sequence of N times 1 min NTP treatment and The term of "P-1min*N-Z3" represents the Z3 zone of skin treated by a sequence of N times 1 min NTP treatment;

2) similarly, the skin is heated with an oven either in a thermal continuous treatment or a thermal sequential treatment. The term "T50-6min" represents the skin which is thermally treated for a 6 min continuous treatment using a 50 ℃ oven. The term "T50-6min-T60-6min" represents the skin which is first thermally treated for a 6 min continuous treatment using a 50 ℃ oven and then thermally treated for another 6 min continuous treatment using a 60 ℃ oven. The term of T60-1min*N represents the skin which is treated for N times 1 min thermal treatment using a 60 ℃ oven. It is same for skins continuously or sequentially treated with the oven in other temperature and treatment times;

3) the temperature of SAP in the skin treated with NTP is measured by an IR camera during the whole treatment. the temperature of thermally treated skin is measured by the IR camera at the end of thermal treatments;

4) the Mueller polarimetric parameters (Δ, δ and α) of mice skin tissue are calculated based on the method of Lu-Chipman algorithm using MATLAB [233]. Each histogram of Mueller polarimetric parameters of the selected zone in the skins are obtained by dividing all the pixels of selected zone into 200 equal interval using MATLAB. Y axis of the histogram is the sum of all pixels in each interval. The value of Y axis is proportional to the area of the selected zone, which is not considered in the present chapter. It will be studied in the further work by normalizing the intensity.

6.1 *Ex vivo* Mueller Polarimetric Imaging of mice skin treated by plasma jet

6.1.1 MPI for investigating the effect of plasma continuous treatment on *ex vivo* mice skin

NTP treatment dose is crucial to the influence of NTP on the modification of skin microstructure. The structure of skin can either be slightly affected by NTP treatment with a low dose or be damaged by NTP with a high dose. In this chapter, the aim of skin treatments with plasma continuous treatment is to study the polarimetric properties of skin treated with NTP for different treatment times (The treatment "dose" is proportional to treatment time) and to select a NTP treatment time which can change but cannot damage the skin structure for a further investigation. In this subsection, the MPI and infrared camera imaging are used to analyze mice skin for different conditions of plasma treatment. MPI aims to study the modifications in the microstructure of the tissue. Camera infrared is used to monitor the variation of temperature of the tissue. A mice skin without NTP treatment is used as reference and labeled CTRL. The skin samples used in this experiment come from the same mice and are cut into several small pieces. Four different pieces have been treated with plasma jet continuously for different exposure times: sample a for 0.5 min, sample b for 1 min, sample c for 2 min and sample d for 6 min. Mueller polarimetric images have been acquired for each sample before and after plasma treatment. Also, thermal images have been acquired during the whole NTP treatment.

The corresponding temperature of the SAP zone in skin treated by NTP in different times are shown in Table 6. 1. The temperature in all CTRL skins are same, which is the room temperature (20 ℃). The temperature of SAP increases with NTP treatment time. Temperature of SAP is increased by 65% (from 20 ℃ to 33 ℃) after a 0.5 min treatment, but is quickly increased by 195.5 % (from 20 ℃ to 58.9 ℃) by treating with NTP for 1 min. SAP temperature is stale around 70 ℃ when the NTP treatment time is over 2 min.

Table 6. 1 Temperature of the skin treated by plasma continuous treatments

NTP treatment time	CTRL	0.5 min	1 min	2 min	6 min
Skin temperature	20 ℃	33 ℃	58.9 ℃	69 ℃	72 ℃
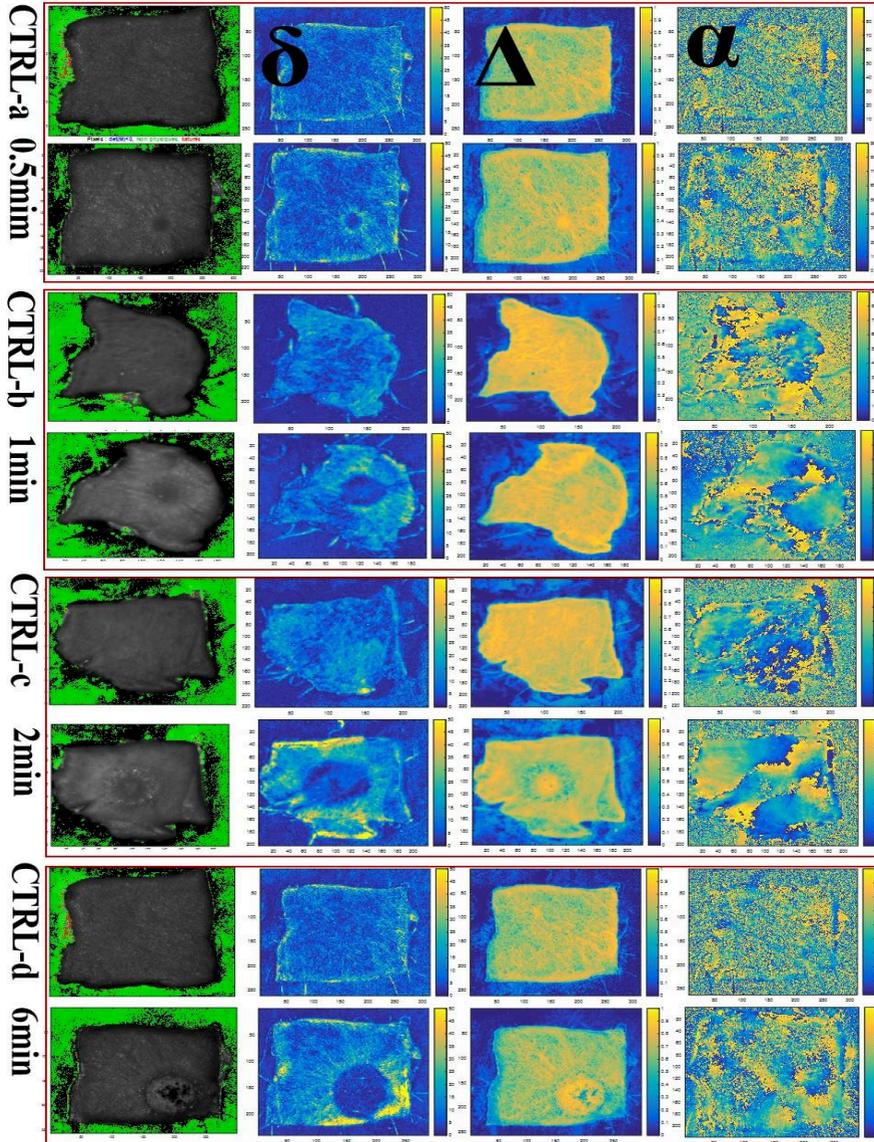
Figure 6. 2 MPI of different mice skins treated continuously by a plasma jet in different treatment times. The plasma jet discharge conditions for all treatments are same. The wavelength of MPI is 550 nm. δ represents the linear retardance of skin, α represents the Azimuth of linear retardance of skin and Δ represents the total depolarization of skin.

Figure 6. 2 shows the images of Mueller polarimetric parameters of untreated mice skin and the skins treated with plasma continuous treatments. Mice skins are

treated by the helium plasma jet for 0.5 min, 1 min, 2 min and 6 min, respectively. It is found that extending the NTP treatment time expands the area of SAPs. The area of SAP in the skin treated by NTP for 0.5 min is roughly similar to the cross-section of the plasma jet, while this area is largely increased due to the spread of NTP on the surface of skin when NTP treatment time is increased to 2 min. Area of SAP of 2 min NTP treated skin is similar to the skin treated with NTP for 6 min. The polarimetric properties of skins will be presented in histograms and be analyzed next.

Figure 6. 3 Histograms of linear retardance and depolarization of different zones in the skin treated continuously with NTP for 0.5 min and the corresponding untreated skins

Figure 6. 3 shows the histogram of δ and Δ of different zones in the skin treated continuously with NTP for 0.5 min and the corresponding untreated skins. The δ of CTRL-a skin ranges from 0 to 30 degree and the peak of histogram is at 7 degree. The Δ of CTRL-a skin ranges from 0.45 to 0.86 and Δ histogram has peak at 0.7. CTRL skin evidences Δ mainly due to multiple scattering. A retardance can be observed in CTRL skin indicating the applied mice skin in this work is an anisotropic biological medium. Polarimetric parameters of SAP are influenced by the plasma continuous treatment. The δ of peripheral skin adjacent to SAP is increased by the NTP treatment, which leads to maximum δ of Z1 increase to 40 degree (increased by 33 % with respect to CTRL-a). This histogram is larger than that without treatment showing that globally the retardance is increased with respect to the sample without a treatment. In particular a strong increasing of retardance is observed around the SAP zone. However, in the treated zone (SAP) the retardance is globally decreased as shown by the histogram for Z2 which range from 0 to 12. The entire

SAP (Z2) shows an evenly distributed retardance and the δ histogram of Z3 (not given) is same with Z2. The Δ of Z1 is similar to CTRL-a, which shows a histogram with the depolarization ranging from 0.4 to 0.83. The Δ of SAP (Z2) is increased with respect to untreated skin, which ranges from 0.6 to 0.83.
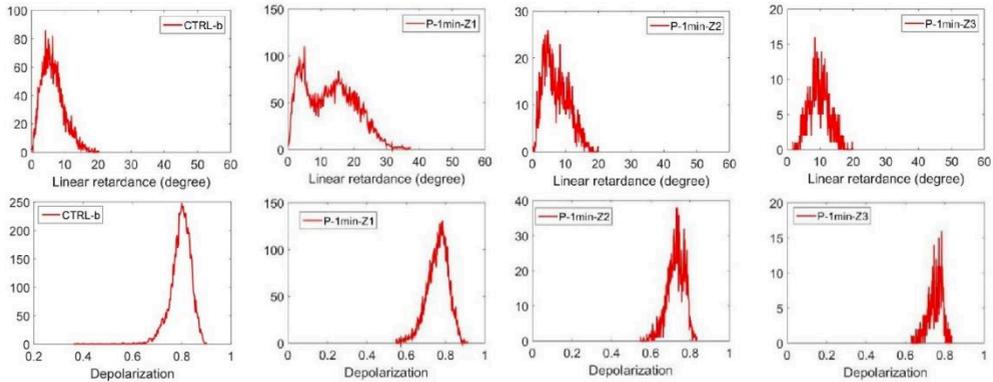
Figure 6. 4 Histograms of linear retardance and depolarization of different zones in the skin treated continuously with NTP for 1 min and the corresponding untreated skins

Figure 6. 4 shows the histogram of δ and Δ of different zones in the skin treated continuously with NTP for 1 min and the corresponding untreated skins. The δ of CTRL-b skin ranges from 0 to 20 degree and the peak of δ histogram is at 5 degree. The Δ of CTRL-b skin ranges from 0.6 to 0.9 and Δ histogram has peak at 0.8. Globally the effect of treatment is an increasing of the retardance. The δ of peripheral skin adjacent to SAP is increased by the NTP treatment, which leads to the maximum δ of Z1 increase to 30 degree (increased by 50 % with respect to CTRL-a). Z2 exhibits two zones with different histogram peaks. The first around 8 degree (very similar to CTRL-b) and the second around 18 degree which corresponds to the part around the treated zone. The entire SAP (Z2) shows a similar δ histogram to CTRL-b skin. The peak of δ histograms of the central part of SAP (Z3) is increased to 10 degree, which is higher than the CTRL-b (increased by 100 %). The Δ of Z1 is similar to CTRL-a. It ranges from 0.6 to 0.9 and the peak of histogram is 0.8. The Δ of Z2 and Z3 are slightly decreased by NTP treatment. The peak of Δ histogram is decreased to ca. 0.7 (decreased by 12.5 % with respect to CTRL-b) and the maximum Δ is 0.8 (decreased by 12.5 % with respect to CTRL-b).
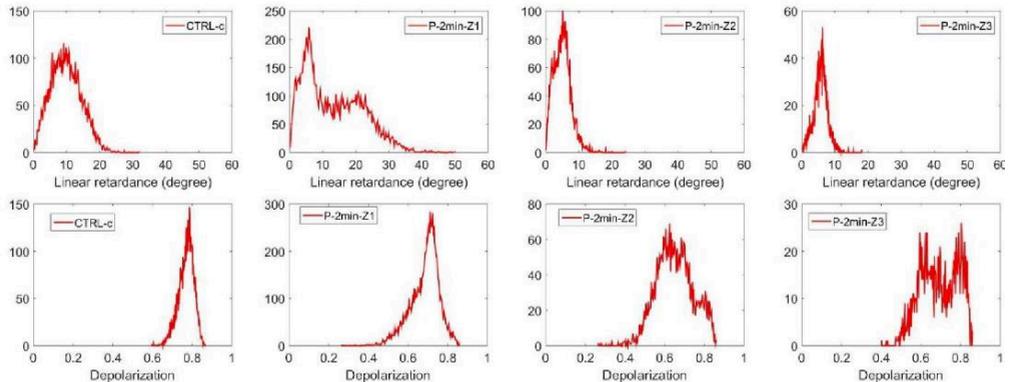
Figure 6. 5 Histograms of linear retardance and depolarization of different zones in the skin treated continuously with NTP for 2 min and the corresponding untreated skins

Figure 6. 5 shows the histogram of δ and Δ of different zones in the skin treated continuously with NTP for 2 min and the corresponding untreated skins. The δ of CTRL-c skin ranges from 0 to 20 degree and the peak value of histogram is ca. 10 degree. The Δ of CTRL-c skin ranges from 0.6 to 0.84 and Δ histogram has peak at 0.76. The δ of peripheral skin adjacent to SAP is significantly increased by the NTP treatment, which leads to maximum δ of Z1 increase to 40 degree (increased by 100 % with respect to CTRL-c). Two peaks appear in the δ histogram of Z1. The first 5-degree peak is attributed to the histogram of SAP (Z2), which is even decreased with respect to the corresponding untreated skin. The second 20-degree peak belongs to the δ histogram of boundary of plasma treated zone (SAP). The retardance of SAP is globally decreased as shown by the δ histogram for Z2 which ranges from 0 to 12. The peak of δ histograms of Z2 is decreased to 5 degree (decreased by 50 % with respect to the CTRL-c). The retardance of Z3 is same with Z3. Similar observations can be made for the Δ of plasma treated skin. The Δ histogram peak of CTRL-c is similar to that of Z1, which is at 0.76. This peak is greatly decreased to 0.6 in the region of entire SAP (Z2) (decreased by 21 % with respect to CTRL-c). The Δ histogram of Z2 also exhibits a small peak at 0.8. The histogram of Z3 is similar to that of Z2, but the second peak at 0.8 is more significant than the one in Z2. Based on the MPI of P-2min-Z3 (Figure 6. 2), it indicates that NTP treatment for 2 min decreases the Δ of the edge region of SPA, while show less influence on the central part of SAP.
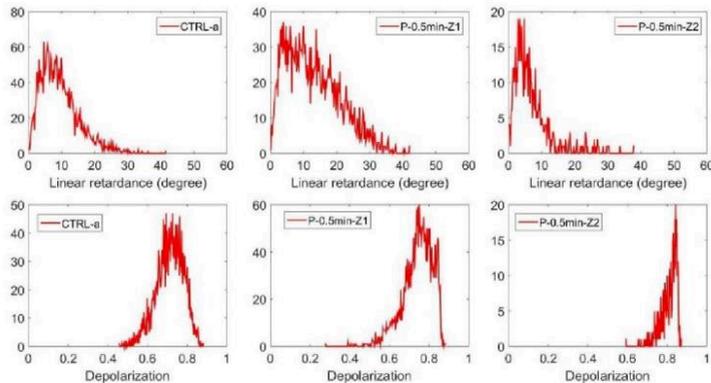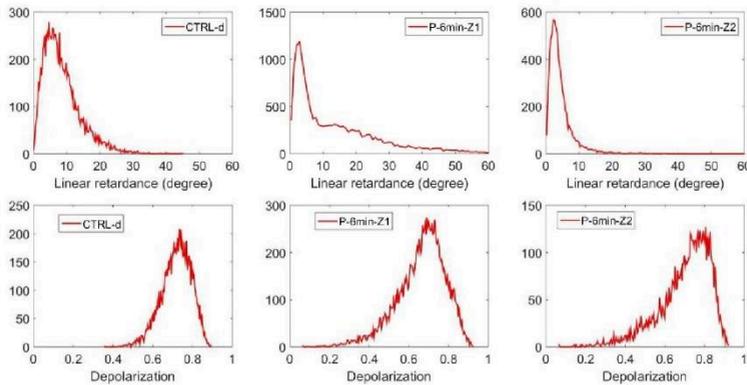
Figure 6. 6 Histograms of linear retardance and depolarization of different zones in the skin treated continuously with NTP for 6 min and the corresponding untreated skins

Figure 6. 6 shows the histogram of δ and Δ of different zones in the skin treated continuously with NTP for 6 min and the corresponding untreated skins. The δ of CTRL-d skin ranges from 0 to 30 degree and the peak value of histogram is ca. 7 degree. The δ of peripheral skin adjacent to SAP is slightly increased by the NTP treatment, which leads to maximum δ of Z1 increase to 50 degree. However, the retardance of SAP (Z2) is declined significantly with the respect to untreated skin, which is consistent with the sample of P-1min*2-Z2. The maximum δ of Z2 is 10 degree and the peak of histogram is 3 degree. Similarly, the Z3 is not appeared in the central part of SAP, which means the retardance in the entire SAP is decreased by the 6 min NTP treatment. The value of Δ histogram of CTRL-d skin ranges from 0.4 to 0.87, while the Z2 and Z3 show a decreased histogram ranging from 0.2 to 0.87. The distribution of depolarization of Z2 is same to that of Z1.

As shown in Figure 6. 2, untreated skins exhibit a randomly distributed Azimuth (α), but with a plasma treatment the distribution of α is globally tend to specific directions. α histograms of all the selected zones in each sample are listed in Appendix C (Figure C. 1, Figure C. 2, Figure C. 3 and Figure C. 4). The α histogram has two peaks that are at 28 degree and at 45 degree in P-1min-Z1, has one peak at 20 degree in P-1min-Z2 and has one peak at 25 degree in P-1min-Z3. The Azimuth has one peak at 30 degree in P-2min-Z1, has one peak at 40 degree in P-2min-Z2 and has one peak at 45 degree in P-2min-Z3. The α of skin of P-0.5min and P-6min is randomly distributed, which is similar to the corresponding untreated skins. Note

that the influence of NTP on the α of skins are not only reflected in the selected regions but the entire skin. The effect of NTP treatment on the modification of α of skin should depends on the observation of the whole skin.

In summary, four different *ex vivo* mice skins are treated continuously with NTP for 0.5 min, 1 min, 2 min and 6 min, respectively. The corresponding temperature of the SAPs zone are measured using an infrared camera imager during the whole treatment. The temperature in CTRL skins are stable at the room temperature (20 °C). The temperature of SAP increases with NTP treatment time and the SAP can be heated to 72 °C maximum. The surface of SAPs expands with the treatment time. All the untreated skins exhibit a retardance, a strong depolarization and a randomly distributed Azimuth. The specific polarimetric properties of different untreated sample have a small difference in each other. The δ of peripheral skin adjacent to SAP is increased regardless the treatment time, while the δ of SAP varies with treatment time. The peak of δ histogram of SAP (Z2) is first decreased when skin is treated with NTP for a 0.5 min, then is increased to a value which is similar to that of the corresponding untreated skin when skin is treated with NTP for 1 min, and then is globally decreased again when the skin is treated with NTP for more than 2 min and this decline is more significant in the treatment of 6 min. SAP exhibits a Z3 zone when NTP treatment time over 0.5 min, but Z3 disappears when skin is treated with NTP for 6 min. The response of δ of Z3 to NTP treatment is similar to that of Z2 that the peak of δ histogram is decreased first, then is increased and then is decreased again with the increasing of plasma continuous treatment time. The depolarization of SAP (Z2) is globally increased with a 0.5 min of NTP treatment, then is lightly decreased with a 1 min of NTP treatment and then is greatly decreased with a further increased plasma continuous treatment dose.

6.1.2 MPI for investigating the effect of plasma sequential treatment on ex vivo mice skin

The linear retardance is a parameter enabling to characterize the anisotropy of medium. Note that skin treated with NTP for 1 min shows an increased retardance in the central part of SAP and the retardance of entire SAP strongly affected by the treatment dose, the polarimetric properties of skins treated with a sequence plasma

treatment has been further studied. Contrary to the continuous treatment described above, in a sequential treatment, the NTP is applied in series of 1 min treatment; the time between two NTP treatment is in the range of 20~30 min in order to perform MPI measurements. The interest of this method is that the same skin sample is monitored after each 1 min NTP dose. Mice skin samples are treated for 1 min sequentially by the helium plasma jet up to 9 times in total. The thermal images have been acquired during the whole NTP treatment. The maximum temperature of the skin samples treated by NTP is approximately the same after each 1 min dose and is equal to 59 ± 3 °C. Figure 6. 7 shows the *ex vivo* MPI of skin treated by NTP and the histograms of the Mueller polarimetric parameters of skin treated with NTP are shown in Figure 6. 8, Figure 6. 9, Figure 6. 10 and Figure 6. 11. The selected region for CTRL, Z1, Z2 and Z3 are listed in Appendix C (Figure C. 5, Figure C. 6 and Figure C. 7). The Azimuth of selected zones in the untreated and plasma sequentially treated skins are also listed in the Appendix C (Figure C. 5, Figure C. 6 and Figure C. 7). As mentioned before, Azimuth distribution of the whole surface of skin is modified by NTP treatments. The effect of NTP treatment on the modification of α of skin should depend on the observation of the whole skin. In this experiment the Azimuth of whole surface of skin treated by plasma sequential treatment has been analyzed and the histograms are shown in Figure 6. 11.

The SAP region of each NTP treated sample is very visible on MPI images. Its surface increases with the increasing treatment dose. The expansion of the SAP area of the skin is partly due to the special uncertainties in positioning the skin sample under the plasma jet device after each MPI, between two dose treatments. But this area is no longer increased when the skin is treated by NTP four times.

The histograms of Mueller polarimetric parameters of skins will be analyzed in the following order: i) The retardance and depolarization of untreated skin; ii) the retardance of different zones in the skin treated with plasma sequential treatment in different doses; iii) the depolarization of different zones in the skin treated with plasma sequential treatment in different doses; iv) the Azimuth of the whole surface of skin treated with plasma sequential treatment in different doses.
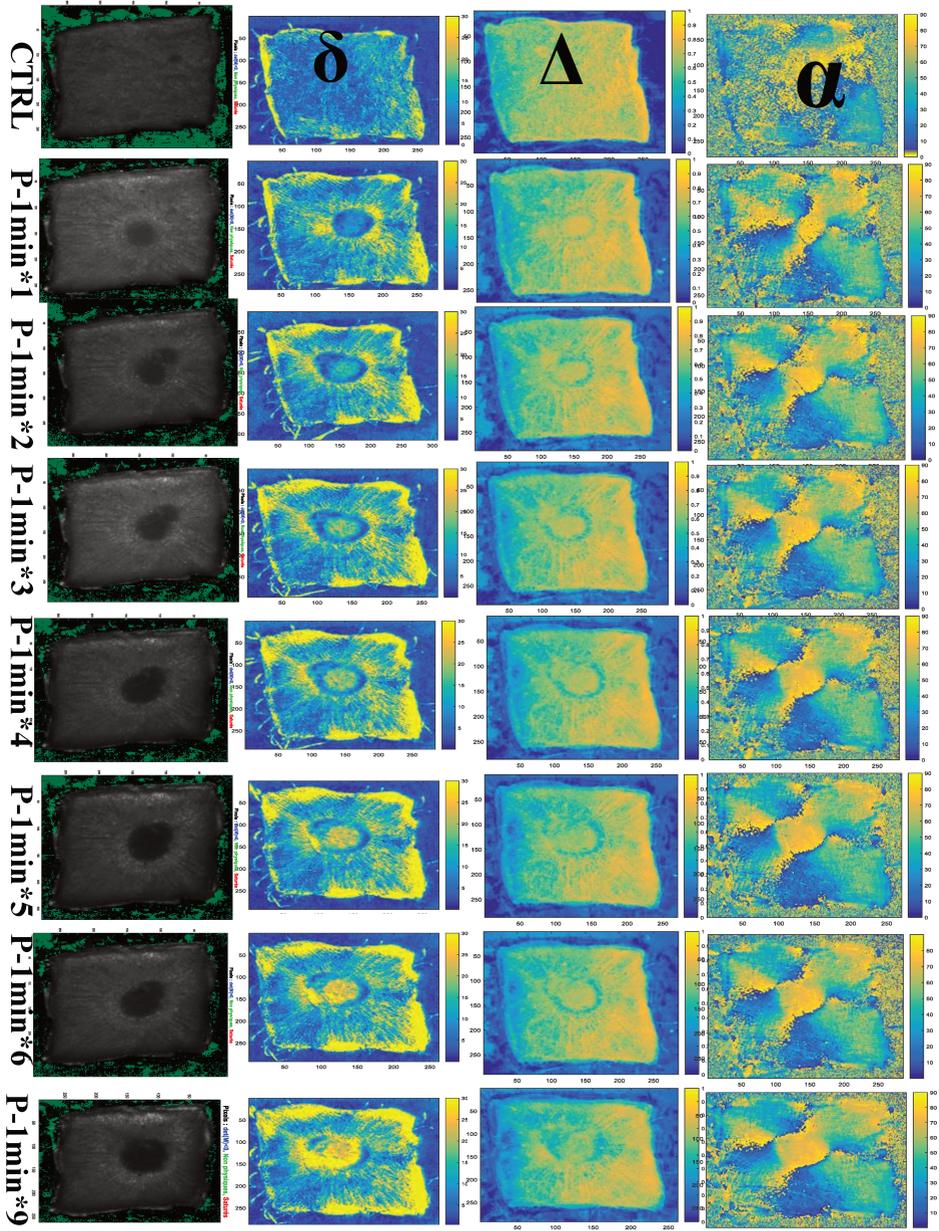
Figure 6. 7 MPI of mice skin treated sequentially by plasma jet. The discharge condition of plasma jet for all treatments are same. The temperature of CTRL skins is ca. 20 °C (room temperature) and the skins treated by NTP is equal to 59 ± 3 °C. The wavelength of MPI is 550 nm.

Figure 6. 8 shows the histograms of δ and Δ of untreated skin. The selected zone

in the CTRL skin is same with the region of Z1 in terms of the size and position. Untreated skin shows a narrow distribution of δ. The maximum δ is 20 degree and the peak of δ histogram is at 7 degree. The Δ of untreated skin ranges from 0.4 to 0.83 and the Δ histogram has a peak at 0.7.
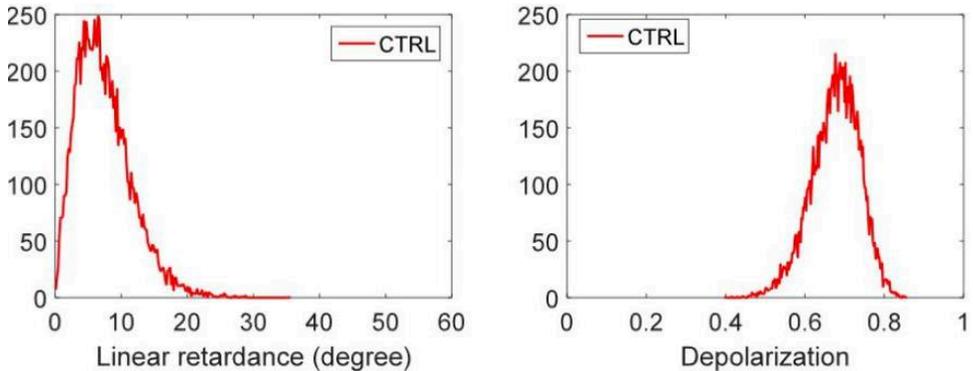
Figure 6. 8 Histograms of the linear retardance and depolarization of untreated skin

Figure 6. 9 shows the δ histograms of Z1, Z2 and Z3 region of skin treated with NTP under different sequential treatment doses. Z1 is a region containing the entire SAP and the adjacent region to SAP, so the δ histogram of Z1 is an assessment of the overall impact of the plasma on the modification of retardance of skins. The δ of SAP is globally increased by the NTP treatments. The δ of skin treated with NTP increases to 40 degree maximum (20 degree for untreated skin and increase by 100%). This increase is not influenced by the treatment dose. However, the peak of δ histogram of NTP treated skins increases as the increasing of treatment dose and in can be increased by 186 % maximum (from 7 degree of CTRL to 20 degree of P-1min*9-Z1). The peak increase of retardance histogram of Z1 is mainly attributed to the retardance increase of SAP (Z2) since it is the region with a continuously increased retardance under a higher treatment dose while the retardance of region around SAP is relatively less affected by the treatment doses.

Z2 is the entire SAP and Z3 is the central part of SAP. When skin is treated by NTP for one time (P-1min), the δ of Z2 is similar to that of Z3. Retardance histogram of Z2 and Z3 zone has a same peak at 10 degree and the maximum δ is 20 degree.

When the skin is treated by NTP for three times (P-1min*3), δ histogram of Z2 exhibits two peaks. The first peak is at 7 degree which is attributed to the boundary part of Z2 (very similar to CTRL skin). The second peak is at 17 degree which is equal to the peaks shown in the δ histogram of Z3 which has only one peak. Both the δ histogram of Z2 and Z3 ranges from 0 to 27 degree. When the skin is treated with NTP for 6 times (P-1min*6), the first peak of δ histogram of Z2 is increased to 11 degree and the second peak is increased to 22 degree. The second peak of δ histogram of Z2 is equal to the one of Z3 and the maximum δ of Z2 is similar to that of Z3 (34 degree). When skin treated with NTP for 9 times (P-1min*9), the first peaks of δ histogram of Z2 disappears and the second peak increases to 25 degree. The maximum δ of Z2 and Z3 is same, which is 45 degree. In short, i) the central part of SAP (Z3) exhibits a bigger δ than that of the boundary part of SAP; ii) δ of the entire SAP (Z2) increases with the increasing of plasma sequential treatment dose; iii) the δ of Z3 shows a faster increase than that of the boundary part of SAP when the treatment dose increases.
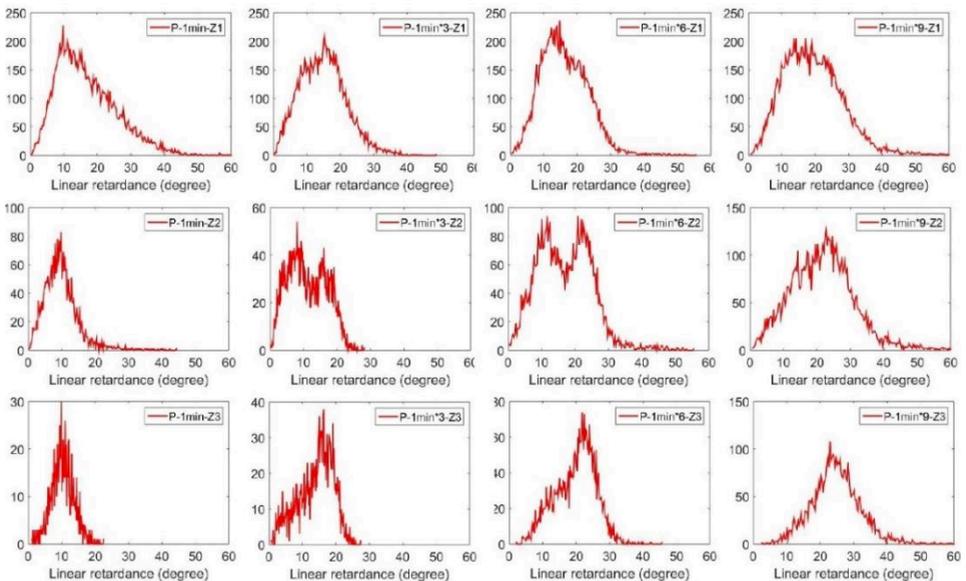
Figure 6. 9 Histograms of the linear retardance of Z1, Z2 and Z3 in skins treated sequentially with NTP in different doses

Figure 6. 10 shows the Δ histograms of Z1, Z2 and Z3 region of skin treated with NTP with different plasma sequential treatment doses. The Δ of SAP is much less

affected by the NTP treatments, compared to the δ of SAP. The Δ in all sample ranges from 0.4 to 0.83, which is similar to the untreated skin, but the peak of Δ histogram is decreased with the increasing of treatment dose. The peak of Δ histograms of Z1 (the entire SAP) is 0.76 when skin is treated by NTP for one time (P-1min), while it decreases to 0.59 when skin with the maximum treatment dose (P-1min*9). The peak is decreased by 15.7 % maximum with respect to the untreated skin (0.7 for the untreated skin). The peak of Δ histogram of Z1, Z2 and Z3 under a same treatment dose is same. Note that the Δ of boundary of SAP (Z2) is decreased and is smaller than the Δ of central part of SAP (Z3) visually, shown in Figure 6. 7. However, this difference is not reflected in the Δ histogram of Z2 and Z3.
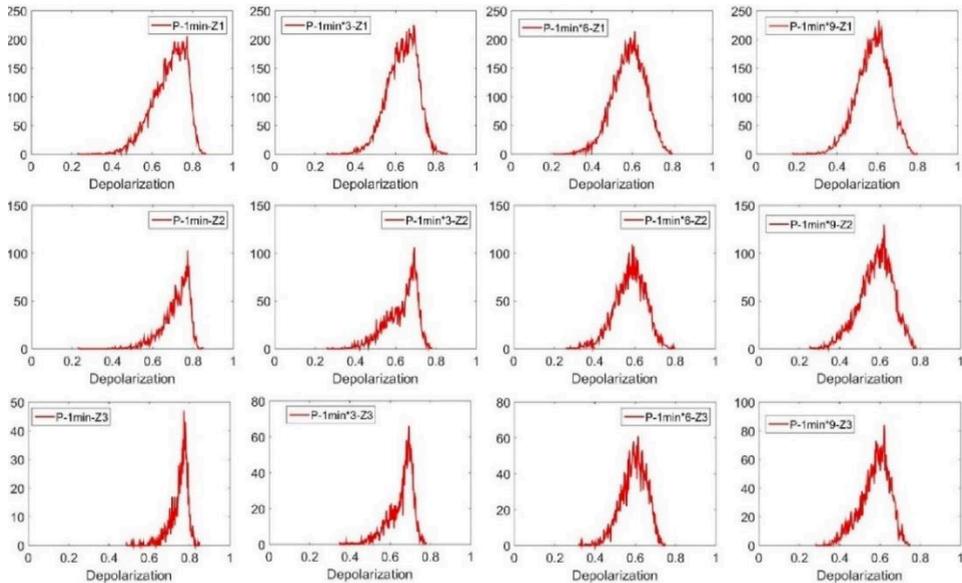
Figure 6. 10 Histograms of the depolarization of Z1, Z2 and Z3 in skins treated sequentially with NTP in different doses

As mentioned before, Azimuth distribution of the whole surface of skin is modified by NTP treatments. The effect of NTP treatment on the modification of α of skin should depend on the observation of the whole skin. In this experiment the whole surface of skin has been analyzed, as shown in Figure 6. 11. Without NTP treatment we observe a random distribution of the α while after plasma treatment the α orientation distribute in the range of 0~90 degree and the α histograms appear two

peaks. The first peak is at 22 degree and the second peak is at 53 degree. The second peak is the dominant direction of the α orientation but is free from the influence of the plasma sequential treatment dose, whereas the first peak becomes more significant in the skin treated with NTP under a bigger treatment dose. The α histograms of Z1, Z2 and Z3 has also been analyzed, which listed in Appendix C (Figure C. 8). α histogram of Z1 is similar to Z2 and Z3 under the same NTP treatment dose. Only one peak is observed in the histogram of each sample. The peak ranges from 70 degree to 80 degree. The bigger the treatment dose the smaller the peak.
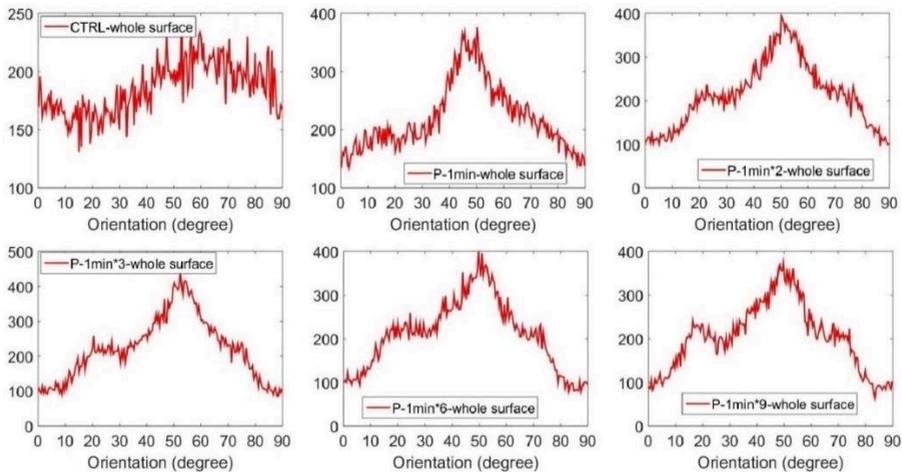
Figure 6. 11 Histograms of the Azimuth of the whole surface of untreated skin and the skins treated with a sequence of N times 1 min NTP treatment. N here includes 1, 2, 3, 6 and 9.

6.2 *Ex vivo* Mueller Polarimetric Imaging of mice skin heated in an oven

6.2.1 MPI for investigating the effect of thermal continuous treatment on *ex vivo* mice skin

According to the work of Hambleton et al. who investigated the thermal damage to collagen in skin, structure of collagen begins to be changed when temperature over 50-52 °C [296]. It starts from weakening the chemical bands crosslinking different collagen fibers and ends with the protein denaturation [296]. In this section, the skin

is first thermally treated for 6 min using a 50 °C oven (labeled with T50-6min); then structural changes and characteristics of polarimetric states of these skin samples are measured with the MPI. Same samples are then placed in the oven again at the temperature of 60 °C for another 6 min (labeled with T50-6min-T60-6min) and then analyzed with MPI. The objective is to compare the polarimetric parameters of the thermally treated skin to the polarimetric parameters of NTP treated skins having a temperature around 60 °C. The imaging and histograms of the Mueller polarimetric parameters of skin are shown in Figure 6. 12 and Figure 6. 13, respectively.
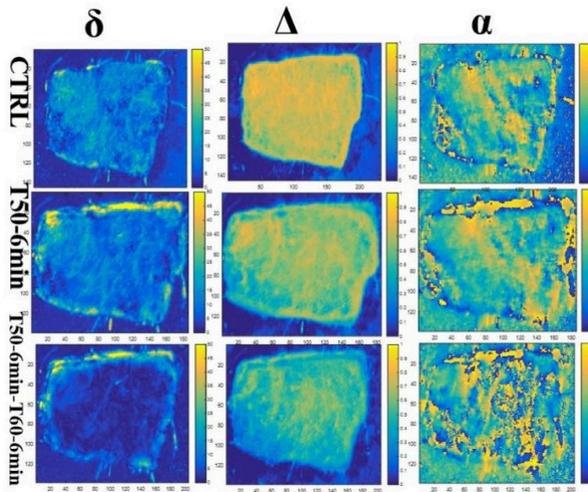
Figure 6. 12 MPI of mice skin treated by a thermal continuous treatment using an oven with different temperatures. Skin temperature is measured by an IR camera. The temperature of CTRL skin is ca. 20 °C (room temperature), the temperature of skin of T50-6min is 50 °C and the temperature of skin of T50-6min-T60-6min is 60 °C. The wavelength of MPI is 550 nm

Figure 6. 12 show the image of Mueller polarimetric parameters of the whole surface of CTRL skin and Figure 6. 13 shows the histograms of Mueller polarimetric parameters of the whole surface of CTRL skin. The images with selected zone are listed in Appendix C (Figure C. 9). As can be seen that the CTRL skin group has a retardance ranging from 0 to 25 degree and a strong depolarization (0.6~0.8). The α orientation distribution is wide but is most distributed at 45 degree. When skin is thermally heated for 6 min using a 50 °C oven, the image and histograms of δ and Δ of skin are influenced while the α is similar to the CTRL skin. The peak of δ

histogram of T50-6min is decreased to 10 degree from 13 degree (decreased by 23 % with the respect to CTRL skin). The peak of Δ histogram of T50-6min is decreased to 0.61 from 0.76 (decreased by 18.7 % with the respect to CTRL skin). When this thermally treated skin is further heated with a 60 °C oven for another 6 min, the decrease of δ and Δ of skin become more significant. The peak of δ histogram is decreased to 2 degree from 13 degree (decreased by 86% with respect to the untreated skin) and maximum δ is decrease to 9 degree from 25 degree (decrease by 64% with respect to the untreated skin). The peak of Δ histogram is decreased to 0.5 from 0.76 (decreased by 34 % with respect to the untreated skin) and maximum Δ is decrease to 0.7 from 0.82 (decreased by 14.6 % with respect to the untreated skin). The distribution of α orientation becomes more random than the untreated skin. In short, the thermal treatment with an oven can affect the microstructure of skin and this modification becomes stronger with a higher treatment temperature (a bigger thermal treatment dose). In the following, the experiment with different skins heated continuously with a 60 °C oven for different times aims to simulate the influence of thermal effect of the NTP treatment on the polarimetric properties of skin.
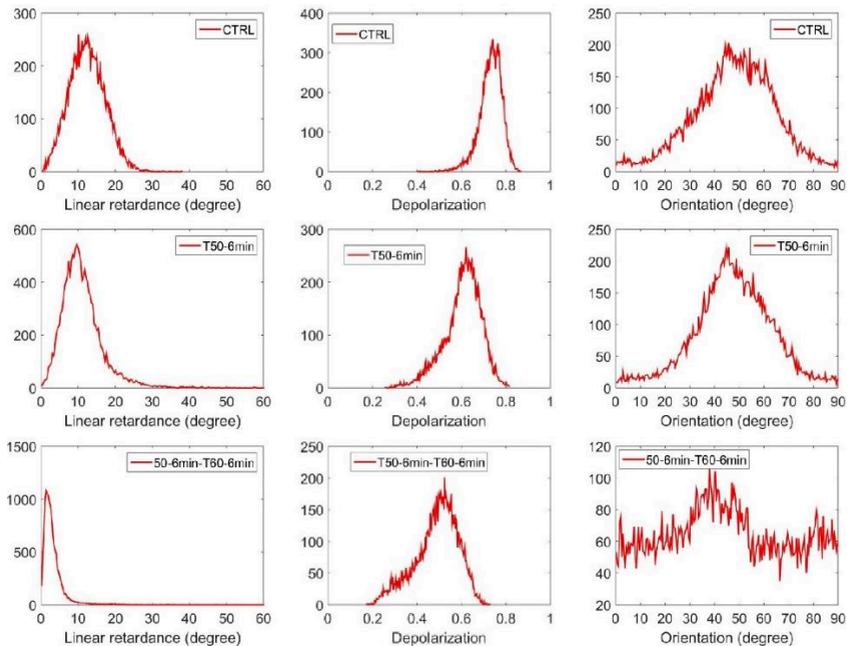
Figure 6. 13 The histogram of Azimuth, depolarization and linear retardance of the entire surface of skins thermally treated with an oven

In this experiment, three different skins are selected for the thermal continuous treatment with a 60 ℃ oven for different treatment times. CTRL-a skin is treated for 1 min, CTRL-b skin is treated for 2 min and CTRL-c skin is treated for 6 min. The temperature of thermally treated skin is measured with the IR camera at the end of each treatment and temperature of all the thermally treated skin is 60 ℃. All samples are placed on the surface of an ice before the measurement with MPT. The images of polarimetric parameters of skins are shown in Figure 6. 14, and the histograms of each Mueller polarimetric parameters of skins are shown in Figure 6. 15 and Figure 6. 16, and the images of the selected zone are listed in Appendix C (Figure C. 11).
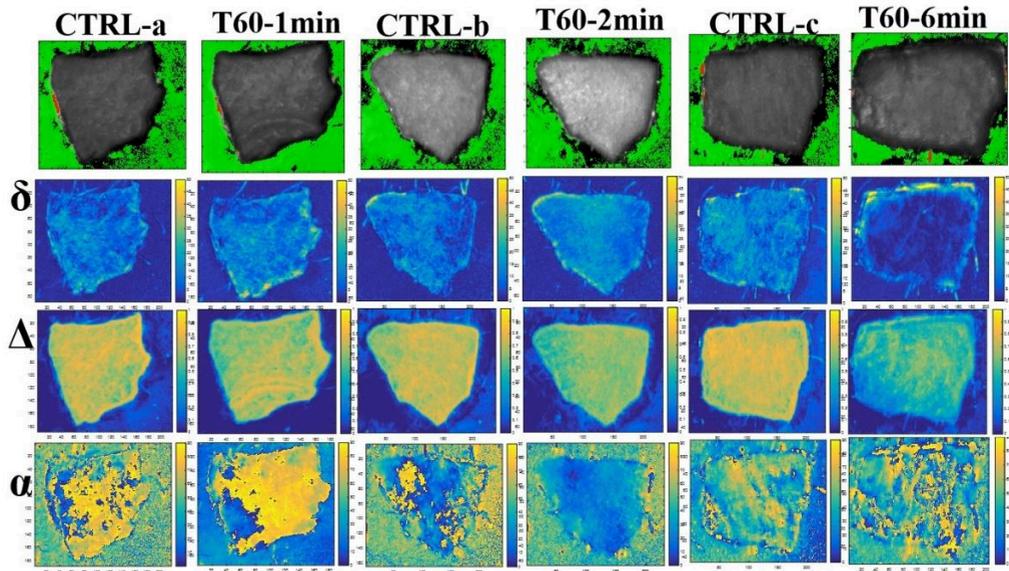
Figure 6. 14 MPI of mice skin treated by a thermal continuous treatment using a 60 ℃ oven. The skin temperature is measured by an IR camera. The temperature of CTRL skins is ca. 20 ℃ (room temperature) and temperature of all the thermally treated skins is 60 ℃. The thermally treated skin is always stored on the surface of an ice before measuring with MPI. The wavelength of MPI is 550 nm

Figure 6. 15 shows the histograms of α, Δ and δ of the entire surface of CTRL skin and skins thermally treated with a 60 ℃ oven for 1 min continuously. The δ of the CTRL-a skin ranges from 0 to 25 degree and the δ histogram has a peak at 10 degree. The Δ of CTRL-a skin ranges from 0.5 to 0.83 and the Δ histogram has a peak in 0.74. α histogram of CTRL-a skin has a peak at 80 degree and a loopback at

0 degree. With a thermal treatment, the maximum δ is increased to 37 degree (increased by 48 % with respect to CTRL) and the peak of δ histogram is increased to 15 degree (increased by 50 % with respect to CTRL), the peak of Δ histogram is decreased to 0.67 (decreased by 9.5 % with respect to CTRL) and α orientation of skin is more distributed to 80 degree.

Figure 6. 15 The histogram of Azimuth, depolarization and linear retardance of the entire surface of untreated skin and skins thermally treated with a 60 ℃ oven for 1 min continuously

Figure 6. 16 shows the histograms of α, Δ and δ of the entire surface of CTRL skin and skins thermally treated with a 60 ℃ oven for 2 min continuously. The δ of the CTRL-b skin ranges from 0 to 20 degree and the histogram has a peak at 10 degree. The Δ of CTRL-b skin ranges from 0.53 to 0.8 and the Δ histogram has a peak in 0.74. α histogram of CTRL-b skin has a peak at 10 degree and a loopback at 90 degree. With a thermal treatment, the maximum δ is increased to 25 degree (increased by 25 % with respect to CTRL) and the δ histogram peak is increased to 15 degree (increased by 50 % with respect to CTRL), the peak of Δ histogram is decreased to 0.6 (decreased by 18.9 % with respect to CTRL) and α orientation of skin is more distributed to 20 degree.

When the thermal treatment time is increased to 6 min, the thermally treated skin exhibits totally different influences on the modification of polarimetric properties of skins, as have shown in Figure 6. 13. The thermal treatment disturbs the α

orientations of skin, decreases the α of skin and greatly declines the δ. The peak of δ histogram is decreased to 2 degree (decrease by 86% with respect to CTRL) and maximum δ is decrease to 9 degree (decrease by 64%). The peak of Δ histogram is decreased to 0.5 (decrease by 34 % with respect to CTRL) and maximum Δ is decrease to 0.7 (decrease by 14.6 % with respect to CTRLs). The distribution of Δ orientation becomes more random than the untreated skin.
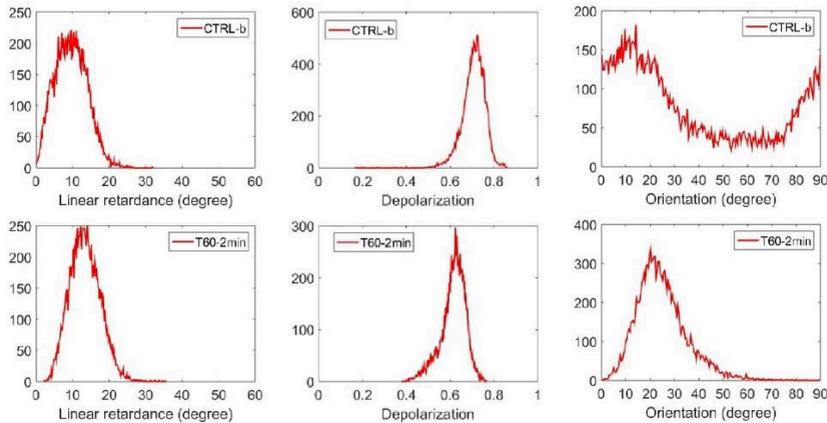
Figure 6. 16 The histogram of Azimuth, depolarization and linear retardance of the entire surface of untreated skin and skins thermally treated with a 60 °C oven for 2 min continuously

In summary, by comparing to the corresponding untreated skins, i) the maximum δ is increased 50 % by both the 1 min and 2 min thermal continuous treatment, but is dramatically decreased 86 % by the 6 min thermal continuous treatment; ii) the peak of δ histogram is increased 48 % by 1 min thermal continuous treatment and is increased 25 % by 2 min thermal continuous treatment, while is dramatically decreased 64 % by the 6 min thermal continuous treatment; iii) the peak of Δ histogram of skin is decreased in each samples; iv) the α orientation of skin is more distributed to 80 degree after the 1 min thermal continuous treatment and to 20 degree after the 2 min thermal continuous treatment, but become more random with respect to the untreated skin.

6.2.2 MPI for investigating the effect of thermal sequential treatment on *ex vivo* mice skin

The plasma sequential treatments increase the retardance (δ) of SAP and

decrease the depolarization (Δ) of SAP. The influence of plasma sequential treatment on the modification of δ and Δ of SAP is strengthened by increasing the treatment dose (Figure 6. 7). The distribution of Azimuth (α) orientation of skin become less random with the plasma sequential treatments (Figure 6. 7). Similarly, the thermal continuous treatment with an oven have been found can affect the microstructure of skin and this modification becomes more significant when the temperature of oven increases from 50 °C to 60 °C (Figure 6. 14). In the following, the experiment with one skin heated by a sequential of several times 1 min thermal treatment with a 60 °C oven has been carried out. The objective is to compare the polarimetric properties of the thermally treated skin to the untreated skin, and to simulate the influence of thermal effect of the plasma sequential treatment on the modification of polarimetric properties of mice skin. The images of Mueller polarimetric parameters of thermally treated skin are shown in Figure 6. 17, the histograms of the polarimetric parameters are shown in Figure 6. 18, and the images of selected zone of the thermally treated skin are listed in Appendix C (Figure C. 10).
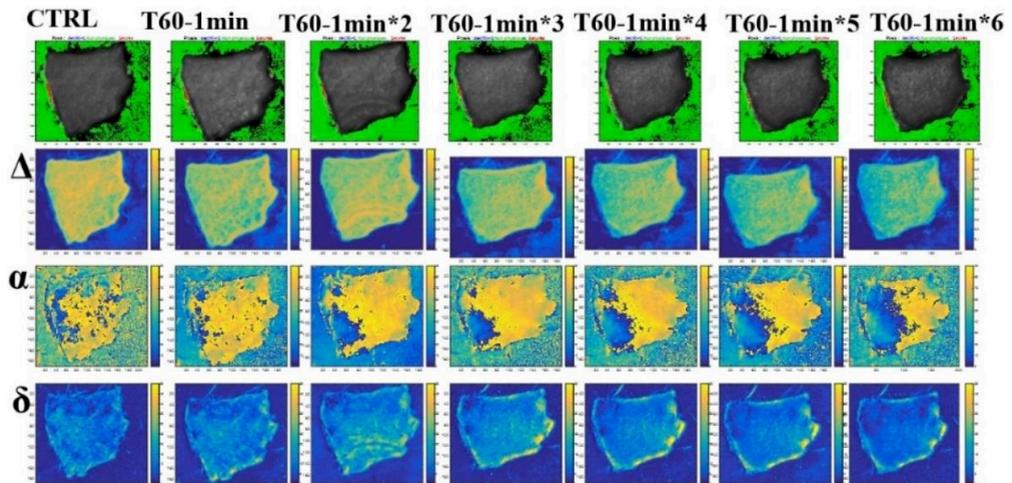
Figure 6. 17 MPI of mice skin heated sequentially in a 60 °C oven. Each single thermal treatment time is 1 min. Skin temperature is measured by an IR camera. The temperature of CTRL skins is ca. 20 °C (room temperature) and the temperature of all the heated skins is 60 °C. The thermally treated skin is always stored on the surface of an ice before measuring with MPI. The wavelength of MPI is 550 nm

The CTRL skin group has a δ ranging from 0 to 22 degree and has a δ histogram peak at 9 degree. The Δ of CTRL skin ranges from 0.5 to 0.83 and the peak of Δ histogram is 0.74. The histogram of α orientation of CTRL skin has a peak at 80

degree and has loopback at 0 degree. Polarimetric properties of the thermally treated skins are affected by the treatments and the treatment doses. The δ of skin is increased first and then is decreased. The peak of δ histogram is at 11 degree when skin is thermally treated for 1 time (increased by 22 % with respect to the untreated skin) and is 15 degree when skin is further thermally treated for 3 times (increased by 67 % with respect to the untreated skin). However, the peak of δ histogram is decreased when skin is thermally treated for 6 times (decreased by 44 % with respect to the untreated skin). The Δ of skin continuously decreases when the treatment dose decreases, compared to the untreated skin. The peak of Δ histogram is decreased by 24 % maximum (from 0.74 to 0.56). The thermal treatment exhibits a less influence on the modification of α of skin.
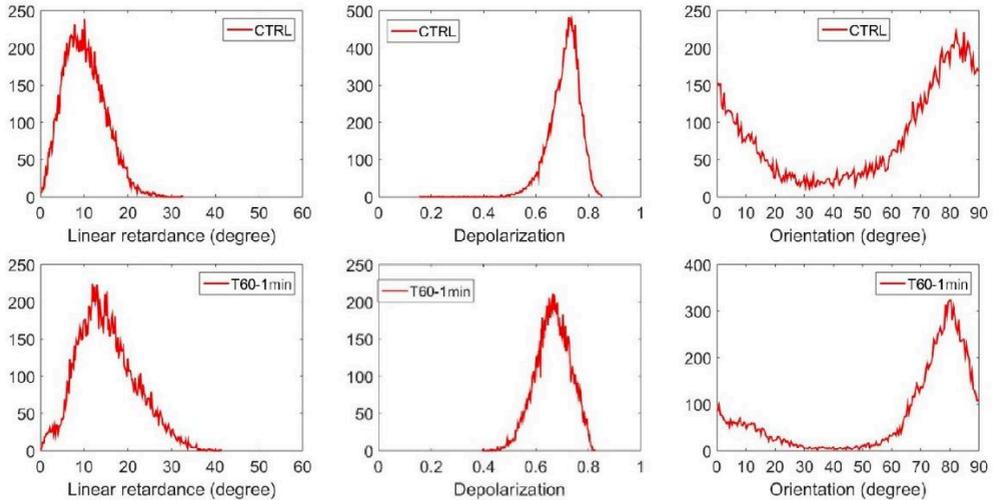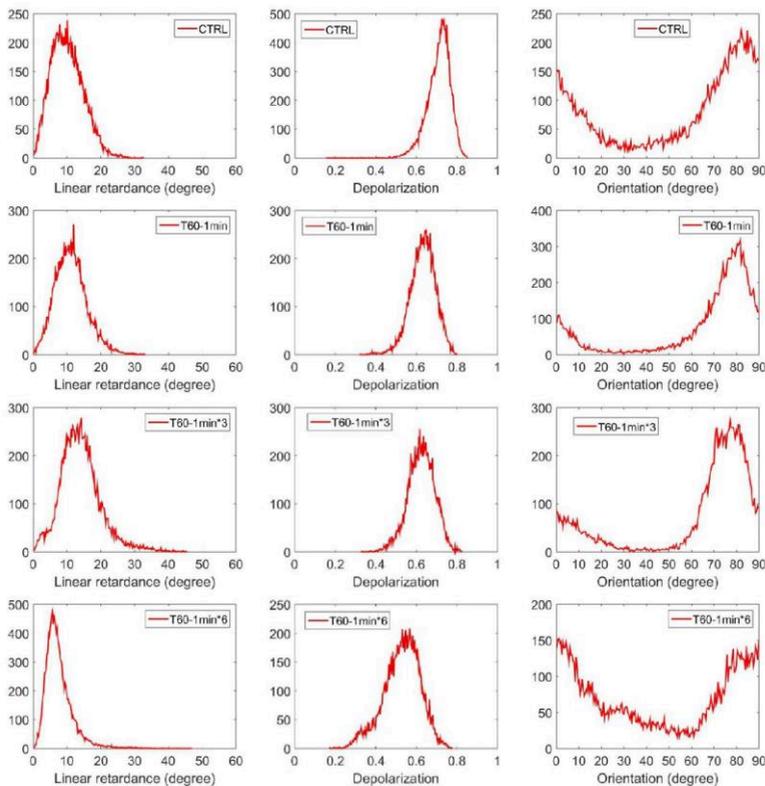

Figure 6. 18 The histogram of Azimuth, depolarization and linear retardance of the entire surface of untreated skin and skins thermally treated with a 60 °C oven sequentially under different treatment doses

When skin is treated with a sequential of different times 1 min NTP treatment, temperature of skin sample is around 59 ± 3 °C, which is similar the temperature of the thermal sequential treatment with a 60 °C oven. The NTP treatments significantly and continuously increases the δ as the increasing of treatment dose, whereas the thermal treatments slightly increase the δ first but dramatically decrease the δ under a bigger treatment dose. The distribution of α orientation of skin becomes less random and the histogram shows a specific peak after the NTP treatment, while α of skin is much less influenced by the thermal treatment. The responses of Δ to NTP treatment is similar to that of the thermal treatment that it is decreased by the treatments. Hence, thermal effect of the thermal sequential treatment with an oven on the modification of skin microstructure is different from the effect of plasma sequential treatment on this modification of skin microstructure.
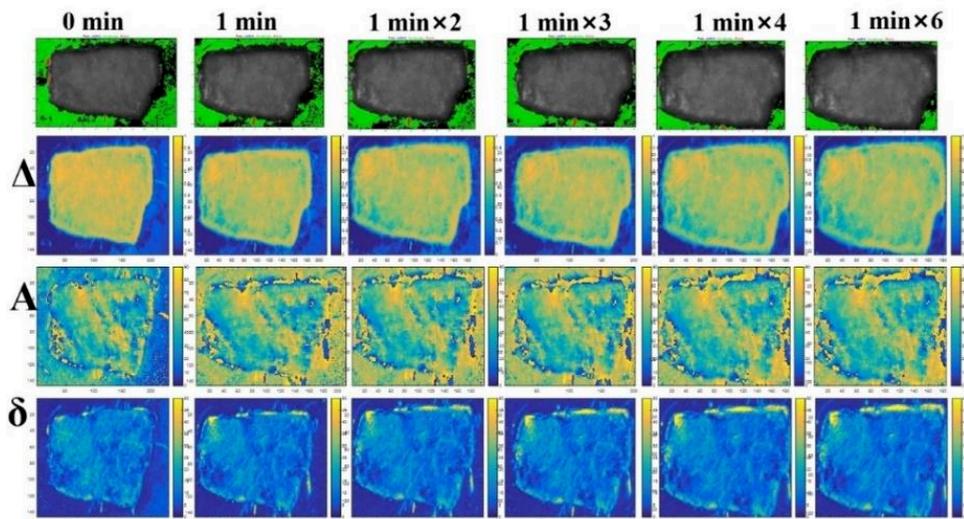
Figure 6. 19 MPI of mice skin heated sequentially in a 50 °C oven. Each single thermal treatment time is 1 min. The skin temperature is measured by an IR camera. The temperature of CTRL skins is ca. 20 °C (room temperature) and the temperature of all the heated skins is 50 °C. The thermally treated skin is always stored on the surface of an ice before measuring with MPI. The wavelength of MPI is 550 nm.

The skins are also thermally treated by a 50 °C oven sequentially and the MPI of thermally treated skins are shown in Figure 6. 19. The histograms of Mueller polarimetric parametric parameters of all skins are listed in Appendix C (Figure C. 12).

CTRL skin in this experiment exhibits a δ (0~20 degree), a strong Δ (0.6~0.8) and randomly distributed Azimuth (0~90 degree). Apparently, the polarimetric properties of skin are changed by thermal sequential treatments using a 50 ℃ oven, except for the Δ that it is slightly decreased by this thermal sequential treatment (the peak of Δ histogram is decreased by 6% maximum when skin is thermally treated for 6 times).

6.3 Discussion

The effect of NTP treatment on the modification of skin structure have been investigated by characterizing the Mueller polarimetric parameters of skins. This discussion is divided into three parts depending on the temperature of treated skins.

i) Skins at a temperature below 50 ℃ max (included 50 ℃)

The temperature of CTRL skins is 20 ℃ (room temperature). Skin samples without treatment are characterized by a strong depolarization (ca. 0.6~0.8), as well as a non-negligible retardance (ca. 0~0.2). As seen above, 50 ℃ thermal treatment, even the 6 min thermal continuous treatment, does not alter the MPI parameters of skin compared to the control group: the retardance and Azimuth of the thermally treated skin are similar to the corresponding CTRL skins, regardless the dose of thermal continuous treatment (Figure 6. 12) and dose of thermal sequential treatment (Figure 6. 19). Based on the literature, the retardance can be caused by the skin birefringence which is tightly related to the structure of skin, e.g. the spatial structure of collagens [232]. Structure of collagen begins to be changed when temperature over 50℃, starting from weakening the chemical bands crosslinking different collagen fibers [296]. Note that the peak of depolarization histogram of thermally treated skins is decreased both in the 50℃ thermal continuous treatment and 50℃ sequential treatments, compared to the corresponding CTRL skin (Figure 6. 12 and Figure 6. 19). The bigger the treatment dose, the more significant the depolarization decreased. It is known that multiple scattering is a dominating depolarization process

in biological tissues [236]. It is strongly related to the surface topography (e.g. roughness) of the medium. The skin surface is probably influenced by the thermal treatment and it is probably this modified skin surface that intensifies the multiple scattering of skin surface and then decreases the depolarization of skin.

The temperature of SAP in the skin treated with NTP for 0.5 min reaches 33 ℃, which is even lower than 50 ℃. Although the temperature of NTP treated skin is even lower than the lowest oven temperature treatment performed in this study, the peak of retardance histogram of SAP in P-0.5min skin is decreased, unlike the thermally treated skin. This suggests that the effect of a 30 s NTP treatment on the modification of retardance of skin observed on Figure 6. 2 is not due to a thermal effect. It could be due to the plasma reactive species or other plasma reagents. The depolarization of SAP is similarly decreased as that of the thermally treated skin, which could be caused by the thermal effect.

ii)   Skins at a temperature around 59±3 ℃

Temperature of skins placed in an oven at 60 ℃ is comparable to temperature of the SAP in the skin treated with NTP for 1 min. In this case, both NTP and thermal treatments exhibit influences on all the Mueller polarimetric parameters of skins.

Compared to the CTRL skins, the value of depolarization of skins is decreased by the NTP treatments or thermal treatments probably due to the intensified multiple scattering of skin surface. This decrease becomes more significant as the treatment dose increases. At the opposite, the retardance is increased in the central regions of SAP (Z3) of skins treated by NTP. This increase becomes more significant in a bigger dose of plasma sequential treatment (Figure 6. 7). Meanwhile, the distribution of Azimuths in the skins treated by NTP becomes more evenly than the CTRL skins (Figure 6. 7). Azimuth is the orientation of eigenvalue axis indicating the orientation of the fibrous collagen [241]. We think that the plasma sequential treatments change the orientation of collagen fibers and rearrange them more regularly. It is probably the effect of NTP treatment on the optimization of spatial structure of the skin collagen that enhances the birefringence of the skin, resulting in an increased retardance. As shown in Figure 6. 11Figure 6. 11 Histograms of the Azimuth of the

whole surface of untreated skin, the peak of Azimuth histogram of the skins treated by plasma sequential treatments is more evenly distributed in 22 degree and 53 degree and this trend is more significant in the skin treated by NTP with a higher treatment dose.

The response of Mueller polarimetric parameters of skin to the 60 ℃ thermal sequential treatment is different to that of plasma sequential treatment which similarly heats the SAP to 60 ℃, in practically the retardance. The peak of retardance histogram of thermally treated skins is firstly increased (it is same with plasma treatment), but then is decreased as the dose of thermal sequential treatment increases (Figure 6. 12 and Figure 6. 17). This indicates that 60 ℃ thermal effects can modify the retardance of skin but contribute differently with NTP treatment in this modification. As can be seed from Figure 6. 17 that the Azimuths of thermally treated skins become less random with respect to the untreated skins and the depolarization of skin is also affected by this thermal treatment, indicating the 60 ℃ thermal effects can modify the microstructure of skin tissues.

iii) Skins at a temperature around 70±3 ℃

Only when the skin is treated by the plasma continuous treatments for more than 2 min, temperature of SAP can reach 70 ℃.

The coagulation and denaturation of collagen can occur when the skin temperature reaches 60 ℃. The collagen shrinkage temperature occurs around 65 ℃ [295]. 70 ℃ is then a temperature which can burn or damage the skin structure easily. The signs of skin burns can be found in the edges zone of SAP of skins treated by NTP (Figure 6. 2). The retardance and depolarization in these regions has been greatly decreased and the distribution of Azimuths become random again. The randomly distributed Azimuth indicates the orientation of collagen fibers is disordered. The decreased retardance and depolarization mean this skin tissue has a very weak characteristics of the anisotropy, such as birefringence. This indicates the microstructure of skin treated with a plasma continuous treatment for 6 min have been significantly changed and is probably damaged. The six minutes 60 ℃ thermal continuous treatment can also lead to a similar influence on the modification of

polarimetric properties of skin (Figure 6. 14 and Figure 6. 12).

The investigation about the microstructure modification of NTP treated skins will be further studied using a higher resolution microscopic imaging, since it can give the information of the changes of skin collagen.

6.4 Summary

Ex vivo Mueller Polarimetry Imaging (MPI) has been used in this work to evaluate and quantify the influence of a helium plasma jet treatment on the modification of structure of the mice skin by characterizing the polarimetric parameters of skin such as linear retardance, total depolarization and orientation of the eigenvalue axis. As a comparison, *ex vivo* MPI of thermally treated mice skins by heating skins in an oven are used to understand what is the role of heat on skin modification during a plasma treatment. Mice skin tissue used in this work is characterized by a strong anisotropy and the Mueller polarimetric parameters of mice skin can be significantly affected by the plasma treatments. Detailed results are as follows:

1) The untreated skin has a linear retardance (ca. 0~20 degree), strong depolarization (ca. 0.6~0.8) and randomly distributed Azimuth;
2) The temperature of the skin at the end of a the plasma continuous treatment is strongly related to the treatment time (treatment dose); the temperature of skin treated by plasma for 0.5 min, 1 min, 2 min and 6 min can reach 33 ℃, 59 ℃, 69 ℃ and 72 ℃, respectively; Plasma continuous treatment are also compared to sequences of 1 min plasma treatment which keeps the skin maximum temperature close to 60 C.
3) The peak of linear retardance histogram of the SAP in skin treated with the plasma treatment continuously increases as the dose of plasma sequential treatment increases, while the peak in the thermal treated skin increases first and then decreases with the increasing of dose of 60 ℃ thermal sequential treatment;
4) The plasma and thermal treatments can decrease the peak of depolarization histogram of skins;

5) The microstructure of skin, in particular the collagen of skin, can be strongly modified by a plasma and thermal continuous treatment when plasma treatment time over 2 min and 60 °C thermal treatment time over 6 min. The peak of retardance and depolarization histogram of these affected skins are significantly decreased with respect to the corresponding untreated skins. These affected skins exhibit a randomly distributed Azimuth;

6) Such results evidence a modification of the collagen observed in a preliminary study using confocal microscopy.

General conclusions

The principle objective of this thesis is to investigate non-thermal atmospheric pressure plasma interacting with water and biological samples including seeds and skin. Three different home-made plasma reactors have been used to produce NTP in this work. The first one is single electrode DBD plasma setup, which is used to study the reactive species produced in gas and liquid phase when operated in different carrier gases. The second one is a scale-up of the latter, coupling 9-electrode DBD in parallel. Finally, a plasma jet flown in helium is used to investigate effect of NTP treatments on *ex vivo* mice skin. The main results from this thesis can be summarized as:

1. Plasma-liquid interaction with the single electrode DBD plasma setup

In chapter 3, plasma reactive species produced by NTP in gas and liquid phase have been monitored. The first step is to operate a single electrode DBD reactor in order to investigate the influence working parameters such as, i) the gas flow and composition, ii) the presence or not of liquid water at the bottom of the reactor, iii) the localization of the NTP either touching or not touching the water surface, iv) the carrier gas (N_2, O_2, Air) with or without humidity, v) the applied high voltage and vi) the treatment time.

1) The O_2 discharge produce more O_{3g} than Air discharge, dry gases discharges produce more O_{3g} than humid gases discharges depending on the flow rate. On the other hand, NO_{2g} and NO_g are not detected in all working conditions, probably because they are readily transformed to NO_3 and HNO_3.

2) In the Non-touching Bubble Plasmas configuration, the production of aqueous NO_2^-, NO_3^- and H_2O_{2aq} has been quantified for the different working conditions: the production of all aqueous species increases first and then

decreases with the gas flow rate, when the gas is dry; on the other hand, when the carrier gas contains 74 % humidity, the productions of species increase continuously with the gas flow rate. Since the NTP is not in direct contact with water these RNOS are likely to be formed through the solvation of gaseous species produced upstream by the NTP such as HNO_{2g}, HNO_{3g} and H_2O_{2g}.

3) In Touching Bubble configuration, the production of H_2O_{2aq} is independent on the gas flow and gas composition; this species is probably formed in the upper water layer or aqueous phase through the combination of OH_{aq} radicals for touching plasmas. At the opposite, the productions of NO_2^- and NO_3^- decrease continuously with the gas flow rate. They are likely formed through both the solvation of gaseous nitrogen species and reactions in the upper layer and the bulk of water. Besides, concentrations and yields of NO_2^-, NO_3^- and H_2O_{2aq} increase linearly with the plasma treatment time and is an increasing function of the input voltage.

4) Finally, an upscaled reactor designed for germination experiments has been characterized. It is made of 9 electrodes plasma reactor working in parallel. The production of NO_2^-, NO_3^-, H_2O_{2aq} and OH_{aq} radical is measured as a function of the treatment time, for different working gases in Touching Bubbling Plasma configuration.

2. Seeds treatment with the 9-electrode DBD plasma setup

Chapter 4 investigated the biological effects of non-thermal DBD plasma on a selection of eight types of seeds in order to select the best seeds being the target to explore how this plasma biological effect works: they wheat, mung bean, tomato, radish, mustard, sticky bean, lettuce and dianthus. Two types of treatments are performed: i) direct treatment, seeds are placed in water and the plasma is operated few minutes directly above the water; ii) indirect treatment: water is first treated by plasma and enriched by long-lived reactive species, then seeds are placed inside this

treated water. Brief conclusions are:

1) After an indirect plasma treatment, germination rate of mung beans, radish, and mustard are statistically significant increased, while tomato, lettuce, dianthus, wheat and sticky bean are less influenced;

2) After a direct plasma treatment, germination rate of mung bean is greatly increased and wheat are seeds is less influenced, while mustard seeds are inhabited;

3) Mung bean exhibits a positive germination response both to plasma indirect treatment and plasma direct treatment, it is selected as the main target used to fully explore how this non-thermal plasma improving germination in the next step.

In Chapter 5 various treatment conditions have been studied on Mung bean seeds in order to clarify the role of the plasma parameters. First, the effect of plasma produced chemical aqueous species and electric field on germination are studied. This includes seeds treatment under different discharge gases, different discharge times, chemical solutions, various distances to water surface, acidic water and electric field alone. The key conclusions include:

4) Effect of NTP produced aqueous species on mung bean seeds germination

   i) Germination curves of seed directly treated with NTP show more effective acceleration in germination rate than that of indirect plasma treated seeds in all gases discharge, which argues in favor of the role of short-lived species produced in liquid phase by NTP;

   ii) Germination promoting effect of NTP treatment is relatively insensitive to treatment time in our operating conditions, i.e. from 1 to 10 min;

   iii) Acidification of the water from (From pH 7 to 4) increases germination rate for seeds without NTP direct treatments but has no

influence in the case of NTP treatment;

iv) Germination percentage of NTP treated groups does not depend on the distance to the water surface, which indicates short lived reactive species are not the main candidates which are likely to affect germination.

5) Then, the effect of electric field on mung bean seeds germination has been studied.

i) Electric field intensity of 20 kV at the position of the seeds top surface is 10~30 kV/cm without water and 3~7 kV/cm at the same position with water;

ii) Germination curves of seeds treated by electric field show same promoting effect with seeds treated by plasma;

iii) Wet seeds and immersed seeds response to electric field in a similar way and both with a much better performance in germination promoting than that of dry seeds;

iv) Intensity and treating time of electric field have very little influence on germination;

v) Water is necessary in accelerating germination rate of mung bean of electric field.

vi) No marks of being etched and signs of crack on seeds surface are noticed;

vii) The higher the initial moisture the faster water uptake rate;

viii) Germination of seeds treated by plasma is similar to the seeds treated by electric field;

ix) Influence of plasma on germination relates to seeds hydration process that the higher the degree of hydration of seeds, the weaker

the effect of plasma and electric field on promoting germination;

x) Treatments of plasma or electric field treatment improve germination mainly through the interaction with germination related hydration and metabolic processes.

Part of these results has already been published in Journal of Physics D: Applied Physics. The rest of these results, have been submitted to the same journal and now is under its first correction.

3. *Ex vivo* Mueller Polarimetric Imaging of mice skin treated by the plasma jet

Chapter 6 aims at studying the effect of plasma treatment on skin tissue using Mueller polarimetric imaging. It is aim to explore new characterization methods for diagnosing the effects of plasma on the internal structure of living tissue. The microstructure and optical properties of the biological tissue, such as the birefringence, shape, density, and refractive index of the scatterer, can change the polarization state of the light. Therefore, the microstructure and optical properties of the superficial layer of the biological tissue can be obtained by the Mueller polarimetric imaging method. Higher resolution microscopic imaging can give an observation of structure analysis of tissue in the level of nano size. The temperature of the skin at the end of the plasma continuous treatment is strongly related to the treatment time (treatment dose); the temperature of skin treated by plasma for 0.5 min, 1 min, 2 min and 6 min can reach 33 ℃, 59 ℃, 69 ℃ and 72 ℃, respectively. Plasma continuous treatments are also compared to sequences of 1 min plasma treatment which keeps the skin maximum temperature close to 60 ℃. Continuous and sequential plasma treatment are benchmarked with thermal treatment where skin samples are placed in an oven at different controlled temperature for different treatment times. The main conclusions are below:

1) The untreated skin has a linear retardance (ca. 0~20 degree), strong depolarization (ca. 0.6~0.8) and randomly distributed Azimuth;

General conclusions

2) The peak of linear retardance histogram of the of SAP in skin treated with the plasma treatment continuously increases as the dose of plasma sequential treatment increases, while the peak in the thermal treated skin increases first and then decreases with the increasing of dose of 60 ℃ thermal sequential treatment;

3) The plasma and thermal treatments can decrease the peak of depolarization histogram of skins;

4) The microstructure of skin, in particular the collagen of skin, can be strongly modified by a plasma and thermal continuous treatment when plasma treatment time over 2 min and 60 ℃ thermal treatment time over 6 min. The peak of retardance and depolarization histogram of these affected skins are significantly decreased with respect to the corresponding untreated skins. These affected skins exhibit a randomly distributed Azimuth;

5) Such results evidence a modification of the collagen observed in a preliminary study using confocal microscopy.

Reference

1. Freidberg JP: **Plasma physics and fusion energy**: Cambridge university press; 2008.
2. Francis FC: **Introduction to plasma physics and controlled fusion**: Springer International Publishing; 1984.
3. Fridman A: **Plasma chemistry**: Cambridge university press; 2008.
4. Inagaki N: **Plasma surface modification and plasma polymerization**: CRC Press; 2014.
5. Federici G, Skinner CH, Brooks JN, Coad JP, Grisolia C, Haasz AA, Hassanein A, Philipps V, Pitcher CS, Roth J: **Plasma-material interactions in current tokamaks and their implications for next step fusion reactors**. *Nuclear Fusion* 2001, **41**(12):1967.
6. Denes FS, Manolache S: **Macromolecular plasma-chemistry: an emerging field of polymer science**. *Progress in polymer science* 2004, **29**(8):815.
7. Samir U, Wright Jr K, Stone NH: **The expansion of a plasma into a vacuum: Basic phenomena and processes and applications to space plasma physics**. *Reviews of Geophysics* 1983, **21**(7):1631.
8. Kirk JG, Melrose DB, Priest ER: **Plasma Astrophysics: Saas-Fee Advanced Course 24. Lecture Notes 1994. Swiss Society for Astrophysics and Astronomy**, vol. 24: Springer Science & Business Media; 2006.
9. Dyakonov MI, Shur MS: **Plasma wave electronics: novel terahertz devices using two dimensional electron fluid**. *IEEE Transactions on Electron Devices* 1996, **43**(10):1640.
10. Knoll AJ, Zhang S, Lai M, Luan P, Oehrlein GS: **Infrared studies of gas phase and surface processes of the enhancement of catalytic methane decomposition by low temperature Plasma**. *Journal of Physics D: Applied Physics* 2019.
11. Yao Y, Hu S, Chen W, Huang Z-Q, Wei W, Yao T, Liu R, Zang K, Wang X, Wu G: **Engineering the electronic structure of single atom Ru sites via compressive strain boosts acidic water oxidation electrocatalysis**. *Nature Catalysis* 2019:1.
12. Yao XM, Jiang N, Peng BF, Guo H, Lu N, Shang KF, Li J, Wu Y: **Characteristics of a corona discharge ignited by a MgO/NiO/Ni sandwich cathode with high secondary electron emission for VOC degradation**. *Journal of Physics D: Applied Physics* 2018, **51**(43):10.
13. Kaiser M, Emmerich R, Urban H, Joos M, Elsner P: **Bifocal plasma source for treatment of gaseous pollutants**. *Surf Coat Technol* 2003, **174**:498.
14. Odic E, Parissi L, Goldman A, Goldman M, Amouroux J: **Depollution processes correlated to temperature control in non equilibrium plasmas. Application to the removal of volatile organic compounds**. New York: Begell House, Inc; 1999.
15. Khaledian HR, Zolfaghari P, Elhami V, Aghbolaghy M, Khorram S, Karimi A, Khataee A: **Modification of Immobilized Titanium Dioxide Nanostructures by Argon Plasma for Photocatalytic Removal of Organic Dyes**. *Molecules* 2019, **24**(3):19.
16. Sarangapani C, Ziuzina D, Behan P, Boehm D, Gilmore BF, Cullen PJ, Bourke P: **Degradation kinetics of cold plasma-treated antibiotics and their antimicrobial activity**. *Scientific Reports* 2019, **9**:15.
17. Kramer A, Bekeschus S, Matthes R, Bender C, Stope MB, Napp M, Lademann O, Lademann J, Weltmann KD, Schauer F: **Cold Physical Plasmas in the Field of Hygiene-Relevance, Significance, and Future Applications**. *Plasma Processes and Polymers* 2015, **12**(12):1410.
18. Liu FX, Sun P, Bai N, Tian Y, Zhou HX, Wei SC, Zhou YH, Zhang J, Zhu WD, Becker K *et al*: **Inactivation of Bacteria in an Aqueous Environment by a Direct-Current, Cold-Atmospheric-Pressure Air Plasma Microjet**. *Plasma Processes and Polymers* 2010, **7**(3-4):231.

19.   Benidris E, Ghezzar MR, Ma A, Ouddane B, Addou A: **Water purification by a new hybrid plasma-sensitization-coagulation process**. *Sep Purif Technol* 2017, **178**:253.

20.   Niessen W, Wolf O, Schruft R, Neiger M: **The influence of ethene on the conversion of NOx in a dielectric barrier discharge**. *Journal of Physics D: Applied Physics* 1998, **31**(5):542.

21.   Miessner H, Francke KP, Rudolph R: **Plasma-enhanced HC-SCR of NOx in the presence of excess oxygen**. *Appl Catal B-Environ* 2002, **36**(1):53.

22.   Miessner H, Francke KP, Rudolph R, Hammer T: **NOX removal in excess oxygen by plasma-enhanced selective catalytic reduction**. *Catal Today* 2002, **75**(1-4):325.

23.   Stere CE, Adress W, Burch R, Chansai S, Goguet A, Graham WG, De Rosa F, Palma V, Hardacre C: **Ambient Temperature Hydrocarbon Selective Catalytic Reduction of NOx Using Atmospheric Pressure Nonthermal Plasma Activation of a Ag/Al2O3 Catalyst**. *ACS Catal* 2014, **4**(2):666.

24.   Von Woedtke T, Metelmann HR, Weltmann KD: **Clinical plasma medicine: state and perspectives of in vivo application of cold atmospheric plasma**. *Contributions to Plasma Physics* 2014, **54**(2):104.

25.   Gan L, Zhang S, Poorun D, Liu D, Lu X, He M, Duan X, Chen H: **Medical applications of nonthermal atmospheric pressure plasma in dermatology**. *JDDG: Journal der Deutschen Dermatologischen Gesellschaft* 2018, **16**(1):7.

26.   Keidar M, Yan D, Beilis II, Trink B, Sherman JH: **Plasmas for treating cancer: opportunities for adaptive and self-adaptive approaches**. *Trends in biotechnology* 2018, **36**(6):586.

27.   Graves DB: **Low temperature plasma biomedicine: A tutorial reviewa)**. *Physics of Plasmas (1994-present)* 2014, **21**(8):080901.

28.   Shashurin A, Keidar M, Bronnikov S, Jurjus R, Stepp M: **Living tissue under treatment of cold plasma atmospheric jet**. *Applied Physics Letters* 2008, **93**(18):181501.

29.   Karahan A, Abbasoglu A, Isik SA, Cevik B, Saltan C, Elbas NO, Yalili A: **Factors Affecting Wound Healing in Individuals With Pressure Ulcers: A Retrospective Study**. *Ostomy Wound Manag* 2018, **64**(2):32.

30.   Koban I, Duske K, Jablonowski L, Schröder K, Nebe B, Sietmann R, Weltmann KD, Hübner NO, Kramer A, Kocher T: **Atmospheric Plasma Enhances Wettability and Osteoblast Spreading on Dentin In Vitro: Proof‐of‐Principle**. *Plasma Processes and Polymers* 2011, **8**(10):975.

31.   Größner‐Schreiber B, Teichmann J, Hannig M, Dörfer C, Wenderoth DF, Ott SJ: **Modified implant surfaces show different biofilm compositions under in vivo conditions**. *Clinical oral implants research* 2009, **20**(8):817.

32.   Dubinov AE, Kozhayeva JP, Zuimatch EA: **Changing germination rate of brown mustard seeds after treatment with plasmas of nanosecond electric discharges**. *IEEE Transactions on Plasma Science* 2017, **45**(2):294.

33.   Junior CA, de Oliveira Vitoriano J, Da Silva DLS, de Lima Farias M, de Lima Dantas NB: **Water uptake mechanism and germination of Erythrina velutina seeds treated with atmospheric plasma**. *Scientific reports* 2016, **6**:33722.

34.   Puač N, Petrović ZL, Živković S, Giba Z, Grubišić D, Đorđević A: **Low‐Temperature Plasma Treatment of Dry Empress‐Tree Seeds**. *Plasma Processes and Polymers* 2005:193.

35.   Sivachandiran L, Khacef A: **Enhanced seed germination and plant growth by atmospheric pressure cold air plasma: combined effect of seed and water treatment**. *RSC Advances* 2017, **7**(4):1822.

36.   Roy N, Hasan M, Kabir A, Reza M, Talukder M, Chowdhury A: **Atmospheric pressure gliding arc discharge plasma treatments for improving germination, growth and yield of wheat**. *Plasma Science and Technology* 2018, **20**(11):115501.

37.	Oehmigen K, Hähnel M, Brandenburg R, Wilke C, Weltmann KD, Von Woedtke T: **The role of acidification for antimicrobial activity of atmospheric pressure plasma in liquids**. *Plasma Processes and Polymers* 2010, **7**(3‐4):250.

38.	Zhang K, Perussello CA, Milosavljević V, Cullen P, Sun D-W, Tiwari BK: **Diagnostics of plasma reactive species and induced chemistry of plasma treated foods**. *Critical reviews in food science and nutrition* 2019:1.

39.	Thevenet F, Guillard C, Rousseau A: **Acetylene photocatalytic oxidation using continuous flow reactor: Gas phase and adsorbed phase investigation, assessment of the photocatalyst deactivation**. *Chemical Engineering Journal* 2014, **244**:50.

40.	Baloul Y, Seignour N, Foucher F, Khacef A: **Experimental assessment of ozone production by multichannel plasma discharges for automotive applications**. *Journal of Physics D: Applied Physics* 2019, **52**(27):275204.

41.	Huu TP, Adamowska M, Da Costa P, Cormier JM, Khacef A: **Combination of Non-Thermal Plasma and Pd-based catalyst for VOCs removal from air: case of CH4 and C3H6**. In*: 2012*; 2012.

42.	Khayrullina R, Tizaoui C, Williams P, Spacie C: **Application of Ozone-Assisted Membrane Cleaning for Natural Organic Matter Fouled Membranes**. *Ozone: Science & Engineering* 2017, **39**(5):310.

43.	Ben Fredj S, Novakoski RT, Tizaoui C, Monser L: **Two-phase ozonation for the removal of estrone, 17β-estradiol and 17α-ethinylestradiol in water using ozone-loaded decamethylcyclopentasiloxane**. *Ozone: Science & Engineering* 2017, **39**(5):343.

44.	Malik MA, Ghaffar A, Malik SA: **Water purification by electrical discharges**. *Plasma Sources Science and Technology* 2001, **10**(1):82.

45.	Glaze WH, Kang J-W, Chapin DH: **The chemistry of water treatment processes involving ozone, hydrogen peroxide and ultraviolet radiation**. 1987.

46.	Abdelmalek F, Gharbi S, Benstaali B, Addou A, Brisset JL: **Plasmachemical degradation of azo dyes by humid air plasma: Yellow Supranol 4 GL, Scarlet Red Nylosan F3 GL and industrial waste**. *Water Res* 2004, **38**(9):2339.

47.	Ayrault C, Barrault J, Tatibouet JM, Blin-Simland N, Jorand F, Pasqulers S, Rousseau A: **Oxidation of 2-heptanone in air by a DBD-type plasma generated within a honeycomb monolith supported PT-based catalyst**. *Abstr Pap Am Chem Soc* 2003, **225**:U55.

48.	Wang X, Romanias M, Thévenet F, Rousseau A: **Geocatalytic uptake of ozone onto natural mineral dust**. *Catalysts* 2018, **8**(7):263.

49.	Jia Z, Barakat C, Dong B, Rousseau A: **VOCs Destruction by Plasma Catalyst Coupling Using AL-KO PURE Air Purifier on Industrial Scale**. *Journal of Materials Science and Chemical Engineering* 2015, **3**(06):19.

50.	Tizaoui C, Grima N: **Kinetics of the ozone oxidation of Reactive Orange 16 azo-dye in aqueous solution**. *Chemical Engineering Journal* 2011, **173**(2):463.

51.	Abdelaziz AA, Ishijima T, Tizaoui C: **Development and characterization of a wire-plate air bubbling plasma for wastewater treatment using nanosecond pulsed high voltage**. *Journal of Applied Physics* 2018, **124**(5):053302.

52.	Nobbs J, Tizaoui C: **A Modified Indigo Method for the Determination of Ozone in Nonaqueous Solvents**. *Ozone: Science & Engineering* 2014, **36**(1):110.

53.	Leray A, Makarov M, Cormier J-M, Khacef A: **Diesel oxidation catalyst for CO and unburned hydrocarbons removal from diesel exhaust under plasma discharge conditions**. In*: 2015*; 2015.

54.	Leray A, Guy A, Makarov M, Lombaert K, Cormier JM, Khacef A: **Plasma-Assisted Diesel Oxidation Catalyst on Bench Scale: Focus on Light-off Temperature and NOx Behavior**. *Topics in Catalysis* 2013, **56**(1-8):222.

55.	Khacef A, Da Costa P, Djéga-Mariadassou G: **Plasma assisted catalyst for NOx remediation from lean gas exhaust**. *Journal of Engineering And Technology Research* 2013, **1**(1):112.

56. Leray A, Cormier JM, Makarov M, Khacef A: **Improvement of Diesel Oxidation Catalyst Light-Off Temperature by Non-Thermal Plasma**. In*: 2012*; 2012.

57. Barakat C, Gravejat P, Guaitella O, Thévenet F, Rousseau A: **Oxidation of isopropanol and acetone adsorbed on TiO2 under plasma generated ozone flow: Gas phase and adsorbed species monitoring**. *Applied Catalysis B: Environmental* 2014, **147**:302.

58. Jia Z, Wang X, Foucher E, Thevenet F, Rousseau A: **Plasma-catalytic mineralization of toluene adsorbed on CeO2**. *Catalysts* 2018, **8**(8):303.

59. Zhuang H, Rothrock Jr MJ, Hiett KL, Lawrence KC, Gamble GR, Bowker BC, Keener KM: **In-Package Air Cold Plasma Treatment of Chicken Breast Meat: Treatment Time Effect**. *Journal of Food Quality* 2019, **2019**.

60. Ling L, Jiangang L, Minchong S, Chunlei Z, Yuanhua D: **Cold plasma treatment enhances oilseed rape seed germination under drought stress**. *Scientific reports* 2015, **5**.

61. Wang W, Zheng H, Fan C, Li J, Shi J, Cai Z, Zhang G, Liu D, Zhang J, Vang S: **High rate of chimeric gene origination by retroposition in plant genomes**. *The Plant Cell* 2006, **18**(8):1791.

62. Judée F, Simon S, Dufour T: **Plasma-activation of tap water using DBD for agronomy applications: Identification and quantification of long lifetime chemical species and production/consumption mechanisms**. *Water Res* 2017.

63. Surowsky B, Fischer A, Schlueter O, Knorr D: **Cold plasma effects on enzyme activity in a model food system**. *Innovative Food Science & Emerging Technologies* 2013, **19**:146.

64. Park DP, Davis K, Gilani S, Alonzo C-A, Dobrynin D, Friedman G, Fridman A, Rabinovich A, Fridman G: **Reactive nitrogen species produced in water by non-equilibrium plasma increase plant growth rate and nutritional yield**. *Current Applied Physics* 2013, **13**:S19.

65. Yang B, Chen JR, Yu QS, Li H, Lin MS, Mustapha A, Hong LA, Wang Y: **Oral bacterial deactivation using a low-temperature atmospheric argon plasma brush**. *J Dent* 2011, **39**(1):48.

66. Goree J, Liu B, Drake D, Stoffels E: **Killing of S-mutans bacteria using a plasma needle at atmospheric pressure**. *Ieee Transactions on Plasma Science* 2006, **34**(4):1317.

67. Hoffmann C, Berganza C, Zhang J: **Cold Atmospheric Plasma: methods of production and application in dentistry and oncology**. *Medical gas research* 2013, **3**(1):21.

68. Kaushik NK, Ghimire B, Li Y, Adhikari M, Veerana M, Kaushik N, Jha N, Adhikari B, Lee S-J, Masur K: **Biological and medical applications of plasma-activated media, water and solutions**. *Biological chemistry* 2018, **400**(1):39.

69. Boehm D, Bourke P: **Safety implications of plasma-induced effects in living cells–a review of in vitro and in vivo findings**. *Biological chemistry* 2018, **400**(1):3.

70. Jablonowski HM: **Generation of highly reactive species by plasma-liquid interaction**. Dissertation, Greifswald, Ernst-Moritz-Arndt-Universität, 2016; 2016.

71. Cha S, Park Y-S: **Plasma in dentistry**. *Clinical plasma medicine* 2014, **2**(1):4.

72. Kim C-H, Kwon S, Bahn JH, Lee K, Jun SI, Rack PD, Baek SJ: **Effects of atmospheric nonthermal plasma on invasion of colorectal cancer cells**. *Applied physics letters* 2010, **96**(24):243701.

73. Zhang X, Li M, Zhou R, Feng K, Yang S: **Ablation of liver cancer cells in vitro by a plasma needle**. *Applied Physics Letters* 2008, **93**(2):021502.

74. Kolb JF, Mohamed A-AH, Price RO, Swanson RJ, Bowman A, Chiavarini R, Stacey M, Schoenbach K: **Cold atmospheric pressure air plasma jet for medical applications**. *Applied Physics Letters* 2008, **92**(24):241501.

75. Fridman G, Friedman G, Gutsol A, Shekhter AB, Vasilets VN, Fridman A: **Applied plasma medicine**. *Plasma Processes and Polymers* 2008, **5**(6):503.

76. Fridman G, Peddinghaus M, Balasubramanian M, Ayan H, Fridman A, Gutsol A, Brooks A: **Blood coagulation and living tissue sterilization by floating-electrode dielectric barrier discharge in air**. *Plasma Chemistry and Plasma Processing* 2006, **26**(4):425.

77. Laroussi M: **Low temperature plasma‐based sterilization: overview and state‐of‐the‐art**. *Plasma processes and polymers* 2005, **2**(5):391.

78. Gomes A, Fernandes E, Lima JL: **Fluorescence probes used for detection of reactive oxygen species**. *Journal of biochemical and biophysical methods* 2005, **65**(2):45.

79. Amit SK, Uddin MM, Rahman R, Islam SR, Khan MS: **A review on mechanisms and commercial aspects of food preservation and processing**. *Agriculture & Food Security* 2017, **6**(1):51.

80. Ekezie F-GC, Sun D-W, Cheng J-H: **A review on recent advances in cold plasma technology for the food industry: Current applications and future trends**. *Trends in Food Science & Technology* 2017, **69**:46.

81. Thirumdas R, Sarangapani C, Annapure US: **Cold plasma: a novel non-thermal technology for food processing**. *Food Biophysics* 2015, **10**(1):1.

82. Thirumdas R, Kothakota A, Annapure U, Siliveru K, Blundell R, Gatt R, Valdramidis VP: **Plasma activated water (PAW): Chemistry, physico-chemical properties, applications in food and agriculture**. *Trends in Food Science & Technology* 2018.

83. Galiè S, García-Gutiérrez C, Miguélez EM, Villar CJ, Lombó F: **Biofilms in the food industry: health aspects and control methods**. *Frontiers in microbiology* 2018, **9**:898.

84. Bourke P, Ziuzina D, Boehm D, Cullen PJ, Keener K: **The Potential of Cold Plasma for Safe and Sustainable Food Production**. *Trends in biotechnology* 2018.

85. Rowan NJ, Espie S, Harrower J, Anderson J, Marsili L, MacGregor S: **Pulsed-plasma gas-discharge inactivation of microbial pathogens in chilled poultry wash water**. *Journal of Food Protection* 2007, **70**(12):2805.

86. Ma R, Wang G, Tian Y, Wang K, Zhang J, Fang J: **Non-thermal plasma-activated water inactivation of food-borne pathogen on fresh produce**. *Journal of hazardous materials* 2015, **300**:643.

87. Min SC, Roh SH, Niemira BA, Boyd G, Sites JE, Uknalis J, Fan X: **In-package inhibition of E. coli O157: H7 on bulk Romaine lettuce using cold plasma**. *Food microbiology* 2017, **65**:1.

88. Montenegro J, Ruan R, Ma H, Chen P: **Inactivation of E. coli O157: H7 using a pulsed nonthermal plasma system**. *Journal of food science* 2002, **67**(2):646.

89. Shi X-M, Zhang G-J, Wu X-L, Li Y-X, Ma Y, Shao X-J: **Effect of low-temperature plasma on microorganism inactivation and quality of freshly squeezed orange juice**. *IEEE Transactions on Plasma Science* 2011, **39**(7):1591.

90. Perni S, Shama G, Kong MG: **Cold atmospheric plasma disinfection of cut fruit surfaces contaminated with migrating microorganisms**. *Journal of food protection* 2008, **71**(8):1619.

91. Dobrynin D, Fridman G, Friedman G, Fridman A: **Physical and biological mechanisms of direct plasma interaction with living tissue**. *New Journal of Physics* 2009, **11**(11):115020.

92. Pankaj S, Misra N, Cullen P: **Kinetics of tomato peroxidase inactivation by atmospheric pressure cold plasma based on dielectric barrier discharge**. *Innovative Food Science & Emerging Technologies* 2013, **19**:153.

93. Wang R, Zhou H, Sun P, Wu H, Pan J, Zhu W, Zhang J, Fang J: **The effect of an atmospheric pressure, DC nonthermal plasma microjet on tooth root canal, dentinal tubules infection and reinfection prevention**. *Plasma Medicine* 2011, **1**(2).

94. Pan J, Sun K, Liang Y, Sun P, Yang X, Wang J, Zhang J, Zhu W, Fang J, Becker KH: **Cold plasma therapy of a tooth root canal infected with Enterococcus faecalis biofilms in vitro**. *J Endod* 2013, **39**(1):105.

95. Kang SK, Choi MY, Koo IG, Kim PY, Kim Y, Kim GJ, Mohamed A-AH, Collins GJ, Lee JK: **Reactive hydroxyl radical-driven oral bacterial inactivation by radio frequency atmospheric plasma**. *Applied Physics Letters* 2011, **98**(14):143702.

96. Jiang C, Chen MT, Gorur A, Schaudinn C, Jaramillo DE, Costerton JW, Sedghizadeh PP, Vernier PT, Gundersen MA: **Nanosecond pulsed plasma dental probe**. *Plasma Processes and Polymers* 2009, **6**(8):479.

97. Schaudinn C, Jaramillo D, Freire M, Sedghizadeh P, Nguyen A, Webster P, Costerton J, Jiang C: **Evaluation of a nonthermal plasma needle to eliminate ex vivo biofilms in root canals of extracted human teeth**. *International endodontic journal* 2013, **46**(10):930.

98. Pei X, Lu X, Liu J, Liu D, Yang Y, Ostrikov K, Chu PK, Pan Y: **Inactivation of a 25.5 μm Enterococcus faecalis biofilm by a room-temperature, battery-operated, handheld air plasma jet**. *Journal of Physics D: Applied Physics* 2012, **45**(16):165205.

99. Miletić M, Mojsilović S, Đorđević IO, Maletić D, Puač N, Lazović S, Malović G, Milenković P, Petrović ZL, Bugarski D: **Effects of non-thermal atmospheric plasma on human periodontal ligament mesenchymal stem cells**. *Journal of physics D: Applied physics* 2013, **46**(34):345401.

100. Kim JY, Ballato J, Foy P, Hawkins T, Wei Y, Li J, Kim SO: **Single‐Cell‐Level Cancer Therapy Using a Hollow Optical Fiber‐Based Microplasma**. *Small* 2010, **6**(14):1474.

101. Honnorat B: **Application of cold plasma in oncology, multidisciplinary experiments, physical, chemical and biological modeling**. 2018.

102. Heinlin J, Isbary G, Stolz W, Morfill G, Landthaler M, Shimizu T, Steffes B, Nosenko T, Zimmermann JL, Karrer S: **Plasma applications in medicine with a special focus on dermatology**. *J Eur Acad Dermatol Venereol* 2011, **25**(1):1.

103. Zhong SY, Dong YY, Liu DX, Xu DH, Xiao SX, Chen HL, Kong MG: **Surface air plasma-induced cell death and cytokine release of human keratinocytes in the context of psoriasis**. *Br J Dermatol* 2016, **174**(3):542.

104. Duchesne C, Banzet S, Lataillade JJ, Rousseau A, Frescaline N: **Cold atmospheric plasma modulates endothelial nitric oxide synthase signalling and enhances burn wound neovascularisation**. *The Journal of Pathology* 2019, **249**(3).

105. Duchesne C, Frescaline N, Lataillade J-J, Rousseau A: **Comparative Study between Direct and Indirect Treatment with Cold Atmospheric Plasma on In Vitro and In Vivo Models of Wound Healing**. *Plasma Medicine* 2018, **8**(4).

106. Kilmer S, Semchyshyn N, Shah G, Fitzpatrick R: **A pilot study on the use of a Plasma Skin Regeneration device (PSR) in full facial rejuvenation procedures**. *Journal of the American Academy of Dermatology* 2005, **52**(3).

107. Kilmer S, Fitzpatrick R, Bernstein E, Brown D: **long Term Follow-up On The Use Of Plasma Skin Regeneration (psr) In Full Facial Rejuvenation Procedures: 70**. *Lasers in Surgery and Medicine* 2005, **36**:23.

108. Kubinova S, Zaviskova K, Uherkova L, Zablotskii V, Churpita O, Lunov O, Dejneka A: **Non-thermal air plasma promotes the healing of acute skin wounds in rats**. *Scientific reports* 2017, **7**:45183.

109. Barton A, Wende K, Bundscherer L, Hasse S, Schmidt A, Bekeschus S, Weltmann K-D, Lindequist U, Masur K: **Nonthermal plasma increases expression of wound healing related genes in a keratinocyte cell line**. *Plasma Medicine* 2013, **3**(1-2).

110. Arjunan KP, Friedman G, Fridman A, Clyne AM: **Non-thermal dielectric barrier discharge plasma induces angiogenesis through reactive oxygen species**. *Journal of the Royal Society Interface* 2011, **9**(66):147.

111. Chatraie M, Torkaman G, Khani M, Salehi H, Shokri B: **In vivo study of non-invasive effects of non-thermal plasma in pressure ulcer treatment**. *Scientific reports* 2018, **8**(1):5621.

112. Arndt S, Unger P, Wacker E, Shimizu T, Heinlin J, Li Y-F, Thomas HM, Morfill GE, Zimmermann JL, Bosserhoff A-K: **Cold atmospheric plasma (CAP) changes gene expression of key molecules of the wound healing machinery and improves wound healing in vitro and in vivo**. *PloS one* 2013, **8**(11):e79325.

113. Vanraes P, Nikiforov AY, Leys C: **Electrical discharge in water treatment technology for micropollutant decomposition**. *Plasma Science and Technology—Progress in Physical States and Chemical Reactions* 2016:429.

114.   Siefermann KR, Liu Y, Lugovoy E, Link O, Faubel M, Buck U, Winter B, Abel B: **Binding energies, lifetimes and implications of bulk and interface solvated electrons in water**. *Nature chemistry* 2010, **2**(4):274.

115.   Lukes P, Locke BR: **Plasmachemical oxidation processes in a hybrid gas–liquid electrical discharge reactor**. *Journal of Physics D: Applied Physics* 2005, **38**(22):4074.

116.   Foster JE: **Plasma-based water purification: Challenges and prospects for the future**. *Physics of Plasmas* 2017, **24**(5):16.

117.   Bruggeman P, Leys C: **Non-thermal plasmas in and in contact with liquids**. *Journal of Physics D: Applied Physics* 2009, **42**(5):28.

118.   An W, Baumung K, Bluhm H: **Underwater streamer propagation analyzed from detailed measurements of pressure release**. *Journal of Applied Physics* 2007, **101**(5):10.

119.   Bruggeman P, Kushner MJ, Locke BR, Gardeniers JG, Graham W, Graves DB, Hofman-Caris R, Maric D, Reid JP, Ceriani E: **Plasma–liquid interactions: a review and roadmap**. *Plasma sources science and technology* 2016, **25**(5):053002.

120.   Marinov I, Guaitella O, Rousseau A, Starikovskaia S: **Modes of underwater discharge propagation in a series of nanosecond successive pulses**. *Journal of Physics D: Applied Physics* 2013, **46**(46):464013.

121.   Lietz AM, Kushner MJ: **Air plasma treatment of liquid covered tissue: long timescale chemistry**. *Journal of Physics D: Applied Physics* 2016, **49**(42):425204.

122.   Somorjai GA: **Principles of Surface Chemistry (Fundamental Topics in Physical Chemistry)**: Prentice-Hall, Inc, Englewood Cliffs, NJ; 1972.

123.   Rumbach P, Bartels DM, Go DB: **The penetration and concentration of solvated electrons and hydroxyl radicals at a plasma-liquid interface**. *Plasma Sources Science and Technology* 2018, **27**(11):115013.

124.   Lindsay A, Anderson C, Slikboer E, Shannon S, Graves D: **Momentum, heat, and neutral mass transport in convective atmospheric pressure plasma-liquid systems and implications for aqueous targets**. *Journal of Physics D: Applied Physics* 2015, **48**(42):424007.

125.   Attri P, Kim YH, Park DH, Park JH, Hong YJ, Uhm HS, Kim K-N, Fridman A, Choi EH: **Generation mechanism of hydroxyl radical species and its lifetime prediction during the plasma-initiated ultraviolet (UV) photolysis**. *Scientific reports* 2015, **5**.

126.   Luo YC, Lietz AM, Yatom S, Kushner MJ, Bruggeman PJ: **Plasma kinetics in a nanosecond pulsed filamentary discharge sustained in Ar-H2O and H2O**. *Journal of Physics D: Applied Physics* 2019, **52**(4):17.

127.   Gorbanev Y, O'Connell D, Chechik V: **Non‐Thermal Plasma in Contact with Water: The Origin of Species**. *Chemistry–A European Journal* 2016, **22**(10):3496.

128.   Elg DT, Yang I-W, Graves DB: **Production of TEMPO by O atoms in atmospheric pressure non-thermal plasma–liquid interactions**. *Journal of Physics D: Applied Physics* 2017, **50**(47):475201.

129.   Chen Z, Liu D, Chen C, Xu D, Liu Z, Xia W, Rong M, Kong MG: **Analysis of the production mechanism of H2O2 in water treated by helium DC plasma jets**. *Journal of Physics D: Applied Physics* 2018, **51**(32):325201.

130.   Hefny MM, Pattyn C, Lukes P, Benedikt J: **Atmospheric plasma generates oxygen atoms as oxidizing species in aqueous solutions**. *Journal of Physics D: Applied Physics* 2016, **49**(40):404002.

131.   Takeuchi N, Ishibashi N: **Generation mechanism of hydrogen peroxide in dc plasma with a liquid electrode**. *Plasma Sources Sci Technol* 2018, **27**(4):9.

132.   Rodebush W, Wahl M: **The reactions of the hydroxyl radical in the electrodeless discharge in water vapor**. *The Journal of Chemical Physics* 1933, **1**(10):696.

133.   Locke BR, Shih K-Y: **Review of the methods to form hydrogen peroxide in electrical discharge plasma with liquid water**. *Plasma Sources Science and Technology* 2011, **20**(3):034006.

134. Peyrous R, Pignolet P, Held B: **Kinetic simulation of gaseous species created by an electrical discharge in dry or humid oxygen**. *Journal of Physics D: Applied Physics* 1989, **22**(11):1658.

135. He X, Lin J, He B, Xu L, Li J, Chen Q, Yue G, Xiong Q, Liu QH: **The formation pathways of aqueous hydrogen peroxide in a plasma-liquid system with liquid as the cathode**. *Plasma Sources Science and Technology* 2018, **27**(8):085010.

136. Albertos P, Romero-Puertas MC, Tatematsu K, Mateos I, Sánchez-Vicente I, Nambara E, Lorenzo O: **S-nitrosylation triggers ABI5 degradation to promote seed germination and seedling growth**. *Nature communications* 2015, **6**:8669.

137. He B, Ma Y, Gong X, Long Z, Li J, Xiong Q, Liu H, Chen Q, Zhang X, Yang S: **Simultaneous quantification of aqueous peroxide, nitrate, and nitrite during the plasma–liquid interactions by derivative absorption spectrophotometry**. *Journal of Physics D: Applied Physics* 2017, **50**(44):445207.

138. Uchida G, Nakajima A, Ito T, Takenaka K, Kawasaki T, Koga K, Shiratani M, Setsuhara Y: **Effects of nonthermal plasma jet irradiation on the selective production of H2O2 and NO2− in liquid water**. *Journal of Applied Physics* 2016, **120**(20):203302.

139. Tian W, Lietz AM, Kushner MJ: **The consequences of air flow on the distribution of aqueous species during dielectric barrier discharge treatment of thin water layers**. *Plasma Sources Science and Technology* 2016, **25**(5):055020.

140. Bruggeman P, Leys C: **Non-thermal plasmas in and in contact with liquids**. *Journal of Physics D: Applied Physics* 2009, **42**(5):053001.

141. Măgureanu M, Sîrbu R, Dobrin D, Gîdea M: **Stimulation of the Germination and Early Growth of Tomato Seeds by Non-thermal Plasma**. *Plasma Chemistry and Plasma Processing* 2018:1.

142. Altieri MA: **Agroecology: the science of sustainable agriculture**: CRC Press; 2018.

143. Bruggink G, Ooms J, Van der Toorn P: **Induction of longevity in primed seeds**. *Seed Science Research* 1999, **9**(1):49.

144. Capanoglu E: **The potential of priming in food production**. *Trends in food science & technology* 2010, **21**(8):399.

145. Bewley J: **Black, m. 1994. seeds; physiology of development and germination**. In.: New York: Plenum Press.

146. Nonogaki H, Bassel GW, Bewley JD: **Germination—still a mystery**. *Plant Science* 2010, **179**(6):574.

147. Finch-Savage W, Bassel G: **Seed vigour and crop establishment: extending performance beyond adaptation**. *Journal of Experimental Botany* 2015, **67**(3):567.

148. Wojtyla Ł, Lechowska K, Kubala S, Garnczarska M: **Different modes of hydrogen peroxide action during seed germination**. *Frontiers in plant science* 2016, **7**.

149. Galland M, Huguet R, Arc E, Cueff G, Job D, Rajjou L: **Dynamic proteomics emphasizes the importance of selective mRNA translation and protein turnover during Arabidopsis seed germination**. *Molecular & Cellular Proteomics* 2014, **13**(1):252.

150. Paparella S, Araújo S, Rossi G, Wijayasinghe M, Carbonera D, Balestrazzi A: **Seed priming: state of the art and new perspectives**. *Plant cell reports* 2015, **34**(8):1281.

151. TT DT, Puthur JT: **UV radiation priming: A means of amplifying the inherent potential for abiotic stress tolerance in crop plants**. *Environmental and Experimental Botany* 2017, **138**:57.

152. Mahmood A, Turgay OC, Farooq M, Hayat R: **Seed biopriming with plant growth promoting rhizobacteria: a review**. *FEMS microbiology ecology* 2016, **92**(8).

153. Ibrahim EA: **Seed priming to alleviate salinity stress in germinating seeds**. *Journal of Plant Physiology* 2016, **192**:38.

154. Ashraf M, Foolad M: **Pre‐sowing seed treatment—A shotgun approach to improve germination, plant growth, and crop yield under saline and non‐saline conditions**. *Advances in Agronomy* 2005, **88**:223.

155. Holdsworth MJ, Bentsink L, Soppe WJ: **Molecular networks regulating Arabidopsis seed maturation, after‑ripening, dormancy and germination**. *New Phytologist* 2008, **179**(1):33.

156. Osborne DJ: **Biochemical control systems operating in the early hours of germination**. *Canadian Journal of Botany* 1983, **61**(12):3568.

157. Gallardo K, Job C, Groot SP, Puype M, Demol H, Vandekerckhove J, Job D: **Proteomic analysis of Arabidopsis seed germination and priming**. *Plant physiology* 2001, **126**(2):835.

158. Heydecker W, Coolbear P: **Seed treatments for improved performance survey and attempted prognosis**. *Seed science and technology* 1977.

159. Pill WG: **Low water potential and presowing germination treatments to improve seed quality**. *Seed quality* 1995:319.

160. Whalley W, Ober E, Jenkins M: **Measurement of the matric potential of soil water in the rhizosphere**. *Journal of experimental botany* 2013, **64**(13):3951.

161. Miano AC, da Costa Pereira J, Castanha N, da Matta Júnior MD, Augusto PED: **Enhancing mung bean hydration using the ultrasound technology: description of mechanisms and impact on its germination and main components**. *Scientific reports* 2016, **6**:38996.

162. Koornneef M, Alonso-Blanco C, Bentsink L, Blankenstein-de Vries H, Debeaujon I, Hanhart C, Leon-Kloosterziel K, Peeters A, Raz V: **The genetics of seed dormancy**. *CAB International, Wallingford, Oxon, UK* 2000.

163. Rajjou L, Duval M, Gallardo K, Catusse J, Bally J, Job C, Job D: **Seed germination and vigor**. *Annual review of plant biology* 2012, **63**:507.

164. Bethke PC, Gubler F, Jacobsen JV, Jones RL: **Dormancy of Arabidopsis seeds and barley grains can be broken by nitric oxide**. *Planta* 2004, **219**(5):847.

165. El-Maarouf-Bouteau H, Meimoun P, Job C, Job D, Bailly C: **Role of protein and mRNA oxidation in seed dormancy and germination**. *Frontiers in plant science* 2013, **4**.

166. McCourt P: **Genetic analysis of hormone signaling**. *Annual review of plant biology* 1999, **50**(1):219.

167. Gniazdowska A, Krasuska U, Czajkowska K, Bogatek R: **Nitric oxide, hydrogen cyanide and ethylene are required in the control of germination and undisturbed development of young apple seedlings**. *Plant growth regulation* 2010, **61**(1):75.

168. Liu Y, Ye N, Liu R, Chen M, Zhang J: **H2O2 mediates the regulation of ABA catabolism and GA biosynthesis in Arabidopsis seed dormancy and germination**. *Journal of experimental botany* 2010, **61**(11):2979.

169. El-Maarouf-Bouteau H, Sajjad Y, Bazin J, Langlade N, Cristescu SM, Balzergue S, Baudouin E, Bailly C: **Reactive oxygen species, abscisic acid and ethylene interact to regulate sunflower seed germination**. *Plant, cell & environment* 2015, **38**(2):364.

170. Arc E, Sechet J, Corbineau F, Rajjou L, Marion-Poll A: **ABA crosstalk with ethylene and nitric oxide in seed dormancy and germination**. *Frontiers in plant science* 2013, **4**:63.

171. Liu X, Deng Z, Cheng H, He X, Song S: **Nitrite, sodium nitroprusside, potassium ferricyanide and hydrogen peroxide release dormancy of Amaranthus retroflexus seeds in a nitric oxide-dependent manner**. *Plant Growth Regulation* 2011, **64**(2):155.

172. Kacharava N, Chanishvili S, Badridze G, Chkhubianishvili E, Janukashvili N: **Effect of seed irradiation on the content of antioxidants in leaves of Kidney bean, Cabbage and Beet cultivars**. *Australian Journal of Crop Science* 2009, **3**(3):137.

173. Parera CA, Cantliffe DJ: **Improved stand establishment of shrunken-2 sweet corn by seed treatments**. *Plant Physiol* 1990, **39**:245.

174. Kaushik P, Shakil NA, Kumar J, Singh MK, Singh MK, Yadav SK: **Development of controlled release formulations of thiram employing amphiphilic polymers and their bioefficacy evaluation in seed quality enhancement studies**. *Journal of Environmental Science and Health, Part B* 2013, **48**(8):677.

175. de Groot GJ, Hundt A, Murphy AB, Bange MP, Mai-Prochnow A: **Cold plasma treatment for cotton seed germination improvement**. *Scientific reports* 2018, **8**(1):14372.

176. Zhang JJ, Jo JO, Do Luong Huynh RKM, Ghosh M, Singh AK, Lee SB, Mok YS, Hyuk P, Jeong DK: **Growth-inducing effects of argon plasma on soybean sprouts via the regulation of demethylation levels of energy metabolism-related genes**. *Scientific Reports* 2017, **7**.

177. Khamsen N, Onwimol D, Teerakawanich N, Dechanupaprittha S, Kanokbannakorn W, Hongesombut K, Srisonphan S: **Rice (Oryza sativa L.) seed sterilization and germination enhancement via atmospheric hybrid nonthermal discharge plasma**. *ACS applied materials & interfaces* 2016, **8**(30):19268.

178. Hammond Jr EC, Bridgers K, Berry FD: **Germination, growth rates, and electron microscope analysis of tomato seeds flown on the LDEF**. *Radiation measurements* 1996, **26**(6):851.

179. Kitazaki S, Koga K, Shiratani M, Hayashi N: **Growth enhancement of radish sprouts induced by low pressure O2 radio frequency discharge plasma irradiation**. *Japanese Journal of Applied Physics* 2012, **51**(1S):01AE01.

180. Srisonphan S: **Tuning Surface Wettability through Hot Carrier Initiated Impact Ionization in Cold Plasma**. *ACS applied materials & interfaces* 2018, **10**(13):11297.

181. Mildaziene V, Pauzaite G, Malakauskiene A, Zukiene R, Nauciene Z, Filatova I, Azharonok V, Lyushkevich V: **Response of perennial woody plants to seed treatment by electromagnetic field and low‑temperature plasma**. *Bioelectromagnetics* 2016, **37**(8):536.

182. Gómez-Ramírez A, López-Santos C, Cantos M, García JL, Molina R, Cotrino J, Espinós J, González-Elipe AR: **Surface chemistry and germination improvement of Quinoa seeds subjected to plasma activation**. *Scientific reports* 2017, **7**(1):5924.

183. Randeniya LK, de Groot GJ: **Non‑Thermal Plasma Treatment of Agricultural Seeds for Stimulation of Germination, Removal of Surface Contamination and Other Benefits: A Review**. *Plasma Processes and Polymers* 2015, **12**(7):608.

184. Saberi M, Modarres-Sanavy SAM, Zare R, Ghomi H: **Amelioration of Photosynthesis and Quality of Wheat under Non-thermal Radio Frequency Plasma Treatment**. *Scientific reports* 2018, **8**(1):11655.

185. Zhou Z, Huang Y, Yang S, Chen W: **Introduction of a new atmospheric pressure plasma device and application on tomato seeds**. *Agricultural Sciences* 2011, **2**(1):23.

186. Dobrin D, Magureanu M, Mandache NB, Ionita M-D: **The effect of non-thermal plasma treatment on wheat germination and early growth**. *Innovative Food Science & Emerging Technologies* 2015, **29**:255.

187. Selcuk M, Oksuz L, Basaran P: **Decontamination of grains and legumes infected with Aspergillus spp. and Penicillum spp. by cold plasma treatment**. *Bioresource technology* 2008, **99**(11):5104.

188. Laroussi M, Leipold F: **Evaluation of the roles of reactive species, heat, and UV radiation in the inactivation of bacterial cells by air plasmas at atmospheric pressure**. *International Journal of Mass Spectrometry* 2004, **233**(1):81.

189. Pizá MCP, Prevosto L, Zilli C, Cejas E, Kelly H, Balestrasse K: **Effects of non–thermal plasmas on seed-borne Diaporthe/Phomopsis complex and germination parameters of soybean seeds**. *Innovative Food Science & Emerging Technologies* 2018, **49**:82.

190. Görsdorf S, Appel KE, Engeholm C, Obe G: **Niltrogen dioxide induces DNA single-strand breaks in cultured Chinese hamster cells**. *Carcinogenesis* 1990, **11**(1):37.

191. Norberg SA, Johnsen E, Kushner MJ: **Helium atmospheric pressure plasma jets interacting with wet cells: delivery of electric fields**. *Journal of Physics D: Applied Physics* 2016, **49**(18):185201.

192. da Silva A, Farias M, da Silva D, Vitoriano J, de Sousa R, Alves-Junior C: **Using atmospheric plasma to increase wettability, imbibition and germination of physically dormant seeds of Mimosa Caesalpiniafolia**. *Colloids and Surfaces B: Biointerfaces* 2017, **157**:280.

193. Ling L, Jiafeng J, Jiangang L, Minchong S, Xin H, Hanliang S, Yuanhua D: **Effects of cold plasma treatment on seed germination and seedling growth of soybean**. *Scientific reports* 2014, **4**.

194. Rahman MM, Sajib SA, Rahi MS, Tahura S, Roy NC, Parvez S, Reza MA, Talukder MR, Kabir AH: **Mechanisms and Signaling Associated with LPDBD Plasma Mediated Growth Improvement in Wheat**. *Scientific reports* 2018, **8**.

195. Zhou R, Zhou R, Zhang X, Zhuang J, Yang S, Bazaka K, Ostrikov KK: **Effects of atmospheric-pressure N2, He, air, and O2 microplasmas on mung bean seed germination and seedling growth**. *Scientific reports* 2016, **6**:32603.

196. Pawlat J, Starek A, Sujak A, Kwiatkowski M, Terebun P, Budzeń M: **Effects of atmospheric pressure plasma generated in GlidArc reactor on Lavatera thuringiaca L. seeds' germination**. *Plasma Processes and Polymers* 2018, **15**(2):1700064.

197. Dubinov AE, Kozhayeva JP, Zuimatch EA: **Scarification of Altaic Flax Seeds With High-Power UV Radiation Generated by Plasma of Nanosecond Electric Discharges**. *IEEE Transactions on Plasma Science* 2018(99):1.

198. Wang X-Q, Zhou R-W, De Groot G, Bazaka K, Murphy AB, Ostrikov KK: **Spectral characteristics of cotton seeds treated by a dielectric barrier discharge plasma**. *Scientific reports* 2017, **7**(1):5601.

199. Ji SH, Kim T, Panngom K, Hong YJ, Pengkit A, Park DH, Kang MH, Lee SH, Im JS, Kim JS: **Assessment of the effects of nitrogen plasma and plasma‐generated nitric oxide on early development of Coriandum sativum**. *Plasma Processes and Polymers* 2015, **12**(10):1164.

200. Ren H, Huang Z, Chen Z, Yuan M, Lu T: **Effects of nitrogen ion implantation on lily pollen germination and the distribution of the actin cytoskeleton during pollen germination**. *Chinese Science Bulletin* 2000, **45**(18):1677.

201. Wei Z, Han G, Zhou G, Li Q, Xie H, Gao Q: **An important mechanism of crop breeding with ultralow energy ion injection**. *Shengwu Wuli Xuebao* 1996, **12**(2):315.

202. Guoping L, Qunce H, Guangyong Q, Yuping H: **The effects of low-energy nitrogen ion implantation on pollen exine substructure and pollen germination of Cedrus deodara**. *Plasma Science and Technology* 2005, **7**(6):3176.

203. Grzegorzewski F, Rohn S, Kroh LW, Geyer M, Schlüter O: **Surface morphology and chemical composition of lamb's lettuce (Valerianella locusta) after exposure to a low-pressure oxygen plasma**. *Food Chemistry* 2010, **122**(4):1145.

204. Richards SL, Wilkins KA, Swarbreck SM, Anderson AA, Habib N, Smith AG, McAinsh M, Davies JM: **The hydroxyl radical in plants: from seed to seed**. *Journal of experimental botany* 2014, **66**(1):37.

205. Schopfer P, Plachy C, Frahry G: **Release of reactive oxygen intermediates (superoxide radicals, hydrogen peroxide, and hydroxyl radicals) and peroxidase in germinating radish seeds controlled by light, gibberellin, and abscisic acid**. *Plant Physiology* 2001, **125**(4):1591.

206. Nguyen T-P, Cueff G, Hegedus DD, Rajjou L, Bentsink L: **A role for seed storage proteins in Arabidopsis seed longevity**. *Journal of experimental botany* 2015, **66**(20):6399.

207. Job C, Rajjou L, Lovigny Y, Belghazi M, Job D: **Patterns of protein oxidation in Arabidopsis seeds and during germination**. *Plant Physiology* 2005, **138**(2):790.

208. Wheaton FW: **Effects of various electrical fields on seed germination**. *Doctor of philosophy*. Iowa State University; 1968.

209. Zhao Y, Hu M, Gao Z, Chen X, Huang D: **Biological mechanisms of a novel hydro-electro hybrid priming recovers potential vigor of onion seeds**. *Environmental and Experimental Botany* 2018, **150**:260.

210. Sudsiri CJ, Jumpa N, Kongchana P, Ritchie RJ: **Stimulation of oil palm (Elaeis guineensis) seed germination by exposure to electromagnetic fields**. *Scientia horticulturae* 2017, **220**:66.

211. Leong SY, Burritt DJ, Oey I: **Electropriming of wheatgrass seeds using pulsed electric fields enhances antioxidant metabolism and the bioprotective capacity of wheatgrass shoots**. *Scientific reports* 2016, **6**:25306.
212. Isobe S, Ishida N, Koizumi M, Kano H, Hazlewood CF: **Effect of electric field on physical states of cell-associated water in germinating morning glory seeds observed by 1H-NMR**. *Biochimica et Biophysica Acta (BBA)-General Subjects* 1999, **1426**(1):17.
213. Arc E, Galland M, Cueff G, Godin B, Lounifi I, Job D, Rajjou L: **Reboot the system thanks to protein post‐translational modifications and proteome diversity: How quiescent seeds restart their metabolism to prepare seedling establishment**. *Proteomics* 2011, **11**(9):1606.
214. Liu B, Honnorat B, Yang H, Arancibia J, Rajjou L, Rousseau A: **Non-thermal DBD plasma array on seed germination of different plant species**. *Journal of Physics D: Applied Physics* 2019, **52**:025401.
215. Zhang S, Rousseau A, Dufour T: **Promoting lentil germination and stem growth by plasma activated tap water, demineralized water and liquid fertilizer**. *RSC Advances* 2017, **7**(50):31244.
216. Wang S, Doona CJ, Setlow P, Li Y-q: **Use of Raman spectroscopy and phase-contrast microscopy to characterize cold atmospheric plasma inactivation of individual bacterial spores**. *Applied and environmental microbiology* 2016, **82**(19):5775.
217. Lukes P, Dolezalova E, Sisrova I, Clupek M: **Aqueous-phase chemistry and bactericidal effects from an air discharge plasma in contact with water: evidence for the formation of peroxynitrite through a pseudo-second-order post-discharge reaction of H2O2 and HNO2**. *Plasma Sources Science and Technology* 2014, **23**(1):015019.
218. Liu Y, Zhang J: **Rapid accumulation of NO regulates ABA catabolism and seed dormancy during imbibition in Arabidopsis**. *Plant signaling & behavior* 2009, **4**(9):905.
219. Singh R, Singh S, Parihar P, Mishra RK, Tripathi DK, Singh VP, Chauhan DK, Prasad SM: **Reactive oxygen species (ROS): beneficial companions of plants' developmental processes**. *Frontiers in plant science* 2016, **7**.
220. Arc E, Galland M, Godin B, Cueff G, Rajjou L: **Nitric oxide implication in the control of seed dormancy and germination**. *Frontiers in Plant Science* 2013, **4**:346.
221. Bailly C, El-Maarouf-Bouteau H, Corbineau F: **From intracellular signaling networks to cell death: the dual role of reactive oxygen species in seed physiology**. *Comptes rendus biologies* 2008, **331**(10):806.
222. Wong AR, Pearson JS, Bright MD, Munera D, Robinson KS, Lee SF, Frankel G, Hartland EL: **Enteropathogenic and enterohaemorrhagic Escherichia coli: even more subversive elements**. *Molecular microbiology* 2011, **80**(6):1420.
223. Puač N, Škoro N, Spasić K, Živković S, Milutinović M, Malović G, Petrović ZL: **Activity of catalase enzyme in Paulownia tomentosa seeds during the process of germination after treatments with low pressure plasma and plasma activated water**. *Plasma Processes and Polymers* 2018, **15**(2):1700082.
224. Frantz C, Stewart KM, Weaver VM: **The extracellular matrix at a glance**. *J Cell Sci* 2010, **123**(24):4195.
225. Samouillan V, Merbahi N, Yousfi M, Gardou J-P, Delaunay F, Dandurand J, Lacabanne C: **Effect of low-temperature plasma jet on thermal stability and physical structure of type I collagen**. *IEEE Transactions on Plasma Science* 2012, **40**(6):1688.
226. Wiegand C, Fink S, Beier O, Horn K, Pfuch A, Schimanski A, Grünler B, Hipler U-C, Elsner P: **Dose-and time-dependent cellular effects of cold atmospheric pressure plasma evaluated in 3D skin models**. *Skin pharmacology and physiology* 2016, **29**(5):257.
227. Choi FD, Sung CT, Juhasz M, Mesinkovsk N: **Oral Collagen Supplementation: A Systematic Review of Dermatological Applications**. *Journal of drugs in dermatology: JDD* 2019, **18**(1):9.
228. Abreu-Velez AM, Howard MS: **Collagen IV in normal skin and in pathological processes**. *North American journal of medical sciences* 2012, **4**(1):1.

229. Qi J, Elson DS: **Mueller polarimetric imaging for surgical and diagnostic applications: a review**. *Journal of biophotonics* 2017, **10**(8):950.

230. Rehbinder J, Haddad H, Deby S, Teig B, Nazac A, Novikova T, Pierangelo A, Moreau F: **Ex vivo Mueller polarimetric imaging of the uterine cervix: a first statistical evaluation**. *Journal of biomedical optics* 2016, **21**(7):071113.

231. Pierangelo A, Benali A, Antonelli MR, Novikova T, Validire P, Gayet B, De Martino A: **Ex-vivo characterization of human colon cancer by Mueller polarimetric imaging**. *Optics Express* 2011, **19**:1582.

232. Vizet J, Rehbinder J, Deby S, Roussel S, Nazac A, Soufan R, Genestie C, Haie-Meder C, Fernandez H, Moreau F: **In vivo imaging of uterine cervix with a Mueller polarimetric colposcope**. *Scientific reports* 2017, **7**(1):2471.

233. Lu S-Y, Chipman RA: **Interpretation of Mueller matrices based on polar decomposition**. *JOSA A* 1996, **13**(5):1106.

234. Ghosh N, Wood MF, Vitkin IA: **Mueller matrix decomposition for extraction of individual polarization parameters from complex turbid media exhibiting multiple scattering, optical activity, and linear birefringence**. *Journal of biomedical optics* 2008, **13**(4):044036.

235. Qi J, Ye M, Singh M, Clancy NT, Elson DS: **Narrow band 3× 3 Mueller polarimetric endoscopy**. *Biomedical optics express* 2013, **4**(11):2433.

236. Kim A, Moscoso M: **Influence of the relative refractive index on the depolarization of multiply scattered waves**. *Physical Review E* 2001, **64**(2):026612.

237. Arifler D, Pavlova I, Gillenwater A, Richards-Kortum R: **Light scattering from collagen fiber networks: micro-optical properties of normal and neoplastic stroma**. *Biophysical journal* 2007, **92**(9):3260.

238. Pierangelo A, Nazac A, Benali A, Validire P, Cohen H, Novikova T, Ibrahim BH, Manhas S, Fallet C, Antonelli M-R: **Polarimetric imaging of uterine cervix: a case study**. *Optics express* 2013, **21**(12):14120.

239. Rehbinder J, Deby S, Haddad H, Teig B, Nazac A, Pierangelo A, Moreau F: **Diagnosis of uterine cervix cancer using Müller polarimetry: a comparison with histopathology**. In: *European Conference on Biomedical Optics: 2015*: Optical Society of America; 2015: 95400W.

240. Du E, He H, Zeng N, Sun M, Guo Y, Wu J, Liu S, Ma H: **Mueller matrix polarimetry for differentiating characteristic features of cancerous tissues**. *Journal of biomedical optics* 2014, **19**(7):076013.

241. Bancelin S, Nazac A, Ibrahim BH, Dokládal P, Decencière E, Teig B, Haddad H, Fernandez H, Schanne-Klein M-C, De Martino A: **Determination of collagen fiber orientation in histological slides using Mueller microscopy and validation by second harmonic generation imaging**. *Optics express* 2014, **22**(19):22561.

242. Isbary G, Köritzer J, Mitra A, Li Y-F, Shimizu T, Schroeder J, Schlegel J, Morfill G, Stolz W, Zimmermann J: **Ex vivo human skin experiments for the evaluation of safety of new cold atmospheric plasma devices**. *Clinical Plasma Medicine* 2013, **1**(1):36.

243. Hasse S, Hahn O, Kindler S, von Woedtke T, Metelmann H-R, Masur K: **Atmospheric pressure plasma jet application on human oral mucosa modulates tissue regeneration**. *Plasma Medicine* 2014, **4**(1-4).

244. Antonic V, Münch S, Belfekroun C, Lademann J, Peschke B, Smith M, Kramer A, Hartmann B, Ottomann C: **Preliminary Evaluation of the Effects of Cold Atmospheric Plasma Application Rate on the Proliferation Behavior of Keratinocytes In Vitro Measured Using CK-5, CK-10, CK-14, Ki-67 and p53 Expression**. *Journal of Biomedical Engineering and Medical Devices* 2016:1.

245. Zhadobov M, Chahat N, Sauleau R, Le Quement C, Le Drean Y: **Millimeter-wave interactions with the human body: state of knowledge and recent advances**. *International Journal of Microwave and Wireless Technologies* 2011, **3**(2):237.

246. Keyvani A, Atyab SM: **Effects of cold atmospheric structure in different**. *Basic Research Journal of Medicine and Clinical Sciences* 2017, **6**(7):6.

247. Jacques SL, Ramella-Roman JC, Lee K: **Imaging skin pathology with polarized light**. *Journal of biomedical optics* 2002, **7**(3):329.

248. Schnetger B, Lehners C: **Determination of nitrate plus nitrite in small volume marine water samples using vanadium (III) chloride as a reduction agent**. *Marine Chemistry* 2014, **160**:91.

249. Doane TA, Horwath WR: **Spectrophotometric determination of nitrate with a single reagent**. *Analytical letters* 2003, **36**(12):2713.

250. Feres MA, Reis BF: **A downsized flow set up based on multicommutation for the sequential photometric determination of iron (II)/iron (III) and nitrite/nitrate in surface water**. *Talanta* 2005, **68**(2):422.

251. Titheradge MA: **The enzymatic measurement of nitrate and nitrite**. In: *Nitric oxide protocols.* edn.: Springer; 1998: 83.

252. Schwarzenbach G, Muehlebach J, Mueller K: **Peroxo complexes of titanium**. *Inorganic Chemistry* 1970, **9**(11):2381.

253. Baillon F, Provost E, Fürst W: **Study of titanium (IV) speciation in sulphuric acid solutions by FT-Raman spectrometry**. *Journal of Molecular Liquids* 2008, **143**(1):8.

254. Kosaka K, Yamada H, Matsui S, Echigo S, Shishida K: **Comparison among the methods for hydrogen peroxide measurements to evaluate advanced oxidation processes: application of a spectrophotometric method using copper (II) ion and 2, 9-dimethyl-1, 10-phenanthroline**. *Environmental Science & Technology* 1998, **32**(23):3821.

255. Davies G, Higgins R, Loose DJ: **Reactions of copper complexes. II. Reduction of bis (2, 9-dimethyl-1, 10-phenanthroline) copper (II) complexes by hydrogen peroxide in aqueous perchlorate media**. *Inorganic Chemistry* 1976, **15**(3):700.

256. Compain E, Poirier S, Drevillon B: **General and self-consistent method for the calibration of polarization modulators, polarimeters, and Mueller-matrix ellipsometers**. *Applied optics* 1999, **38**(16):3490.

257. Therneau TM: **A package for survival analysis in S. 2015. Version 2.38**. In.; 2015.

258. Hess K, Gentleman R: **Muhaz: hazard function estimation in survival analysis. R package version 1.2. 6**. In.; 2014.

259. Kassambara A, Kosinski M: **survminer: Drawing Survival Curves using 'ggplot2,**. In.; 2018.

260. Machin D, Cheung YB, Parmar M: **Survival analysis: a practical approach**: John Wiley & Sons; 2006.

261. McNair JN, Sunkara A, Frobish D: **How to analyse seed germination data using statistical time-to-event analysis: non-parametric and semi-parametric methods**. *Seed Science Research* 2012, **22**(2):77.

262. Klein JP, Van Houwelingen HC, Ibrahim JG, Scheike TH: **Handbook of survival analysis**: CRC Press; 2016.

263. Kaplan EL, Meier P: **Nonparametric estimation from incomplete observations**. *Journal of the American statistical association* 1958, **53**(282):457.

264. Kaplan EL: **This week's citation classic**. *Current Contents* 1983, **24**:14.

265. Case LD, Kimmick G, Paskett ED, Lohman K, Tucker R: **Interpreting measures of treatment effect in cancer clinical trials**. *The oncologist* 2002, **7**(3):181.

266. Kogoma M, Okazaki S: **Raising of ozone formation efficiency in a homogeneous glow discharge plasma at atmospheric pressure**. *Journal of Physics D: Applied Physics* 1994, **27**(9):1985.

267. Sivachandiran L, Khacef A: **In situ and ex situ NO oxidation assisted by sub-microsecond pulsed multi-pin-to-plane corona discharge: the effect of pin density**. *Rsc Advances* 2016, **6**(36):29983.

268. Winter J, Tresp H, Hammer M, Iseni S, Kupsch S, Schmidt-Bleker A, Wende K, Dünnbier M, Masur K, Weltmann K: **Tracking plasma generated H2O2 from gas into liquid phase**

and revealing its dominant impact on human skin cells. *Journal of Physics D: Applied Physics* 2014, **47**(28):285401.

269. Brubaker TR, Ishikawa K, Takeda K, Oh J-S, Kondo H, Hashizume H, Tanaka H, Knecht SD, Bilén SG, Hori M: **Dynamic analysis of reactive oxygen nitrogen species in plasma-activated culture medium by UV absorption spectroscopy**. *Journal of Applied Physics* 2017, **122**(21):213301.

270. Page SE, Arnold WA, McNeill K: **Terephthalate as a probe for photochemically generated hydroxyl radical**. *Journal of Environmental Monitoring* 2010, **12**(9):1658.

271. Buxton GV, Greenstock CL, Helman WP, Ross AB: **Critical review of rate constants for reactions of hydrated electrons, hydrogen atoms and hydroxyl radicals (· OH/· O− in aqueous solution**. *Journal of physical and chemical reference data* 1988, **17**(2):513.

272. Penado KNM, Mahinay CLS, Culaba IB: **Effect of atmospheric plasma treatment on seed germination of rice (Oryza sativa L.)**. *Japanese Journal of Applied Physics* 2017, **57**(1S):01AG08.

273. Jiafeng J, Xin H, Ling L, Jiangang L, Hanliang S, Qilai X, Renhong Y, Yuanhua D: **Effect of cold plasma treatment on seed germination and growth of wheat**. *Plasma Science and Technology* 2014, **16**(1):54.

274. Shapira Y, Multanen V, Whyman G, Bormashenko Y, Chaniel G, Barkay Z, Bormashenko E: **Plasma treatment switches the regime of wetting and floating of pepper seeds**. *Colloids and Surfaces B: Biointerfaces* 2017, **157**:417.

275. Wang G, Huang J, Gao W, Lu J, Li J, Liao R, Jaleel CA: **The effect of high-voltage electrostatic field (HVEF) on aged rice (Oryza sativa L.) seeds vigor and lipid peroxidation of seedlings**. *Journal of Electrostatics* 2009, **67**(5):759.

276. Galindo FG, Vernier PT, Dejmek P, Vicente A, Gundersen MA: **Pulsed electric field reduces the permeability of potato cell wall**. *Bioelectromagnetics: Journal of the Bioelectromagnetics Society, The Society for Physical Regulation in Biology and Medicine, The European Bioelectromagnetics Association* 2008, **29**(4):296.

277. Cramariuc R, Donescu V, Popa M, Cramariuc B: **The biological effect of the electrical field treatment on the potato seed: agronomic evaluation**. *Journal of Electrostatics* 2005, **63**(6-10):837.

278. Moon J-D, Chung H-S: **Acceleration of germination of tomato seed by applying AC electric and magnetic fields**. *Journal of electrostatics* 2000, **48**(2):103.

279. Criddle R, Breidenbach R, Hansen L: **Plant calorimetry: how to quantitatively compare apples and oranges**. *Thermochimica Acta* 1991, **193**:67.

280. Zhang Y, Chen B, Xu Z, Shi Z, Chen S, Huang X, Chen J, Wang X: **Involvement of reactive oxygen species in endosperm cap weakening and embryo elongation growth during lettuce seed germination**. *Journal of experimental botany* 2014, **65**(12):3189.

281. Acosta-Santoyo G, Cameselle C, Bustos E: **Electrokinetic–Enhanced ryegrass cultures in soils polluted with organic and inorganic compounds**. *Environmental research* 2017, **158**:118.

282. Dymek K, Dejmek P, Panarese V, Vicente AA, Wadsö L, Finnie C, Galindo FG: **Effect of pulsed electric field on the germination of barley seeds**. *Lwt-food science and technology* 2012, **47**(1):161.

283. Yang L, Shen H-l: **Effect of electrostatic field on seed germination and seedling growth of Sorbus pohuashanesis**. *Journal of Forestry Research* 2011, **22**(1):27.

284. Morar R, Munteanu R, Simion E, Munteanu I, Dascalescu L: **Electrostatic treatment of bean seeds**. *IEEE transactions on industry applications* 1999, **35**(1):208.

285. Lin Z, Wang R, Wang S, Tan M: **Water Dynamics of Mung bean (Vigna radiata) Sprouts Treated with 6-Benzylaminopurine: Discrimination by Low-Field Nuclear Magnetic Resonance and Spectrometry**. *International Journal of Food Engineering* 2018, **14**(4).

286. Shao S, Meyer CJ, Ma F, Peterson CA, Bernards MA: **The outermost cuticle of soybean seeds: chemical composition and function during imbibition**. *Journal of Experimental Botany* 2007, **58**(5):1071.

287. Teusink RS, Rahman M, Bressan RA, Jenks MA: **Cuticular waxes on Arabidopsis thaliana close relatives Thellungiella halophila and Thellungiella parvula**. *International journal of plant sciences* 2002, **163**(2):309.

288. Miano AC, Augusto PED: **From the sigmoidal to the downward concave shape behavior during the hydration of grains: Effect of the initial moisture content on Adzuki beans (Vigna angularis)**. *Food and Bioproducts Processing* 2015, **96**:43.

289. Gomes Filho E, Sodek L: **Effect of salinity on ribonuclease activity of Vigna unguiculata cotyledons during germination**. *Journal of plant physiology* 1988, **132**(3):307.

290. Campos PS, nia Quartin V, chicho Ramalho J, Nunes MA: **Electrolyte leakage and lipid degradation account for cold sensitivity in leaves ofCoffea sp. plants**. *Journal of plant physiology* 2003, **160**(3):283.

291. Demidchik V, Straltsova D, Medvedev SS, Pozhvanov GA, Sokolik A, Yurin V: **Stress-induced electrolyte leakage: the role of K+-permeable channels and involvement in programmed cell death and metabolic adjustment**. *Journal of Experimental Botany* 2014, **65**(5):1259.

292. Bajji M, Kinet J-M, Lutts S: **The use of the electrolyte leakage method for assessing cell membrane stability as a water stress tolerance test in durum wheat**. *Plant growth regulation* 2002, **36**(1):61.

293. Guan Y-j, Hu J, Wang X-j, Shao C-x: **Seed priming with chitosan improves maize germination and seedling growth in relation to physiological changes under low temperature stress**. *Journal of Zhejiang University Science B* 2009, **10**(6):427.

294. Hegarty T: **The physiology of seed hydration and dehydration, and the relation between water stress and the control of germination: a review**. *Plant, Cell & Environment* 1978, **1**(2):101.

295. Miles CA, Bailey AJ: **Thermal denaturation of collagen revisited**. In: *Proceedings of the Indian Academy of Sciences-Chemical Sciences: 1999*: Springer; 1999: 71.

296. Hambleton J, Shakespeare P: **Thermal damage to skin collagen**. *Burns* 1991, **17**(3):209.

Appendix

A. Modeling of 3D printer for 9-electrod DBD plasma setup

```
$fn=50;
incr=13;
dint=7.7;
dext=dint+0.42*12+0.1;
xmax=3;
ymax=3;
//part 3
difference(){
union(){
translate([-incr*1.7,-incr*1.7,0])
cube([(xmax+2.5)*incr,(ymax+2.5)*incr,6+3.5]);
//gaz
translate([-39-20,6,0])
cube(size=[18.8+20,15,15]);
//HV
translate([-incr*1.7-5,-incr*1.7-10,0])
cube(size=[30,15,13]);

/fixation support
translate([-incr*1.7-9.9+3,-incr*1.7,0])
cube([15,15,16]);
translate([-incr*1.7-9.9+3,-incr*1.7+(xmax+2.5)*incr-15,0])
cube([15,15,16]);
translate([-incr*1.7-9.9+(xmax+2.5)*incr+9.9-8,-incr*1.7,0])
cube([7+8,15,16]);
translate([-incr*1.7-9.9+(xmax+2.5)*incr+9.9-8,-incr*1.7+(xmax+2.5)*incr-15,0])
cube([7+8,15,16]);
difference(){
translate([-incr*1.7,-incr*1.7,0])   #cube([(xmax+2.5)*incr,(ymax+2.5)*incr,11+5]);
translate([-incr*1.7+2,-incr*1.7+2,0])
#cube([(xmax+2.5)*incr-4,(ymax+2.5)*incr-4,11+5+1]);
}
for(x=[1:1:xmax]){
for(y=[1:1:ymax]){
translate([incr*(x-1),incr*(y-1),0]){
difference(){
union(){
//cylinder(d=dext,h=70);
```

```
translate([0,0,10])        cylinder(d1=dext+15, d2=        dext,h=20);
}
   }
      }
         }
            }
               }
// support inside
for(k=[1:1:ymax]){
translate([-incr,-1+incr*(k-1),2])
tube(size=[(xmax-1+1)*incr,2,4]);
}
for(k=[1:1:xmax]){
translate([-1+incr*(k-1),-1-incr*0,2])
cube(size=[2,(ymax-3+2)*incr+2,4]);
}
translate([-1+incr*(-1),-1-incr*0,2])
cube(size=[2,(ymax-1+2-2)*incr+2,4]);
//passage HT
for(x=[1:1:xmax]){for(y=[1:1:ymax]){
translate([incr*(x-1),incr*(y-1),-20]){
#cylinder(d=1.5,h=100);
   }
      }
         }
for(x=[1:1:xmax]){for(y=[1:1:ymax]){
translate([incr*(x-1),incr*(y-1),    0]){    union(){
translate([0,0,3])
#cylinder(d=dint-2,h=72);
translate([0,0,6])
#cylinder(d=dint-0.4,h=72);
}
   }
      }
         }
//acces gaz
translate([-32,12,2])
#cube(size=[20,3,4]);
translate([-60,13.7,7.2/2+3]) rotate([0,90,0])
#cylinder(d=7.2,h=36);
//fixation HV
translate([-incr*1.7-20,-incr*1.7-3,5]) rotate([0,90,0])
#cylinder(d=10.5,h=40);
//fixation support
translate([-incr*1.7-9.9,-incr*1.7,0]) translate([10,7,-10]) cylinder(d=6.5,h=50);
translate([-incr*1.7-9.9,-incr*1.7+(xmax+2.5)*incr-10,0])                translate([10,3,-10])
cylinder(d=6.5,h=50);
```

translate([-incr*1.7-9.9+(xmax+2.5)*incr+9.9,-incr*1.7,0])　　　　translate([0,7,-10])
cylinder(d=6.5,h=50);
translate([-incr*1.7-9.9+(xmax+2.5)*incr+9.9,-incr*1.7+(xmax+2.5)*incr-10,0])
translate([0,3,-10]) cylinder(d=6.5,h=50);

B. VBScript for the calculation of power in real time with an oscilloscope

This code works on Lecroy oscilloscopes equipped with the Xdev option which enable to customize the operations performed on waveforms. In order to minimize the numerical error, the signals must be represented on the whole screen (in order to maximize the step-in voltage)

```
Function Update() 'VBS code
coeffaffichage=1e7 'This coefficient enables the display and the calculation of the
integral of power
capa=100*1e-9'value of the capacitance Cm = 100 nF
Rsonde=10e6 'probe resistance = equivalent resistance of measurement system
fs=10*1e6 'frequency of sampling
ts=1.0/fs 'time between two samples
startData = 0
endData = InResult1.Samples
scaledData1 = InResult1.DataArray(True)
scaledData2= InResult2.DataArray(True)
Redim Tension(endData) 'High voltage,
Redim ucm(endData) 'Voltage cross the capacitance
Redim Courant(endData) 'current
For i = 0 To endData-1-1
Tension(i)=scaledData1(i)
ucm(i)=scaledData2(i)
ucm(i+1)=scaledData2(i+1)
Courant(i)=capa*(ucm(i+1)-ucm(i))/ts+ucm(i)/Rsonde 'current crossing the DBD
Next
'This code provides the sliding average on 2 *taillefen-1 samples
```

```
'LastPoint = endData - 1 '
'ReDim lisse1(endData)
'ReDim lisse2(endData)
'For i = 0+taillefen To LastPoint-taillefen
' somme1=0
' somme2=0
' For j=i-taillefen TO i+taillefen
' somme1 = somme1+scaledData1(j)
' somme2 = somme2+scaledData2(j)
' Next
' lisse1(i)=somme1/(2*taillefen+1)
' lisse2(i)=somme2/(2*taillefen+1)*capa
'Next
'OutResult.DataArray(True) = lisse1 'ou 2 affichage du signal lissé
OutResult.Samples=endData ' Trace length + 1
ReDim somme(endData) 'contains the primitiv function of power as a function of t
somme(0)=0
for i=1 TO endData-1 'integral calculation
somme(i)=somme(i-1)+coeffaffichage*((Tension(i-1)*Courant(i-1)-ucm(i-1)*ucm(i-1)/Rsonde)*Ts)
Next
OutResult.DataArray(True) = somme
    End Function
```

C. Histogram of Mueller polarimetric parameters of ex vivo mice skin
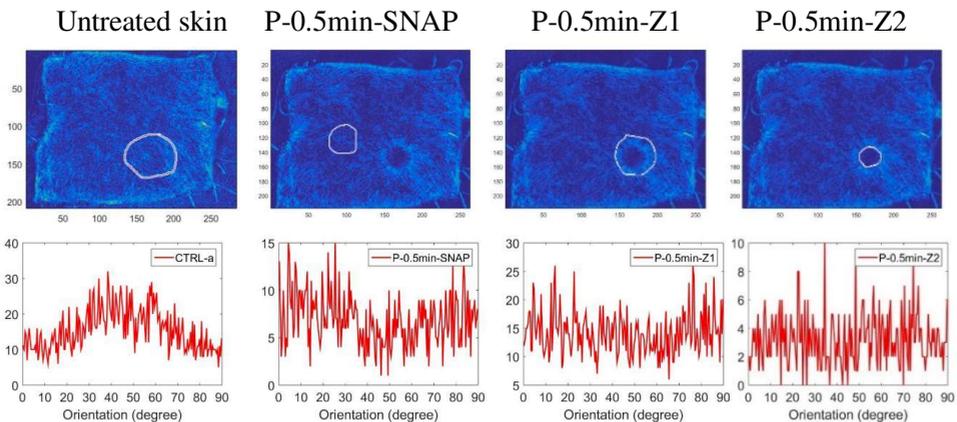

Figure C. 1 The zone selection of mice skin treated continuously by plasma jet for 0.5 min and the Azimuth histogram of selected zone
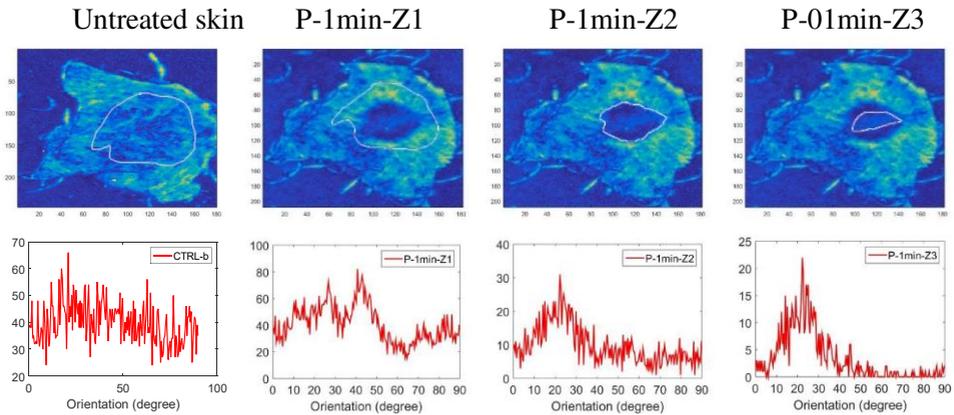
Figure C. 2 The zone selection of mice skin treated continuously by plasma jet for 1 min and the Azimuth histogram of selected zone
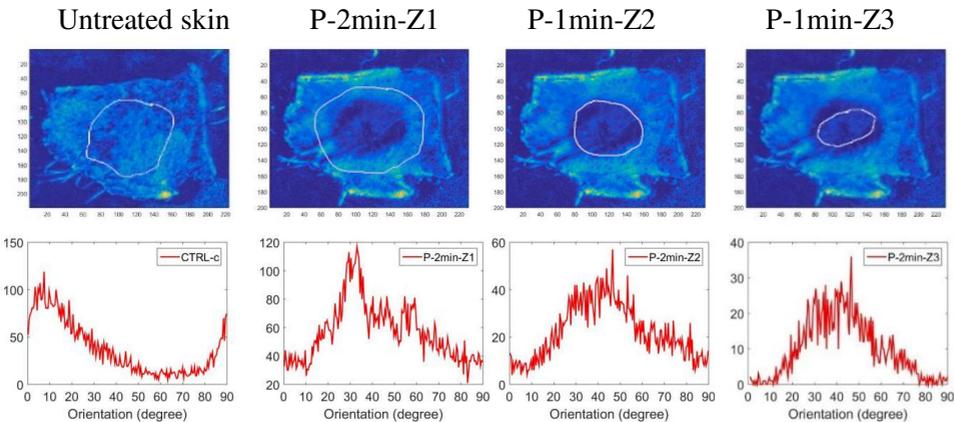

Figure C. 3 The zone selection of mice skin treated continuously by plasma jet for 2 min and the Azimuth histogram of selected zone
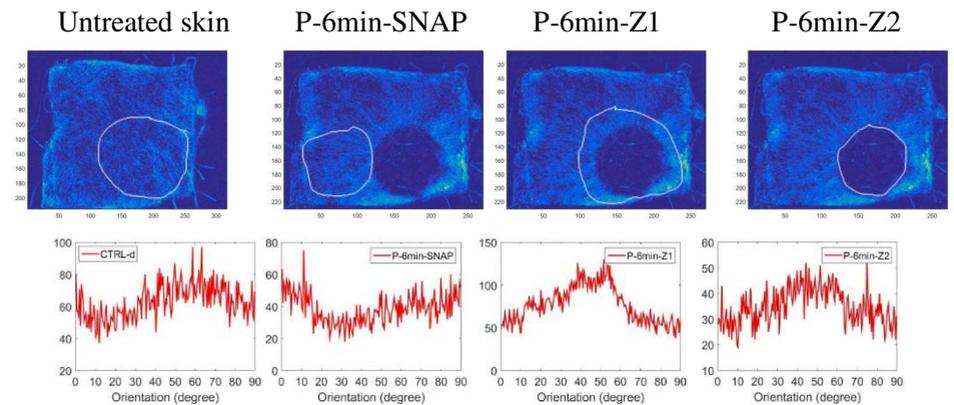

Figure C. 4 The zone selection of mice skin treated continuously by plasma jet for 6 min and the Azimuth histogram of selected zone

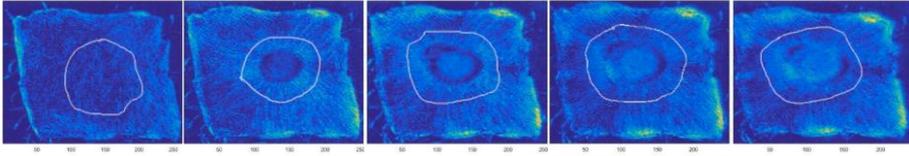Untreated ski   P-1min*1-Z1   P-1min*3-Z1   P-1min*6-Z1   P-1min*9-Z1

Figure C. 5 The Z1 selection of skin treated sequentially by plasma

Untreated skin   P-1min*1-Z1   P-1min*3-Z1   P-1min*6-Z1   P-1min*9-Z1
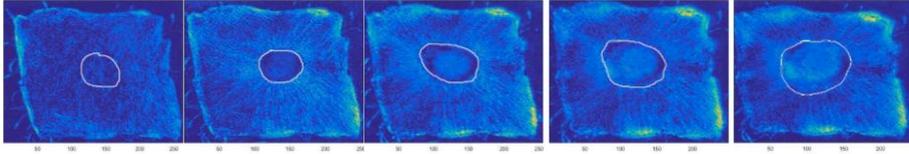

Figure C. 6 The Z2 selection of skin treated sequentially by plasma

P-1min*1-Z1   P-1min*3-Z1   P-1min*6-Z1   P-1min*9-Z1
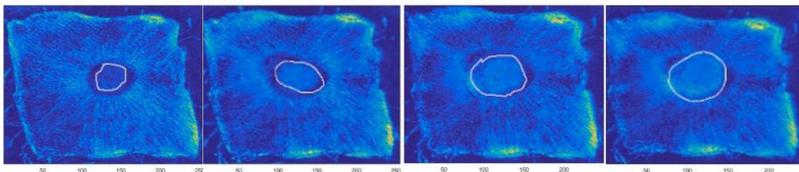

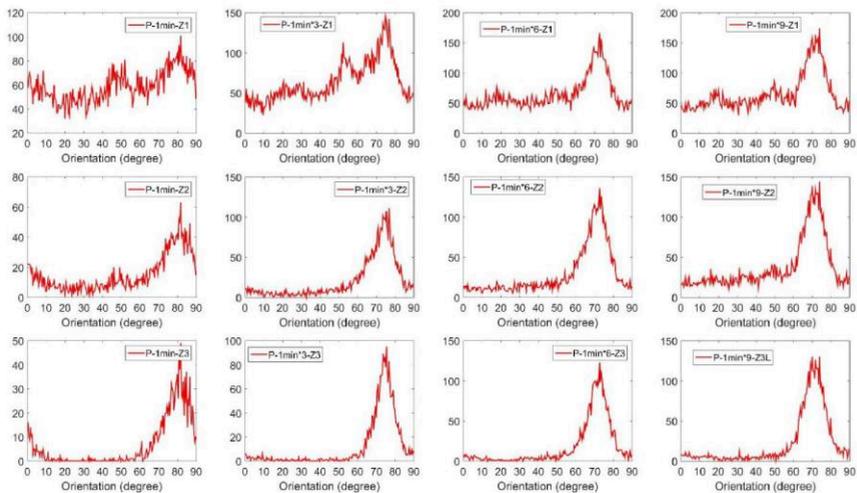Figure C. 7 The Z3 selection of skin treated sequentially by plasma

Figure C. 8 The Azimuth of different zones in skin treated with plasma sequential treatment for different doses

Untreated skin   T50-6min   T50-6min-T60-6min
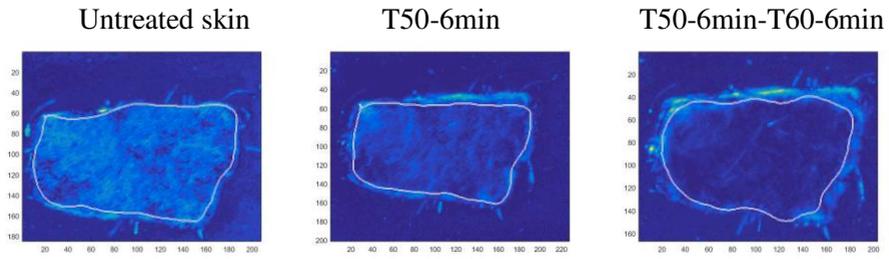
Figure C. 9 The zone selection of thermally treated skin with oven for continuous 6 min under different temperature

Untreated skin   T60-1min*1   T60-1min*3   T60-1min*6

Figure C. 10 The zone selection of thermally treated skin using 60-degree oven for different sequential time

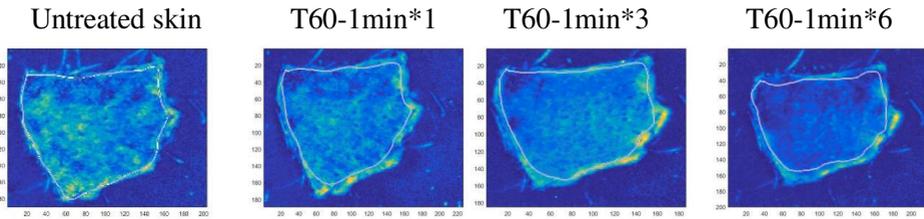Untreated skin   T60-1min

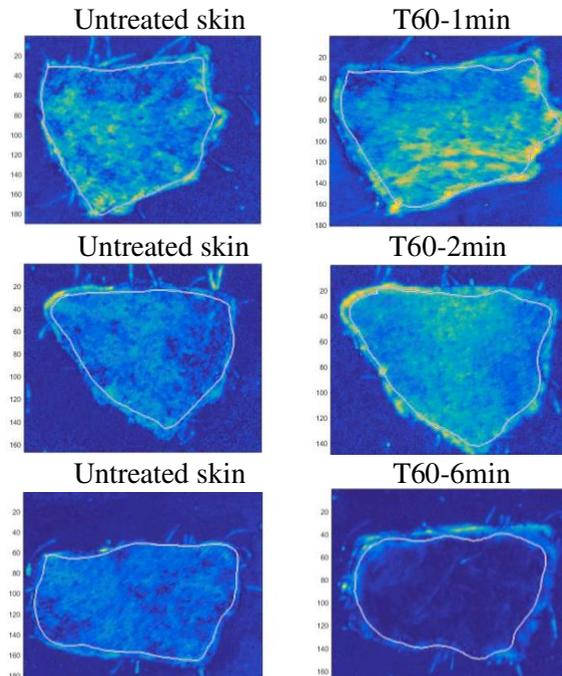Untreated skin   T60-2min

Untreated skin   T60-6min

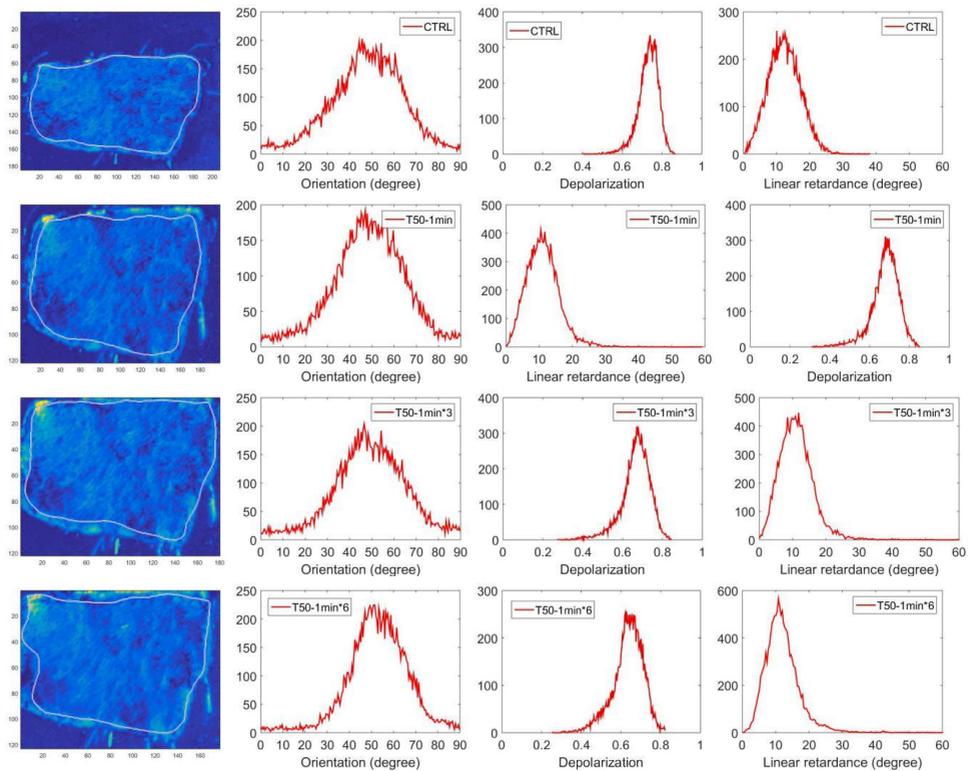Figure C. 11 The zone selection of thermally treated skin with 60-degree oven for different continuous times

Figure C. 12 Histogram of the mice skin thermally treated sequentially with a 50 °C oven in different doses

D. Résumé en français de la thèse

Plasma à pression atmosphérique non thermique interagissant avec l'eau pour applications biologiques

Les plasmas froids (ou plasma non thermique NTP) sont des gas partiellement ionisés dont la température est proche de la température ambiante. Au cours des dernières décennies, les applications des NTP à la biologie, dans des domaines comme l'agriculture et la médecine, ont permis l'émergence de nouvelles recherches multidisciplinaires basées sur les interactions entre les NTP et les organismes vivants traités. Ces nouveaux domaines de recherche sont fortement liés à la chimie issue de l'interaction NTP-liquide. En effet, les cibles biologiques sont usuellement recouvertes d'une couche d'eau. L'objectif du travail de cette thèse est demieux

comprendre les processus physiques et chimiques impliqués dans l'interaction NTP-liquide, en particulier dans le cadre de traitement de graines. Cette étude s'appuie donc sur des recherches à la fois fondamentales et appliquées.

L'utilisation des NTP dans le domaine de l'agriculture a pour objectif d'accélérer la germination des graines en assurant l'uniformité temporelle de cette germination entre les différentes graines. La germination est un processus physiologique très complexe par lequel un semis se développe à partir d'une graine. Cette germination est essentielle pour la croissance des plantes, la production alimentaire ainsi que la sécurité alimentaire. Les mécanismes d'interaction des NTP et dégraines n'ont toujours pas été complètement décrits.

Nous nous sommes également intéressés dans cette thèse aux modifications structurelles d'un tissue cutanée engendrées par les NTP lors d'un traitement de peaux de souris *ex vivo*. Pour ce faire, la technique utilisée est l'imagerie polarimétrique de Mueller (MPI). Cela peut être fait en mesurant la dépolarisation de la peau, le retard linéaire de la peau et l'orientation de l'axe de la peau. Le nut de cette étude est de détecter et de quantifier l'effet du traitement par plasma sur la microstructure de la peau de souris, en particulier le collagène. Le collagène est une protéine majeure de la matrice extracellulaire du derme. Une altération de la structure spatiale du collagène peut entraîner des modifications des propriétés polarimétriques du tissu cutané détectable par la polarimétrie s'agit d'une recherche préliminaire car très peu de travaux connexes ont été réalisés à ce jour.

Les principaux résultats résumés de cette thèse sont présentés ci-dessous :

1. Interaction NTP-liquide avec la configuration plasma DBD à électrode unique

Pour étudier l'interaction NTP-liquides, les espèces réactives produites par les NTP plasma en phase gazeuses et liquides ont été mesurées. En phase gazeuse, l'ozone (O_{3g}) est détecté à la fois dans les rejets d'Air et d'oxygène, tandis que le NO_{2g} et le NO_g ne sont pas détectés dans tous les rejets de gaz. La production d'O_{3g} dépend fortement du débit de gaz. La production de toutes les espèces en phase aqueuse dépend du débit de gaz dans les plasmas à bulles non touchants. Les productions augmentent d'abord puis diminuent avec l'augmentation du débit lorsque les gaz de décharge sont secs, tandis que les productions d'espèces augmentent continuellement avec l'augmentation du débit lorsque les gaz de décharge sont

humides. Nous avons fait l'hypothèse dans cette thèse que toutes ces espèces aqueuses sont formées par la solvatation des espèces gazeuses correspondantes. La production de H_2O_{2aq} sont indépendantes du débit et du mélange de gaz, tandis que les productions de NO_2^- et NO_3^- diminuent de manière continue à mesure que le débit augmente dans tous les plasmas à bulles touchantes. Nous pensons que le NO_2^- et le NO_3^- sont principalement formés dans la couche d'eau ou la phase aqueuse, à la fois par la solvatation d'espèces azotées gazeuses et par des réactions aqueuses pour toucher les plasmas. H_2O_{2aq} est principalement formé dans la couche supérieure d'eau ou dans la phase aqueuse par la combinaison de radicaux OH_{aq} pour le contact des plasmas. De plus, dans le cas des plasmas à bulles touchantes, les concentrations et les rendements en NO_2^-, NO_3^- et H_2O_{2aq} augmentent linéairement avec le temps de traitement au plasma et la tension d'entrée.

2. Traitement des graines

Dans le cadre de l'étude de l'effet des NTP pour la germination des graines, un plasma DBD à 9 électrodes a été utilisé. Les graines réagissent différemment aux traitements NTP selon leurs natures. Le taux de germination des haricots mungo augmente après un traitement direct par les NTP a. Cette augmentation est plus importante que dans le cas de semences traitées indirectement par les NTP dans des décharges d'Air, N_2 et O_2. Ce résultat suggère que clés espèces à vie courte produites par plasma jouent un rôle important pour la germination en phase liquide. L'effet du traitement Air NTP sur la germination des haricots mungo est peu dépendante de la durée du traitement, de pH de l'eau et de la distance des graines à la surface de l'eau. Les effect sur la germination du champ électrique sont comparables à ceux des NTP. Cependant, le taux de germination ne dépend pas dans ce cas de l'intensité du champ électrique et de la durée du traitement. Les graines mouillées et les graines immergées réagissent de manière similaire au champ électrique, les deux offrant de bien meilleures performances en germination que celles des graines sèches. Cela signifie que l'eau est nécessaire pour accélérer le taux de germination du haricot mungo par le champ électrique. En outre, nous avons démontré que l'influence du plasma sur la germination est liée au processus d'hydratation des graines de haricot mungo. En effet plus le degré d'hydratation des graines est élevé, plus l'effet du plasma et du champ électrique sur la promotion de la germination est faible. Nous pensons que les traitements du plasma ou des champs électriques améliorent la

germination principalement par l'interaction avec l'hydratation et les processus métaboliques liés à la germination.

3.Effet des NTP sur la microstructure de peau de souris

La peau non traitée présente une retardance linéaire, une forte dépolarisation et un azimut réparti de manière aléatoire. Tous les paramètres polarimétriques de Mueller des peaux sont affectés par les traitements au plasma et les traitements thermiques. La valeur de retard linéaire dans les régions centrales du traitement au plasma augmente continuellement à mesure que la dose de traitement séquentiel plasmatique augmente, tandis que la valeur dans la peau traitée thermiquement augmente en premier puis diminue avec l'augmentation de la dose de traitement séquentiel thermique 60 °C. Les traitements plasmatiques et thermiques peuvent diminuer la valeur de la dépolarisation des peaux. Un plasma et un traitement thermique continu peuvent endommager la structure de la peau si la durée du traitement au plasma est supérieure à 2 min et la durée du traitement thermique à 60 est supérieure à 6 min. La peau endommagée présente un retard linéaire proche de zéro, une dépolarisation fortement réduite et un azimut réparti aléatoirement.

Titre : Plasma à pression atmosphérique non thermique interagissant avec l'eau pour applications biologiques

Mots clés : Plasmas froids, milieu activé par plasma, médecine par plasma, agriculture par plasma, interaction plasma-liquide, traitements de la peau, traitement des semences, imagerie polarimétrique de Mueller

Les plasmas froids produits par les décharges électriques sont des gaz faiblement ionisés, ce qui maintient la température du gaz à une température proche de la température ambiante, contrairement à la température de l'électron qui peut atteindre plusieurs électron-volts. Les applications des plasmas froids en médecine et en agriculture sont des nouveaux domaines de recherche multidisciplinaires basés sur les interactions de ces plasmas avec des organismes vivants. Le champ électrique ainsi que les espèces réactives de l'oxygène et de l'azote peuvent inactiver les bactéries, stimuler la régénération de la peau (dermatologie), la réduction tumorale (oncologie) et la germination des graines (agriculture). Ce nouveau domaine de recherche, basé sur la chimie plasma-liquide, est très prometteur et se développe rapidement. L'objectif de ce travail est basé sur des recherches fondamentales et appliquées sur le plasma à pression atmosphérique non thermique en interaction avec l'eau pour des applications biologiques et vise à une meilleure compréhension des processus physiques et chimiques de l'interaction plasma-liquide et en particulier du processus biologique de traitements au plasma avec des graines et de la peau de souris ex vivo.

Ce manuscrit est divisé en cinq chapitres: i) On présente tout d'abord une revue de la littérature présentant l'état de l'art concernant l'interaction plasma-liquide et les principales avancées en matière d'applications des plasmas froids à la germination des semences ; ii) Deuxièmement, les dispositifs expérimentaux sont décrits, en particulier la fabrication de réacteurs à plasma utilisant l'impression 3D ; iii) Ensuite, la production d'espèces réactives gazeuses et aqueuses formées par des plasmas de type DBD a été mesurée quantitativement et l'interaction plasma-liquide a été analysée; iv) Puis, plusieurs variétés de graines ont été sélectionnées pour évaluer l'effet un traitement par plasma DBD ; l'étude des mécanismes de promotion de la germination du plasma a été spécifiquement étudiée en traitant les graines de soja vert dans différentes conditions de décharge, dans différents milieux, avec un champ électrique seul et dans différentes conditions de cultures ou de niveau d'hydratation des graines ; v) Enfin, l'imagerie paramétrique de Mueller (MPI) a été appliquée pour la modification de la peau de souris ex vivo traitées par un plasma à jet d'hélium.

Titre : Non-thermal atmospheric pressure plasma interacting with water for biological applications

Key words: Cold plasmas, plasma activated media, plasma medicine, plasma agriculture, plasma-liquid interaction, skin treatments, seeds treatment, Mueller polarimetric imaging

Non-Thermal-Plasmas (NTP) produced by electric discharges are weakly ionized gases, which keeps the gas temperature at near room temperature contrary to the electron temperature which can reach several electron-Volts. Applications of plasma to medicine and agriculture are new multidisciplinary research fields based on interactions of the Non-Thermal-Plasmas with living organisms. Electric field as well as Reactive Oxygen and Nitrogen Species produced by plasma may inactivate bacteria, stimulate skin regeneration (dermatology), tumor reduction (oncology) and seeds germination (agriculture). These new fields of research are based on the plasma-liquid chemistry. These new field of researches, based on the plasma-liquid chemistry are very promising and develops quickly. The objective of this work is based on both fundamental and applied researches in non-thermal atmospheric pressure plasmas interacting with water for biological applications and aim at a better understanding of the physical and chemical processes of plasma-liquid interaction and of particularly the biological process of plasma treatments with seeds and ex vivo mice skin.

This manuscript is divided in five chapters: i) First a literature review is presented showing the state of the art of the plasma-liquid interaction, and the main advances of the application of non-thermal plasmas to seed germination; ii) Second, experimental set ups are described, in particular the manufacturing of plasma reactors using 3D printing; iii) then, the production of gaseous and aqueous reactive species formed by DBD plasmas was measured quantitatively and plasma-liquid interaction was analyzed; iv) Next, different varieties of seeds were selected to evaluate the effect of a DBD plasma treatment and the study of the mechanisms of plasma germination promotion was specifically investigated by treating mung bean seeds in different discharge conditions, in different mediums, in electric field alone and in different hydration levels of seeds; iv) Finally, Mueller parametric imaging (MPI) was applied to study the modification of ex vivo mice skin treated by a helium jet plasma